DESIGN, MODELING AND CONSTRUCTION OF A NOVEL ABLATIVE FAST PYROLYSIS REACTOR AND PRODUCT COLLECTION SYSTEM

Nicholas Matthew Robinson

Doctor of Philosophy

Aston University

September 2000

SUMMARY

The objective of this work was to design, construct and commission a new ablative pyrolysis reactor and a high efficiency product collection system. The reactor was to have a nominal throughput of 10 kg/hr of dry biomass and be inherently scaleable up to an industrial scale application of 10 tones/hr. The whole process consists of a bladed ablative pyrolysis reactor, two high efficiency cyclones for char removal and a disk and doughnut quench column combined with a wet walled electrostatic precipitator, which is directly mounted on top, for liquids collection.

In order to aid design and scale-up calculations, detailed mathematical modeling was undertaken of the reaction system enabling sizes, efficiencies and operating conditions to be determined. Specifically, a modular approach was taken due to the iterative nature of some of the design methodologies, with the output from one module being the input to the next. Separate modules were developed for the determination of the biomass ablation rate, specification of the reactor capacity, cyclone design, quench column design and electrostatic precipitator design. These models enabled a rigorous design protocol to be developed capable of specifying the required reactor and product collection system size for specified biomass throughputs, operating conditions and collection efficiencies.

The reactor proved capable of generating an ablation rate of 0.63 mm/s for pine wood at a temperature of 525 ^{o}C with a relative velocity between the heated surface and reacting biomass particle of 12.1 m/s. The reactor achieved a maximum throughput of 2.3 kg/hr, which was the maximum the biomass feeder could supply. The reactor is capable of being operated at a far higher throughput but this would require a new feeder and drive motor to be purchased. Modeling showed that the reactor is capable of achieving a reactor throughput of approximately 30 kg/hr. This is an area that should be considered for the future as the reactor is currently operating well below its theoretical maximum. Calculations show that the current product collection system could operate efficiently up to a maximum feed rate of 10 kg/hr, provided the inert gas supply was adjusted accordingly to keep the vapour residence time in the electrostatic precipitator above one second. Operation above 10 kg/hr would require some modifications to the product collection system.

Eight experimental runs were documented and considered successful, more were attempted but due to equipment failure had to be abandoned. This does not detract from the fact that the reactor and product collection system design was extremely efficient. The maximum total liquid yield was 64.9 % liquid yields on a dry wood fed basis. It is considered that the liquid yield would have been higher had there been sufficient development time to overcome certain operational difficulties and if longer operating runs had been attempted to offset product losses occurring due to the difficulties in collecting all available product from a large scale collection unit.

The liquids collection system was highly efficient and modeling determined a liquid collection efficiency of above 99% on a mass basis. This was validated due to the fact that a dry ice/acetone condenser and a cotton wool filter downstream of the collection unit enabled mass measurements of the amount of condensable product exiting the product collection unit. This showed that the collection efficiency was in excess of 99% on a mass basis.

ACKNOWLEDGMENTS

I would like to take this opportunity to thank all those people who helped me throughout this work. In particular I would like to express my thanks to Tony Bridgwater and Cordner Peacocke who's continued support has made this project possible.

Special thanks must go to Ian Murkett for making my designs a reality and improving them in the process, Mike Lea for installing and checking electrical equipment, Dave Bleby for correcting any computer problems and Steve Ludlow for purchasing all my equipment.

Dr. Sotos Generalis for help with all things mathematical.

My colleagues in the Bio-Energy Research Group, in particular Nigel Overton, Robert Hague, Liz Salter, Dr. H Sheena, Claire Humphreys and Nina Ahrendt.

My parents, Graham and Jean Robinson, for all their help and support in many ways.

Melissa Fleming, for giving me a place to stay and ensuring that I learnt to cook by generally being so bad at it herself.

TABLE OF CONTENTS

LIST OF FIGURES

LIST OF TABLES

1. INTRODUCTION

The objectives of this chapter are:

- to describe the environmental and commercial reasons for the development of renewable energy and introduce biomass as a renewable energy technology.
- to describe the possible biomass conversion techniques and focus on pyrolysis as conversion technology.
- to define the objectives of this research project which is principally the design and development of an Ablative Fast Pyrolysis Reactor.
- to define important parameters which influence the Fast Pyrolysis Process.
- to define biomass, its constituents and structure.

1.1 BACKGROUND

The "Earth Summit" held in Rio de Janeiro in 1992, and the subsequent "Earth Summit II" held in New York in 1997, highlighted the growing international concern over the deleterious effects of carbon dioxide (CO_2) emissions on the global environment and particularly on the green house effect. A number of the developed nations present signed up to the "Rio Accord", a commitment to reducing or freezing their national CO_2 emissions. In line with their newly acquired sense of environmental responsibility was a desire to stay away from the use of nuclear power to achieve the desired reductions in emissions. In the short term the international community turned to the use of improved combustion technology and greater reliance on natural gas to achieve their targets. However, it was realised that long term strategy would have to be based around the use of renewable energy sources to reduce global CO_2 emissions. Research was and is conducted into developing technologies such as photovoltaics, wind power, hydroelectric power, fuel cells and biomass conversion.

1.2 BIOMASS TECHNOLOGIES

Biomass includes woods, grasses and agricultural crops and these can be used as an energy source, which has a neutral effect on CO_2 emissions. Carbon dioxide emitted during combustion is absorbed by new vegetation growth, and the use of biomass

permits reduction of the quantities of fossil fuels employed. In addition most biomass has very low sulphur contents and this has the added effect of reducing sulphur dioxide emissions.

Biomass used in its virgin form makes a poor fuel due to low calorific content (compared to fossil fuels), high moisture content and poor combustion characteristics. It is normal to convert the fuel to a more viable alternative. There are two main routes for the conversion of biomass into potential fuels, biological conversion and thermochemical conversion. In biological conversion the fermentation of sugars from agricultural crops such as sugar beet and sugar cane to produce ethanol is technically feasible and commercially available. However, the cost of the raw material in the EC makes the process uneconomic.

The other route is thermochemical conversion by heat and reaction. Thermochemical conversion processes seem more promising than biological conversion processes because it is a faster and more intensive process. Two main methods are being investigated, gasification and pyrolysis. Gasification involves the partial combustion of biomass to produce a fuel gas, tar and a solid char. The fuel gas can, for example, be used to drive an engine or turbine to produce electricity. Pyrolysis involves the thermal degradation of biomass in the absence of an oxidising agent to produce a condensable vapour, non-condensable gases and a solid char. The liquid produced is easily transportable and can be used as a fuel or as a source of specialty chemicals (1). Pyrolysis liquid production is the main focus of this thesis as it is currently less developed than gasification, yet enjoys a greater potential and diversity of possible applications.

1.3 PYROLYSIS PROCESSES

Pyrolysis can be classified further into distinctive separate regimes commonly defined as slow, conventional, flash, fast and ablative pyrolysis. The criteria identifying these regimes are based on process parameters such as reaction temperature, gas/vapour residence time and temperature, reactor pressure, biomass heating rate and product thermal quenching rate. The main criteria for each regime are categorised below, it

should be noted that three products are always produced; a solid char, a gas and a condensable vapour consisting of complex, oxygenated hydrocarbons.

1.3.1 Slow Pyrolysis

Slow pyrolysis produces approximately equal proportions of char, gases and a viscous tarry liquid due to the slow degradation rate and the extensive secondary vapour phase reactions. Slow pyrolysis can be characterised by:

- relatively low reactor temperature, < 400 °C
- long vapour residence time, typically > 5 s
- atmospheric pressure
- very slow biomass heating rate, typically 0.01-2 °C/s
- very slow rate of product thermal quenching, minutes to hours

Slow pyrolysis has been used for centuries to produce charcoals, tars, alcohols and other solvents. It is usually carried out in batch processes using kilns or retort furnaces (2, 3, 4).

1.3.2 Conventional Pyrolysis

Conventional pyrolysis gives typical yields of 20 % char, 20 % organic liquids, 20 % water with the remaining 40% comprising of non-condensable gases. Conventional pyrolysis is characterised by:

- relatively low reactor temperature, < 450 °C
- long vapour residence time, typically < 5 s
- atmospheric pressure
- slow biomass heating rate, typically 2-10 °C/s
- very slow rate of product thermal quenching, (5, 6)

1.3.3 Fast Pyrolysis

Fast pyrolysis generally involves high temperatures and rapid product quenching to ensure high liquid yields; typical reaction product compositions are liquids 73%, gases 12% and char 15%. Fast Pyrolysis is categorised by:

- high reactor temperature, > 450 °C
- short vapour residence time, typically < 2 s
- high biomass heating rate, typically > 1000 °C/s
- rapid product thermal quenching, < 40 ms (7)

1.3.4 Ablative Pyrolysis

Ablative pyrolysis can be considered to be a specific technique for achieving fast pyrolysis that may offer advantage over conventional methods. In ablative pyrolysis the reaction products are rapidly removed from the reaction interface to expose fresh biomass for pyrolysis. This serves to maximise the heat transfer rates into the particles and hence ablation rates. The reaction products, and specifically the produced char, are removed due to the high contact pressure and relative motion (>1.2 m/s) between the biomass particles and the heated surface. Ablative pyrolysis can be categorised by:

- high reactor temperature, > 450 °C
- high applied pressure, > 1 x 10^5 Pa
- high relative motion between particle and heated surface, > 1.2 m/s
- short vapour residence time, typically < 2 s
- rapid product thermal quenching, < 40 ms (7)

1.4 OBJECTIVE

Currently the main area of interest for research purposes is fast pyrolysis of biomass. This is because it offers the highest yields of liquids, which is the main product of interest. Various reactor configurations can be used for fast pyrolysis, some with more success than others. Current reactor technologies of interest will be discussed further in

Chapter 3 and can broadly be broken down into fluidised bed reactors, transported bed reactors, entrained flow reactors, vacuum pyrolysis reactors and ablative reactors.

The objective of this project is to model, design and construct a novel pilot plant scale ablative pyrolysis reactor. Ablative fast pyrolysis was chosen because it offers advantages over conventional techniques. This is because the primary mode of heat transfer is from wall conduction. This serves to increase the heat transfer and biomass reaction rate several fold. This allows small compact reactors to be designed without sacrificing capacity. The high contact pressure and relative motion also serve to remove reaction products from the reaction interface, which increases the heat transfer and reaction rate. This process is known as ablation, which is why this type of fast pyrolysis is known as ablative fast pyrolysis. Another benefit is that because the primary heat transfer mechanism is conduction, large quantities of hot gas are not required to provide the heat input needed. This means that smaller, simpler and cheaper product collection systems can be utilised which offers a significant cost saving.

The reactor will be designed to have a nominal capacity of 10 kg/hr and will need to be inherently scaleable with a view to an industrial application of 10 t/hr. The reactor will use a bladed mechanism to provide the necessary high contact pressure and relative velocity. A new, high efficiency product collection system will also be modeled, designed and constructed as this is an area of research to which insufficient attention has been paid.

1.5 PROCESS PARAMETERS

The yields and compositions of the pyrolysis products can be significantly altered by manipulation of the process parameters employed. This can have a major impact on the quality and viability of any product and therefore an overview of the significant factors is given below. These factors should be considered in the specification and design of a reaction system. It is not possible to accurately isolate the effects of individual parameters due to the significant interaction that occur in the reaction. Most researchers consider the following list to represent the controllable parameters that have the most significance.

Substantially controllable parameters:

- The reactor temperature is simple to control and the reaction rate of the biomass is proportional to the temperature of the wall against which the biomass particle ablates. Typically fast pyrolysis reactors operate using woody biomass at a temperature between 450 °C and 600 °C. The reactor must operate at 450 °C or above as this is the minimum temperature at which fast pyrolysis can occur. Reactors are not typically operated above 600 °C as this leads to substantial product losses of the condensable vapour product, which is clearly undesirable.
- The gas/vapour residence time is controllable both by specifying the initial reactor operational volume and operationally by controlling the vapour/gas temperature and flowrate. If necessary nitrogen can be used to lower the vapour residence time, it is necessary to maintain the vapour residence time below 2 seconds in order to minimise any secondary vapour phase condensation reaction or product cracking.
- The gas/vapour temperature will depend upon the reactor temperature and the temperature and flowrate of any diluting nitrogen gas. The vapour temperature must be maintained above 400 °C to prevent the product char sticking to the process pipe work and causing blockages. In addition at temperatures below 400 °C condensation reactions can occur leading to product organic vapour losses and water production. The vapour temperature must also be maintained below 500 °C to prevent any vapour cracking which can lead to vapour losses.
- The pressure applied to the biomass particle affects the ablation rate, with a higher particle pressure leading to a higher ablation rate. This is limited by the available heat flux supply and by the fact that at large particle pressures the particle may be mechanically degraded. The particle pressure is controlled both by the angle of the blades used in the reactor and the relative velocity of the particle compared to the reactor wall. Therefore the speed of rotation of the reactor blades can be used to control the applied pressure. Lédé (8) recommended that the relative velocity be maintained above 1.2 m/s so as to prevent char accumulating on the reactor interface, leading to reduced reaction rates
- Biomass pretreatment (additives, washing, etc.) can be used to influence the chemicals produced during pyrolysis, shifting the composition of the product liquid to favour the higher value added chemicals.

Many of the above parameters were comprehensively in the Ph.D. thesis of G.V.C. Peacocke (9), in addition he considered many more parameters that were controllable to a lesser extent such as particle size and biomass physical properties. As these properties will normally be fixed by the application of the process and the feed material available they will not be considered further.

1.6 BIOMASS COMPOSITION

The composition and structure of biomass is reviewed below due to the effect it has on product yields and compositions. It is beyond the scope of this thesis to give an extensive review but relevant references are given throughout this Chapter.

The structure of biomass has a profound effect on how easy or difficult it is to break apart, both physically and chemical. The chemical components contained in biomass are known to degrade to certain chemicals during pyrolysis. Thus if the composition of the biomass is known it may be possible to determine the chemical composition of the resulting pyrolysis oil.

Biomass is mainly comprised of cellulose, hemicellulose and lignin; with minor components including resin, ash and extractives. These major constituents are composed of carbon, hydrogen and oxygen with other constituents of interest being minor amounts of sulphur and nitrogen.

Typically woody biomass has a lower heating value of 19.8-21.0 MJ/kg (9), this compares to 30-38 MJ/kg for coal (10) and 44 MJ/kg for light fuel oil and gas (10). Typical compositions of biomass are in Table 1 below and typical elemental compositions of biomass and other fuels are Table 2 below.

Table 1 Typical composition of different biomasses (wt% dry) (11)

Biomass	Ash	Lignin	Hemicellulose	Cellulose	Others
Bagasse	1.6	20.2	38.5	38.1	1.6
Beechwood	0.5	23.2	26.8	40.1	9.4
Hardwood	0.3	19.5	35.0	39.0	6.2
Softwood	0.4	27.8	24.0	41.0	6.8
Wheat straw	6.6	16.7	28.2	39.9	8.6

Table 2 Elemental Composition of Biomass and Other Fuels (11)

Material	C	H	O	N	S	Ash
Beech	51.6	6.3	41.5	-	-	0.6
Maple	50.6	6.0	41.7	0.3	-	1.4
Oak waste	49.2	5.7	41.3	0.2	-	3.3
Wheat Straw	48.6	5.2	45.4	0.7	0.1	8.4
Sweet Sorghum	49.9	5.4	33.8	1.4	0.1	10.5
Anthracite coal	94.4	2.9	0.9	1.1	0.7	6
No.6 fuel oil	87.2	10.7	2.1	-	1.47	.02
Natural gas	75	25	-	-	-	-

1.6.1 CELLULOSE

Cellulose is the main constituent of wood and has therefore attracted interest as a model component for the study of biomass fundamentals. It is the primary component of the cell walls. Cellulose can be represented by the formula $[C_6H_{10}O_5]_n$ and is a linear polymer linked together by glycosidic bonds which can be seen in Fig. 1 below. Cellulose chemistry is not discussed here but it is known that the functional groups on the cellulose molecule have a significant effect on the chemical and physical properties of the biomass (12). Cellulose pyrolyses via two competing reaction, fragmentation and depolymerisation. Fragmentation is the breaking apart of the glucose monomer in the cellulose polymer, whereas depolymerisation leads to the breaking of the bonds holding the monomers together. Both feedstock parameters and process parameters determine the choice of pathway. The main feedstock parameters are the morphology of the cellulose, its degree of polymerisation and the presence of alkali metal cations associated with the cellulose polymer. The morphology of the cellulose and degree of

polymerisation are only altered when the wood has been chemically modified (1) or altered by effects such as heating in a vacuum (13). High temperatures and the presence of inorganic material tends to produce more fragmentation reactions and products such as Acetic Acid and Hydroxyacetaldehyde are formed. More depolymerisation reaction occur in the absence of inorganic material (e.g. ash) producing products such as Levoglucosan and Cellobiosan. This has implications if any biomass pretreatment is used to influence the product composition.

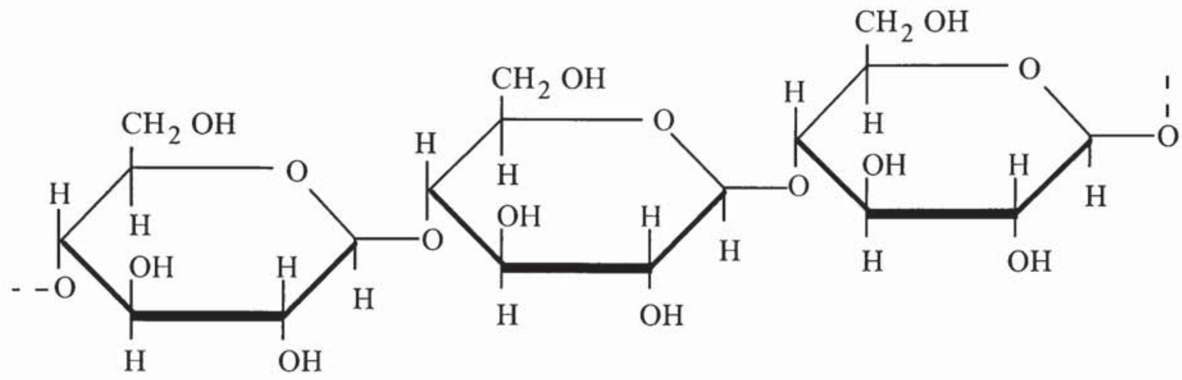

Fig. 1 The Cellulose Polymer.

1.6.2 HEMICELLULOSE

Hemicellulose is a complex polymer based on a variety of sugars such as d-glucose, d-xylose, d-galactose and l-arabinose. Hemicellulose is a branched chain polymer with 1, 4 β-linkages between the sugar units. Hemicellulose is closely associated with cellulose in the cell wall and lignin in the middle lamella (12) and may be seen in Fig. 2 and Fig. 3 below.

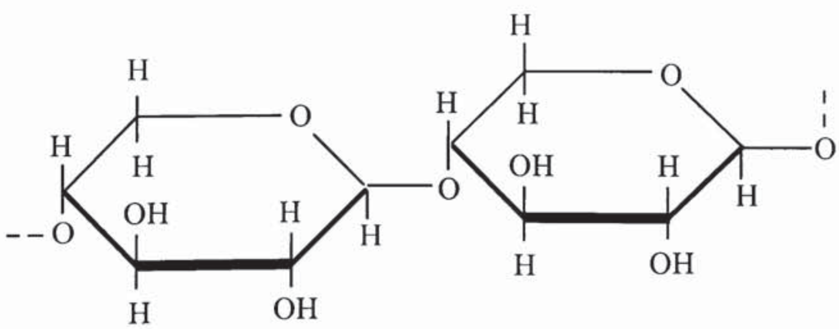

Fig. 2 Xylan hemicellulose structure.

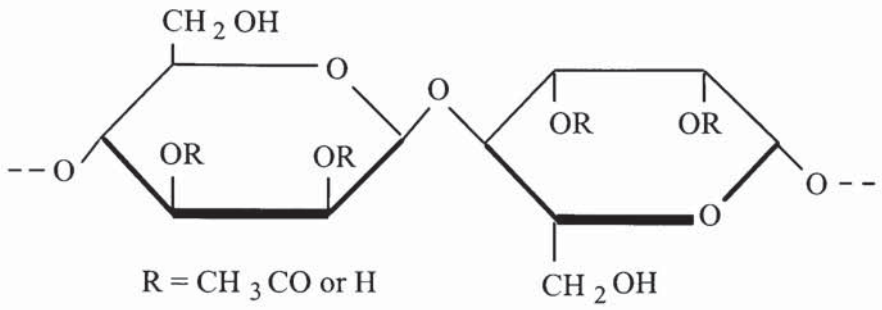

Fig. 3 Mannan hemicellulose structure.

Hemicellulose has received less attention due to its lower abundance, variety of constituents, high reactivity and rapid degradation at low temperatures (150-350 °C). Due to its lack of crystallinity and low degree of polymerisation, fragmentation rather than depolymerisation reactions are likely to occur (5). Hemicellulose is a likely source of furan derivatives and gives higher yields of char, water and acetic acid during pyrolysis due to its higher reactivity compared to that of cellulose.

1.6.3 LIGNIN

Lignin is an amorphous material that surrounds cellulose fibres in the middle lamella and cements them together. Lignin is composed of phenolic polymers consisting of C_3-C_6 phenyl propane units, some examples of which may be seen in Fig. 4 and Fig. 5 below. Lignin is a random three dimensional polymer; the phenyl propane units can consist of guaicyl, syringyl or hydroxyl units. The exact physical structure of lignin is not known but the units are commonly joined with α- or β- linkages (14, 15, 16).

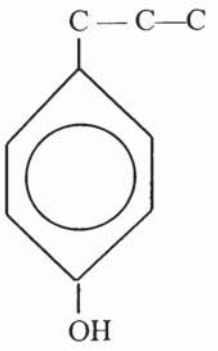

p-Hydroxylphenylpropane

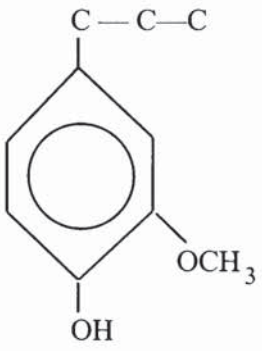

Guaiacylpropane

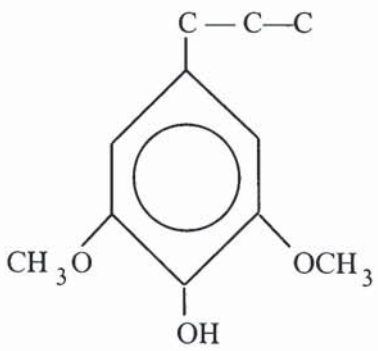

Syringylpropane

Fig. 4 Lignin monomers.

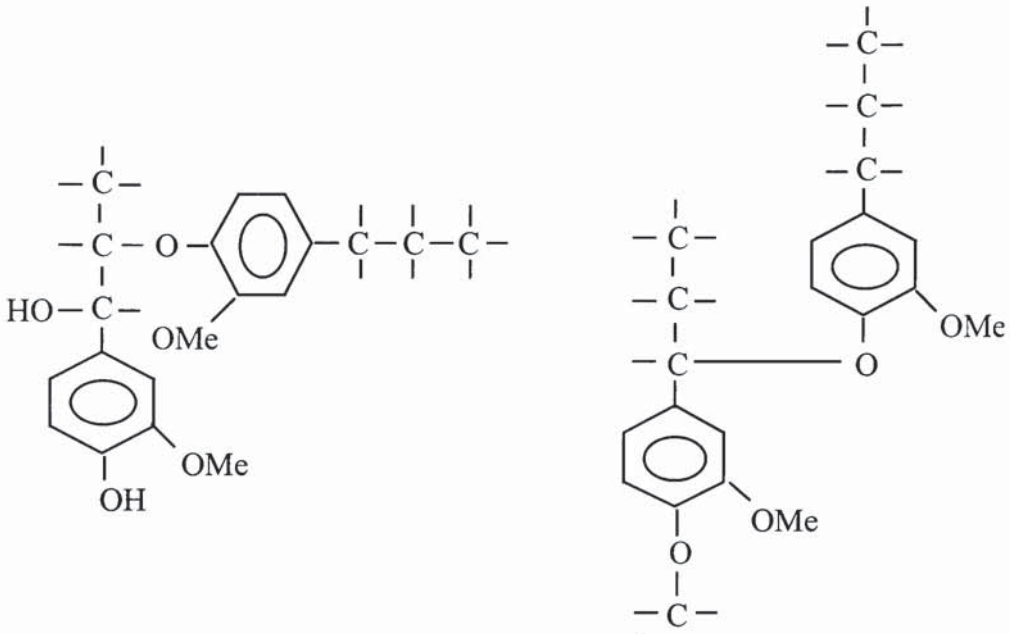

a - Alkylether bonding

b - 4' Ether bonding

Fig. 5 Ether bonds in lignin.

The complex structure of lignin has led to a lack of understanding of the pyrolysis of this biomass component. Lignin is the most thermally stable component of wood but its chemical structure varies according to its source and the method of isolation. Minor decomposition of lignin begins at 250 °C but most significant lignin pyrolysis occurs above this temperature.

2. MECHANISMS OF BIOMASS PYROLYSIS

Biomass is primarily composed of cellulose, hemicellulose and lignin. Many studies have been performed to determine the reaction scheme for each of the major three components: cellulose (12, 17, 18, 19, 20), hemicellulose (21, 22, 23, 24) and lignin (25, 26, 27, 28). The pyrolysis of whole wood is more complicated and only general, rather than detailed, reaction mechanisms have been identified. There is evidence that the pyrolysis of wood may be represented by a linear combination of the pyrolysis products of the three major wood components. Three major whole wood reaction schemes have been proposed; that developed by Diebold et al. (31), that developed by a meeting of specialists at a workshop in 1980 (29), and that developed by Evans and Milne (30). As this project focuses on the development of a reactor for the ablative pyrolysis of whole wood, only the reaction scheme of Diebold (31) is described below as it is considered the most relevant to ablation. This is because it includes a step for degradation of biomass to a liquid intermediary before subsequent vaporisation. This is a key feature of ablative pyrolysis.

2.1 DIEBOLD MODIFIED REACTION SCHEME (1985)

Diebold (31) proposed a simplified global reaction scheme in which the biomass initially decomposes to a viscous primary precursor (termed "Active" by Shafizadeh). The "Active" liquid layer can then subsequently vapourise or crack to produce char and gases. The "Active" layer has been confirmed in work by Diebold (32) and Lédé et al. (8, 33). The model can be seen in Fig. 6 below, however, it should be noted that no pathway is provided for secondary char formation from the gas/vapour phase which is known to occur.

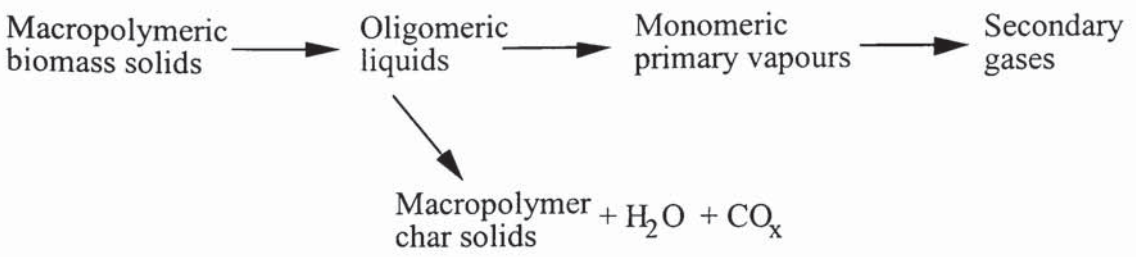

Fig. 6 Diebold modified reaction scheme [1985]

2.2 MODELING OF PYROLYSIS

Mathematical modeling of pyrolysis is used to primarily assess the effects of various parameters on the yields and compositions of the final products. Models of interest are empirical models, kinetic models for primary product yields and secondary vapour phase decomposition kinetics for the gas phase reactions of the primary products before condensation.

Analytical models are required for large particles (>100 μm) to obtain the global pyrolysis rate. These must consider known parameters that affect the pyrolysis process, these include:

a) Heat transfer from the reactor to the particle surface by convection, radiation and conduction.
b) Heat transfer from the outside of the particle to the inside via conduction and possibly convection.
c) Connective heat transfer between the volatile reaction products leaving the reaction zone and the solid matrix.
d) Primary pyrolysis leading to the conversion of biomass to a gas, char and liquid product.
e) Secondary vapour phase decomposition kinetics.
f) Changes in physical properties, enthalpy and heats of reaction.
g) Diffusion of volatiles out of the solid and away from the particle surface, a possible consequence of this being the establishment of pressure gradients.

These processes are all temperature dependent and as the temperature is a function of both time and space this must also be considered.

Analytical models are therefore exceedingly complex and beyond the scope of this report. Readers are referred to the work of Bridge (34) who conducted an extensive review of analytical models and to the recent work of di Blasi et al. (35, 36, 37).

Empirical and Kinetic models are described below.

2.3 EMPIRICAL MODELING

This is a simple form of model in that it is based on the overall mass balance as follows:

$$\text{Biomass} \rightarrow \alpha\ \text{Char} + \beta\ \text{Liquid} + \gamma\ \text{Gas}$$

Where α,β and γ are the mass fractions of the products at specified conditions. A model of this form was developed by Toft (108) and the following relationships determined:

Organics, wt %	$= -16.4 \times 10^{-6} (T)^2 + 0.164 (T) - 3.47$
Water, wt %	$= 4.70 \times 10^{-6} (T)^2 - 0.0049 (T) + 1.20$
Char, wt %	$= 8.60 \times 10^{-6} (T)^2 - 0.0099 (T) + 2.95$
Gas, wt %	$= 8.06 \times 10^{-6} (T)^2 - 0.0071 (T) + 1.64$

A more detailed review is given in Chapter 8.2.2.

2.4 KINETIC MODELING

Kinetic modeling is an attempt to represent the overall reaction kinetic of the pyrolysis process as a series of reaction steps. Kinetic models are derived from experimental studies using Thermogravimetric Analysis (TGA), Differential Scanning Calorimetry (DSC) and Differential Thermal Analysis (DTA). The kinetics of wood pyrolysis are still derived by measuring the rate of weight loss of a wood sample as a function of time and temperature. The most common technique used is thermogravimetric analysis. This involves the continuous weighing and recording of data obtained from a sample heated at either constant temperature or fixed heating rate (18, 38, 39, 40, 41, 24, 42,

43). This is normally carried out under vacuum or a nitrogen atmosphere. As there is no provision for collection of the volatile pyrolysis products, the data obtained is normally used to derive overall kinetic expressions based on the weight loss of the original biomass. The overall thermal degradation process can be represented by.

$$\text{Biomass} \rightarrow \text{Char} + \text{Volatiles} \qquad \textbf{Eq. 1}$$

The rate of the above reaction can be represented by a first order Arrhenius type rate equation.

$$-\left(\frac{dW}{dt}\right) = A(W - W_f)EXP\left(\frac{-E}{RT}\right) \qquad \textbf{Eq. 2}$$

W = Initial mass fraction

W_f = Final mass fraction

A = Pre-exponential constant, s^{-1}

E = Activation energy, J/mol

R = Universal gas constant. J/mol

T = Reaction Temperature, K

If the sample is heated at a constant rate M (M=dT/dt), then:

$$-\left(\frac{dW}{dt}\right) = \left(\frac{A}{M}\right)(W - W_f)EXP\left(\frac{-E}{RT}\right) \qquad \textbf{Eq. 3}$$

The activation energy and the pre-exponential factor are determined by obtaining the best fit curves through experimental data.

The kinetic constant κ for first order reactions is defined:

$$\kappa = A \times EXP\left(\frac{-E}{RT}\right) \qquad \textbf{Eq. 4}$$

This is used to determine the change in mass or composition of the original material by:

$$V = V^{*}\left[1 - EXP(-\kappa t)\right] \qquad \textbf{Eq. 5}$$

Where:

V^{*} = Maximum attainable product yield at temperature T

V = Yield at time t

As there are a large variety of biomass types that can be used, there is a large amount of kinetic data available; in addition is it possible for different researchers to obtain different kinetic data for similar biomass types. A comparison of different kinetic parameter estimation methods has been made by Vovelle et al. (44), which highlights the variability in values obtained by using different methods. The variability of kinetic data due to differences in sample size, shape and origin may be seen in the small selection of kinetic data given in the table below.

Table 3 Experimental kinetic parameters for overall reaction rate expressions.

Source	Sample	Temperature Range °C	Activation Energy kJ/mol	Frequency Factor s^{-1}
Bilbao et al. 45 46	Pinaster pine	290-325 >325	16.4 52.9	6×10^{2} 1.6×10^{16}
Stamm 47	Douglas fir sawdust Coniferous wood	10-220 95-250	104.7 123.5	2.4×10^{5} 6.2×10^{7}
Thurner et al. 48	Oak sawdust	300-400	106.5	2.5×10^{6}
Tran & Rai 49	Douglas fir bark Catalysed bark *	100-850 100-850	101.7 + 142.7 X** 102.6 + 86.2 X **	2.1×10^{8} 2.3×10^{8}
Samolada et al. 50	Fir wood	400-500	56.5 v 94.5 g	136 2.4×10^{33}

*	Bark with 15% K_2CO_3
**	X denotes fractional conversion
V	Total volatiles
G	Total gases

More comprehensive data can be obtained from the work of Peacocke (9). The variation of kinetic parameters occurs even for similar feedstocks and conditions. This variation may be accounted for by a number of factors. The effect of neglecting the temperature variation of the sample during heat up and the use of the steady state temperature as the overall reaction temperature were reviewed by Williams and Besler (23). The problems with the kinetic modeling of biomass where both heat and mass transfer effects must be considered has already been reviewed in Chapter 2. Other discrepancies can be due to too simplistic modeling or the presence of impurities or ash which may influence the kinetic parameters.

2.5 PRIMARY LIQUIDS FORMATION AND SECONDARY VAPOUR PHASE DECOMPOSITION

The vapours produced during pyrolysis are subject to a time-temperature history (Vapours are produced then progressively cooled/condensed) before their recovery as a liquid product. Because the vapours are subjected to this time-temperature history, secondary vapour phase reactions can occur. Secondary vapour phase reaction and kinetics are essential in the design of a reactor for optimal liquids production

2.5.1 LIQUIDS FORMATION AND VAPOUR PHASE DECOMPOSITION

Lidén et al. (51), Diebold (52) and Gorton and Knight (53) have proposed models for the formation of product vapours followed by subsequent secondary decomposition. Lidén and Diebold used different reactor configurations yet proposed similar kinetic models. The kinetic model of Lidén et al. and Diebold can be seen in Fig. 7 below.

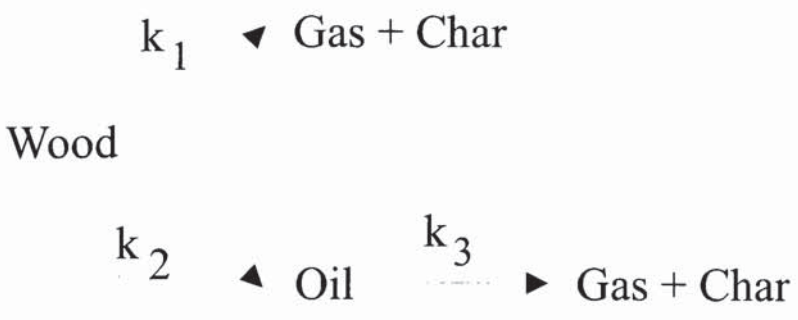

Fig. 7 Kinetic model of Lidén et al. (51) and Diebold (52).

The yield of liquid products can be estimated from the following relationship:

$$x = x_o\left(\frac{1-\mathrm{EXP}(-k_3\theta)}{k_3\theta}\right) \qquad \textbf{Eq. 6}$$

Where:

k_3 = The reaction rate constant for vapour decomposition, s^{-1}

θ = Mean residence time, s

x_o = Theoretical maximum oil yield, wt%

x = Yield of oil, wt%

The kinetic constants may be obtained from:

$$k_3 = 4.28\times10^6\,\mathrm{EXP}\left(\frac{-17500}{RT}\right) \qquad x_o = 0.703 \qquad \textbf{Eq. 7}$$

$$k_3 = 1.55\times10^5\,\mathrm{EXP}\left(\frac{-87634}{RT}\right) \qquad x_o = 0.78 \text{ or } 0.76 \qquad \textbf{Eq. 8}$$

Gorton and Knight (53) determined the following kinetic model.

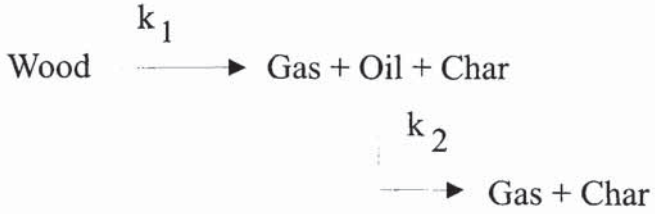

Fig. 8 Kinetic model of Gorton and Knight.

Where the yield of liquid products can be determined from:

$$x = \left(\frac{k_1 x_0}{(k_2 - k_1)[EXP(-k_2\theta)]} \right) \qquad x_0 = 0.811 \qquad \textbf{Eq. 9}$$

Where:

$$k_1 = 1.483 \times 10^6 EXP\left(\frac{-21380}{RT}\right) \qquad \textbf{Eq. 10}$$

$$k_2 = 23.12 \times EXP\left(\frac{-7060}{RT}\right) \qquad \textbf{Eq. 11}$$

Where:

k_1 = Reaction rate constant for liquids production, s^{-1}

k_2 = Reaction rate constant for decomposition of vapour, s^{-1}

Vasalos et al. (54) and Piskorz et al. (55) tested these models using their own experimental data. Vasalos et al. found that Diebolds parameters gave a best fit for the particle size range of 500-600 μm, and estimated the liquids yields to ± 20%. Lidéns parameters gave a best fit for the particle size range 300-425 μm, and estimated the liquid yields to ± 10%. Vasalos et al. found that the model Knight et al. proposed did not satisfactorily predict liquid yields for either particle size range. The conclusion of this work was that variations between the predicted yields and the experimental yields was due to the exclusion of the water yield in the reaction mechanism, the residence times used, the type and size of biomass used and the use of the constant x_o.

3. LITERATURE REVIEW

Chapter 1.2 described the two primary methods of achieving fast pyrolysis, conventional fast pyrolysis and ablative fast pyrolysis. In this chapter examples of these types of technologies are reviewed, in addition vacuum pyrolysis is reviewed as it shares many of the characteristics of both conventional and ablative pyrolysis.

In conventional fast pyrolysis the heat transfer to the particle is achieved predominantly by convection. Ideally, in conventional pyrolysis a small particle size should be used to maximise the reaction rates and product yield. This is because large particle sizes (say having a minimum linear dimension of 2 mm) would react similarly to a shrinking core model, with an inner core of reacting biomass and an outer shell of reaction char. This char layer presents a resistance to heat transfer and reaction rates. In addition, the product vapours are forced to diffuse out through the accumulated char layer. This char layer can catalytically crack the product vapours, significantly reducing the liquid yield, which is undesirable. However, in practice small particle sizes are more expensive to produce and a balance needs to be struck. Conventional fast pyrolysis is typically accomplished in fluidised bed, transported bed and entrained flow reactors. Examples of these types of reactor are reviewed below.

Ablative fast pyrolysis utilises conduction to provide the necessary heat transfer to the reacting biomass particle. This is far more effective than convection heat transfer and serves to increase the reaction rate. In addition the ablative effect removes any char from the reaction interface, this means that large size particles can be utilised in ablative reactors with minimum product losses due to cracking reactions. As ablative fast pyrolysis is the focus of this project it is reviewed extensively below.

Pyrovac (56) have developed a novel vacuum moving bed reactor, which relies upon a mixture of conductive and convective heat transfer. In addition the process is capable of utilising large size wood chips because the vacuum rapidly removes the pyrolysis vapours helping to minimise product cracking. The Pyrovac technology does not sit

comfortably under the heading of either conventional or ablative fast pyrolysis but is reviewed here as it is a commercialised technology.

A more comprehensive review of existing fast pyrolysis process has been undertaken by Bridgwater and Peacocke (57), which includes many more examples of conventional pyrolysis systems.

3.1 EGEMIN, BELGIUM (ENTRAINED FLOW)

3.1.1 BACKGROUND

The aim of the Egemin plant was the production of bio-oil by the flash pyrolysis of fine wood particles in a 200 kg/h vertical, down flowing entrained flow pilot plant shown in Fig. 9 (58, 59). The plant was commissioned in October 1991 and the research was finished in 1993 with the project being abandoned due to lack of funding and less promising results. A basic problem of this plant was obtaining a sufficiently high rate of heat transfer in the short residence time needed for high liquid yields. This resulted in incomplete pyrolysis of the biomass feed and therefore low efficiency.

3.1.2 DESCRIPTION

The feed was small wood particles of 1 to 5 mm with a reported feed moisture content of 16%. Wood was transferred from a storage silo to a small buffer hopper before being fed into the reactor using a water cooled screw auger provided with a nitrogen purge. Wood particles were entrained into the down flowing vertical reactor in a stream of hot gas, at a temperature between 700 and 800°C, produced by a 90% sub-stoichiometric burner fuelled by propane diluted with nitrogen to limit the temperature. The reactor was designed to give an average particle residence time of 0.6 seconds (height 1.2m, diameter 0.4m).

The pyrolysis products left the reactor at approximately 490°C and passed through a cyclone to remove the product char. The liquid products were separated by quenching in a venturi scrubber using product oil as the scrubbing medium. The recycled oil was cooled with a water cooled heat exchanger.

Approximately 75-80% of the oil product was collected by the venturi scrubber system and 20-25% was collected from the fan drain (see below). Gas separated from the liquid products left the venturi scrubber disentrainment tank through fibre mist eliminators using a downstream fan. The oil collected from the fan was highly viscous compared with the oil collected by the venturi scrubber. The non-condensable product gas was flared, but still contained up to 5% of the oil produced.

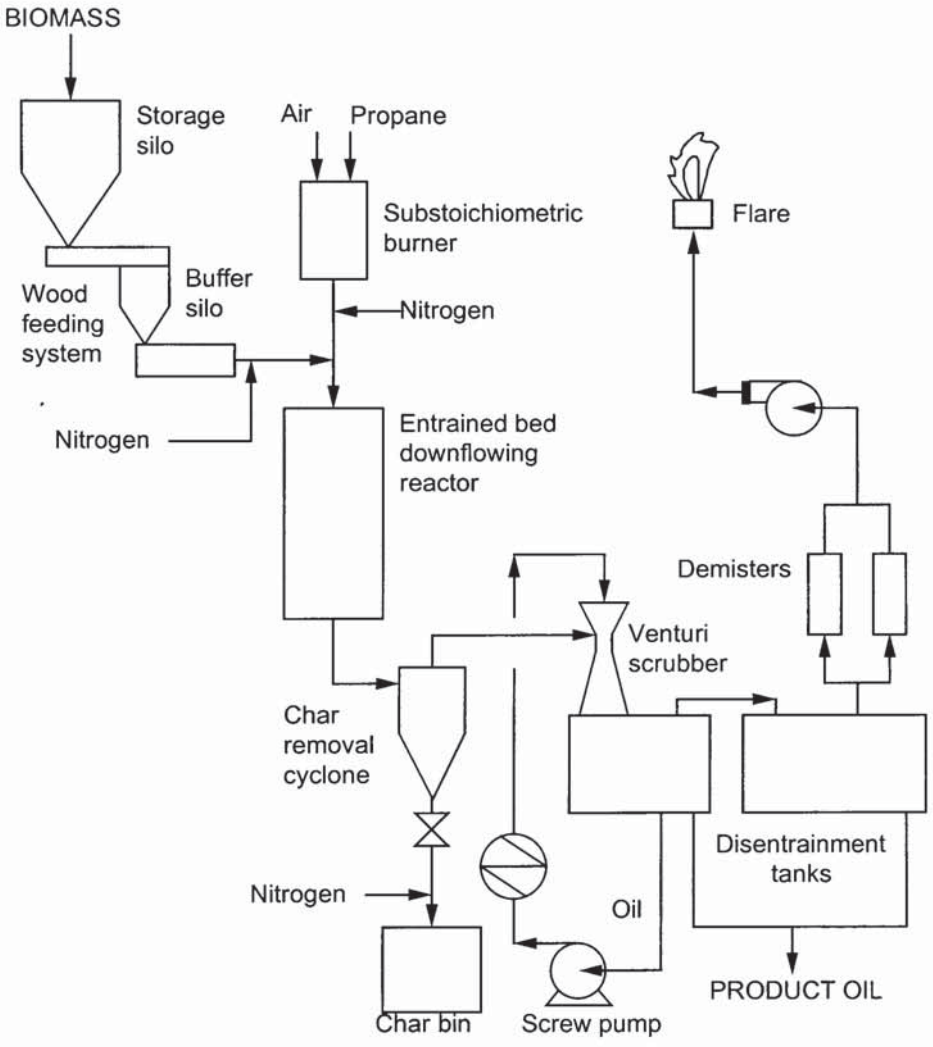

Fig. 9 Egemin Flash Pyrolysis Process (58, 59).

3.1.3 PRODUCTS

The bio-oil was collected from three points; the primary collection vessel, the secondary collection vessel and the drain at the fan. A mass balance is given in Table 4 below. The gas mass flow rate was not measured and was obtained by difference.

Table 4 Mass Balance - Egemin Flash Pyrolysis Process (58)

	Mass flowrate, kg/h	**Yield, %**
Wood (dry)	84.0	N.A.
Oil	33.5	39.9
Gas (by difference)	13.6	29.0
Char	24.4	16.2
Water	12.5	14.9

3.1.4 DISCUSSION

A problem encountered during operation was that the feed was not completely pyrolysed, particularly at high feed rates in excess of 100 kg/h. This is due to insufficiently rapid heat transfer to the particles in the short residence experienced, as almost all heat transfer is by convection.

Another problem encountered was char carry-over from the cyclone collecting in the liquid lines and causing blockages in the heat exchanger and pipework. Bio-oil separation from the non condensable gas was poor with up to 5 % of the product vapour being flared. Efficient product collection is a common problem with most flash pyrolysis systems as the large ratio of non-condensable gas to condensable vapour volumes makes product collection difficult. Heat exchangers suffer fouling problems and are incapable of removing aerosols unless highly over specified and conventional demisters do not appear to be effective at removing aerosols. Use of electrostatic precipitators would remove this problem.

By virtue of their design entrained flow reactors will require large inert/transport gas volumes. This makes them inherently expensive due to the need to produce this gas and the increased equipment sizes needed to handle the gases and, more importantly, to condense the valuable product. Furthermore, in order that a significant fraction of the

biomass feed entering the reactor is pyrolysed, either a long vapor residence time or small biomass particle sizes are required.

A long vapour residence time is undesirable due to the possibility of vapour cracking and product loss. With an entrained flow reactor the vapour residence time is linked to the particle residence time. If a low vapour residence time is used than a low particle residence time will inevitably result. Unless a small particle size is used, a consequence of a low particle residence time is that only a small fraction of the feed is pyrolysed Although this can be mitigated by using a partial feed recycle it adds further complexities to the reaction system.

Small particle sizes are inherently expensive to produce and therefore undesirable.

Therefore, entrained flow reactors were not considered when identifying a suitable design for a new pyrolysis reactor as they offer significant disadvantages compared to other techniques.

3.2 UNIVERSITY OF WATERLOO, CANADA (FLUIDISED BED)

3.2.1 INTRODUCTION

This program was initiated in the early 1980's with the main objective of establishing conditions for maximising liquid yields from biomass, particularly from forest materials. Their research is probably the most extensively published and publicised in this area; for example (60, 61, 62, 63, 64, 65).

A 50 g/h bench scale continuous flash pyrolysis unit using a fluidised bed at atmospheric pressure was initially employed to determine the most efficient operating regime. Particles sized between 105 μm and 250 μm were fed in a nitrogen atmosphere over a temperature range of 400-650°C. Organic liquid yields of 60-70% (moisture free basis) could be achieved using hardwoods such as aspen poplar with a vapour residence time of approximately 0.5 seconds. A 3 kg/hr unit was then constructed by utilising the design data obtained from the bench scale unit. This has been extensively studied and a

200 kg/h pilot plant based on results from this unit has been constructed in Spain by Union Fenosa.

3.2.2 DESCRIPTION

A flow diagram of the 3 kg/h process unit at Waterloo is shown in Fig. 10 below. The wood feed is air dried to a moisture content of 7% before being hammer milled and then screened to a particle size of 595 μm. The wood is then conveyed from the hopper by a variable speed twin screw feeder into a cavity where it is entrained into the reactor by recycled product gas. The reactor bed material is sand and the fluidising agent is recycled product gas (a CO-CO_2-CH_4 mixture) which is preheated by electric heaters. The reactor is wrapped with heating coils allowing extra heat to be added either to the bed of sand or to the freeboard space.

The fluidised bed is operated in a "blow-through" mode which means that the char is entrained out of the reactor whilst the bed material (sand) remains within the reactor. This is done by careful selection of sand size, biomass particle size, bed velocity and reactor configuration.

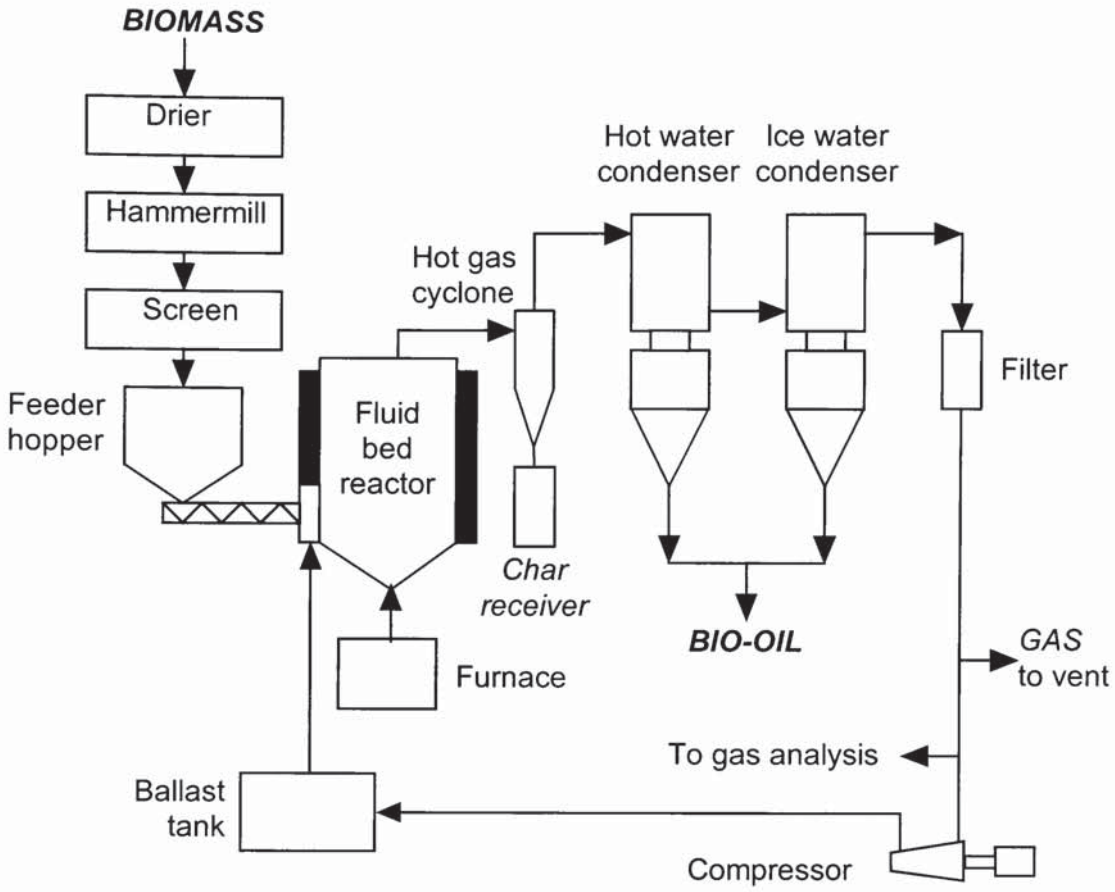

Fig. 10 Waterloo fast pyrolysis unit.

The reaction products pass through a cyclone where char is removed. The vapours and the gaseous product then pass through two vertical condensers in series where the majority of the condensable vapour is collected. The first condenser is held at about 60°C while the second one uses chilled water at around 0°C as the cooling medium. The effluent gases then pass through a filter to remove any residual aerosols before being passed to a recycle compressor. A proportion of this gas stream is taken from the compressor discharge and used to fluidise the reactor bed and convey feed into the reactor, while the excess is vented through a gas analyser and gas meter as product gas. The product gas is analysed for CO and CO_2 in an on-line infra-red gas analyser-recorder. Samples of the product gas are also taken periodically and analysed by gas chromatography.

3.2.3 PRODUCTS

Table 5 below details the yields of the various constituents of the pyrolysis products. It can be seen that liquids were produced in high yields at temperatures around 500 °C. The liquid product is highly oxygenated with no phase separation. It has a low viscosity and contains 10 to 20 wt% water depending on the moisture content of the feedstock and the reaction temperature employed. Some properties of the liquid product are outlined in Table 6.

Table 5 Reported Pyrolysis Yields from Different Woods at Optimal Conditions

	Brockville Poplar	**White Spruce**	**Red Maple**
Temperature, °C	504	500	508
Moisture content, wt %	5.2	7	5.9
Particle top size, mm	1000	1000	590
Apparent residence time, sec	0.47	0.65	0.47
Feed rate, kg/h	2.1	1.91	1.98
Yields, wt % (dry wood basis)			
Water (reaction product)	9.7	11.6	9.8
Char	16.5	12.2	13.75
Organic liquids (dry)	62.9	66.5	67.9
Gas composition wt % (dry wood basis)			
CO	4.71	3.82	4.12
CO2	5.89	3.37	4.89
H2	0.02	0.02	0.01
CH4	0.44	0.38	0.36
C2H4	0.19	0.17	0.16
Others	0.25	0.04	0.26
Total Gas	11.5	7.8	9.8

The gas produced has a higher heating value of about 14.4 MJ/Nm^3. This value increases at higher reaction temperatures as the CH_4 content increases and the CO_2 content decreases.

Table 6 Properties of Pyrolytic Liquids

Elemental Analysis	Brockville Poplar	White Spruce	Red Maple
C	54.7	54	54.7
H	6.9	6.8	6.4
O (by difference)	38.4	39.2	38.9
H/C ratio	1.51	1.55	1.4
O/C ratio	0.53	0.54	0.53
Water content (wet)	18.7	22.4	18
PH	2.4	2.1	2.4
Density, g/cm3	1.2	1.22	1.19
Higher Heating Value, MJ/kg	23.2	22.7	22.4

3.2.4 DISCUSSION

Fluidised beds have many advantageous properties that make them suitable for use as a pyrolysis reactor.

- The fluidised bed is capable of handling a variety of feed type, sizes and shapes and is unlikely to block or clog up.
- The bed material, typically sand, is inert and provides an effective medium through which to transport heat to the pyrolysing particles.
- The fluidising action of the bed may serve to mechanically abrade the accumulating char layer from the reacting biomass particle. The product vapours do not then have to diffuse through the char layer and this reduces the product vapour cracking.
- The particle residence time and the vapour residence time are effectively de-coupled enabling a high biomass conversion rate to be achieved. This is due to the fact that the particles remain suspended in the bed until they are light enough to be entrained out (typically when they become char).

Disadvantages include

- The vapour residence time is dependent upon a number of factors and becomes increasingly difficult to control, and more importantly limit, as reactor sizes increase. This is because as bed diameters increase the bed depth must also increase in order for the bed to fluidise effectively. As the gas/vapour velocity is

limited by the fact that at high velocities bed material would be entrained from the reactor, this means that the vapour residence time must increase.

- The bed will retain a portion of char from the pyroysis process; this is in intimate contact with the product vapours and will lead to an amount of catalytic product cracking.
- Large particle sizes may not degrade to a fine char and may be difficult to entrain out of the reactor.
- Out of necessity fluidised beds require large gas volumes which complicates product collection and adds to the capital and operating cost of the system.

3.3 ENSYN, CANADA (TRANSPORTED BED)

3.3.1 INTRODUCTION

In the late 1970s and early 1980s Ensyn's RTP™ technology developed at least four configurations of reactor which evolved from the research on fast pyrolysis carried out at the University of Western Ontario. These reactors are essentially transported bed reactors and the various configurations are referred to as RTP-I, RTP-II (66), RTP-III and RTP-IV. The main objective of their research is to employ fast pyrolysis to produce both gaseous and liquid fuels and chemicals (67, 66). The process was commercialised in 1989 (68) and several commercial plants were sold to Red Arrow in the USA for recovery of food flavorings and additives (68, 69).

There are currently eight operational plants (57): 30 dry t/d, 25 dry t/d and 3 dry t/d units at Red Arrow in Wisconsin, a 15 t/d demonstration plant at ENEL in Italy, a 100 kg/h unit, 40 kg/h unit and 10 kg/h R&D units at Ensyn in Ottawa, and a 20 kg/h unit at VTT in Finland. A number of facilities are currently at a design or construction stage at up to 350 t/d capacities. Ongoing development work includes hot vapour filtration to reduce ash and char, liquid filtration to reduce char, supply of oil for engine and turbine testing in Canada and Europe, combustion testing, upgrading and product characterisation.

3.3.2 DESCRIPTION

The RTP-III configuration as designed for the ENEL Italian plant can be seen in Fig. 11 below.

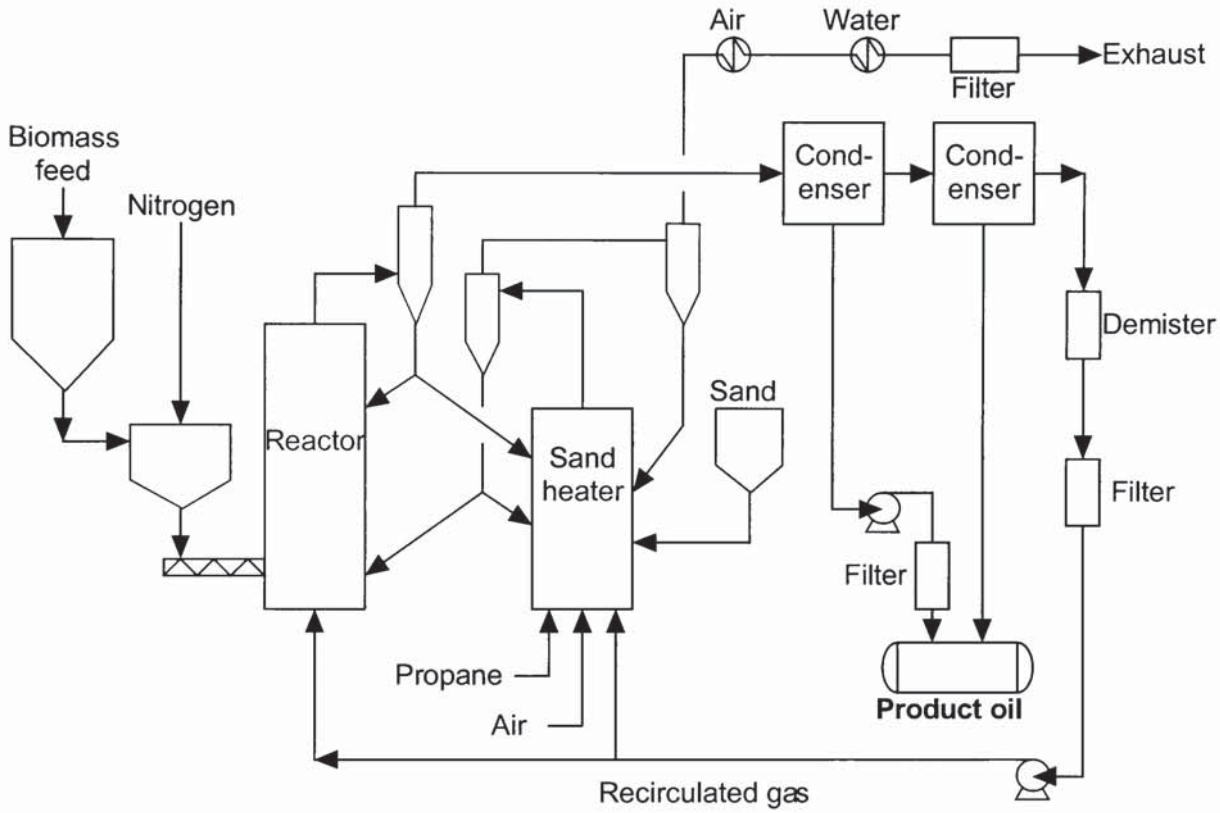

Fig. 11 Ensyn RTP III Process Flowsheet of the ENEL Bastardo plant (70)

The transported bed reactor contacts hot recirculated sand with biomass in an upflowing reactor. The biomass is comminuted to under 6 mm and dried to not more than 10% moisture before being fed to the reactor. The pyrolysis products are passed through two cyclones to remove the char before the vapour is rapidly quenched and cooled in a multiple stage system. The total residence time for the hot vapours can be controlled down to a hundred milliseconds preventing secondary vapour phase reactions. Very low residence times are used for chemicals production, whilst longer residence times are used for liquid fuels in order to more completely crack the lignin. R&D is currently underway to reduce the char and ash levels in the liquid by hot vapour filtration and oil filtration (71).

3.3.3 PRODUCT AND YIELDS

A maximum total liquid yield of 83% by weight (moisture free basis) has been achieved using typical woody biomass feeds. The typical physical properties of the liquids can be seen in Table 7 below (72, 73).

Table 7 Wood Derived Pyrolysis Oils from Ensyn.

	Typical value	Range
Physical property		
Moisture content	22%	14 - 31%
PH	2.5	2.1-3.4
Specific gravity	1.18	1.16-1.22
Elemental analysis, % (moisture free)	1	1
C	56.4	55.3-63.5
H	6.2	5.2-7.0
O (by difference)	37.1	39.43-28.98
N	0.2	0.07-0.39
S	<0.01	0.00-0.05
Ash	0.1	0.04-0.25
C/H molar ratio	0.76	0.89-0.76
C/O molar ratio	2.02	1.87-2.92
HHV, MJ/kg (moisture free basis)	23.1	22.1-24.3
HHV, MJ/kg as produced	17	15-19
Viscosity, cp (@ 40°C)	45	35 - 55
Kinematic viscosity, cSt @ 25°C	233	
ASTM Vacuum Distillation, %	1	1
160 °C	10	
193 °C	20	
219 °C	40	
Distillate	50	
Flash point °C	55	51 - 58
Pour point °C	-25	
Solubility	1	1
Hexane insoluble, %	99	
Toluene insoluble, %	84	
Acetone/acetic acid insoluble, %	0.14	

3.3.4 APPLICATIONS

The Ensyn Technology was commercial applied by Red Arrow Products in Wisconsin, USA, which produce chemicals with the residual oil used as a boiler fuel (69).

Combustion tests showed that the fast pyrolysis bio-oils could be used in place of heavy and light fuels oils in industrial boiler applications (71, 73). Recent tests at Canmet (74) and at MIT (75) show that the liquid oil is more similar to light fuel oil in its combustion characteristics. Therefore special combustion chambers would not be required and a fossil fuel fired boiler or furnace could be easily converted to use this oil. Currently Ensyn is working with a number of companies to test fire bio-oil in an internal combustion engine and in gas turbines (68).

3.3.5 Discussion

The Ensyn systems are one of the few examples of successfully commercialised technologies. Although termed a transported bed reactor it is in fact highly similar to a fluidised bed reactor and the same advantages and disadvantages apply with the following exceptions.

- The gas vapour velocity is not as limited as the sand is actively removed from the bed and therefore entrainment is not as much of a problem.
- The sand is unlikely the have the same char level as a fluidised bed as it is continuously regenerated in the sand heater unit.
- The bed agitation is likely to be greater than in a fluidised bed, with a more effective removal of the accumulating char layer.

3.4 PYROVAC, CANADA (VACUUM PYROLYSIS)

3.4.1 Introduction

Dr. Christian Roy and his research team developed the *Pyrocycling*^{TM} process initially at the Université de Sherbrooke (1981 - 1985) and then at Université Laval (1985 - present). In 1988 Roy created Pyrovac Institute Inc., a private research and development centre devoted to improving the process and the products obtained from various industrial wastes. The engineering firm Pyro Systems Inc. was created in 1996 to scale-up the process. The *Pyrocycling*^{TM} process is being commercialised by Pyrovac

International Inc., a Canadian company created in 1990 whose business office is in Montreal, Canada.

3.4.2 DESCRIPTION

The patented process involves the thermal decomposition of organic materials under specific conditions such as a temperature of 450°C and under a total pressure of 15 kPa. These conditions enable the recovery of large quantities of pyrolytic oils as well as solid carbonaceous materials that possess distinct surface properties.

The feedstock is dried and shredded before being fed into the reactor under vacuum. The reactor is known as a Pyrocycler™, a specially designed integrated equipment system shown in Fig. 12 below. Molten salts are used to heat two horizontal plates that are maintained at a temperature of 530 °C. The molten salts are heated by burning the process waste non-condensable gases. The feed is conveyed over the heated plates and pyrolyses producing vapours that are rapidly removed from the reactor by means of a vacuum pump. These vapours pass through two condenser units in which the heavy and light oils are recovered followed by an aqueous phase. The residual solid products (char) exit the reactor and are collected and cooled. There is an extensive bibliography of which a few key references are included (76, 56, 77).

Fig. 12 The Pyrocycling™ Vacuum Pyrolysis Process.

3.4.3 PRODUCTS.

Typical yields of pyrolysis products obtained from woody biomass during the vacuum pyrolysis and their physical properties are given in Table 9 below.

Table 8 Yields and compositions of the Pyrocycling™ process.

Typical Yields (wt. %, dry wood basis)

	Fir/Spruce Bark	Spruce Wood
Pyrolysis oils	35%	47%
Pyrolytic water	20%	17%
Wood charcoal	34%	24%
Gas	11%	12%

Pyrolysis Oil (Spruce Wood)	
Elemental Comp. (wt.%, @23% moist.)	
C	55.4
H	8.4
O	35.3
N	0.6
S	<0.01
Ash	0.3
Density, kg/m^3 @25°C	1140
HHV, MJ/kg	23.0
Water, wt.%	23.0
Viscosity @ 50°C, cSt	5.6
Flash point, °C	>95
V, Na, ppm	each: <1
Ca, ppm	107
K, ppm	22
pH	3

Charcoal	
HHV, MJ/kg	30.4
Volatile Matter	20.3
Ash	7.6
Fixed Carbon	72.1
Gas composition (vol. %)	
Hydrogen	6.6
Methane	10.0
Carbon monoxide	32.0
Carbon dioxide	41.5
Ethane	1.5
Ethene	1.5
Propene	1.4
Propane	0.4
Methanol	0.4
Butane	0.4
Butene	0.6
Pentane	0.6
Others	3.1
HHV, MJ/kg	10.9

3.4.4 APPLICATIONS

Possible commercial applications apart from energy provision include recycling of automobile shredder residues, biomedical wastes, waste plastics, municipal solid wastes, petroleum sludge's and other industrial wastes with organic components. In most cases, the wastes are completely transformed into pyrolysis oils, water, solid residues and non condensable gases. The process can also be used for the remediation of soils contaminated with hydrocarbons or to extract bitumen from tar sands.

3.4.5 DISCUSSION

Again the Pyrocycling technology is an example of a commercialised technology, the following advantages and disadvantages apply.

Advantages include

- large particle sizes can be used as the vacuum product collection system helps to remove the product vapours through any accumulated char layer.
- the char is removed from the system without the need for cyclones as there does not appear to be significant char breakup and entrainment.

Disadvantages include

- The system is mechanically complex, making it capital intensive and potentially more unreliable.
- Vacuum technology is inherently an expensive process.
- Despite the use of a vacuum, the reaction products are significantly cracked with a resulting loss of organic liquids.

3.5 NREL ENTRAINED FLOW VORTEX REACTOR (ABLATION)

3.5.1 BACKGROUND

Diebold conducted research into pyrolysis of lignocellulosic feedstocks at the Solar Energy Research institute (SERI), now the National Renewable Research Laboratory (NREL). Diebold demonstrated the phenomenon of ablative fast pyrolysis when he used a red hot nichrome wire to ablatively cut a piece of wood (32). The pyrolysis rates obtained appeared to be roughly 3.5 times the order of magnitude of those recorded for slow pyrolysis rates at a similar temperature. Diebold went on the design and construct a 50 kg/h entrained flow ablative pyrolysis reactor, although only a throughput of 36 kg/hr has been achieved to date (57).

3.5.2 PROCESS DESCRIPTION

The reactor consists of a horizontal cylinder with an internal diameter of 13.4 cm and a length of 70 cm and is heated by three wall heaters. Wood chips approximately 5 mm square are tangentially entrained into the reactor via a screw feeder. The entrainment gases (steam or nitrogen) are at a temperature of approximately 700°C and can accelerate the particles to velocities of over 400 m/s. The wood particles ablatively pyrolyse and the gas, vapours and char fines exit the reactor through an axial takeoff. The reactor is capable of generating a particle pressure in the region of 7.0×10^6 N/m^2. Relevant literature is available in the proceedings of the U.S. D.o.E. Biomass Thermochemical Conversion Contractors Meetings (78, 79, 80, 81, 82).

3.5.3 COMMISSIONING STUDIES

Cold flow studies indicated that only 20% of the available heat transfer surface was being utilised by the wood chips. A fabricated helical rib was placed inside the reactor to force the particles to take a more preferential path through the reactor. This proved partially effective as some of the particles managed to bypass the helix due to poor sealing of the helix against the reactor wall. Diebold noted that at temperatures of less than 625°C, 30% of the feedstock remained only partially pyrolysed on a once though basis (78). In order to improve the conversion of biomass a new reactor was built with an integral helical rib (25mm pitch, width 6mm, height 3mm) and a solids recycle loop was added, see Fig. 13 below.

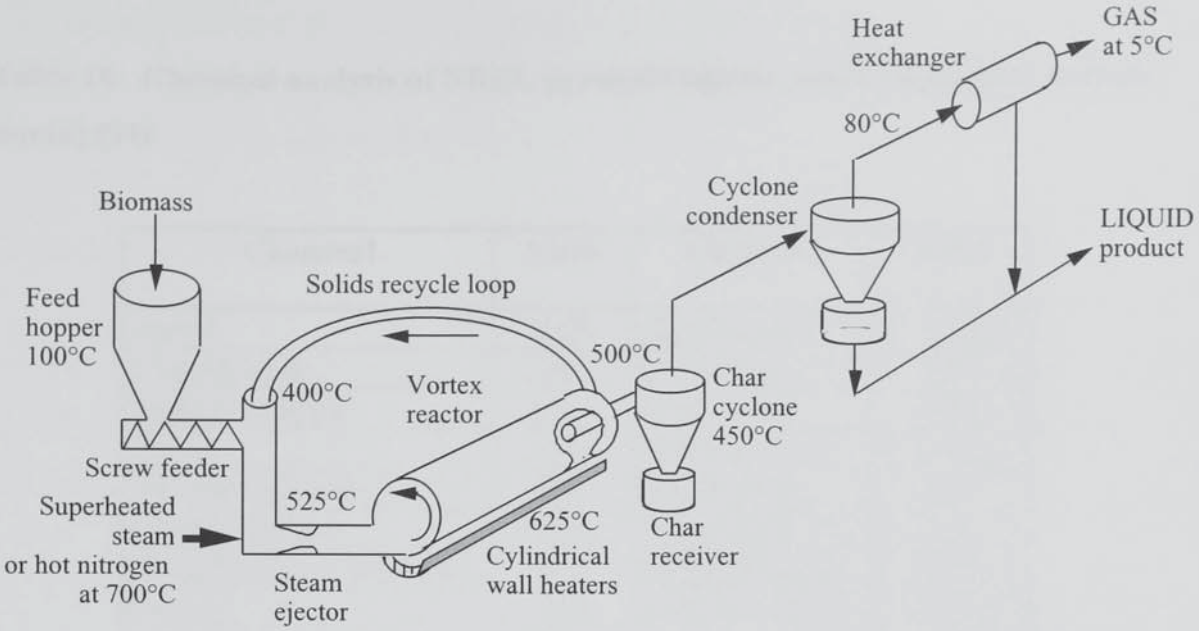

Fig. 13 NREL ablative pyrolysis reactor.

Installation of both the helical rib and solids recycle reduced losses from approximately 30% to 7-10% and this can be assumed to be char rather than unreacted biomass. Calculations showed that the particles had to be recycled approximately 23 times achieving a particle size of <50 μm before being entrained out with the gas and vapour products. Some of the results obtained may be seen in Table 9 and Table 10 below.

Table 9 Mass balances for the NREL vortex reactor [wt% dry feed basis] (83)

Feedstock	Organic Liquids	Char	Gases	Water	Reactor Temp.(°C)	Residence time (s)
Aspen poplar	53.4	12	16	10.9	500	0.75
Aspen poplar	55.4	13.1	13.8	11.8	625	--

Table 10 Chemical analysis of NREL pyrolysis liquids, [wt% chemical in biomass liquid] (84)

Chemical	Yield	Chemical	Yield
Acetol	4.08	Glycolic acid	0.54
2 furaldehyde	0.66	Formic acid	0.97
Furfuryl alcohol	0.1	Acetic acid	4.08
Phenol	0.73	Propionic acid	0.33
5-methyl furfural	0.06	Butyric acid	0.43
4-butyrolactone	0.26	Valeric acid	0.26
Methyl cyclopenten-l-one	0.44	Hexanoic acid	0.26
p-cresol	0.09	Heptanoic acid	0.03
m-cresol	0.04		
Eugenol	0.13	Levoglucosan	1.99
2,6-dimethoxyphenol	0.66	Syringaldehyde	0.37

Central to Diebolds work was the proposition that the wood initially formed a liquid film that lubricated particle motion. The film was thought to consist of large oligomeric compounds that vapourise slowly; or cannot vapourise but decompose to lower molecular weight compounds that can. It was proposed that the larger oligomeric molecules are derived from lignin, and are more thermally stable than those derived from carbohydrates.

The reactor is currently not in use for liquid production, however it can be adapted to produce liquids when required.

3.5.4 Discussion

The NREL reactor is essentially an entrained flow reactor, but by virtue of the high contact pressures generated with the reactor wall the reaction process is also ablative. The following advantages and disadvantages apply.

Advantages include

- low vapour residence times resulting in a minimal product loss due to cracking reactions.

- a high particle contact pressure resulting in high reaction rates.
- ablation effect serves to remove reaction products from the reaction interface leading to higher reaction rates and less product cracking.

Disadvantages include

- large volumes of transport gas are difficult to heat to the minimum temperature of 450 °C necessary to prevent product sticking
- large volumes of transport and product gas require complex and more costly collection systems.
- additional complexity in order to generate high velocity transport gases which are required to achieve high particle contact pressure.
- unable to effectively decouple the particle residence time and vapour residence time, excepting that resulting from partial particle recycles.
- high particle recycle rate needed in order that a significant fraction of the biomass is pyrolysed.
- large particle sizes are more difficult to entrain and therefore limit the system.

3.6 CENTRE NATIONALE DES RECHERCHES SCIENTIFIQUES, UNIVERSITY OF NANCY (ABLATION)

3.6.1 BACKGROUND

This work developed from an analysis of the criteria for fast pyrolysis, ablative pyrolysis was viewed as satisfying the requirements for high heat transfer rates coupled with minimum char production. Lédé carried out fundamental research into ablative fast pyrolysis and derived detailed heat transfer relationships from empirical results and heat transfer theory. These results were fundamental to the ablative pyrolysis design methodology employed by Peacocke (9) in the construction of his ablative pyrolysis reactor.

3.6.2 PROCESS DESCRIPTION: ROTATING DISK RIG

Lédé et al's. experimental system can be seen in Fig. 14 below (8, 85, 33, 86). The rig consists of a stainless steel disk of 7.5 cm diameter capable of being rotated at a constant and controllable speed. The disk was heated from below by four gas burners. Wood rods of diameter 2 to 10 mm were pressed vertically onto the hot surface. The applied pressure was controlled using weights, with the ablation rates of the wood being determined by measuring the change in rod length over a specified period of time. The reaction zone of the wood rod was investigated by a microscope after the experimental run had ended. The experiments were carried out under an atmosphere of argon to prevent combustion of the volatiles. No provision was made for the recovery or measurement of the vapours produced so mass balances were unable to be determined.

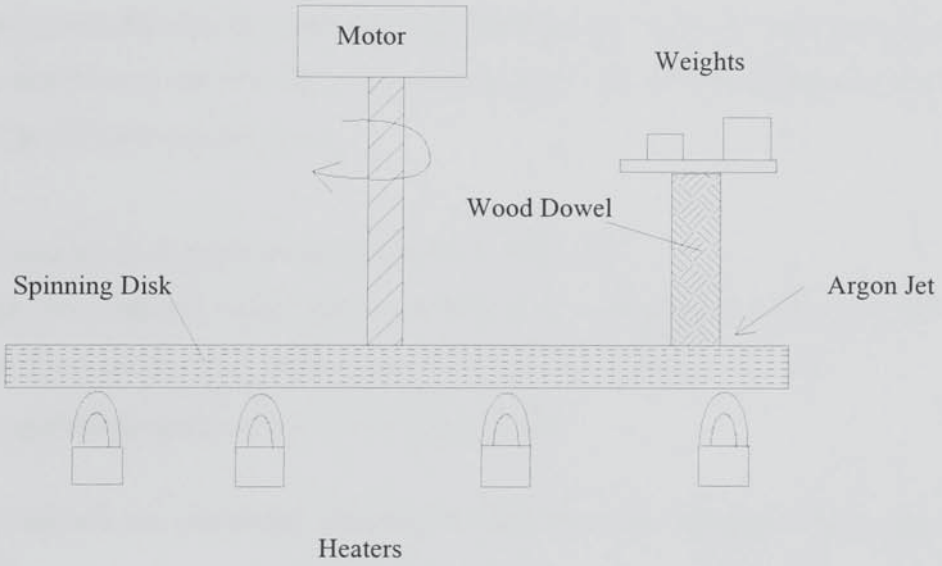

Fig. 14 Lédé's Spinning disc reactor.

The ablation rate of the wood rod was measured as a function of disk temperature, relative motion and applied pressure. Empirical correlations and fundamental relationships were then determined (86, 87). The range of variables used were:

a) disk temperature between 550°C and 900°C.
b) relative motion velocities between 0.3 m/s and 3 m/s.
c) applied pressures of 2×10^5 Pa and 3.5×10^5 Pa.

Separate experiments were also carried out for the case of no relative motion between the disk and wood rod (88).

3.6.3 Results Of The Work

A range of correlations were determined relating to the ablative pyrolysis of biomass. These correlations can be used in the design of ablative pyrolysis but are neither accurate enough nor conducted in sufficient depth to be used in the design of the ablative pyrolysis reactor which is the focus of this project. An overview of some of the more important parameters is given below.

Biomass Decomposition Temperature, T_d

Lédé proposed that the biomass decomposition temperature, T_d, had an average value of 739 K, determined empirically in a series of experiments. Experiments were conducted within the following parameters:

- an average heat transfer coefficient of 10,000 w/m^2.
- disk temperatures, which the wood rods were contacted with, of 500-900°C.
- relative motion between the wood rod and heated disk of 0-3 m/s.
- an applied pressure of 1 x 10^5 to 3.5 x 10^5 Pa.

Lédé proposed an analytical solution for the biomass decomposition temperature as follows:

$$T_w = T_d + \frac{T_d - T_o}{h}\sqrt{\left(\kappa\lambda_w\rho_w C_{pw}\right)} \qquad \textbf{Eq. 12}$$

Where:

T_w = Temperature of the wall, K

T_d = Biomass decomposition temperature, K

T_o = Datum temperature, K

h = Heat transfer coefficient, W/m^2.K

C_{pw} = Biomass heat capacity, J/kg.K

λ_w = Wood dry thermal conductivity, W/mK

ρ_w = Wood dry density, kg/m^3

κ = First order decomposition kinetic constant, s^{-1}

It should be noted that the average value of 739 K for T_d is determined from a range of data with the deviation being as much as ± 30 K.

Ablation Rate, V

The ablation rate of the wood rod was determined for a range of experimental conditions and the following empirical relationship determined:

$$V = \hat{A}P^F \qquad \textbf{Eq. 13}$$

Where:

V = Ablation rate, m/s

P = Applied pressure, Pa

$\hat{A}$ = Function of the reactor heated surface temperature, m/s.Pa.F

F = Constant dependent upon solid, ≈ 1 for wood

Lédé proposed the following empirical relationship for F.

$$F = \frac{C_p(T_d - T_o)}{C_p(T_d - T_o) + \Delta H_{pyr}} \qquad \textbf{Eq. 14}$$

Where:

ΔH_{pyr} = Enthalpy of pyrolysis, J/kg

Heat Transfer Coefficient

The heat transfer coefficient, h, was also empirically determined from a range of experimental data for wood.

$$h = \Re p^F \qquad \textbf{Eq. 15}$$

Where:

$\Re$ = empirically determined parameter equal to 0.017 $w/m^2.K.Pa^F$

At present, there is no further experimental work being carried out, however fundamental work on ablation and the nature of the formation of "active" is ongoing.

3.6.4 Discussion

The empirical work undertaken by Lédé et al. enabled the determination of the biomass decomposition temperature and showed that the value was roughly constant. This was an important discovery as it is one of the fundamental operating limits of a pyrolysis reactor.

Lédé et als. work attempted to link parameters such as the biomass decomposition temperature or ablation rate to physical properties and kinetics. As only a limited amount of experiments had been undertaken, with a just a few subject materials, the results are very much case specific and a simple empirical relationship would have been more appropriate.

The equation used to determine the heat transfer coefficient, h, ignores influences such as vapour formation below the biomass and char accumulation on the reaction interface.

Further work by Lédé et al (85, 86, 87, 88) developed analytical relationships, largely based on the classic Osborne-Reynolds work (101), enabling the determination of the ablation rate from applied temperature, pressures and physical properties for a round wood rod. An alternative approach, based on a rectangular wood rod, is developed in

Chapter 6 and is used in the design of the ablative pyrolysis reactor that is the focus of this thesis.

3.7 INTERCHEM INDUSTRIES INC., USA (FORMELY PYROTECH) (ABLATION)

3.7.1 BACKGROUND

Interchem Industries Inc. was founded in 1985. Initial work to scale up the ablative pyrolysis process was carried out by Pyrotech Corporation to solve an energy deficit problem at a pulp mill at Samoa, California. The reactor was a coiled tube designed by Bill Ayres (ref) based upon the NREL technology (89, 90). The company entered into an agreement with Midwest Research Institute Ventures, a subsidiary of Midwest Research Institute, of which NREL is a division, and a consortium of Fortune 500 companies formed in 1989 to commercially develop the technology (91). The main objective of the consortium was to develop and exploit the commercial potential of the NREL process. Possible areas of interest being in the production of a phenol adhesive and alternative fuels. Interchem obtained a license to construct a scaled up reactor based on the NREL process, although NREL were not involved with providing any technical expertise at this point. Subsequently a 32.7 t/d facility was designed and constructed. The facility was termed the Petroleum Synthesis Unit (PSU) and was used for the production of fuel oil and charcoal; construction was finished in September 1990 with testing until January 1991 (92, 93).

3.7.2 PROCESS DESCRIPTION: PETROLEUM SYNTHESIS UNIT

The plant was built in Missouri for the conversion of sawmill wastes, Fig. 15. The heat required for pyrolysis was generated by combustion of the non-condensable process gases, this being used to heat the reactor walls. The products are condensed by direct contact heat transfer in a 6 tray column, initially using a diesel quench liquid followed by product liquid quench. The remaining gases and vapours are recycled to the reactor with part being combusted for process heat as explained earlier.

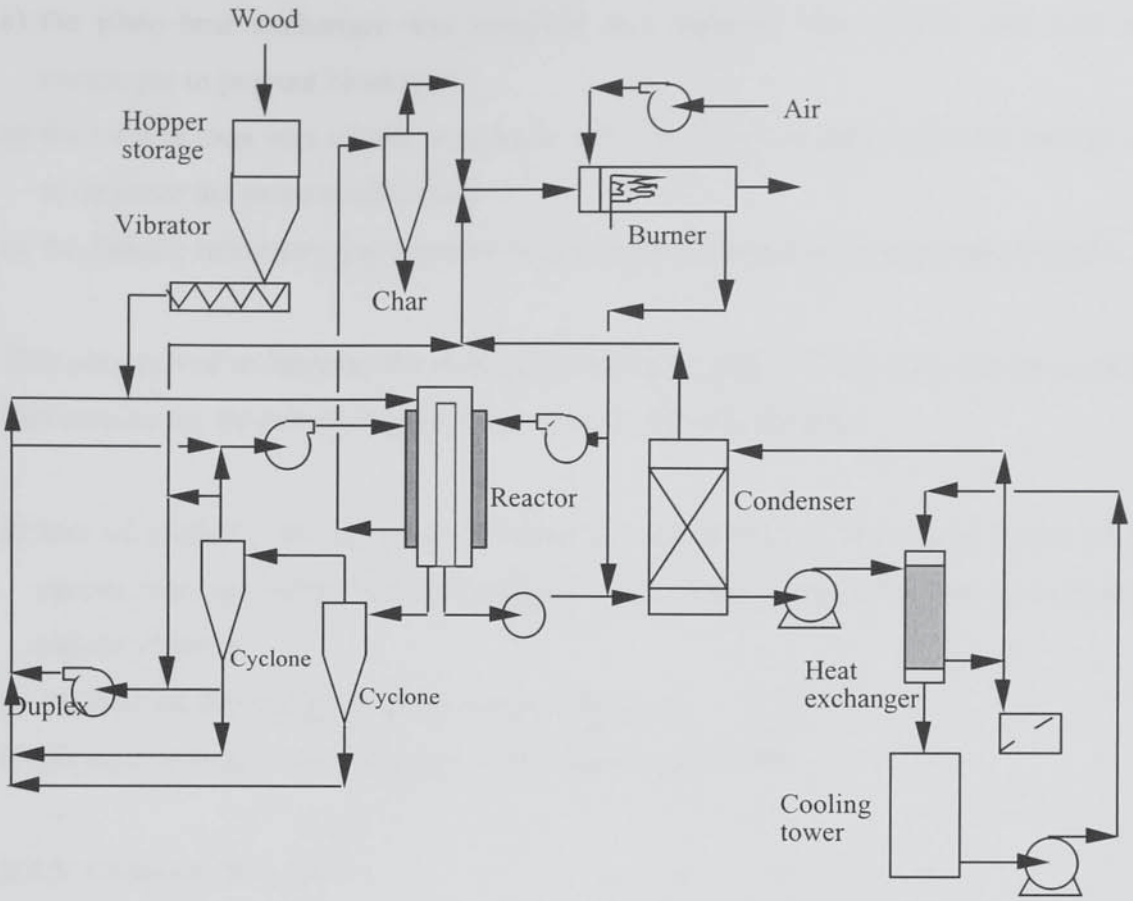

Fig. 15 Interchem Petroleum Synthesis Process.

The first plant was shut down in 1992 due to operational and technical difficulties that could not be solved with the existing equipment. The design capacity of 1360 kg/h was not achieved, this was principally due to the following reasons: (94)

a) the furnace refractory for the reactor had been damaged during transport.
b) particle recycle problems.
c) particle carryover into the product collection system.
d) low particle velocities in the reactor leading to low throughputs.
e) plugging of the plate heat exchanger in the product collection system.
f) gas leaks from the reactor.

Initial throughputs of only 90 kg/h were achieved due to the problems noted earlier. The following changes were then made to the system to try and improve the throughput:

a) the plate heat exchanger was removed and replaced with a shell and tube heat exchanger to prevent blockages.
b) the recycle loop was rebuilt in order to retain more of the particle kinetic energy and to improve the process efficiency.
c) the furnace refractory was repaired to minimise leaks and to improve heat transfer.

This only served to increase throughput to 180 kg/h, only 13.2 % of the design capacity. The reasons for the low throughput were then deduced to be due:

a) loss of particle velocity upon entering the reactor due to the initial 0.6 m of the reactor tube not being heated, leading to a dry friction condition and consequential loss of velocity.
b) insufficient recycle gas heating in the condenser.
c) the recycle loop was overloaded with unreacted particles.

3.7.3 CURRENT STATUS

The pre-treatment and handling units were relocated to Kansas City where Interchem were to build a second generation plant based upon the operational experience gained and utilising a radically different reactor design with input from NREL.

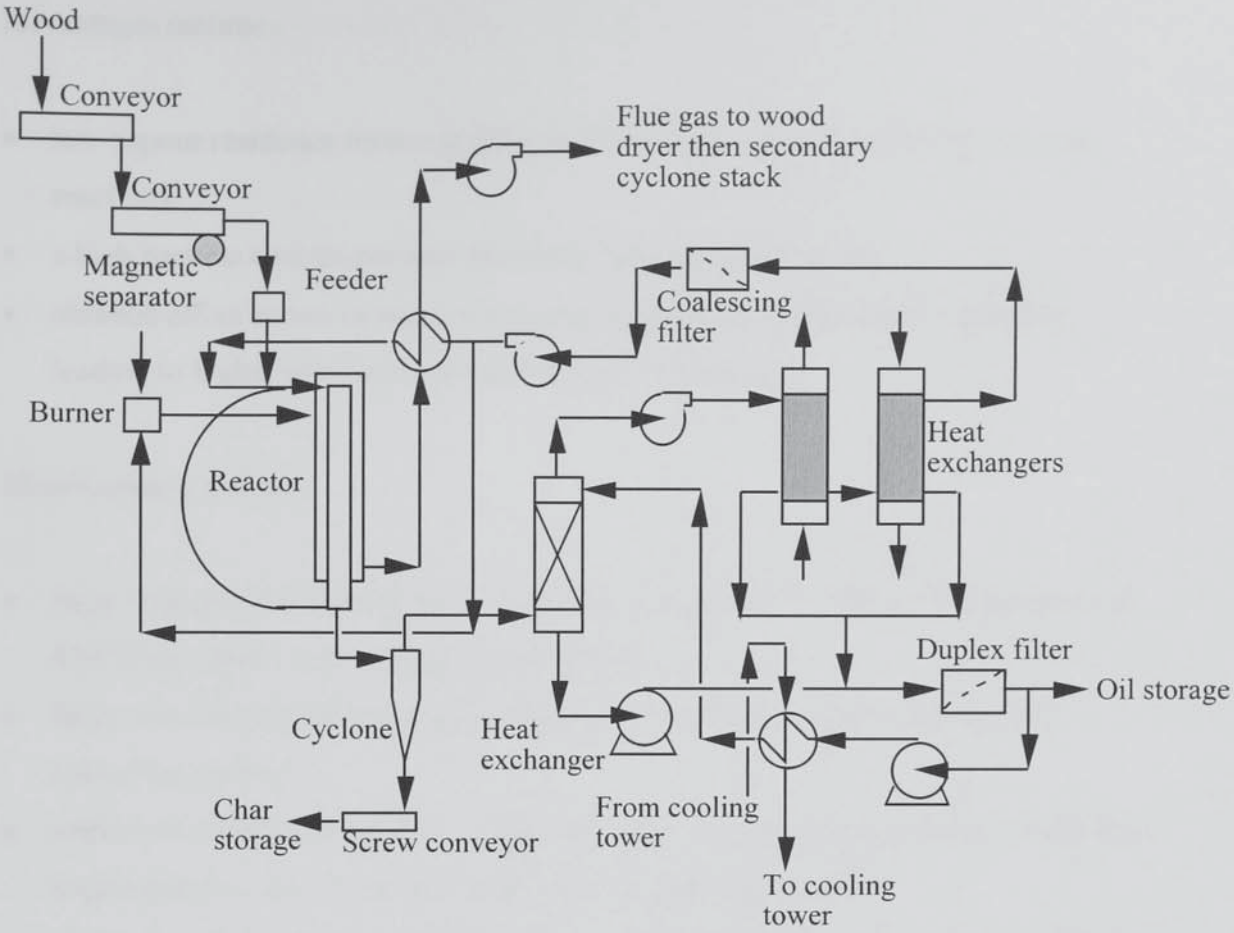

Fig. 16 Second generation Petroleum Synthesis Process.

This unit was never operated and has now been abandoned; there are no plans to restart or redevelop any of the reactors.

3.7.4 DISCUSSION

The Interchem reactor is essentially an entrained flow reactor, but by virtue of the high contact pressures generated with the reactor wall the reaction process is also ablative.

The fact that the first 0.6 m of the reactor was unheated is difficult to understand as it is a fundamental requirement. The friction factor of a dry biomass particle against a cold surface, compared to an ablating biomass particle against a hot surface, is significantly different. An unheated first section will therefore significantly reduce the velocity and kinetic energy of the particle, which will impact on the reactor efficiency.

The following advantages and disadvantages apply to this type of reactor design.

Advantages include

- low vapour residence times resulting in a minimal product loss due to cracking reactions.
- a high particle contact pressure resulting in high reaction rates.
- ablation effect serves to remove reaction products from the reaction interface leading to higher reaction rates and less product cracking.

Disadvantages include

- large volumes of transport gas are difficult to heat to the minimum temperature of 450 °C necessary to prevent product sticking
- large volumes of transport and product gas require complex and more costly collection systems.
- additional complexity in order to generate high velocity transport gases, which is a requirement in order to achieve high particle contact pressure.
- unable to effectively decouple the particle residence time and vapour residence time, excepting that resulting from partial particle recycles.
- high particle recycle rate needed in order that a significant fraction of the biomass is pyrolysed.
- large particle sizes are more difficult to entrain and therefore limit the system.

3.8 UNIVERSITY OF TWENTE (ABLATION/TRANSPORTED)

3.8.1 BACKGROUND

This project was to develop a new reactor technology for the ablative pyrolysis of biomass under the auspices of the EEC JOULE program. Ablative pyrolysis was to be achieved by having the particles slide up a heated rotating cone. Particle pressure being generated by the centrifugal force of the particles on the wall. This concept was initially only partially successful.

3.8.2 Process Description: Conceptual Design and Cold Flow Studies

The concept is that biomass particles are fed onto a vaned impeller at the base of the reactor. This propels particles onto a heated rotating cone. The expectation was that the centrifugal motion of the cone both generates particle pressure and has an ablative effect, the required heat for pyrolysis being supplied from the heated cone walls (95).

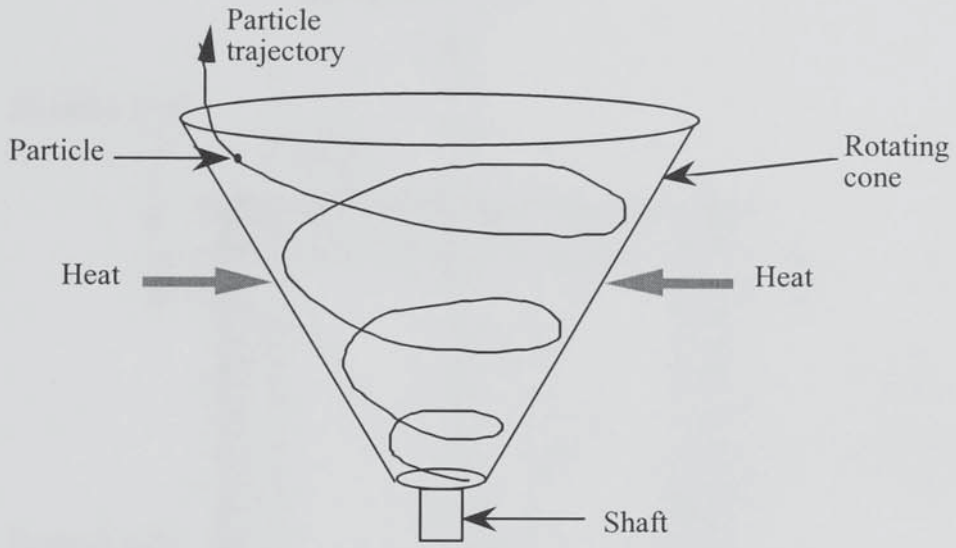

Fig. 17 Schematic of particle behaviour in rotating cone reactor.

A cold flow rig was constructed to investigate the dynamic behavior of the particles in the reactor. Mono-sized spherical PVC particles (140-780 μm, density 1.1 g/cm^3) were used as the test particles because they could easily be seen and photographed (95). Two cones were tested; one at an angle of 60°, the other at an angle of 90°. Cone rotational speeds of up to 1800 rpm were used to determine the influence of gas flow on particle residence time and motion. An endoscopic camera was used to record these experiments. PVC particles greater than 400 μm appeared to be unaffected by gas viscous forces and the particle residence time appeared to be independent of the particle diameter. At particle sizes less than 200 μm, viscous forces became dominant and the residence time of particles was a function of both particle diameter and cone rotational speed.

3.8.3 Process Description: Working Model

A heat transfer rig, see Fig. 18, was constructed with a cone angle of 60° to investigate the heat transfer to ablatively pyrolysing particles (95, 96). Measurement of particle temperature was achieved by fluoroptic methods.

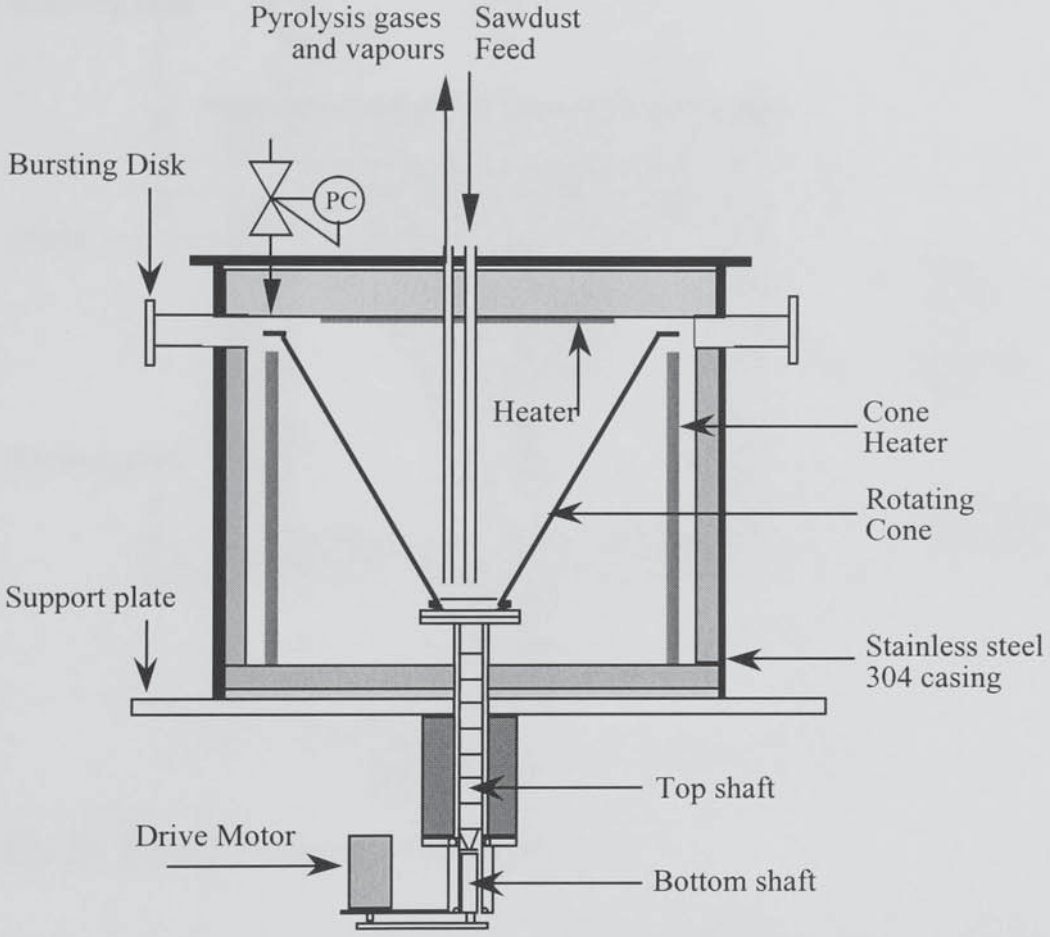

Fig. 18 Prototype rotating cone reactor.

Initial experiments showed that biomass particles less than 250 μm in size adhered to the cone surface, quickly reducing the reactor throughput. The reactor was modified to allow the addition of sand as a carrier medium to promote the flow of solids (97). Initial experiments were carried out mainly at a temperature of 600°C with a rotational speed of 900 rpm.

The initial experimental reactor had a large empty volume and consequently a large vapour/gas residence time of approximately 80 s. This made product collection difficult and significantly reduced liquid yields due to vapour cracking. The reactor interior was

modified by adding an internal cone to reduce the operational volume from 0.25 m^3 to 0.003 m^3.

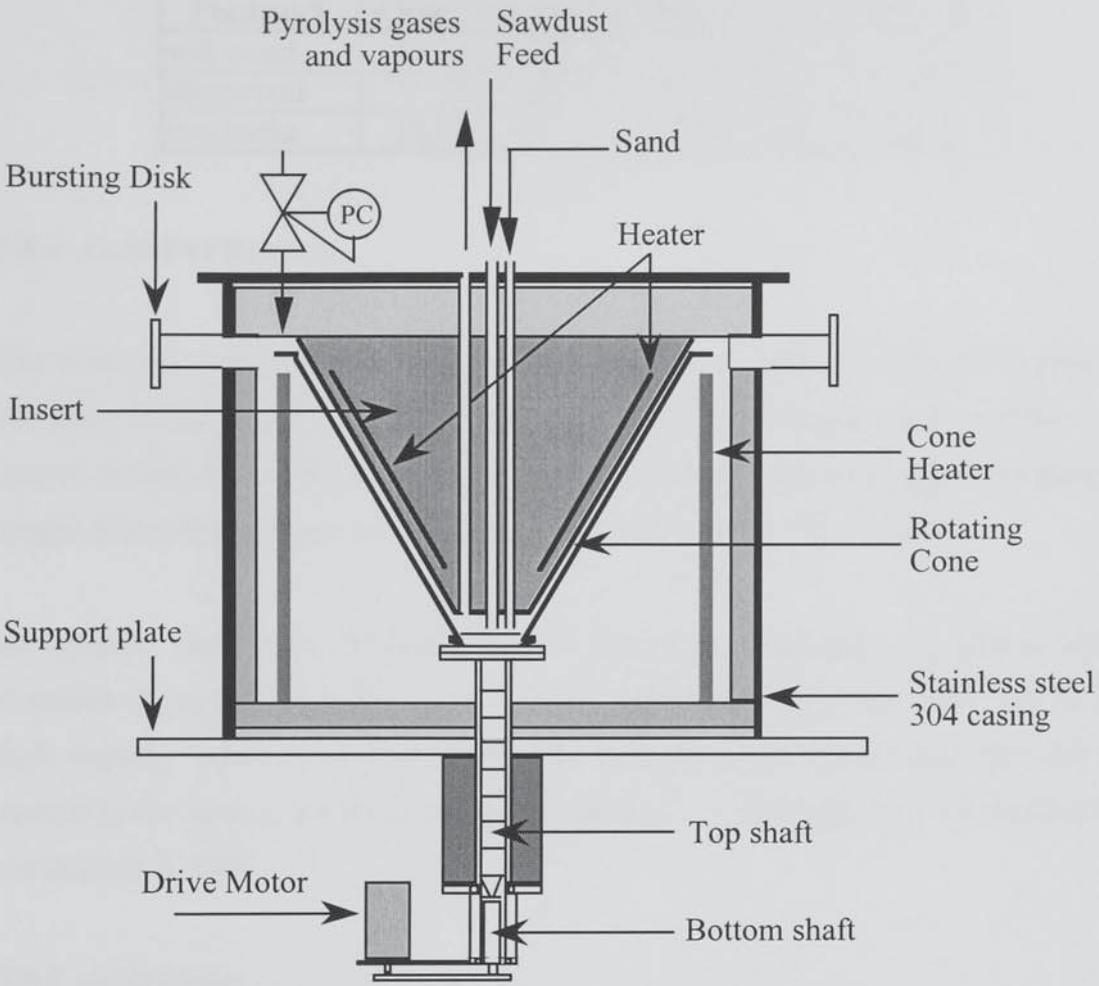

Fig. 19 Modified rotating cone reactor.

The sand to biomass ratio used varied between 10 and 20:1 as a mass ratio. The liquids produced were collected in a system of six condensers in a series followed by gas filtering, with gas analysis performed batchwise using a gas chromatograph. Run times were limited to a maximum of ten minutes due to the char collection region outside of the heated zone being undersized. Reactor throughputs of 7.2 kg/h of biomass are claimed.

Table 11 Results for the rotating cone reactor, reactor temperature 600°C [wt% dry feed basis](98).

Feedstock	Char	Organics	Water	Gas	Closure
soft wood	10	31	15.5	35.5	92
Hardwood	7	19	21	38	85
rice husks	18	11	20.5	32	81.5

3.8.4 CURRENT STATUS.

The reactor is to be modified so that the carrier sand is removed from the reactor with the char, followed by combustion and recycling of the hot sand to the reactor. This system is intended to be scaled up by having a sequential series of cones mounted on a single drive shaft, each cone capable of pyrolysing biomass particles (99).

At present, there is a 50 kg/h unit at Shengyang University in China with 30 experiments completed to date (99). A second generation rotating cone reactor of 10 kg/h capacity which is an integrated unit comprising char combustion and hot sand recycle to the reactor has been tested and operated. A 200 kg/h unit is proposed to be constructed in 1997.

3.8.5 DISCUSSION

The original concept was that the centrifugal force generated by the rotating cone would serve to ablatively pyrolyse the biomass particle. However, ablative pyrolysis requires a very high contact pressure, greater than 1×10^5 Pa, in order to successfully remove all the reaction products (especially char) from the reaction interface; and to achieve a thin liquid film, in order to maximise heat transfer rates. This is simply not achievable with a rotating cone approach.

Sand was used to prevent particles sticking to the reactor walls. Therefore the system, which was intended to be an ablative reactor, is in actual fact a transported bed reactor. Because sand is used as the transporting material the biomass particle will be mechanically abraded, removing accumulated char and enhancing reaction rates, and the sand can be used as a heat carrier. A benefit of using this method to generate a

transported bed is that inert gases do not have to necessarily be used. This makes the product collection potentially easier and cheaper as smaller collection units could be used.

The rotating cone is a complex way of achieving pyrolysis and therefore is difficult to scale up. The concept of having multiple cones on a single axis has some merits but again is a very complex system.

3.9 ASTON UNIVERSITY

3.9.1 BACKGROUND

The primary objective of Peacocke's (9) work was to design, construct, test and operate a novel ablative pyrolysis reactor and product recovery system. Other key objectives included the development of an ablative pyrolysis design methodology, mathematical modeling of the ablation process and measurement of empirical ablation data at 500°C.

3.9.2 PROCESS DESCRIPTION: ABLATIVE PYROLYSIS REACTOR

The concept derived used a fixed heated surface and a second non-heated rotating surface to apply both relative motion and pressure to the biomass particle.

The final design incorporated an angled rotating blade as the second surface to apply mechanical pressure to the ablating particle. As the particles ablate they are reduced in size and moved to the back of the blade, finally being reduced to fine char with a particle size dependent upon the blade clearance.

3.9.3 COMMISSIONING STUDIES

A small cold flow test rig was constructed to assess the effect of blade size, shape and number on the pyrolysis process. The effect of blade number, angle and rotational speed on particle behavior was empirically determined. A maximum of four blades, five cm long, and of variable angle could be positioned radially from the drive shaft and rotated at various speeds above a metal plate.

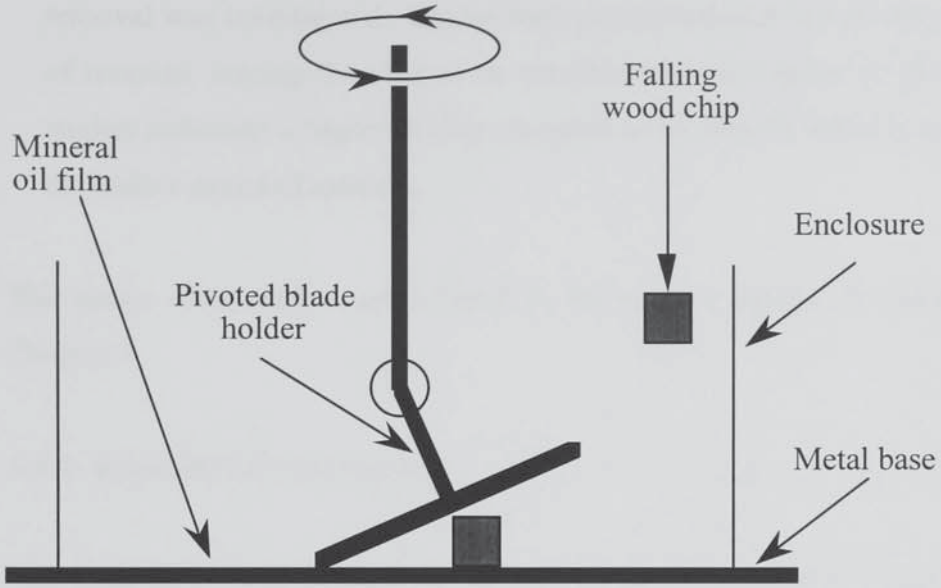

Fig. 20 Cold flow experimental rig.

The test rig shown had an internal diameter of 150 mm with a variable speed motor attached to the drive shaft. Blades 50 mm wide and 30 mm deep could be attached to pivoting holders to enable the assessment of various blade angles with or without the use of a lubricating film.

The following results were determined:

a) regularly spaced blades are beneficial in giving uniform particle distribution, maximising the available heat transfer area usage and minimising the effect of voidage due to uneven particle distribution below the blades. Four blades were specified in the final design, the addition of more blades not being possible due to space and maneuverability limitations.
b) at low rotational speeds less than 20 rpm and blade angles above 20^{o} (relative to the horizontal) the blades merely pushed particles around on the surface. This was due to the oil film not being displaced and the particles sliding on the mineral oil film. A study of the mechanics of particle motion due to centripetal force suggested the particles would not move out along the rotational blades due to contact pressure generated by a low angled blade.

c) to avoid the use of transport gas to remove the char, the possibility of mechanical removal was investigated. Blades were positioned asymmetrically to the normal axis of rotation, forcing the char to be transported to the center of rotation. Cold flow studies indicated a degree of char transport so the reactor outlet was positioned below the blades centre of rotation.

The above observations are utilised in the reactor design and discussed further in Chapter 4.

3.9.4 Final Reactor Design

The final reactor was designed to have a biomass throughput of 5 kg/h and may be seen in Fig. 21 below.

The reactor has an internal diameter of 258 mm with an internal height from the heated base to the interior of the reactor lid of 68 mm. A side inlet port for the addition of nitrogen is used as both a thermal quenching medium and to entrain the fine char particles out of the reactor. The reactor external walls are heated using a band knuckle heater rated to 2.25 kW at 450°C to minimise the deposition of product vapours on the wall. The reactor base is heated with 14 x 400 W compact cartridge heaters, these are capable of generating a heat flux of 11.4 w/cm^2 at 600°C.

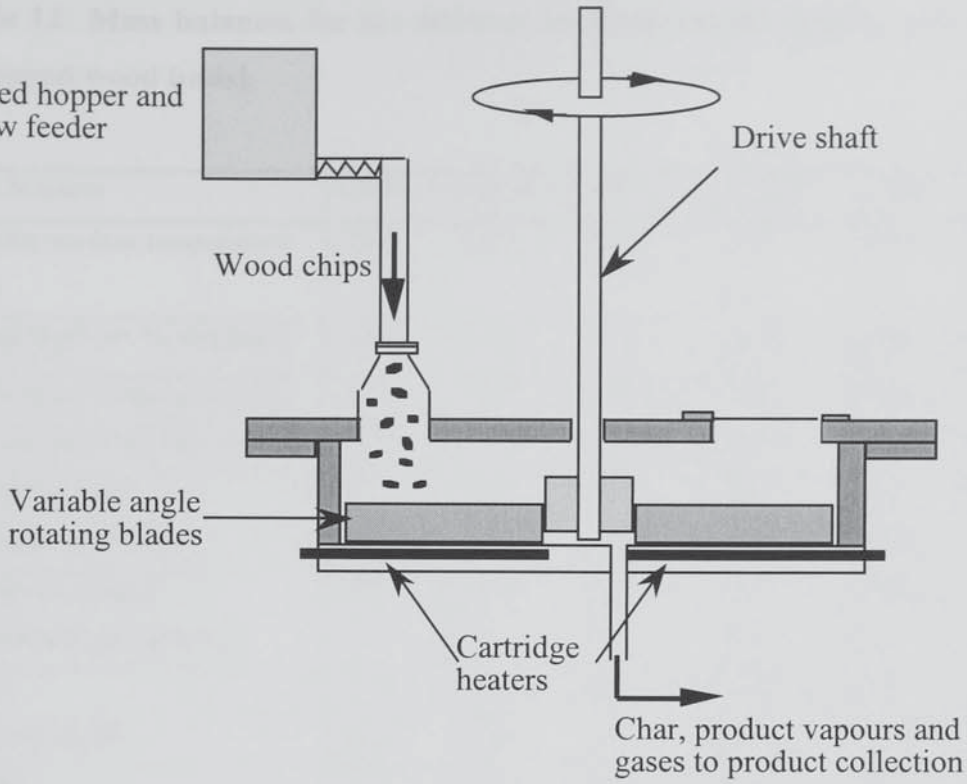

Fig. 21 Peacocke's ablative pyrolysis reactor.

The product collection system consisted firstly of a cyclone to remove the char entrained in the product vapours. The vapours then enter two ice/water cooled condenser before being passed through a cotton wool filter to remove any persistent vapours/aerosols. A molecular sieve (3Å size) was finally used to remove any water vapours. Batch samples of the non-condensable gases were taken for analysis by a gas chromatograph.

Although the reactor worked effectively it only ever achieved a biomass throughput of 3.7 kg/h, 74.7 % of the original specified throughput of 5 kg/h. This was believed to be largely due to an incorrectly assumed biomass density of 530 kg/m^3 as against the actual value of 396 kg/m^3.

Some of the results obtained can be see in Table 12.

Table 12 Mass balances for the ablative pyrolysis reactor [yields, dry ablatively pyrolysed wood basis].

Run Number	CR09	CR14	CR15	CR13	CR07	CR08
Reactor surface temperature [°C]	456	458	501	505	550	550
Wood H_2O [wt %, dry basis]	2.86	1.37	1.2	1.21	2.44	2.08
Gas/vapour temperature [°C]	318	323	350.3	278	389	366
Reactor pressure [kPa, abs.]	101.9	101.3	100.4	100.4	91.0	101.9
Run time [min]	45	27	35	18	15	33
Ablated wood [wet]	260.4	117.2	301.7	264.6	412.4	1003
Residence time of Gas/vapour products [s]	2.45	5.83	6.57	2.73	2.83	2.02
Char	12.8	18.8	22.1	12.2	13.8	21.1
Organic liquid	60.3	50.4	41.4	56.6	58.3	48.6
Water	17.7	20.3	17.4	24.5	22.7	10.3
Gas [N_2 free]	10.0	5.8	6.0	12.9	9.0	6.6
Closure	100.7	95.4	86.9	106.2	103.8	86.6

3.9.5 DISCUSSION

The reactor developed was a highly successful initial concept, but was limited in its scale up potential. Any scaling up of the reactor would involve increasing the disc diameter.

The reactor effectively de-coupled the biomass particle residence time and the product vapour residence time. The reactor could also be operated without the need for large volumes of inert gas. This makes product collection easier, as the product vapours are more concentrated, and less expensive as smaller collection units can be used.

The reactor was designed based on the relationships determined by Lédé (see Chapter 3.6). However, the methodology used was not rigorous and small mistakes are also evident in the calculations.

The collection system used was not ideal, the ice/acetone condensers used were too small for the task, necessitating the use of cotton wool filters to capture much of the aerosols generated, as these could not be removed in the condensers. Calculations also showed that the inlet velocity in the collection cyclone was too small for efficient char collection.

An improved collection system has been developed in collaboration with Peacocke as an integral part of this thesis, see Chapter 9.

4. REACTOR DESIGN

4.1 INTRODUCTION

The aim of this chapter is to identify the key requirements for the design of a new type of ablative pyrolyser and to develop new design concepts. It is intended to design and construct a new ablative pyrolyser with a nominal throughput of 10 kg/h, this being a suitable pilot plant scale. Consideration will given during the design to scale up requirements to an industrial application of up to 10 tons/h

4.2 REQUIREMENTS FOR ABLATIVE PYROLYSIS

An ablative fast pyrolysis reactor has several key requirements that must be met, which are (9,100):

a) High particle pressure on heated surface, >100,000 N/m^2.
b) High particle heating rate, >1,000 K/s.
c) Reactor surface temperature not greater than 600 °C.
d) High relative motion between heated surface and biomass particle (>1.2 m/s).
e) Short vapour residence time before cooling and condensation.
f) Relatively easy scale-up (technically and economically feasible).

These requirements are discussed in more detail below.

a) A high particle pressure against the heated surface increases the overall ablation rate. This is because the higher the contact pressure the thinner the produced liquid film is (see Chapter 6). The produced liquid film presents a resistance to heat transfer and the thinner it is the lower the resistance to heat transfer will be and consequently a higher rate of ablation can be achieved. The high contact pressure can be generated either by pneumatic means or by a bladed approach to ablation, see Chapter 3 for examples.

b) A high heat transfer rate from the reactor wall to the particle is needed to maximise the particle pyrolysis rate. Conductive heat transfer is desirable as it gives a higher heat transfer rate than gas-solid convective heat transfer. The heat flux capacity of the heat source is a limiting factor with regard to the reaction rate of the biomass particle and consequently the reactor capacity. Therefore high heat fluxes are desirable for any reactor design.

c) Reactor surface temperatures greater than 600 °C will tend to lead to secondary cracking reactions, see Chapter 2, and consequently reduced liquid yields and carbon deposition in process pipelines.

d) As the relative motion between the particle and ablative surface is increased, the ablation rate of the particle increases up to a maximum limiting value, see Chapter 6. This value is a function of the applied pressure and temperature. The reason that this effect occurs is twofold. The primary reason that the ablation rate is lower at low relative velocities is due to char formation. Biomass is not a true phase change material, rather than simply melting to a liquid and then vaporising, a large proportion of the biomass melts with some char formation. This char coats the reaction interface and serves to inhibit heat transfer leading to lower ablation rates. As the relative velocity increases so does the shear stress that the char layer is experiencing. The char layer is therefore reduced and the heat transfer rate is higher leading to higher ablation rates. Lédé (8) discovered that at a relative velocity of 1.2 m/s the ablation rate became constant, indicating that the shear stress was sufficient to ensure complete char removal.

The secondary reason that lower relative velocities cause lower ablation rates is due to the inability of the heated wall to satisfy the heat flux demands of the ablating particle. Because the heat flux demands cannot be met the wall temperature at that specific point must fall to provide the necessary heat input to the particle. This serves to lower the ablation rate. However because the particle is being moved relative to the heated surface, the heat demand is spread over a large area rather than a single point. Therefore the heat demand is shared and the temperature drop experienced is lower and the ablation rate is higher. Therefore, the higher the relative velocity, the higher the ablation rate. This effect is more pronounced at

lower relative velocities because as the velocity gets higher, a larger surface area is employed and the increase in ablation rate gradually diminishes until the rate is effectively constant. This effect can be seen graphically in Chapter 7.

e) Short vapour residence times will reduce the possibility of secondary vapour phase reactions such as thermal cracking, repolymerisation and recondensation reactions. Any possible catalytic effects due to ash or contaminants will be reduced.

f) Successful scale-up is an important consideration so that any economic potential of the design may be exploited. The requirements for scale-up will be discussed in Chapter 13.

4.3 REACTOR DESIGN CONCEPT

4.3.1 ROTATING BLADE CONCEPT

A rotating blade approach was utilised by Peacocke (9) in the design of his ablative fast pyrolysis reactor, see Chapter 3.9. The rotating blade is used to generate relative motion against a fixed heated surface. The resistance to motion of the particles causes the blades to exert a mechanical force on the particles causing rapid ablation. The particles ablate and are reduced in size, moving towards the back of the blades leaving space for new particles. Peacocke (9) used a cold flow rig to experimentally determine the effect of a number of blade properties. The cold flow rig used may be seen in Fig. 20.

The flat, horizontal surface had an internal diameter of 150 mm with a variable speed motor attached to the drive shaft. One or two blades could be mounted on pivotable holders, each blade being 50 mm wide and 30 mm deep. A lubricating film comprising mineral oil was used to simulate the combined melting and lubrication effect that accompanies ablation. The effect of the number of blades, blade angle, blade rotational speed, blade orientation and blade clearance were studied. The two effects pertinent to this investigation are the blade angle and the blade clearance and Peacocke's results are summarised below.

- Blade angles up to 60° to the horizontal were studied by Peacocke to assess the generation of pressure on the biomass particles and the resulting particle motion beneath the blades. Blade angles greater than 30° tended to simply push the particles around the reactor without developing any contact pressure. At angles less than 20°, the blades tended to ride up over the particles, suggesting that there was a resistance to lateral motion. This was due to the increased pressure reducing the liquid film beneath the particles leading to an increased friction force.
- The effect of blade clearance (gap between blade and heated surface) was investigated using both the cold flow studies and from actual commissioning runs. Ablation produces very fine char that can easily be removed from the reactor via entrainment. However, the blade clearance determines the minimum particle size remaining after ablation, which exits through the back of the blade. Although these minimum sized particles may get caught up in subsequent blade passes, it is more likely that they will undergo conventional pyrolysis within the reactor environment. This will produce larger char particles leading to char hold-up and possible catalytic cracking reactions. Therefore the minimum blade clearance achievable is recommended, subject to mechanical limitations.

The reactor design criterion was to develop the most suitable, efficient reactor system that would also be inherently easy to scale-up and could be designed and constructed using the resources and equipment available to this institute.

After careful deliberation and evaluation the final reactor design was termed the Rotating Column Reactor and can be seen in Fig. 22 below. The biomass would be forced against the reactor walls by the rotating blades, because the reactor wall surface area is dependent on both the reactor diameter and the reactor length this design has the potential for flexibility scale-up potential.

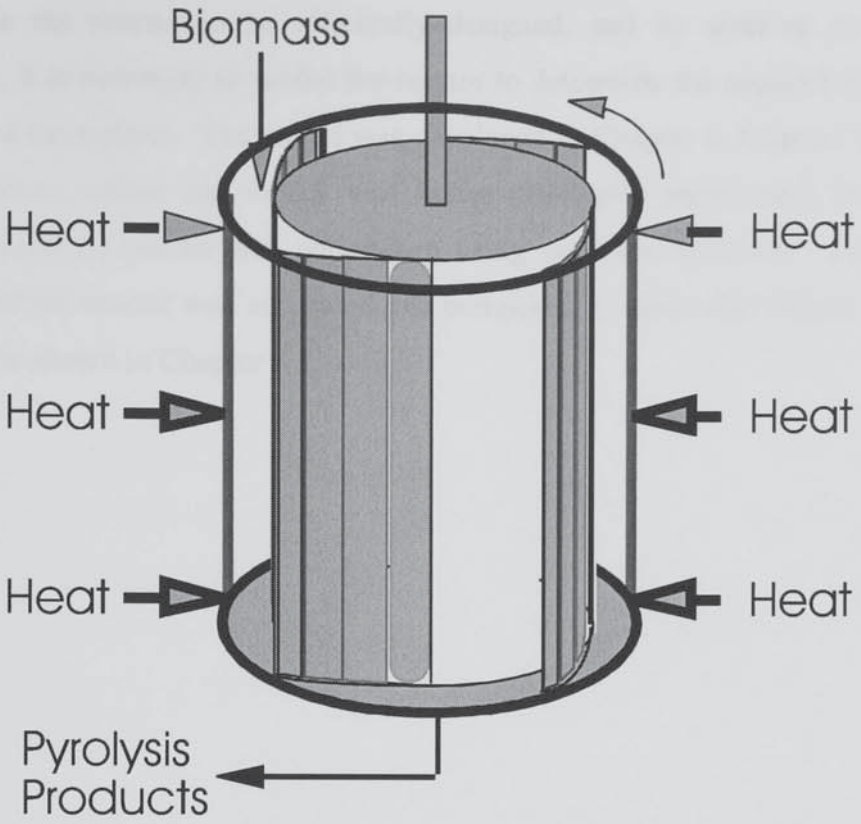

Fig. 22 Rotating column reactor concept.

Heating will be achieved via the reactor walls. On a small scale reactor such as that which will be used in this project electrical resistance heating will be used. Large scale industrial application would require the use of a more economic medium such as gas fired heaters. Potential problems include particle distribution and vapour residence times. Long vapour residence times (> 2s) lead to a loss of liquids products due to extensive cracking reactions. This would be overcome by use of a large diameter central cylinder to reduce the vapour space available. Good biomass particle distribution is essential in order to fully utilise the available space beneath the blades ensuring maximum capacity. A large scale reactor would have a long path length and therefore the reactor would have to be mounted vertically in order to ensure good particle distribution. The particles would enter at the top of the reactor and cascade down until they become swept along behind the blades. The small scale reactor that will be employed in this project will only have a short path length and therefore particle distribution will not be a problem. Therefore the reactor will be mounted horizontally as this is easier to engineer on a small scale.

To enable the reactor to be efficiently designed, and its scale-up potential to be evaluated, it is necessary to model the reactor to determine the required dimensions for a specified throughput. The model was developed in Chapter 6, Chapter 7 and Chapter 8. However, whilst the model was being developed preliminary machining and fabrication of the reactor was undertaken using available materials. Then the actual capacity of the reactor was estimated and compared to achievable results. The reactor specified is shown in Chapter 5.

5. REACTOR SPECIFICATION

In order to be able to design and specify equipment for the reactor and product collection system the reactor throughput has to be specified. Naturally the throughput and hence size of the system will be limited by the available space, equipment and funding. A 3 kg/hr feeder is available for use on the new rig. However, the focus of this Ph.D. is to design an inherently scaleable reactor capable of operating at high feed throughputs. Therefore the reactor will be designed to operate at much higher feed throughput than feeder is capable of supplying. This allows the concept to be tested and leaves scope for future capacity upgrades as and when funding becomes available for a new feed and product collection system. The reactor being designed will essentially be a slice or section of a larger reactor. The section taken is intended to be a $1/10^{th}$ length of a large scale reactor.

The reactor was initially sized based upon extrapolation from the work of Peacocke (9) and designed to have a capacity of 10 kg/hr. Subsequent modeling, see Chapter 6, 7 and 8, showed that the reactor could have a capacity of 30 kg/hr. This means that if the reactor had been constructed to scale instead of simply being a $1/10^{th}$ slice the reactor would have a capacity of 300 kg/hr. As it is the reactor is a $1/10^{th}$ slice is estimated to have a capacity of 30 kg/hr. However the feeder only has a maximum throughput of 3 kg/hr and the reactor will therefore have to be limited to this capacity.

5.1 REACTOR SHELL

The reactor design utilises a circular heated wall against which biomass particles are ablated. The reactor interior dimensions were specified as a diameter of 256 mm and a length of 130 mm. The heating source for the reactor is a 5.5 kW band heater, to reduce the weight of the reactor and to fix the band heater in place it was decided that the heater would be recessed into the reactor shell. Mechanical strength would be retained by the use of two raised rims around the outermost perimeter, to which flanges would be welded to enable the front and back plates to be attached. To reduce the vapour space inside the reactor and to provide a structure for the blades to be attached to an

inner cylinder was also fabricated, this had an exterior diameter of 190 mm. The reactor shell and interior cylinder may be seen in Fig. 23 below.

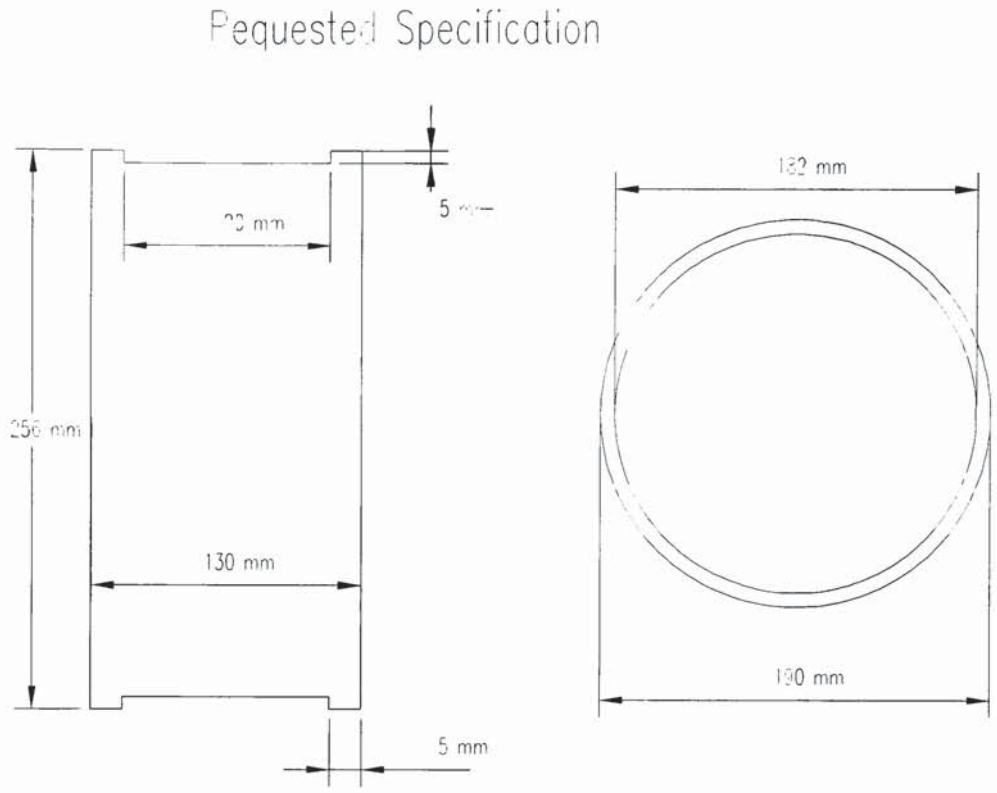

Fig. 23 Diagram of reactor shell and interior cylinder.

Provisions were made for the reactor blades to be bolted to the inner cylinder every 45° giving 8 blades in total. The whole assembly is attached via a 1-inch drive shaft to a variable speed drive motor with an initial power rating of 330 Watt; this was subsequently increased to 1.5 kW. The blade assembly may be seen in Fig. 24 below:

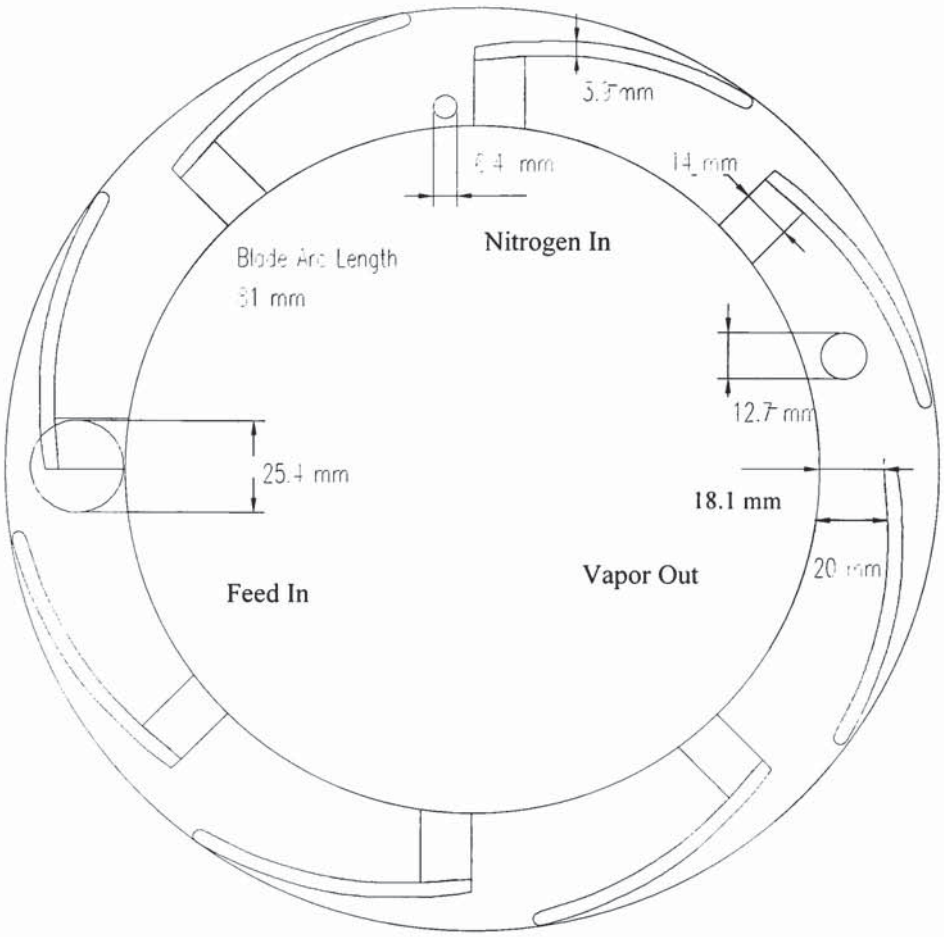

Fig. 24 Reactor shell and blades.

The front and back plates are square and 350 mm on a side, this is to enable easy attachment to the framework. The drive shaft, transport gas and feed enter through the front plate and the product gases and char exit through the front plate also. The drive shaft is attached to the inner cylinder and supported by two bearings. A pressure seal is maintained though the use of an air cooled seal housing containing an aluminium/bronze bush and a high temperature polymer seal.

The vapours exit through the back plate of the reactor and pass through trace heated process pipes to the product collection train. Chapter 6 and 8 and 9 detail the modelling of the reactor and the modelling and design of the product collection system. A schematic of the whole reaction system with detailed explanation of the processes involved is given in Chapter 10.

6. MODELING OF ABLATION PROCESS

Fast pyrolysis of biomass occurs when the solid is subjected to thermal degradation in the absence of an oxidising agent at temperatures above 450 °C. Three basic products are formed; non-condensable gases, char and a condensable vapour. A step preceding is believed to be the partial decomposition of the biomass to form an "Active" intermediate or melt and some char (8, 9, 29, 32, 33, 85). This in turn vapourises, and thermally cracks, to give the three main products detailed above. Close-contact melting occurs when the biomass is pressed against a heated surface. Ablation is a method of close-contact melting where the solid is pressed against a heated surface and is moved relative to that heated surface. The applied relative motion rapidly removes the melt and char from the reaction interface preventing any accumulation, which serves to increase the ablation rate several fold.

This chapter focuses on the ablative fast pyrolysis phenomenon and in particular upon the combined melting and lubrication that occurs at the interface between the wood and heated surface. The fundamentals of ablative pyrolysis have been investigated by a number of researchers and this paper seeks to extend and advance work in this area. Notable research in this field has been carried out by Lédé et al. (8) who made quantitative measurements of the apparent rate of reaction of wood rods by contact with a hot spinning steel disc. Further to this work Martin et al. (88) presented an analytical and experimental study on ablative melting of a solid cylinder perpendicularly pressed against a stationary surface. A mathematical expression for the rate of ablation was determined by solution of the conservation of mass, momentum and energy equations, an extension of the classic work of Osborne Reynolds developed in 1901 (101). To enable the solution of these equations it was necessary to assume that the wood was a true phase change material. The reader is referred to relevant work on "close contact melting" by; Moallemi et al. (102), Saito et al. (103, 104), Bejan (105), Litsek et al. (106).

The ablation process is modeled for a Cartesian co-ordinate system under the assumption that the melting and lubrication of the sliding phase change material is due primarily to direct contact heating. Two similar but different models are developed, a two dimensional isothermal model and a one dimensional adiabatic model. The

accuracy of the models predictions are then determined by experiments on a custom built ablative pyrolysis reactor.

6.1 ISOTHERMAL MODEL

The basic configuration upon which the model is based can be seen in Fig. 25 below and shows a wood chip pressed against a moving solid surface.

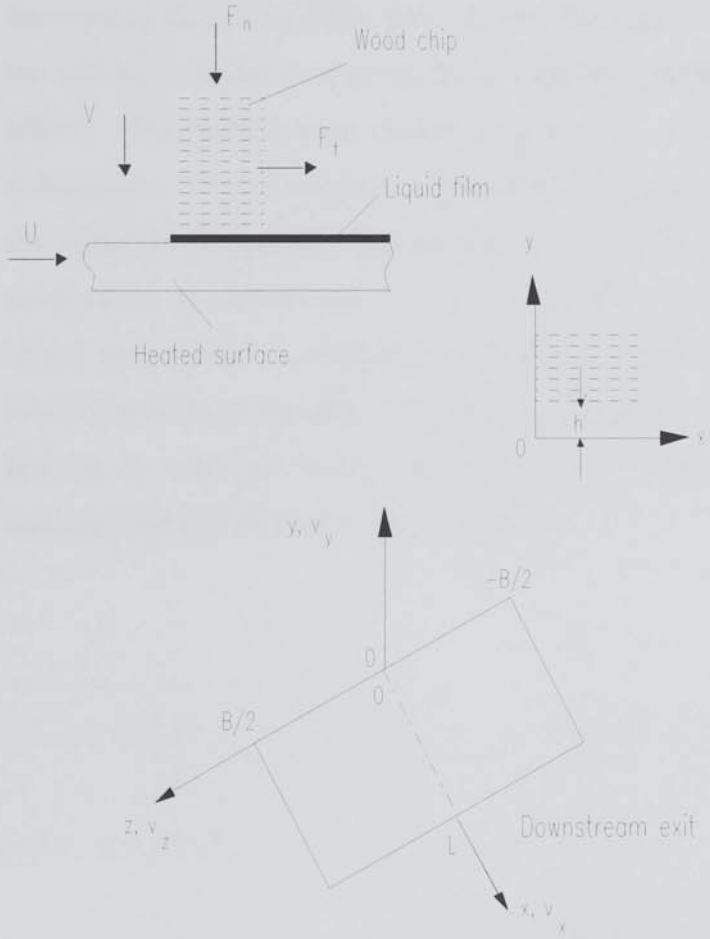

Fig. 25 Diagram of an isothermally ablating wood chip.

The phase change material slides on a produced liquid film, which exits through the edges of the wood chip. The phase change material is modeled as being isothermal and at a known initial temperature T_0. Subsequently at the liquid-wood interface the temperature is instantaneously increased to the wood melting temperature T_m. The heated surface against which the ablation process is occurring is assumed to be at a constant temperature T_s and is also assumed isothermal. Frictional heating is assumed

to be negligible and is ignored (105). The block moves down towards the surface with a constant velocity V that will be termed the ablation velocity. The solid surface is moving relative to the phase change material with a constant velocity U, and as a consequence the produced liquid film is swept out of the downstream edge.

6.2 ADIABATIC MODEL

The simplifying assumption that the heated surface is isothermal has the effect of decoupling the heat transfer process from the liquid-film phenomenon. The objective of the adiabatic model is to relax the isothermal assumption and to establish the resulting effect. The model uses similar terminology as the isothermal model with a few differences. The wood chip is modeled as being at a known initial temperature T_0, at the liquid-wood interface the temperature is at the wood melting temperature T_m. The temperature in side the wood chip, T, decreases from the melting temperature T_m to the initial temperature T_o through a penetration distance d_o. The heated surface against which the ablation process is occurring is assumed to be at a temperature T_s. Frictional heating is assumed to be negligible and is ignored. A diagram of the physical arrangement can be seen in Fig. 26 below.

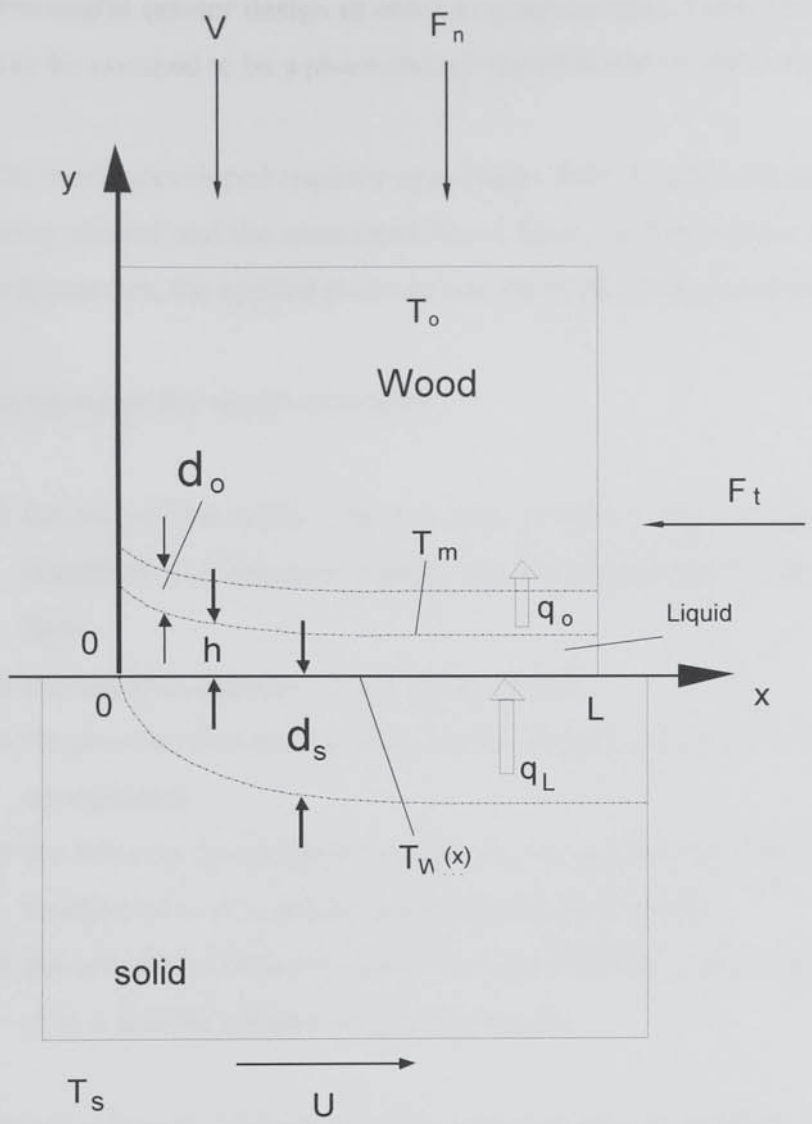

Key

V = ablation velocity, m/s
U = relative velocity, m/s
h = liquid film thickness
$T_{w(x)}$ = temperature of wall at position x, K
T_s = bulk temperature of solid heated surface, K
T_o = bulk temperature of wood chip
T_m = Melting temperature of wood chip
d_o = thermal penetration distance, m
d_s = thermal penetration distance in to solid surface
F_t = friction force, N
F_n = force applied
Q_l = heat flux into liquid layer
Q_o = heat flux into wood chip

Fig. 26 Diagram of an adiabatically ablating wood chip.

6.3 ISOTHERMAL MODEL DEVELOPMENT

The wood chip is modeled as a phase change material, an assumption that is not entirely correct. Lédé (8) showed that above a relative velocity of 1.2 m/s between the wood particle and the heated slider, the ablation rate is independent of the relative velocity. This is typical of a phase change material. However, below a relative velocity of 1.2 m/s, the ablation rate decreases with decreasing relative motion. This is believed to be due to a char layer that is inhibiting heat transfer into the particle. The thickness of the char layer, and hence the resistance to heat transfer, is a function of the relative velocity and is either a minimum or negligible at relative velocities of 1.2 m/s or greater. Therefore at relative velocities greater than 1.2 m/s, which is a prerequisite for any

meaningful reactor design in order to generate high contact pressures, the wood particle may be assumed to be a phase change material and the following model can be applied.

The model developed requires as an input, both the physical properties of the wood chip being ablated and the associated liquid layer, its dimensions, the operating and melting temperatures, the applied pressure and the applied tangential velocity.

As its output the model calculates:

a) the size of the relative motion gap, h (which due to the assumption of isothermal operation is a constant value), and the temperature distribution across this liquid layer.
b) the resulting ablation rate of the wood chip.
c) the pressure distribution beneath the ablating wood chip as a function of the x and z co-ordinates.
d) the velocity distribution beneath the wood chip in both the x and z direction as a function of x, z, y and the applied tangential velocity.
e) the volumetric flow-rate beneath the wood chip in the x and z direction as a function of x, z and the applied tangential velocity.

The model is developed below and attempts to link the film thickness determined from Fouriers law of heat conduction to the pressure distribution determined from a momentum balance. This in turn allows the ablation velocity to be determined.

6.3.1 TEMPERATURE DISTRIBUTION

The primary concern is with the melting caused by direct heat transfer across the sliding contact area, it can be assumed that the phase change material melts at a constant temperature T_m. The moving solid will be assumed to be isothermal and at a temperature T_s, this means the temperature difference across the relative motion gap has a constant value $\Delta T = T_s - T_m$.

The energy conservation equation for a Newtonian fluid (a fluid in which the velocity gradient is directly proportional to the shear stress) with constant density, ρ, and thermal conductivity, k, can be applied to the relative motion gap, h.

$$\rho C_p\left(\frac{\partial T}{\partial t}+v_x\frac{\partial T}{\partial x}+v_y\frac{\partial T}{\partial y}+v_z\frac{\partial T}{\partial z}\right)=k\left(\frac{\partial^2 T}{\partial x^2}+\frac{\partial^2 T}{\partial y^2}+\frac{\partial^2 T}{\partial z^2}\right)+\mu\Phi \qquad \textbf{Eq. 16}$$

Where Φ is the viscous dissipation function:

$$\Phi=2\left[\left(\frac{\partial v_x}{\partial x}\right)^2+\left(\frac{\partial v_y}{\partial y}\right)^2+\left(\frac{\partial v_z}{\partial z}\right)^2\right]+\left(\frac{\partial v_y}{\partial x}+\frac{\partial v_x}{\partial y}\right)^2+\left(\frac{\partial v_z}{\partial y}+\frac{\partial v_y}{\partial z}\right)^2 +\left(\frac{\partial v_x}{\partial z}+\frac{\partial v_z}{\partial x}\right)^2-\frac{2}{3}\left(\frac{\partial v_x}{\partial x}+\frac{\partial v_y}{\partial y}+\frac{\partial v_z}{\partial z}\right)^2 \qquad \textbf{Eq. 17}$$

The viscous dissipation function is normally only considered significant for large velocity gradients and can therefore be ignored in this case. Assume steady state operation and neglecting the effect of thermal diffusion in the x and z directions, gives the following equation.

$$v_x\frac{\partial T}{\partial x}+v_y\frac{\partial T}{\partial y}+v_z\frac{\partial T}{\partial z}=\alpha\frac{\partial^2 T}{\partial y^2}+\frac{\mu\Phi}{\rho C_p} \qquad \textbf{Eq. 18}$$

Where, α, the thermal diffusivity equals

$$\alpha=\frac{k}{\rho C_p} \qquad \textbf{Eq. 19}$$

Scale analysis of the above equation gives

$$\frac{U\Delta T}{L}=\frac{\alpha\Delta T}{h^2}+\frac{\mu}{\rho C_p}\left(\frac{U}{h}\right)^2 \qquad \textbf{Eq. 20}$$

Therefore it can be seen that the effects of convection heating and friction can be ignored if:

$$\frac{U\Delta T}{L} / \frac{\alpha \Delta T}{h^2} \langle 1 \qquad \text{and} \qquad \frac{\mu}{\rho C_p}\left(\frac{U}{h}\right)^2 / \frac{\alpha \Delta T}{h^2} \langle 1 \qquad \textbf{Eq. 21}$$

Considering this in an order of magnitude sense it can be seen that only the vertical diffusion term needs to be retained in order to determine the temperature profile in the liquid film, hence:

$$\alpha \frac{\partial^2 T}{\partial y^2} = 0 \qquad \textbf{Eq. 22}$$

Integrating twice with respect to y gives

$$\alpha T + c_1 y + c_2 = 0 \qquad \textbf{Eq. 23}$$

By utilising the boundary conditions $T = T_m$ at $y = h$ and $T = T_s$ at $y = 0$ the constants can be determined to be

$$c_2 = -\alpha T_s \qquad \text{and} \qquad c_1 = \frac{-\alpha \Delta T}{h} \qquad \textbf{Eq. 24}$$

Where

$$\Delta T = T_s - T_m$$

Substituting into Eq. 23 gives

$$T = T_s - \frac{\Delta T y}{h} \qquad \textbf{Eq. 25}$$

Scale analysis has shown that the effects of longitudinal conduction and frictional heat generation can be ignored. Therefore the only area of interest is the transversal

conduction phenomenon, which overwhelms all other energy effects due to the small film thickness and low liquid viscosity. Fouriers law of heat conduction applied across the liquid film gives

$$q_y = -k\frac{dT}{dy} \qquad \textbf{Eq. 26}$$

The total heat flux, q_y, that crosses the liquid film is equal to the heat flux absorbed by the liquid from the lower heated slider. This is therefore comprised of the heat needed to raise the temperature of the phase change material to its melting point and subsequently to melt it.

$$q_y = \rho_w h_{wf} V + \rho_w C_{pw} V\left(T_m - T_o\right) \qquad \textbf{Eq. 27}$$

Note in the case of wood rods it may be necessary to take account of any moisture present within the wood. Therefore it would be necessary to include the sensible heat required to heat the moisture to its vaporisation point and the latent heat required to subsequently vaporise it. It is not necessary to include the sensible heat required to raise the vaporised moisture to the phase change material melting point, this is because it is more mobile than the "active" layer and would migrate away from the melting front. Contributory evidence to support this assumption is given in the work of Lédé et al. (8), where a thermocouple embedded in an ablating wood rod records a temperature of 100 °C behind the reaction and thermal penetration zone. Assuming moisture is present the heat flux would be given by:

$$q_y = \rho_w h_{wf} V(1 + Ste) + M\rho_w V\left[C_{pm}\left(T_b - T_0\right) + h_{mf}\right] \qquad \textbf{Eq. 28}$$

Where

$$Ste = \frac{C_{pw}\left(T_m - T_o\right)}{h_{wf}} \qquad \textbf{Eq. 29}$$

M represents the wood moisture content on a wt./wt. dry basis, C_{pm} is the moisture heat capacity, h_{mf} is the moisture enthalpy of fusion, T_b is the moisture boiling point at the prevailing pressure and Ste is the Stefan number and accounts for the degree of subcooling of the upper solid phase change material. To simplify the mathematics it will be assumed that there is no moisture present. Applying Fouriers law of heat conduction:

$$-k\frac{dT}{dy} = \rho_w h_{wf} V(1+Ste) \qquad \textbf{Eq. 30}$$

Separating the variables and integrating across the liquid film gives

$$-k\int_{T_s}^{T_m} dT = \rho_w h_{wf} V(1+Ste)\int_0^h dy \qquad \textbf{Eq. 31}$$

$$h = \frac{k(T_s - T_m)}{\rho_w h_{wf} V(1+Ste)} \qquad \textbf{Eq. 32}$$

Therefore it can be noted that h varies inversely with the ablation velocity V.

6.3.2 LUBRICATION EFFECT AND PRESSURE DISTRIBUTION

The unknown in the above equations is the ablation velocity V, this can be determined by considering the mechanical equilibrium of the upper solid. This involves analysing the lubrication effect of the liquid film, this is essentially an extension of the classic Osborne-Reynolds theory of lubrication according to which the liquid inertia and pressure variation in the transverse direction are negligible. The pressure distribution P(x,z) will also be determined in order to connect it to the applied normal force.

The equation of continuity for this system, assuming constant density is:

$$\rho\frac{\partial v_x}{\partial x} + \rho\frac{\partial v_y}{\partial y} + \rho\frac{\partial v_z}{\partial z} = 0 \qquad \textbf{Eq. 33}$$

The x and z components of the equation of motion in rectangular co-ordinates for a Newtonian fluid with constant density and viscosity are.

x-component

$$\rho\left(\frac{\partial v_x}{\partial t}+v_x\frac{\partial v_x}{\partial x}+v_y\frac{\partial v_x}{\partial y}+v_z\frac{\partial v_x}{\partial z}\right)=-\frac{\partial P}{\partial x}+\mu\left(\frac{\partial^2 v_x}{\partial x^2}+\frac{\partial^2 v_x}{\partial y^2}+\frac{\partial^2 v_x}{\partial z^2}\right)+\rho g_x$$

Eq. 34

z-component

$$\rho\left(\frac{\partial v_z}{\partial t}+v_x\frac{\partial v_z}{\partial x}+v_y\frac{\partial v_z}{\partial y}+v_z\frac{\partial v_z}{\partial z}\right)=-\frac{\partial P}{\partial z}+\mu\left(\frac{\partial^2 v_z}{\partial x^2}+\frac{\partial^2 v_z}{\partial y^2}+\frac{\partial^2 v_z}{\partial z^2}\right)+\rho g_z$$

Eq. 35

The system can be assumed to be at steady state in addition the gravitational accelerations g_x and g_z are equal to zero. Scale analysis of the above equations will show that the viscous forces are orders of magnitude greater than the inertial forces, allowing the inertial forces to be ignored. Therefore the following equations are obtained.

$$\frac{\partial P}{\partial x}=\mu\frac{\partial^2 v_x}{\partial y^2}$$

Eq. 36

$$\frac{\partial P}{\partial z}=\mu\frac{\partial^2 v_z}{\partial y^2}$$

Eq. 37

Integrating Eq. 36 with respect to y but noting that $\partial p/\partial x$ is a constant because it only depends on x gives.

$$\frac{1}{\mu}\frac{\partial P}{\partial x}y=\frac{\partial v_x}{\partial y}+c_1$$

Eq. 38

c_1 is some unknown function to be determined later from the boundary conditions, integrating again gives

$$\frac{1}{2\mu}\frac{\partial P}{\partial x}y^2 = v_x + c_1 y + c_2 \qquad \textbf{Eq. 39}$$

Again c_2 is some unknown function to be determined from the boundary conditions. The velocity boundary conditions are

$$v_x = \begin{cases} U & \\ 0 & \text{at} \end{cases} \begin{matrix} y = 0 \\ y = h \end{matrix}$$

Applying the boundary conditions gives

$$c_1 = \frac{U}{h} + \frac{1}{2\mu}\frac{\partial P}{\partial x}h \qquad and \qquad c_2 = -U \qquad \textbf{Eq. 40}$$

The x-velocity component in the gap in terms of the unknown pressure gradient gradient $\partial P/\partial x$ becomes.

$$v_x = \frac{1}{2\mu}\frac{\partial P}{\partial x}y(y-h) + U\left(1-\frac{y}{h}\right) \qquad \textbf{Eq. 41}$$

Similarly Eq. 37 becomes

$$\frac{1}{2\mu}\frac{\partial P}{\partial z}y^2 = v_z + c_3 y + c_4 \qquad \textbf{Eq. 42}$$

Using the velocity boundary conditions

$$v_z = \begin{cases} 0 & \\ 0 & \text{at} \end{cases} \begin{matrix} y = 0 \\ y = h \end{matrix} \qquad \textbf{Eq. 43}$$

And

$$c_3 = \frac{1}{2\mu}\frac{\partial P}{\partial z}h \qquad and \qquad c_4 = 0 \qquad \textbf{Eq. 44}$$

And the z-velocity component in the gap in terms of the unknown pressure gradient $\partial P/\partial z$ becomes

$$v_z = \frac{1}{2\mu}\frac{\partial P}{\partial z}y(y-h) \qquad \textbf{Eq. 45}$$

Next define the height integrated flow rates to be

$$Q_x(x,z) = \int_0^h v_x dy \qquad \text{and} \qquad Q_z(x,z) = \int_0^h v_z dy \qquad \textbf{Eq. 46}$$

Gives

$$Q_x = \frac{1}{12\mu}\left(-\frac{\partial P}{\partial x}\right)h^3 + \frac{1}{2}Uh \qquad \textbf{Eq. 47}$$

And

$$Q_z = \frac{1}{12\mu}\left(-\frac{\partial P}{\partial z}\right)h^3 \qquad \textbf{Eq. 48}$$

Consider again the equation of continuity in the liquid filled gap

$$\frac{\partial v_x}{\partial x} + \frac{\partial v_y}{\partial y} + \frac{\partial v_z}{\partial z} = 0$$

The upper interface can be considered to have the generated liquid instantaneously removed giving, $v_y = -V$ at $y = h$ and $v_y = 0$ for $y < h$, in this case V is the ablation velocity. Integrating the equation of continuity between the limits $y = 0$ and $y = h$ gives

$$\frac{\partial Q_x}{\partial x} - V + \frac{\partial Q_z}{\partial z} = 0 \qquad \textbf{Eq. 49}$$

Where from earlier work

$$\frac{\partial Q_x}{\partial x} = \frac{1}{12\mu}\frac{\partial^2 P}{\partial x^2}h^3 \qquad \textbf{Eq. 50}$$

$$\frac{\partial Q_z}{\partial z} = \frac{1}{12\mu}\frac{\partial^2 P}{\partial z^2}h^3 \qquad \textbf{Eq. 51}$$

Substitution and rearrangement gives

$$\frac{\partial^2 P}{\partial x^2} + \frac{\partial^2 P}{\partial z^2} = -\frac{12\mu V}{h^3} \qquad \textbf{Eq. 52}$$

The boundary conditions of P(x,z) are homogeneous around the perimeter of the wood chip, $P = 0$ at $x = o$, $x = L$, $z = B/2$ and $z = -B/2$, and this provides a basis for solving the above Poisson-type problem. The above equation can be split into two parts, one homogeneous and one in-homogeneous. For example, the pressure distribution P(x, z) can be split up into two parts as follows

$$P(x,z) = P_1(x) + P_2(x,z) \qquad \textbf{Eq. 53}$$

6.3.2.1 SOLVING FOR $P_1(X)$

$P_1(x)$ is in-homogeneous and can be solved by integrating the following expression twice and applying the boundary condition $P = 0$ at $x = 0$ and $x = L$.

$$\frac{\partial^2 P}{\partial x^2} = -\frac{12\mu V}{h^3} \qquad \textbf{Eq. 54}$$

The solution gives

$$P_1(x) = \frac{6\mu V}{h^3} x(L - x) \qquad \textbf{Eq. 55}$$

6.3.2.2 SOLVING FOR $P_2(X, Z)$

$P_2(x, z)$ has a homogeneous solution which may be determined from

$$\frac{\partial^2 P}{\partial x^2} + \frac{\partial^2 P}{\partial z^2} = 0 \qquad \textbf{Eq. 56}$$

This may be solved by seeking a solution of the type $P(x, z) = F(x)G(Z)$, this being a function of x only multiplied by a function of z only. By definition G(z) is independent of x, therefore

$$\frac{\partial^2 P}{\partial x^2} = G\frac{\partial^2 F}{\partial z^2} = GF'' \qquad \textbf{Eq. 57}$$

and

$$\frac{\partial^2 P}{\partial z^2} = F\frac{\partial^2 G}{\partial x^2} = G''F \qquad \textbf{Eq. 58}$$

Substitution back into the equation gives

$$GF'' + G''F = 0 \qquad \textbf{Eq. 59}$$

Dividing by FG gives

$$\frac{F''}{F} + \frac{G''}{G} = 0 \qquad \textbf{Eq. 60}$$

Hence $\frac{F''}{F} = -\frac{G''}{G}$ and the variables have been separated.

The two sides of this equation are function of independent variables and hence cannot be equal unless each is equal to the same constant, C say. Thus the assumption of a solution of this type has reduced the partial differential equation to a pair of ordinary differential equation, these being

$$F'' - CF = 0 \qquad \text{and} \qquad G'' + CG = 0$$

Where the solution is given by $P_2 = FG$. The forms of the function F and G depend on whether C is positive or negative, which is determined by the boundary conditions.

$$P = 0 \quad \text{when} \quad x = 0 \quad \text{or} \quad x = L$$

$$P = 0 \quad \text{when} \quad z = \frac{B}{2} \quad \text{or} \quad z = \frac{-B}{2}$$

The solution for F must oscillate whereas the solution for G is exponential around z = 0. Therefore:

$$F'' - CF = 0$$

To make the solution to this oscillatory, C must be negative. Let $C = -I^2$

$$F'' + I^2F = 0 \qquad \text{and} \qquad G'' - I^2G = 0 \qquad \textbf{Eq. 61}$$

These equations have standard solution of the form

$$F = A \cos Ix + B \sin Ix \qquad \textbf{Eq. 62}$$

And

$$G = C\,EXP(Iz) + D\,EXP(-Iz) \qquad \textbf{Eq. 63}$$

Now

$$P_2(x,z) = FG$$

$$P_2(x,z) = (A\cos Ix + B\sin Ix)(C\,EXP[Iz] + D\,EXP[-Iz]) \qquad \textbf{Eq. 64}$$

It is already known that P = 0 at x = 0 for all z, therefore A is equal to zero. Absorbing B into (C + D) gives

$$P_2 = \sin Ix\,(C\,EXP[Iz] + D\,EXP[-Iz]) \qquad \textbf{Eq. 65}$$

Knowing that P = 0 at x = L for all z, therefore sin IL = 0 for a non-trivial solution. From simple trigonometric functions IL = rΠ, where r is an integer and therefore I = rΠ/L giving.

$$P_2 = \sin\left(\frac{r\Pi x}{L}\right)\left(C\,EXP\left[\frac{r\Pi z}{L}\right] + D\,EXP\left[-\frac{r\Pi z}{L}\right]\right) \qquad \textbf{Eq. 66}$$

There is a line of symmetry at z = 0, therefore dP/dz = 0 at x = 0. Therefore:

$$\frac{dP_2}{dz} = \sin\left(\frac{r\Pi x}{L}\right)\left(\frac{Cr\Pi}{L}EXP\left[\frac{r\Pi z}{L}\right] - \frac{Dr\Pi}{L}EXP\left[-\frac{r\Pi z}{L}\right]\right) \qquad \textbf{Eq. 67}$$

Substituting dP/dz = 0 at z = 0 gives

$$0 = \sin\left(\frac{r\Pi x}{L}\right)\left(\frac{Cr\Pi}{L} - \frac{Dr\Pi}{L}\right) \qquad \textbf{Eq. 68}$$

For a non-trivial solution D must equal C and using the Cosh trigonometric identity Eq. 66 becomes

$$P_2 = 2C \sin\left(\frac{r\Pi x}{L}\right) \cosh\left(\frac{r\Pi z}{L}\right) \qquad \textbf{Eq. 69}$$

Where $r > 0$

This can be solved as a Fourier half-wave series using the boundary conditions already specified giving the solution

$$P_2(x,z) = \sum_{n=0}^{\infty} C_n \sin\left[(2n+1)\Pi\left(\frac{x}{L}\right)\right] \cosh\left[(2n+1)\Pi\left(\frac{z}{L}\right)\right] \qquad \textbf{Eq. 70}$$

Where

$$C_n = \frac{48(-1)^{n+1}\mu V L^2}{(2n+1)^3 \Pi^3 h^3 \cosh\left[(2n+1)\Pi\frac{B}{2L}\right]} \qquad \textbf{Eq. 71}$$

The overall equation for P(x, z) can be determined by combining the solution for $P_1(x)$ and $P_2(x, z)$ giving

$$P(x,z) = \frac{6\mu V}{h^3} x(L-x) + \sum_{n=0}^{\infty} C_n \sin\left[(2n+1)\Pi\left(\frac{x}{L}\right)\right] \cosh\left[(2n+1)\Pi\left(\frac{z}{L}\right)\right] \qquad \textbf{Eq. 72}$$

This in turn can be integrated across the sliding contact area in order to determine F_n, the applied normal force

$$F_n = \int_0^L \int_{-B/2}^{B/2} P(x,z)\,dx\,dz \qquad \textbf{Eq. 73}$$

Integration of P(x, z) gives

$$F_n = \frac{\mu V L^3 B}{h^3}\Theta$$ **Eq. 74**

Where

$$\Theta = 1 - \frac{192\,L}{\Pi^5 B}\sum_{n=0}^{\infty}\frac{\tanh\left[(2n+1)\frac{\Pi}{2}\frac{B}{L}\right]}{(2n+1)^5}$$ **Eq. 75**

Therefore the ablation velocity V may be determined by rearranging Eq. 74 to give

$$V = \frac{F_n h^3}{\mu L^3 B\Theta}$$ **Eq. 76**

Note that P_n, the average pressure, is equal to F_n/LB so an alternative expression is

$$V = \frac{P_n h^3}{\mu L^2 \Theta}$$ **Eq. 77**

Note from earlier work that

$$h = \frac{k(T_s - T_m)}{\rho_w h_{wf} V(1 + Ste)}$$

By both substitution and rearrangement the following equation is obtained

$$h^4 = \frac{k(T_s - T_m)\mu L^2 \Theta}{\rho_w h_{wf}(1 + Ste)P_n}$$ **Eq. 78**

This indicates that the liquid film thickness is inversely proportional to the $P_n^{1/4}$.

Finally deduce the tangential friction force, F_t, from its definition, assuming a Newtonian fluid

$$F_t = -\int_0^L \int_{-B/2}^{B/2} \mu \left(\frac{\partial v_x}{\partial y} \right)_{y=0} dx\, dz \qquad \textbf{Eq. 79}$$

An equation for the velocity of the liquid film in the x-direction has already been derived; it is a simple matter to integrate this as indicated to give

$$F_t = \frac{\mu ULB}{h} \qquad \textbf{Eq. 80}$$

It is also possible to determine the volumetric flowrate in the x and z direction beneath the wood chip and equations have already been derived to enable the evaluation of this, these being

$$Q_x = \frac{1}{12\mu}\left(-\frac{\partial P}{\partial x}\right)h^3 + \frac{1}{2}Uh$$

And

$$Q_z = \frac{1}{12\mu}\left(-\frac{\partial P}{\partial z}\right)h^3$$

The two unknowns in these equation are $\partial P/\partial x$ and $\partial P/\partial z$. These can be determined by the partial differentiation of P(x, z) with respect to x or z giving

$$\frac{\partial P}{\partial x} = \frac{6\mu V}{h^3}(L-2x) + \sum_{n=0}^{\infty} C_n \frac{(2n+1)\Pi}{L} \cos\left[(2n+1)\Pi\left(\frac{x}{L}\right)\right] \cosh\left[(2n+1)\Pi\left(\frac{z}{L}\right)\right] \qquad \textbf{Eq. 81}$$

$$\frac{\partial P}{\partial z} = \sum_{n=0}^{\infty} C_n \frac{(2n+1)\Pi}{L} \sin\left[(2n+1)\Pi\left(\frac{x}{L}\right)\right] \sinh\left[(2n+1)\Pi\left(\frac{z}{L}\right)\right] \qquad \textbf{Eq. 82}$$

Straightforward substitution into the equations given above will enable the volumetric flowrates to be determined.

6.4 ADIABATIC MODEL DEVELOPMENT

The wood chip is modeled as a true phase change material and is therefore the model only valid for an applied normal speed of approximately 1.2 m/s as previously explained.

The model developed requires as an input, both the physical properties of the wood chip being ablated and the associated liquid layer, its dimensions, the operating and melting temperatures, the applied pressure and the applied tangential velocity. In addition the physical properties of the medium against which it is being ablated is required.

As its output the model calculates:

a) the size of the relative motion gap (h), which varies with axial position (x), and the temperature distribution across this liquid layer.
b) the resulting ablation rate of the wood chip.
c) the pressure distribution beneath the ablating wood chip as a function of axial position.
d) the velocity distribution beneath the wood chip in the x direction as a function of x, y and the applied tangential velocity.
e) the volumetric flow-rate beneath the wood chip in the x direction as a function of x, and the applied tangential velocity.

The model is developed below and attempts to link the film thickness determined from Fouriers law of heat conduction to the pressure distribution determined from a momentum balance. This in turn allows the ablation velocity to be determined. The upper solid, the liquid film and the lower solid are considered separately and then meshed using appropriate matching conditions along the interfaces that define the liquid film.

6.4.1 PHASE CHANGE MATERIAL

The primary concern is with the conductive heat transfer into the wood chip across the distance d_0. It is assumed that the penetration distance d_0 is smaller than the length L and that the interface shape is sufficiently flat so that.

$$d_o \langle\langle L \qquad \text{and} \qquad \left|\frac{dh}{dx}\right| \langle 1 \qquad \textbf{Eq. 83}$$

The energy conservation equation with constant density, ρ, and thermal conductivity, k, and negligible shear stress can be applied after insertion of Fourier's Law of heat conduction.

$$\rho_w C_{pw}\left(\frac{\partial T}{\partial t} + v_x \frac{\partial T}{\partial x} + v_y \frac{\partial T}{\partial y} + v_z \frac{\partial T}{\partial z}\right) = k_w\left(\frac{\partial^2 T}{\partial x^2} + \frac{\partial^2 T}{\partial y^2} + \frac{\partial^2 T}{\partial z^2}\right) \qquad \textbf{Eq. 84}$$

Where Φ is the viscous dissipation function:

$$\Phi = 2\left[\left(\frac{\partial v_x}{\partial x}\right)^2 + \left(\frac{\partial v_y}{\partial y}\right)^2 + \left(\frac{\partial v_z}{\partial z}\right)^2\right] + \left(\frac{\partial v_y}{\partial x} + \frac{\partial v_x}{\partial y}\right)^2 + \left(\frac{\partial v_z}{\partial y} + \frac{\partial v_y}{\partial z}\right)^2 + \left(\frac{\partial v_x}{\partial z} + \frac{\partial v_z}{\partial x}\right)^2 - \frac{2}{3}\left(\frac{\partial v_x}{\partial x} + \frac{\partial v_y}{\partial y} + \frac{\partial v_z}{\partial z}\right)^2 \qquad \textbf{Eq. 85}$$

The viscous dissipation function is normally only considered significant for large velocity gradients and can therefore be ignored in this case. Assuming steady state operation and neglect the effect of thermal diffusion and convection heating in the x and z directions. Due to the notation and co-ordinate system used, v_y can be represented by -V the ablation velocity.

$$-V\frac{\partial T}{\partial y} = \alpha_w \frac{\partial^2 T}{\partial y^2} \qquad \textbf{Eq. 86}$$

Where, α, the thermal diffusivity equals

$$\alpha_w = \frac{k_w}{\rho_w C_{pw}} \qquad \textbf{Eq. 87}$$

V is an unknown constant in this equation and the derivative is only a function of y allowing total derivatives to be used. Allowing z to represent dT/dy, gives the following equation.

$$\alpha_w \frac{dz}{dy} + V \cdot z = 0 \qquad \textbf{Eq. 88}$$

The variables of this equation can be separated and integrated between boundary conditions, which for now will be called a and b:

$$\left[\ln z\right]_a^b = \left[\left(\frac{-V}{\alpha_w}\right) y\right]_a^b \qquad \textbf{Eq. 89}$$

These boundary conditions can then be inserted for z and y, leaving the following equation:

$$z_b = z_a \exp\left[\frac{-V}{\alpha_w}(y_b - y_a)\right] \qquad \textbf{Eq. 90}$$

If the boundary condition a is where y = h and T = T_m and noting that b is still the variable term then this can be can substituted in the give:

$$\frac{dT}{dy} = z_a \exp\left[\frac{-V}{\alpha_w}(y - h)\right] \qquad \textbf{Eq. 91}$$

Again the variables of this equation can be separated and the equation integrated to give:

$$\int_{T_m}^{T} dT = \int_{h}^{y} z_a \exp\left[\frac{-V}{\alpha_w}(y - h)\right] \qquad \textbf{Eq. 92}$$

This equation then becomes:

$$T - T_m = \frac{-\alpha_w z_a}{V}\left\langle \exp\left[\frac{-V}{\alpha_w}(y-h)\right] - 1 \right\rangle \qquad \textbf{Eq. 93}$$

The second boundary condition can then be inserted into this equation where $T \rightarrow T_o$ and $y \rightarrow \infty$, giving:

$$T_o - T_m = \frac{-\alpha_w z_a}{V}(0-1) \qquad \textbf{Eq. 94}$$

This can then be substituted back into Eq. 93 to give:

$$T(y) = T_0 + (T_m - T_0)\exp\left(\frac{-V}{\alpha_w}(y-h)\right) \qquad \textbf{Eq. 95}$$

Therefore the temperature profile in the upper solid may be determined. Because V is a constant in the equation derived above, the heat flux that enters the upper solid, q_o, is independent of longitudinal position.

6.4.2 HEAT CONDUCTION IN THE LIQUID FILM

The primary concern is with the melting caused by direct heat transfer across the sliding contact area. It can be assumed that the phase change material melts at a constant temperature T_m. The moving solid will be assumed to at a temperature $T_w(x)$.

The energy conservation equation for a Newtonian fluid with constant density, ρ, and thermal conductivity, k, can be applied to the relative motion gap, h.

$$\rho C_p\left(\frac{\partial T}{\partial t} + v_x\frac{\partial T}{\partial x} + v_y\frac{\partial T}{\partial y} + v_z\frac{\partial T}{\partial z}\right) = k\left(\frac{\partial^2 T}{\partial x^2} + \frac{\partial^2 T}{\partial y^2} + \frac{\partial^2 T}{\partial z^2}\right) + \mu\Phi \qquad \textbf{Eq. 96}$$

The viscous dissipation function, Φ, is normally only considered significant for large velocity gradients and can therefore also be ignored in this case. Assume steady state operation and neglect the effect of thermal diffusion in the x and z directions, gives

$$v_x \frac{\partial T}{\partial x} + v_y \frac{\partial T}{\partial y} + v_z \frac{\partial T}{\partial z} = \alpha \frac{\partial^2 T}{\partial y^2} + \frac{\mu \Phi}{\rho C_p} \qquad \textbf{Eq. 97}$$

Where, α, the thermal diffusivity equals

$$\alpha = \frac{k}{\rho C_p} \qquad \textbf{Eq. 98}$$

Scale analysis of the above equation gives

$$\frac{U\Delta T}{L} = \frac{\alpha \Delta T}{h^2} + \frac{\mu}{\rho C_p}\left(\frac{U}{h}\right)^2 \qquad \textbf{Eq. 99}$$

Therefore it can be seen that the effects of convection heating and friction can be ignored if:

$$\frac{U\Delta T}{L} / \frac{\alpha \Delta T}{h^2} \langle 1 \quad \text{and} \quad \frac{\mu}{\rho C_p}\left(\frac{U}{h}\right)^2 / \frac{\alpha \Delta T}{h^2} \langle 1 \qquad \textbf{Eq. 100}$$

Considering this in an order of magnitude sense only the vertical diffusion term needs to be retained in order to determine the temperature profile in the liquid film, hence:

$$\alpha \frac{\partial^2 T}{\partial y^2} = 0 \qquad \textbf{Eq. 101}$$

Integrating twice with respect to y gives

$$\alpha T + c_1 y + c_2 = 0 \qquad \textbf{Eq. 102}$$

By utilising the boundary conditions $T = T_m$ at $y = h$ and $T = T_w(x)$ at $y = 0$ the constants can be determined to be

$$c_2 = -\alpha T_w(x) \qquad and \qquad c_1 = \frac{-\alpha \Delta T}{h} \qquad \textbf{Eq. 103}$$

where

$$\Delta T = T_w(x) - T_m$$

Substituting into Eq. 102 gives

$$T = T_w(x) - \frac{\Delta T y}{h} \qquad \textbf{Eq. 104}$$

Which enables the temperature profile in the liquid film to be determined.

Scale analysis has shown that the effects of longitudinal conduction and frictional heat generation can be ignored. Therefore only area of interest is the transversal conduction phenomenon, which overwhelms all other energy effects due to the small film thickness and low liquid viscosity. Fouriers law of heat conduction applied across the liquid film gives

$$q_L = -k \frac{dT}{dy} \qquad \textbf{Eq. 105}$$

The total heat flux, q_y, that crosses the liquid film is equal to the heat flux absorbed by the liquid from the lower heated slider. This is therefore comprised of the heat needed to raise the temperature of the phase change material to its melting point and subsequently to melt it, in the case of wood rods it may be necessary to take account of any moisture present and the same arguments as developed for the isothermal case apply.

$$q_L = \rho_w h_{wf} V + \rho_w C_{pw} V\left(T_m - T_o\right) \qquad \textbf{Eq. 106}$$

Letting

$$\mathrm{Ste} = \frac{C_{pw}\left(T_m - T_o\right)}{h_{wf}} \qquad \textbf{Eq. 107}$$

Where Ste is the Stefan number and accounts for the degree of subcooling of the upper solid phase change material.

$$-k\frac{dT}{dy} = \rho_w h_{wf} V(1+\mathrm{Ste}) \qquad \textbf{Eq. 108}$$

Separating the variables and integrating across the liquid film gives

$$-k\int_{T_w(x)}^{T_m} dT = \rho_w h_{wf} V(1+Ste)\int_0^h dy \qquad \textbf{Eq. 109}$$

$$h = \frac{k\left(T_w(x) - T_m\right)}{\rho_w h_{wf} V(1+Ste)} \qquad \textbf{Eq. 110}$$

Therefore it can be noted that h varies inversely with the ablation velocity V.

6.4.3 Heat Conduction in the Solid Slider

The solid slider is moving with a constant velocity U, and therefore a process of time dependent conduction of a constant heat flux into the liquid film is occurring. The thermal penetration region, d_s, is assumed to be small such that:

$$d_s \langle\langle L \qquad \textbf{Eq. 111}$$

The temperature profile in the solid slider can be determined via a similarity profile solution of the energy equation. The solution requires numerical integration and only

the final equation and not the derivation will be given here, the subscript s denotes a property of the solid slider:

$$T_w(x) = T_s - \left[\left(\frac{q_L}{0.886k_s}\right)\left(\frac{x\alpha_s}{U}\right)^{1/2}\right] \qquad \textbf{Eq. 112}$$

Therefore the term $T_w(x)$ in Eq. 110 may be replaced by the above expression to give an expression for the variation of the liquid film gap with longitudinal position:

$$h = \left[\frac{(T_s - T_m)k}{q_L}\right] - \left[\left(\frac{k}{0.886k_s}\right)\left(\frac{x\alpha_s}{U}\right)^{1/2}\right] \qquad \textbf{Eq. 113}$$

6.4.4 CHAR LAYER

It has already been stated that these expressions, when applied to wood, are for the specific case of a tangential velocity greater than 1.2 m/s. At velocities below this the ablation rate decays dramatically indicating that there is an added resistance to heat transfer, this is in addition to the effect of the reduced slider temperature, which is a function of position due to the adiabatic assumption. It is assumed that the added resistance is due to a layer of char and slower reacting cellulose rods between the active layer and the wood interface. Assuming that this layer presents no resistance to mass transfer it becomes simply a case of resistance to heat transfer and Fouriers law of heat conduction can be applied across the composite gap between the slider and wood interface.

If Fouriers law is applied across the char layer, with the subscript c denoting properties of the char layer, gives:

$$q_c = \frac{k_c(T_c - T_m)}{h_c} \qquad \textbf{Eq. 114}$$

The thickness of the liquid layer is given by:

$$q_l = \frac{k\left(T_w(x) - T_c\right)}{h_l} \qquad \textbf{Eq. 115}$$

The heat flux that passes through the liquid layer is equal to that which passes through the char layer. Therefore only a simple rearrangement of the Fouriers equation is required in order to eliminate the unknown temperature at the char/liquid boundary giving the total distance, h_T, between the slider and wood interface as:

$$h_T = \frac{k\left(T_w(x) - T_m\right)}{q_l} - \frac{h_c k}{k_c} \qquad \textbf{Eq. 116}$$

The terms $T_w(x)$ and q_l can be replaced by the expressions that were derived earlier, the term h_c is the thickness of the char layer and will be dependent upon the stresses induced in it via the mechanical forces employed. The char thickness could be determined either mathematically or empirically allowing the model to be employed for situation where the relative velocity is below 1.2 m/s. However as reactors are unlikely to be designed with a relative velocity below the 1.2 m/s threshold the effect of the char layer will not be pursued.

6.4.5 LUBRICATION EFFECT AND PRESSURE DISTRIBUTION

The unknown in the above equations is the ablation velocity V, this can be determined by considering the mechanical equilibrium of the upper solid. This involves analysing the lubrication effect of the liquid film, this is essentially an extension of the classic Osborne-Reynolds theory of lubrication according to which the liquid inertia and pressure variation in the transverse direction are negligible. The pressure distribution P(x) will also be determined in order to connect it to the applied normal force.

The equation of continuity for this system, assuming constant density is:

$$\rho\frac{\partial v_x}{\partial x} + \rho\frac{\partial v_y}{\partial y} = 0 \qquad \textbf{Eq. 117}$$

The x component of the equation of motion in rectangular co-ordinates for a Newtonian fluid with constant density and viscosity are.

x-component

$$\rho\left(\frac{\partial v_x}{\partial t}+v_x\frac{\partial v_x}{\partial x}+v_y\frac{\partial v_x}{\partial y}+v_z\frac{\partial v_x}{\partial z}\right)=-\frac{\partial P}{\partial x}+\mu\left(\frac{\partial^2 v_x}{\partial x^2}+\frac{\partial^2 v_x}{\partial y^2}+\frac{\partial^2 v_x}{\partial z^2}\right)+\rho g_x$$

Eq. 118

The system can be assumed to be at steady state in addition the gravitational acceleration g_x is equal to zero. Scale analysis of the above equations will show that the viscous forces are orders of magnitude greater than the inertial forces, allowing the inertial forces to be ignored. Therefore

$$\frac{\partial P}{\partial x}=\mu\frac{\partial^2 v_x}{\partial y^2} \qquad \textbf{Eq. 119}$$

Integrating Eq.119 with respect to y but noting that $\partial p/\partial x$ is a constant because it only depends on x gives.

$$\frac{1}{\mu}\frac{\partial P}{\partial x}y=\frac{\partial v_x}{\partial y}+c_1 \qquad \textbf{Eq. 120}$$

c_1 is some unknown function to be determined later from the boundary conditions, integrating again gives

$$\frac{1}{2\mu}\frac{\partial P}{\partial x}y^2=v_x+c_1y+c_2 \qquad \textbf{Eq. 121}$$

Again c_2 is some unknown function to be determined from the boundary conditions. The velocity boundary conditions are given below, note that h denotes the relative motion gap defined earlier in Eq. 116:

$$v_x = \begin{cases} U & y = 0 \\ 0 & \text{at} \quad y = h \end{cases}$$

Applying the boundary conditions gives

$$c_1 = \frac{U}{h} + \frac{1}{2\mu}\frac{\partial P}{\partial x}h \qquad and \qquad c_2 = -U \qquad \textbf{Eq. 122}$$

The x-velocity component in the gap in terms of the unknown pressure gradient gradient $\partial P/\partial x$ becomes.

$$v_x = \frac{1}{2\mu}\frac{\partial P}{\partial x}y(y-h) + U\left(1-\frac{y}{h}\right)$$

Defining the height integrated flow rate to be

$$Q_x = \int_0^h v_x dy \qquad \textbf{Eq. 123}$$

Giving

$$Q_x = \frac{1}{12\mu}\left(-\frac{\partial P}{\partial x}\right)h^3 + \frac{1}{2}Uh \qquad \textbf{Eq. 124}$$

Consider again the equation of continuity in the liquid filled gap

$$\frac{\partial v_x}{\partial x} + \frac{\partial v_y}{\partial y} = 0$$

Considering the upper interface to have the generated liquid instantaneously removed gives, $v_y = -V$ at $y = h$ and $v_y = 0$ for $y < h$, in this case V is the ablation velocity. Integrating the equation of continuity between the limits $y = 0$ and $y = h$ gives

$$\frac{\partial Q_x}{\partial x} - V + \frac{\partial Q_z}{\partial z} = 0 \qquad \textbf{Eq. 125}$$

Further integration gives the following relationship:

$$Q_x = -C + Vx \qquad \textbf{Eq. 126}$$

The constant of integration C and the ablation velocity V are determined by first rearranging Eq. 124 to obtain an expression for dP/dx:

$$\frac{dP}{dx} = \frac{6\mu U}{h^2} + \frac{12\mu(C + Vx)}{h^3} \qquad \textbf{Eq. 127}$$

Integration of this equation gives an expression for the pressure at a point x in the liquid film:

$$P(x) = \int_0^x \frac{6\mu U}{h^2} + \frac{12\mu(C - Vx)}{h^3} dx \qquad \textbf{Eq. 128}$$

Integration of Eq. 128 across the phase change material length L gives the applied force F_n.

$$F_n = \int_0^L \int_0^x \frac{6\mu U}{h^2} + \frac{12\mu(C - Vx)}{h^3} dx dx \qquad \textbf{Eq. 129}$$

The boundary conditions of P(x) are homogeneous around the edge of the wood chip, P = 0 at x = o, x = L. Furthermore the applied force F_n is a known variable, therefore there are two unknowns and two equations providing a basis for solution of the above system of equations.

Finally the tangential friction force, F_t, cab be determined from its definition, assuming a Newtonian fluid

$$F_t = -\int_0^L \mu\left(\frac{\partial v_x}{\partial y}\right)_{y=0} dx \qquad \textbf{Eq. 130}$$

As an equation for the velocity of the liquid film in the x-direction has already been derived it is a simple matter to integrate this as indicated to give:

$$F_t = \int_0^L \frac{4\mu U}{h} + \frac{6\mu(C - Vx)}{h^2} dx \qquad \textbf{Eq. 131}$$

6.5 RESULTS

6.5.1 ISOTHERMAL MODEL REQUIREMENTS

The derived equations were solved using a spreadsheet so that the accuracy of the results could be determined by comparison with published results. The following variable and physical property data was required in order to be able to solve the equations. Note that the physical properties will vary from wood to wood, however, it is not practical to have a full analysis of each wood used. Therefore only the wood density and moisture content will be considered variable, any other physical properties will be based upon literature averages specific to the wood type used.

Table 13 Required variable data inputs for model.

Property	Symbol	Units
Length of sliding contact	L	M
Width of sliding contact	B	M
Pressure on cylinder	P_n	Pa
Temperature of wood	T_0	K
Tangential velocity	U	M/s
Biomass dry density	ρ_w	Kg/m^3
Wall temperature	T_s	K
Moisture content %	M	Wt/wt dry basis

Table 14 Required data inputs for isothermal model.

Property	Symbol	Units	Value
Liquid specific heat capacity	C_p	J/kg K	3650 #
Wood specific heat capacity	C_{pw}	J/kg K	2800 #
Liquid density	ρ	kg/m^3	500 #
Liquid thermal conductivity	K	W/m K	0.1-0.42 #
Liquid thermal diffusivity	α	m^2/s	3E-08 #
Liquid viscosity	μ	$N\ s/m^2$	0.07245 #
Latent heat of fusion	h_{sw}	J/kg	40000 #
Biomass decomposition temperature	T_m	K	approx. 710 #
Moisture enthalpy of fusion %	H_{mf}	J/kg	2256700
Moisture specific heat capacity %	C_{pm}	J/kg	4800
Temperature of wood	T_0	K	293

% Factor to take account of fact that wood may not be dry.

Physical property value refers to pine.

The corresponding outputs from the model are:

Table 15 Isothermal model outputs.

Property	Symbol	Units
Applied normal force	F_n	N
Relative motion gap	H	m
Pressure distribution	P(x, z)	N/m^2
x-direction volumetric flowrate	Q_x	m^3/s
z-direction volumetric flowrate	Q_z	m^3/s
Ablation velocity	V	m/s
Calculation term	C_n	
Calculation term	Θ	

6.5.2 ADIABATIC MODEL REQUIREMENTS

The derived equations require numerical integration to be solved, in addition the ablation velocity V and the constant of integration C are both unknown and need to be

obtained iteratively. A technical calculation program was used to solve the system of equations and the numerical integration's were solved using the *Romberg* technique.

There is a small variation in the inputs required by the adiabatic model compared to the isothermal. The adiabatic model is per unit width so the term width term B is not required. Additional physical property data is required for the solid slider, in this case stainless steel, which is given in Table 17 below. There is also some variation in the model outputs, which can be seen in Table 17 below.

Table 16 Physical property data for char layer and stainless steel slider.

Property	Symbol	Units	Value
Steel thermal conductivity	K_s	W/m.K	45
Steel thermal diffusivity	α_σ	m^2/s	1.15×10^{-5}

Table 17 Adiabatic model outputs

Property	Symbol	Units
Applied normal force	F_n	N
Frictional force	F_t	N
Relative motion gap	h(x)	M
Pressure distribution	P(x)	N/m^2
Ablation velocity	V	m/s
Wall temperature	$T_w(x)$	K
Wood temperature	T(y)	K
Penetration distance into wood	d_0	M
Calculation term	C	

6.5.3 ISOTHERMAL MODEL RESULTS

6.5.3.1 PRESSURE AND VOLUMETRIC FLOWRATE DISTRIBUTION

To enable the determination of the pressure and volumetric flowrate distribution a spreadsheet was used to calculate their respective values as a function of x and z; with the results being displayed as a matrix, and subsequently graphed as a three dimensional surface plot. The spreadsheet was set up so that the matrix intervals could be specified,

in this case a 10 x 10 matrix was used. As the data in matrix format is somewhat difficult to assimilate only the surface plots will be given here. It should be noted that as the surface pots are based on a 10 x 10 matrix, the x and z scale vary from 0 to 10 and this corresponds to a linear progression from minimum to maximum in the x and z directions.

The variable values used will be an applied pressure of 2×10^5 N/m^2, a wall temperature of 500 °C and 10 mm square wood chip.

Pressure Distribution

The pressure distribution beneath an ablating wood chip can be seen in Fig. 27 below.

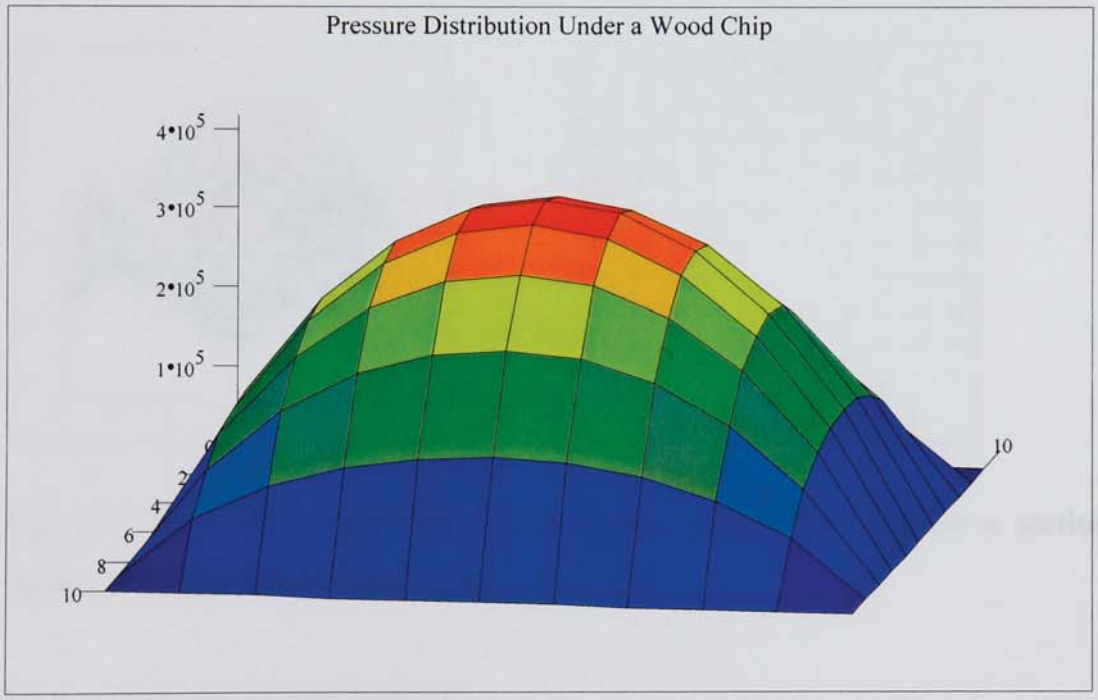

Fig. 27 Pressure distribution beneath an ablating wood chip.

As can be expected, the pressure distribution shows a maximum at the center and decreases to zero at the wood chip edges.

Volumetric Flowrate Distribution

The volumetric flowrate varies in both the x and z directions and therefore cannot be represented on one graph alone. However a resultant volumetric flowrate, Q_r, can be determined from:

$$Q_r = \sqrt{Q_x^2 + Q_z^2} \qquad \textbf{Eq. 132}$$

And the direction of the volumetric flowrate can be determined from a vector field plot. An example of this is shown in Fig. 28 below for the case of a stationary, square, wood chip.

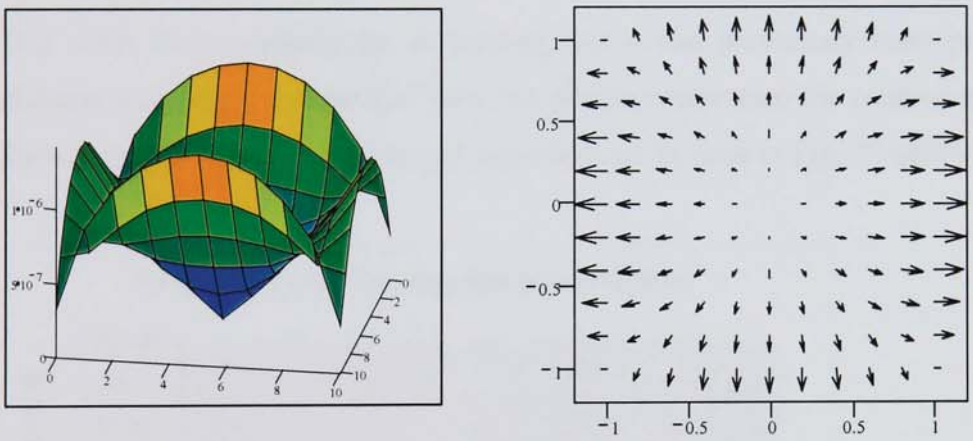

Fig. 28 Resultant volumetric flowrate and vector field plot for a stationary, square, ablating wood chip.

6.5.4 ADIABATIC MODEL RESULTS

6.5.4.1 RELATIVE MOTION GAP AND SOLID SLIDER TEMPERATURE

The solid slider has been assumed to be adiabatic and therefore its temperature changes as a function of axial position. The temperature, $T_w(x)$, can be determined from Eq 112 and is plotted in Fig. 29 below. The variable values used in this and subsequent graphs/tables will be an applied pressure of 2×10^5 N/m^2, a wall temperature of 500 °C, 10 mm square wood chip and a tangential velocity of 1.2 m/s unless stated otherwise.

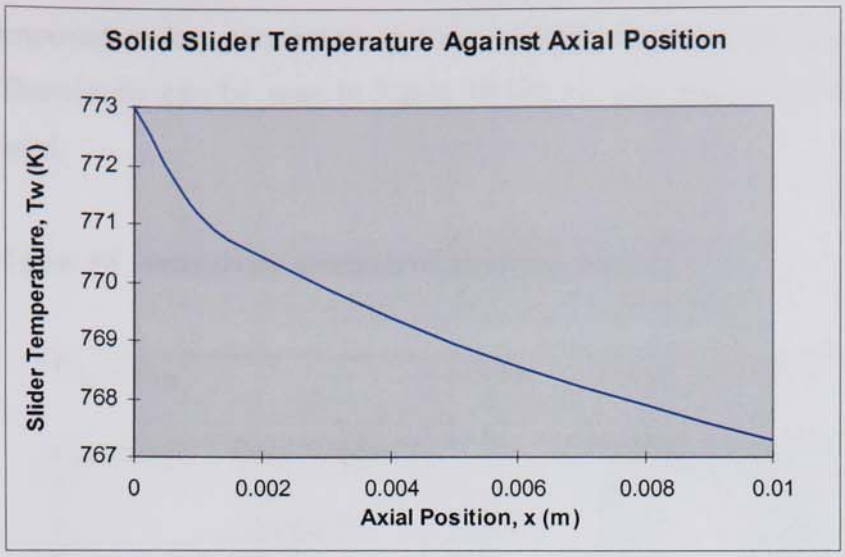

Fig. 29 Variation in solid slider temperature with axial position.

The solid slider temperature is varying, yet it has previously been proved that the ablation velocity is independent of axial position, therefore the relative motion gap (h) must vary. The relative motion gap variation can be seen in Fig. 30 below.

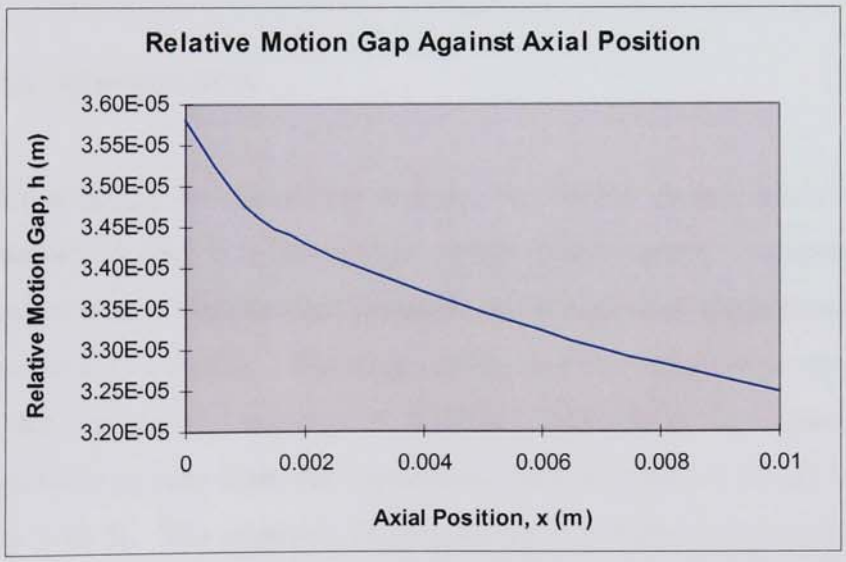

Fig. 30 Variation in relative motion gap with axial position.

6.5.4.2 Sensitivity Analysis of Key Parameters

The adiabatic model derived above can be used to investigate the sensitivity of the ablation velocity to changes in key parameters. Changes of ± 5% and ± 10% were

imposed on key parameters and the variation from a base case ablation velocity noted. The results can be seen in Table 18 below, also shown are the base case parameters used.

Table 18 Sensitivity analysis of ablation process.

Variation		+ 10%	+ 5%	- 5%	- 10%
Parameter	Base Value		% Variation in V		
L	2 cm	-4.86	-2.46	2.59	5.21
P_n	200000 Pa	2.34	1.18	-1.22	-2.55
T_o	293 K	5.21	2.59	-2.46	-5.05
T_s	823 K	34.23	21.40	-32.12	-179.13
T_m	710 K	-142.5	-41.67	23.67	39.21
M	6 % w/w (dry)	-1.21	-0.43	0.51	0.93
U	1.2 m/s	0.08	0.08	0.00	-0.08
C_p	2800 kJ/kg.K	-6.59	-3.28	3.32	6.73
K	0.42 W/m.K	6.58	3.48	-3.74	-7.77
μ	0.07245 $N.s/m^2$	-2.37	-1.21	1.27	2.59
ρ	500 kg/m^3	-7.67	-3.83	3.96	7.83

6.6 DISCUSSION

Considering the sensitivity analysis the results quantitatively show what was already suspected, that in order to have a high ablation rate it was necessary to use small wood chips with a high contact pressure and a high disk temperature with as little moisture present as possible. The large effect that the variation in melting temperature has is only particularly relevant if different feed stocks are considered as wood is vary unlikely to vary from the value determined by Lédé et al. (8), certainly not by as much as 5-10 %. The relatively large increase in ablation rate possible with preheating of the feedstock presents an interesting possibility for the utilisation of low quality waste heat. Also of note is the small impact of variation in the tangential velocity applied to the wood chip, this tends to imply that the assumption of an additional heat transfer resistance below tangential velocities of 1.2 m/s is a valid one. The additional resistance is most likely due to char accumulation on the melt interface that is not removed at low tangential velocities due to low mechanical shear stresses.

7. EXPERIMENTAL INVESTIGATION INTO ABLATION RATE

In this work the aim was to investigate the effects of various parameters on the ablation rate. Easily controllable parameters such as wood rod geometry, temperatures, applied pressures and relative velocities would be investigated. For these experiments the following range of variables were chosen:

- Wood rod geometry's of 2 cm x 0.9 cm and 0.9 cm x 0.9 cm.
- Disk temperatures of 450, 500, 550 and 600 °C
- Applied pressures of 2, 4, 6 and 8 x 10^5 Pa
- 0, 0.3, 0.6, 0.9, 1.2 and 1.5 m/s relative velocity at a disk temperature of 500 °C and an applied pressure of 2 x 10^5 Pa.

In addition, the effect of different physical properties could be investigated by utilising different wood types such as hardwoods and softwoods.

7.1 EXPERIMENTAL SETUP AND PROCEDURE

The experiments were performed using a purpose built experimental rig which may be seen in Fig. 31 below. The wood rods were pressed against a horizontal, planar steel disk rotating at a constant and controllable velocity. The steel disk was heated from below to the desired temperature by custom built ceramic heaters, with the temperature being measured by a thermocouple pressed against the steel disk. The steel disk had a diameter of 214 mm with the wood rods being pressed against it at a distance of 74 mm from the center.

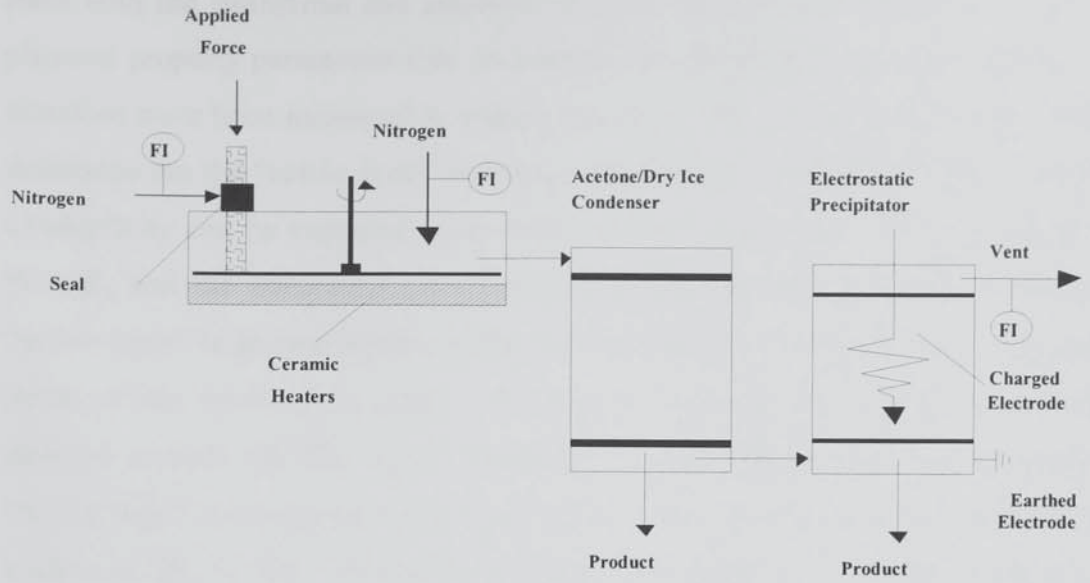

Fig. 31 Experimental Ablation Rig.

- A constant flowrate of nitrogen was maintained through the reactor to provide the required inert atmosphere and to carry the products to the product collection system. This consisted of an acetone/dry ice condenser followed by a wall cooled electrostatic precipitator. Experiments were performed in order to determine the effects of wood rod geometry, relative motion, applied pressure and temperature difference upon the wood rod ablation rate.

Force was applied vertically to the rod and as it ablated against the hot spinning disk the time needed to ablate through a distance of 10 cm was recorded. This enabled the ablation rate to be determined. In addition the products were collected, gas samples taken and the total gas throughput recorded to enable further analysis and for mass balances to be determined.

7.2 RESULTS

Only a limited number of experimental runs were completed due to failure of the ceramic heater used in the equipment. Although further experiments are anticipated this is pending on the replacement of the failed ceramic heater. The experimental runs that were completed are detailed in Table 19 below and are compared to the results obtained

from both the isothermal and adiabatic ablation models detailed earlier. Many of the physical property parameters that are required by the models are easily determined and therefore have been measured to ensure accuracy. Two parameters that are difficult to determine are the "active layer" viscosity and thermal conductivity. The "active layer" conductivity can be expected to lie between the values of the wood conductivity, 0.1 W/m.K, and the condensed oil conductivity, 0.42 W/m.K (107), this is because the "active layer" is an intermediate stage between the two. Therefore the upper and lower limits of the conductivity range were applied for both the isothermal and adiabatic ablation models and the results compared to those determined experimentally. The "active layer" viscosity was chosen to be 0.073 N.s/m^2, this value being that utilised by Lédé et al. (8, 33, 86). As can be seen below the value of 0.1 W/m.K fits best with the isothermal model and the value 0.42 W/m.K fits best with the adiabatic model.

Table 19 Data and results for wood rod ablation studies.

Run	2	2	2	2
Date	13/5/98	13/5/98	13/5/98	13/5/98
Wood Moisture, %	13.43	13.43	13.43	13.43
Wood Density, kg/m^3	552	552	552	552
Wood Length, mm	19.8	19.8	19.8	19.8
Wood Breadth, mm	8	8	8	8
Applied Pressure, kPa	201	411	684	900
Applied Temperature, °C	500	500	500	500
Applied Velocity, m/s	1.8	1.8	1.8	1.8
Ablation Length, mm	100	100	100	100
Time Taken, s	225	209	149	111
Ablation Rate, mm/s	0.44	0.47	0.67	0.90
Isothermal Calculated Rate, mm/s, k = poly	1.13	1.36	1.54	1.65
Isothermal Calculated Rate, mm/s, k = 0.1	0.38	0.46	0.52	0.56
Adiabatic Calculated Rate, mm/s, k = poly	0.48	0.57	0.65	0.70
Adiabatic Calculated Rate, mm/s, k = 0.1	0.17	0.20	0.23	0.25
Value of polynomial k	0.42	0.42	0.42	0.42

In addition the results are displayed graphically and may be seen below in Fig. 32 below.

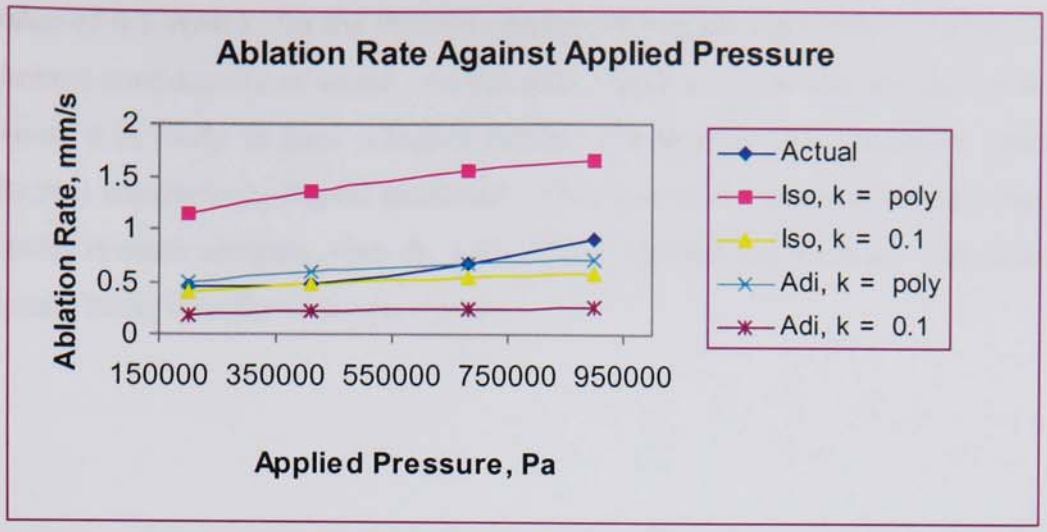

Fig. 32 Ablation rate against applied pressure for run 1.

7.3 DISCUSSION

The experiments described above show a good fit between the ablation rate derived from mathematical models and that determined experimentally. However as only one set of experiments has been performed on one type of wood it is difficult to draw any conclusions without any further experimentation. One major flaw was the inability to directly determine the viscosity and thermal conductivity of the active layer. Perhaps the only possible way would be through extensive experimentation and data fitting, which was not feasible due to the equipment failure.

The value of 0.42 W/m.k was chosen for the "active" layer thermal conductivity in the adiabatic model because an initial first guess value was required and this was based on the thermal conductivity of pyrolysis oil (107), extrapolated to the melt temperature. It was then intended to perform experimental runs in order to determine the actual value of the "active" layer thermal conductivity. However, limited experimental runs over a range of conditions showed the initial guess value of 0.42 W/m.k was an accurate value. The limited experimental runs show that the derived model is highly accurate for this particular case, however, additional work is required on a variety of different wood types to prove this conclusively.

The isothermal model requires that the thermal conductivity be approximately 0.1 W/m.k., a figure similar to that used by Lédé (8), in order to get accurate results. The

value of 0.1 W/m.k for the thermal conductivity of the active layer is equivalent to the thermal conductivity of wood. As the active layer is essentially the melted form of the wood, it is likely to have a higher thermal conductivity that should be similar to the thermal conductivity bio-oil produced. Therefore these results show that the adiabatic model is more accurate, with the active layer thermal conductivity needed to get good results being broadly what was expected.

8. DETERMINATION OF REACTOR THROUGHPUT

8.1 DETERMINATION OF ABLATION RATE

The preceding chapter established and validated a mathematical model that was capable of determining the ablation velocity and tangential friction force for an ablating wood rod. The necessary inputs included the wood rod physical properties, the applied temperature, the relative velocity and the contact pressure. Although the wood rod physical properties, applied temperatures and relative velocity are easy to determine or specify for a reaction system, the same cannot be said of the applied pressure. If there is not a simple method whereby the applied pressure for a reaction system can be determined, enabling the ablation rate and hence reactor throughput to be calculated, then the model developed in Chapter 6 serves little purpose beyond a theoretical exercise.

Taking the case of the reaction system envisaged in Chapter 1, it can be seen that the applied pressure is a function of the tangential friction force (which varies linearly with relative velocity) and blade angle. Therefore there is a need to be able to link the applied pressure to the tangential friction force (which can be determined from the model).

Two options are available:

- A simple empirical method whereby studies are performed on a small reactor with a known blade angle and the effect of the applied temperature and relative velocity on the ablation rate are recorded. This would enable the applied pressure to then be calculated from the model and hence a correlation could be obtained.
- A force diagram of the system would enable the applied pressure to be determined from the tangential friction force and blade angle. The tangential friction force can only be calculated if the ablation velocity is known and the ablation velocity can only be determined if the applied pressure is known. Superficially it appears that the problem cannot be solved, however it can be solved iteratively.

Considering the reactor envisaged in Chapter 5, the curved wall may be approximated to a flat surface and the following force balance applies.

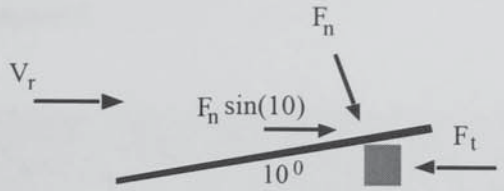

Fig. 33 Force balance for ablation process.

Where F_n is the applied force, F_t is the tangential friction force, v_r is the relative velocity and Φ is the blade angle. From this it can be seen that

$$F_t = F_n \, Sin\, \phi$$

Therefore the applied force and ablation velocity can be determined iteratively provided the particle physical properties, applied temperatures, relative velocity and blade angle are known.

The two most critical factors, which could affect the accuracy of the above iterative calculation, are the liquid film conductivity and viscosity. These are also the two parameters that are unknown and impossible to determine analytically. In Chapter 7 it was demonstrated how these parameters could be determined experimentally by back calculation using the ablation model, however this could still lead to error. Unfortunately there is insufficient time available to enable an exhaustive investigation of the liquid film thermal conductivity and viscosity. Therefore the values determined from the small number of experiments that were performed will be used and any inherent errors will be tolerated.

The premise given above is that the ablation velocity and applied pressure can be determined for a given reactor configuration as long as the physical properties of the materials employed, the temperatures applied and the relative velocity are known. In order to prove this theory, calculated values must be compared with those determined experimentally in order to determine the accuracy of the model employed.

The reactor employed in this experiment is that which was specified in Chapter 5. A simple diagram of the reactor can be seen in the figure below and the dimension of the reactor can be seen in Chapter 5.

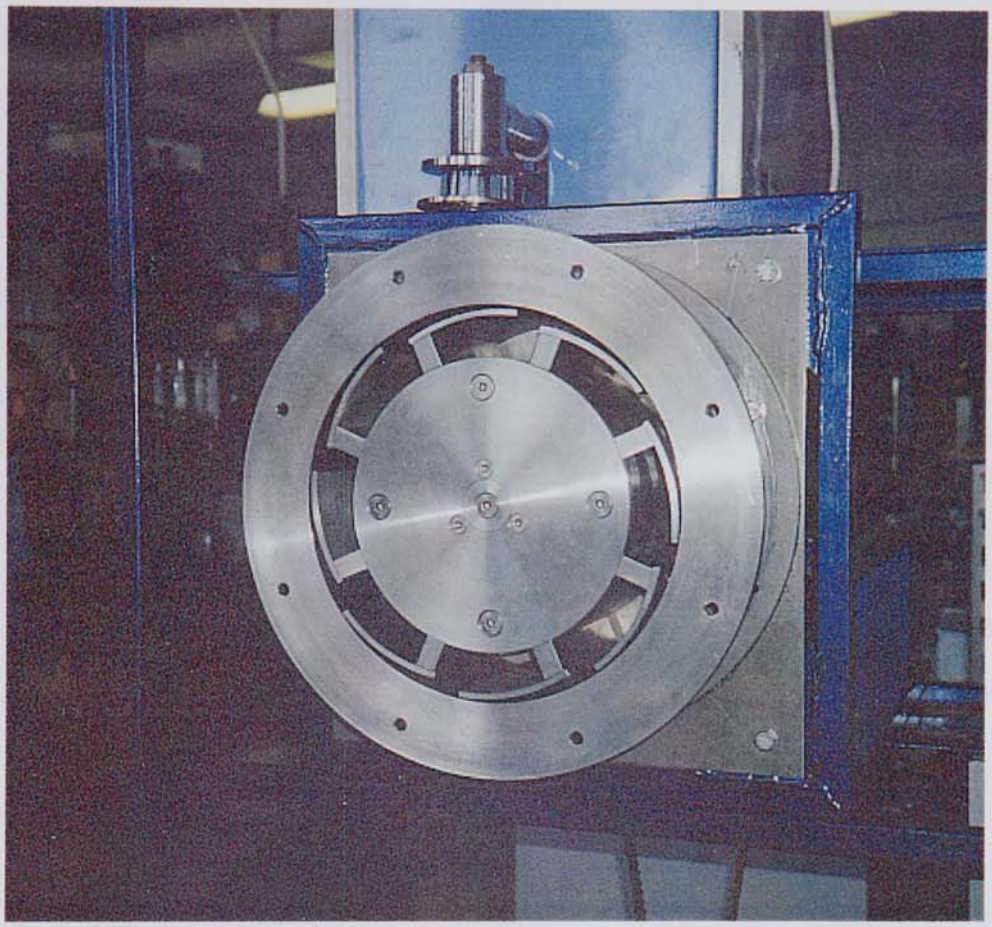

Fig. 34 Front view of rotating column reactor.

The reactor was heated by a 5.5 kW band heater with the temperature being controlled by a digital temperature controller. The relative motion was supplied by a 1.5 kW motor controlled by a variable speed D.C. controller. 7 mm by 20 mm wood chips were ablated at a temperature of 550 ^{0}C with a blade angle of 12^{o} and the time taken for complete ablation was recorded for a variety of relative velocities. A strobe light was used in order to calculate the relative velocities and to isolate the image of the spinning biomass particle at a fixed position in space so that the particle degradation could be observed and timed. The experimental results obtained are compared with those obtained via modelling in Table 20 below.

Table 20 Data comparing experimental determination and model predictions of ablation rate.

Run	1	2	3	4	5
Date	9/9/99	9/9/99	9/9/99	9/9/99	9/9/99
Liquid film Conductivity, W/m.K	0.1	0.1	0.1	0.1	0.1
Liquid Film Viscosity, N.s/m^2	0.075	0.075	0.075	0.075	0.075
Wood Moisture, %	10.43	10.43	10.34	10.43	10.43
Wood Density, kg/m^3	525	525	525	525	525
Wood Breadth, mm	20	20	20	20	20
Wood Length, mm	7	7	7	7	7
Applied Temperature, °C	525	525	525	525	525
Applied Velocity, m/s	12.1	10.9	9.9	8.3	6.1
Time Taken, s	11	12	13	15.25	19
Ablation Rate expm, m/s	0.00063	0.00058	0.00053	0.00045	0.00036
Calculated Rate, m/s	0.0006	0.00058	0.00056	0.0005	0.00048

The experimentally determined ablation rate (V expm) is compared with that predicted by the model (798 K) in Fig. 35 below

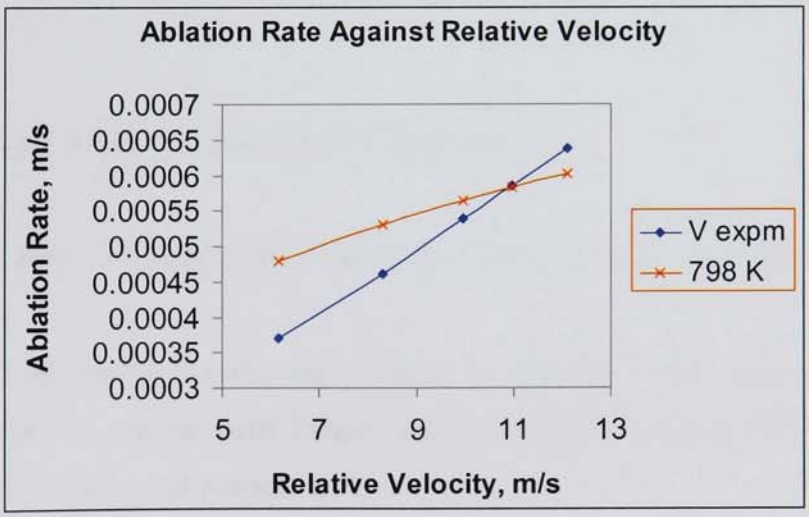

Fig. 35 Ablation rate against relative velocity for experimental and model prediction.

8.1.1 CONCLUSION

A reasonably close fit is obtained over the range of relative velocities investigated. This range is representative of industrial size applications due to the fact that at lower

velocities the biomass particles did not remain fixed beneath the blades and higher velocities could lead to mechanical failure of the biomass particles due to the high contact pressure. Therefore industrial scale applications would operate within these limits.

Due to the small number of experiments performed, these results should be considered qualitative in nature. Far more experimental runs would have to be performed and a detailed investigation of the liquid film thermal conductivity and viscosity undertaken in order to make these results quantitative.

As can be seen there is a difference in the gradient of the two lines, this is most likely due to the assumption of a flat reactor surface leading to an error in the determination of the blade angle.

Despite these problems the ablation velocity can be reasonably accurately determined from knowledge of the reactor configuration, physical properties, applied temperatures and relative velocities.

8.2 CALCULATION OF REACTOR CAPACITY

In order to be able to calculate the reactor throughput 3 important factors need to be known:

- The area available for the ablating particles to initially occupy beneath the blades. This depends on reactor path length, reactor diameter, number of blades, blade angle, blade position and particle size.
- The packing factor of the particles beneath the blades.
- The ablation rate of the particles.

The total area beneath the blades is not of interest (excepting heat flux considerations), only that available for initial occupation by a biomass particle. It is necessary to know how many fresh unablated particles can enter the reactor and find a space beneath the blades to occupy. Once a particle is replaced by a fresh one it is no longer of importance as it can be assumed that it will continue to ablate beneath the blade at the

same rate as the particle at the front, therefore presenting no hindrance, or in the case of curved blades, at a faster rate due the lower contact angle.

The packing factor defines how many particles can occupy the initial space or surface area beneath the blades. In a best case scenario this will be a perfect fit with each particle touching each other and no free space available. In a worst case scenario each particle will be separated by a distance that is a fraction less than the particle size, wasting as much space as possible. In practice the packing factor will lie somewhere between the two extremes and can only be determined empirically.

If all of the above is known the reactor throughput can then be calculated.

8.2.1 Reactor Capacity Calculation

Taking the reactor specified in Chapter 5 the reactor path length is 130 mm, the reactor diameter is 256 mm, the number of blades is 8, the blade angle is 12° and the blade position is known. If a particle size of 20 mm x 7 x 7 mm is used, with a reactor wall temperature of 525 °C, and the maximum relative velocity the reactor is capable of, 12.1 m/s, is specified. Then the best and worst case reactor throughput can be calculated, this is shown below.

Table 21 Calculation of Reactor Throughput

Scenario	**Best Case**	**Worst Case**
Liquid film Conductivity, W/m.K	0.1	0.1
Liquid Film Viscosity, $N.s/m^2$	0.075	0.075
Wood Moisture, %	10.43	10.43
Wood Density, kg/m^3	525	525
Wood Breadth, mm	20	20
Wood Length, mm	7	7
Applied Temperature, °C	525	525
Applied Velocity, m/s	12.1	12.1
Calculated Ablation Rate, m/s	0.0006	0.0006
Packing Factor, %	100	50
Reactor Throughput, kg/hr	40	20

8.2.2 Reaction Products

Once the capacity of the reactor is known the product composition and flow rates can be determined and the product collection system designed accordingly. Detailed modeling and specification of the product collection system is carried out in Chapter 9. A precise calculation of the product yields is currently not possible as sufficient detailed kinetic schemes are not available. An overview of the current knowledge and limitations is given in Chapter 2. An alternative approach was taken by Toft (108) who determined empirical relationships for the product yields based on accumulated data from other researchers efforts. The following conditions apply to the relationships determined:

- Reactor temperature of 450-500 °C.
- Vapour residence time of less than 2 seconds.
- A particle size of less than 2 mm.
- A biomass moisture content of less than 10%.

The particle size limitation of less than 2 mm was specified so as to limit intra-particle reaction and heat transfer effects. During ablation the reaction products are rapidly removed from the reaction interface and intra-particle effects are not an issue. Therefore the restriction on particle size does not apply to ablation and the following empirical equation can be employed:

Organics, wt % $= -16.4 \times 10^{-6} (T)^2 + 0.164 (T) - 3.47$

Water, wt % $= 4.70 \times 10^{-6} (T)^2 - 0.0049 (T) + 1.20$

Char, wt % $= 8.60 \times 10^{-6} (T)^2 - 0.0099 (T) + 2.95$

Gas, wt % $= 8.06 \times 10^{-6} (T)^2 - 0.0071 (T) + 1.64$

Based on these equations the reaction products can then be determined. It should be noted that the reactor itself is sized so as to be able to handle feed rates of upto an average value of 30 kg/hr (average of best and worst case scenario) so as to enable future work at high capacities to be carried out as and when funds for upgrading become available. The feeder that will be employed has a maximum capacity of 3 kg/hr and therefore the products composition and flowrates should be determined for a feed rate of

3 kg/hr. The reaction temperature will be specified to be 525 ^{0}C, with an internal gas temperature of 400 ^{0}C and a feed moisture content of 10%. Based on this data the product composition and flowrates at 400 ^{o}C would be:

Table 22 Calculation of product compositions.

Component	Mass %	R.M.M	kg/hr	kg/s	Mols/s	m^3/s
Organic	61.98	0.400	1.86	5.16E-04	1.29E-03	7.13E-05
Gases	13.40	0.035	0.40	1.12E-04	3.19E-03	1.76E-04
Water generated	12.33	0.018	0.37	1.03E-04	5.71E-03	3.15E-04
Char	12.29	0.012	0.37	1.02E-04	8.53E-03	1.28E-07
Total	100.00		3.00	8.33E-04	1.87E-02	5.63E-04

However, based on the size of the reactor specified in Chapter 5 and estimating the necessary pipework required, the total operating volume could be estimated to be 0.00234 m^3. This means that the residence time of the vapours before quenching will be approximately 4.15 seconds. This is clearly far too long and would lead to substantial product cracking and loss of the valuable organic fraction. Therefore nitrogen will have to be used in order to get the product vapour residence time down to less than 2 second. The maximum amount of nitrogen that can be supplied to the reactor using currently available equipment is 100 ltr/min or 0.0017 m^3/s of nitrogen at 25 ^{o}C. At 400 ^{o}C this is equivalent to 0.0038 m^3/s or 230 ltr/min and would result in a residence time of 0.5 seconds and change the product composition to:

Table 23 Calculation of product composition including nitrogen.

Component	Mass %	R.M.M	kg/h	Kg/s	Mols/s	m^3/s
Organic	18.43	0.4	1.86E+00	5.16E-04	1.29E-03	7.13E-05
Gases	3.98	0.035	4.02E-01	1.12E-04	3.19E-03	1.76E-04
Water generated	3.67	0.018	3.70E-01	1.03E-04	5.71E-03	3.15E-04
Char	3.65	0.012	3.69E-01	1.02E-04	8.53E-03	1.28E-07
Nitrogen	70.27	0.028	7.09E+00	1.97E-03	7.03E-02	3.88E-03
Total	100.00		1.01E+01	2.80E-03	8.91E-02	4.45E-03

From this information it is possible to model and design the product collection system which is described in detail in Chapter 9.

9. PRODUCT COLLECTION SYSTEM

9.1 INTRODUCTION

Fast pyrolysis invariably produces three products; non-condensable gases, a solid char and a condensable organic vapour. Condensation of the vapour produces a liquid product that may be used as a fuel or as a source of specialty chemicals. The products are generally produced from softwood in yields of; char 12 wt.%, gases 12 wt.% and the balance being condensable vapours. The vapours typically consist of:

- condensable vapours of low molecular weight chemicals (acetic acid, formaldehyde, phenols, hydroxy acetone, etc).
- water vapours either present in the original feed or produced during pyrolysis (typically 20%).
- complex oxygenated hydrocarbons formed by partial depolymerisation of the biomass constituents.

As the product vapours cool to around 400°C the hydrocarbons can combine to form visible aerosol consisting of micron and sub-micron particle sizes. These particles will coalesce and stick to any surface at temperatures less than 400°C presenting significant fouling problems. However, if the vapours are maintained at temperatures above 450°C, for longer than one second, secondary vapour phase reactions will occur. This cracks the vapours to form permanent gases, char and lower molecular weight hydrocarbons. The easiest way of minimising liquid losses is to keep the residence time as low as possible (<0.5 s) and to control the temperature to about 400 °C. As pyrolysis is carried out in an oxygen free environment, an inert gas such as nitrogen is used in varying proportions, depending on the reactor configuration. Nitrogen may also be used to control vapour residence time and temperature in the reactor. In the preceding chapter the composition and flowrates of the product vapours were calculated and nitrogen was added to control the vapour residence time. The valuable organic fraction must know be condensed out from a process stream, which is largely non-condensable gases and this presents a number of problems.

Depending on the design of the pyrolysis reactor the process char is typically smaller than the feedstock. In the case of ablative pyrolysis the char is typically a free flowing powder. If pyrolysis oil is produced from biomass for use as a chemical feedstock or energy source it is desirable to have a product that contains a minimum of suspended solids, typically less than 0.5 wt % (109). Typical reasons for this are:

- The solid char is very fine and can lead to fouling problems in condensers and process pipes.
- The solid char tends to settle slowly over time leading to an accumulation of sludge in process storage vessels.
- The char may have some catalytic effect on the long term instability of pyrolysis oil.
- The solid char could block the orifices of atomisers and burners leading to combustion problems.
- The char has a high ash and alkali metals content, which can damage turbine blades and boilers.

Therefore it is typical to remove the product char from the vapour before condensation, as it is difficult to remove from the product liquid. Conventional techniques for char removal in the gas phase involve multiple high efficiency cyclones or hot gas filtration.

In a cyclone, centrifugal force is used to separate the high density solids from the low density gases. In high efficiency cyclones, the gases typically enter with velocities between 9 and 27 m/s, with a higher velocity giving higher collection efficiencies. Two important points with regards to cyclones are:

- The efficiency of a cyclone is a function of the particle diameter with small particles below 10 μm being difficult to remove.
- The amount of centrifugal force generated is proportional to the square of the tangential entering velocity, which is limited by pressure drop constraints, and is inversely proportional to the diameter of the cyclone. This can lead to scale up problems.

In hot gas filtration the solids are filtered from the vapours prior to condensation. Typically bag filters are used and pioneering work by Diebold et al. (110) showed that they could be highly efficient at char removal with a residual char concentration in the condensed liquid of less than 0.01 % wt./wt. The char collection efficiency of a filter is not expected to degrade upon scale up leaving the primary scale up factor to be the ratio of the volumetric gas flowrate to the area of the filter. Simply put a scaled up filter has more surface area.

Superficially hot gas filtration appears an attractive proposition. However there is one major drawback, severe product cracking occurs in the baghouse. Typical baghouse conditions are a residence time of 6 seconds, a temperature of 385 °C and this leads to about 10% of the product vapours being converted to non-condensable gases (110). As this is clearly unacceptable, cyclones remain the collection method of choice. Therefore two cyclones were designed and constructed to enable the removal of the bulk of the particulates present. The design methodology employed is summarised in Chapter 9.2 below.

After char removal, it is then necessary to condense and collect the liquid fraction known as bio-oil. The presence of large volumes of non-condensable gases represents a significant heat and mass transfer resistance, making conventional heat transfer equipment inappropriate due to the large equipment sizes required. In addition, pyrolysis liquids present considerable fouling problems, which can also render conventional heat exchangers inoperable. Although all fast pyrolysis processes have necessarily included liquids collection, little attention has been paid to the fundamentals of design. Bridgwater and Peacocke (9, 57) conducted a review of the current fast pyrolysis technologies and associated collection technologies. The conclusion is that the majority of systems use a direct contact heat exchanger for cooling/condensing process vapours and electrostatic precipitators are the best technique for removing residual vapours after the direct contact heat exchanger. Many of the systems are multi-stage with multiple liquid collection points. One problem associated with the multi-stage collection systems is pyrolysis liquid instability. In multi-stage collection, the product liquid is collected in a number of stages and blended to produce the pyrolysis liquid. This appears to adversely affect the pyrolysis oil instability and lead to phase separation as well as being needlessly complicated. Therefore a single stage collection

system will be specified for this project. This will involve a direct contact heat exchanger coupled to an electrostatic precipitator.

In their simplest form, direct contact heat exchangers consist of open vessels where the process stream and coolant are mixed directly. There is no heat transfer resistance of a separating wall, nor complexity due to arranging this wall to maximise the heat transfer surface. Their attractiveness stems from their potential economy and simplicity, plus their ability to handle a wide variety of fluids and solids, often under conditions that would cause excessive fouling, corrosion or thermal stressing in conventional equipment. A disk and doughnut direct contact heat exchanger was designed and constructed for cooling and partial condensation of the pyrolysis vapours. Due to the lack of specific design techniques for direct contact heat exchangers, the quench column was designed based upon gas flows. An overview of the current knowledge, designs methods and types of direct heat exchangers is given in Chapter 9.3 below.

Although direct contact heat exchangers offer large volumetric heat transfer coefficients and substantial interfacial areas, fugitive aerosols may still pass through the system. These aerosols, termed a "mist" in distillation operations, require the use of an electrostatic precipitator (E.P.) to facilitate collection. In electrostatic precipitation the forces used to separate the aerosols from the gas stream are applied directly to the aerosols themselves. Therefore, the energy needed to effect separation is considerably less than for other types of separating equipment. A detailed model of electrostatic precipitators was developed and used to design an electrostatic precipitator for product collection. As the model is extremely complex and detailed, the development and theory is given in Appendix 1. In order to keep the electrostatic precipitator cold and to prevent fouling, thereby increasing efficiency, a wet walled electrostatic precipitator was used. This was mounted directly on top of the direct contact heat exchanger, with the cooled quench liquid flowing down the walls of the E.P. before entering the direct contact heat exchanger and cascading down through the disk and doughnut section. This arrangement can be seen in Chapter 9.4 below. The quench liquid chosen was octane due to the fact that it is largely immiscible and non-reactive with pyrolysis vapours/liquids and has a sufficiently high vapour pressure to prevent excessive vaporisation. In addition a refrigeration unit was used to cool the octane down to -5 °C before entering the product collection system. The condensed pyrolysis vapours and

octane are recycled through the refrigeration unit and product collection system. Accumulation of product within the system causing capacity problems is not envisaged due to the fact that the continuous mode of operation is limited by feeder constraints, however provision is made for a product stream should this become necessary.

9.2 CYCLONE DESIGN

Cyclones employ centrifugal forces to effect gas-solid separation and are widely used in industry. Cyclones can be used for the separation of particles down to approximately 5 μm in diameter. It is necessary to design a cyclone for the removal of particles entrained in a vapour exiting an ablative pyrolysis reactor. The most common design in use is the reverse-flow cyclone. In this design the gas enters the top of the cyclone tangentially and spirals down to the apex of the conical section; it then moves upwards in a second, smaller spiral and exits through the top of the cyclone via a central vertical pipe. The centrifugal forces move the particles radially to the walls where they slide down and are collected at the bottom.

9.2.1 DESIGN METHODOLOGY

Stairmand (1951) (111) developed two standard designs for gas-solid cyclones: a high efficiency cyclone and a high throughput cyclone. As the throughput from the reactor is minimal, and because it is desirable to minimise the char content of the pyrolysis oil, the high efficiency design will be used. The performance curve for the standard design was obtained experimentally under standard conditions (detailed overleaf); and can be transformed to other cyclone sizes and operating conditions using the following scaling equation. For a given separating efficiency:

$$d_2 = d_1\left[\left(\frac{Dc2}{Dc1}\right)^3 * \frac{Q_1}{Q_2} * \frac{\Delta\rho_1}{\Delta\rho_2} * \frac{\mu_2}{\mu_1}\right]^{1/2} \qquad \textbf{Eq. 133}$$

Where

d_1 = Mean diameter of particle separated at standard conditions, at the chosen separating efficiency.

d_2 = Mean diameter of the particle separated in the proposed design, at the same separating efficiency.

Dc1 = Diameter of the standard cyclone, 203 mm.

Dc2 = Diameter of proposed cyclone, mm.

Q_1 = Standard flow rate, 223 m^3/h.

Q_2 = Proposed flow rate, m^3/h.

$\Delta\rho_1$ = Solid-fluid density difference in standard conditions, 2000 kg/m^3.

$\Delta\rho_2$ = Density difference proposed design, kg/m^3.

μ_1 = Standard fluid viscosity, 0.018 mNs/m^2.

μ_2 = Proposed fluid viscosity, mNs/m^2.

A diagram of the standard high efficiency cyclone is given in Fig. 36 below, showing the dimensions of each section.

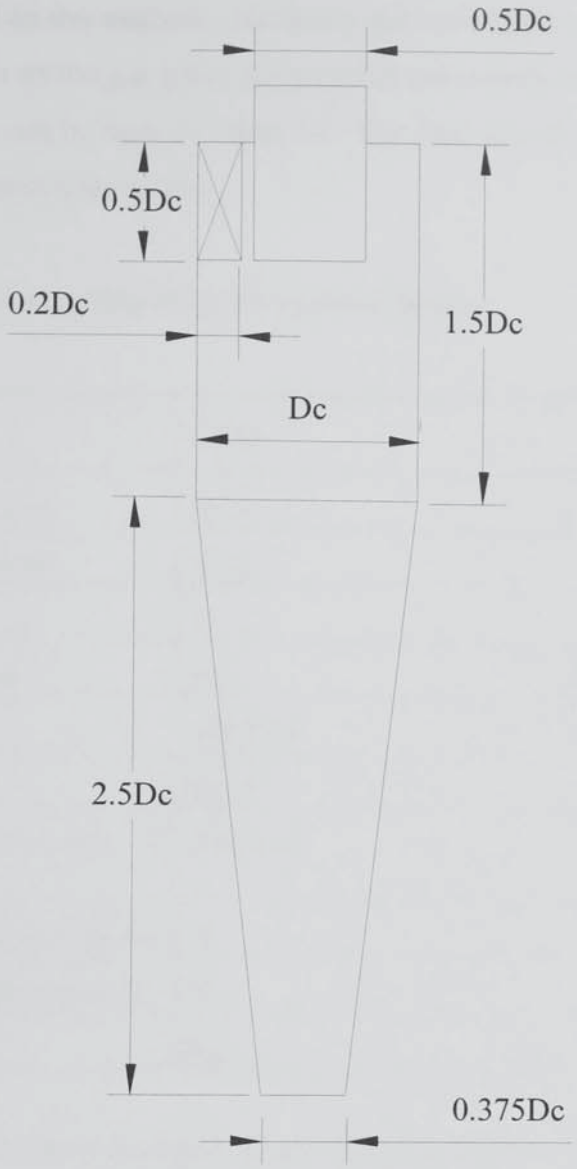

Fig. 36 High efficiency cyclone.

The cyclone should be designed to give an inlet velocity of between 9 and 27 m/s and the optimum inlet velocity to maximise efficiency whilst minimising the resulting pressure drop has been found to be 15 m/s.

9.2.2 CYCLONE SPECIFICATION

To enable an effective design of a cyclone two important things are required: firstly a particle size analysis, obtained in this case by using a Malvern particle size analyser. The char analysed was obtained from the char collected by a cyclone used on a similar type of reactor, this has the weakness that any fines that passed through the cyclone

were not included in the analysis. Secondly the volumetric flow rate, temperature and physical properties of the gas (plus any physical constants) entering the cyclone need to be known. These can be seen in Table 24. The data was obtained from a model of the intended ablative pyrolysis reactor.

Table 24 Physical property data for cyclone design.

Property	Units	Value
Volumetric flow-rate	m^3/s	0.0044
Volumetric flow-rate	m^3/h	15.98
Temperature	K	673
Operating pressure	Pa	101320
Gas viscosity	$mN.s/m^2$	0.028
Particle density	kg/m^3	200
Test fluid viscosity (air, 1 atm, 293K)	$mN.S/m^2$	0.018
Diameter of standard cyclone	M	0.203
Minimum required recovery	%	99
Design velocity	m/s	27

It is desirable to remove as many of the fine particles as possible, therefore a high centrifugal force and consequently a high inlet velocity is required. The maximum inlet velocity of 27 m/s will be specified, the resulting pressure drop being of secondary importance to the collection efficiency. Two important modifications to the standard design need to be made at this point. Firstly, the standard design uses a rectangular inlet duct, this is difficult to design on a small scale and will be replaced by a circular duct. The cyclone diameter calculation will still be based upon the size factors given for a rectangular duct. Secondly, the cyclone design will have to be modified to take account of standard sizes and material availability. This will result in the modification of some sizes and parameters. The calculated parameters and the corresponding specified standard sizes are given in Table 25.

Table 25 Calculated and specified cyclone sizes.

Parameter	Units	Value
Area of inlet duct to give specified velocity	m^2	0.00016
Calculated radius of inlet duct	M	0.0072
Actual radius of inlet duct	M	0.008
Actual area of inlet duct	m^2	0.0002
Diameter of proposed cyclone calc, Dc2	M	0.044
Diameter of proposed cyclone, Dc2	M	0.04
Scaling factor		0.42
Actual velocity	m/s	15.8

The performance calculations, using the particle size analysis, scaling factor and the standard performance curves (112) are shown in Table 26.

Table 26 Calculated performance of cyclone design.

1 Particle size, mm	2 Mean particle size	3 % in range	4 Mean particle size/scaling factor	5 Efficiency at scaled % size	6 Collected (3)*(5)/100	7 Grading at exit (3)-(6)	8 % at exit
>564	564	0	1339.95	100	0	0	0
564-261.7	412.85	23	980.84	100	23	0	0
261.7-160.4	211.05	19.9	501.41	100	19.9	0	0
160.4-112.8	136.6	18.6	324.53	100	18.6	0	0
112.8-84.3	98.55	8.2	234.13	100	8.2	0	0
84.3-64.6	74.45	5.9	176.87	100	5.9	0	0
64.6-50.2	57.4	10.5	136.37	100	10.5	0	0
50.2-39	44.6	4.7	105.96	100	4.7	0	0
39-30.3	34.65	2.2	82.32	100	2.2	0	0
30.3-23.7	27	2.2	64.14	100	2.2	0	0
23.7-18.5	21.1	1.5	50.13	100	1.5	0	0
18.5-14.5	16.5	1.4	39.20	99	1.38	0.014	14
14.5-11.4	12.95	1	30.76	97	0.97	0.03	30
11.4-9	10.2	0.3	24.23	96	0.28	0.012	12
9-7.2	8.1	0.2	19.24	95	0.19	0.01	10
7.2-5.8	6.5	0.2	15.44	94	0.18	0.012	12
<5.8	2.9	0.2	6.89	89	0.17	0.022	22
		100		Overall collection efficiency	99.9	0.1	100

The collection efficiencies shown in column 5 of the table were read from a standard performance curve (111) at the scaled particle size, column 4. The overall collection efficiency satisfies the minimum solids collection requirement. The final cyclone design, based upon the calculated cyclone diameter, can be seen in Fig. 37. The design includes any modifications to the standard design, as described earlier.

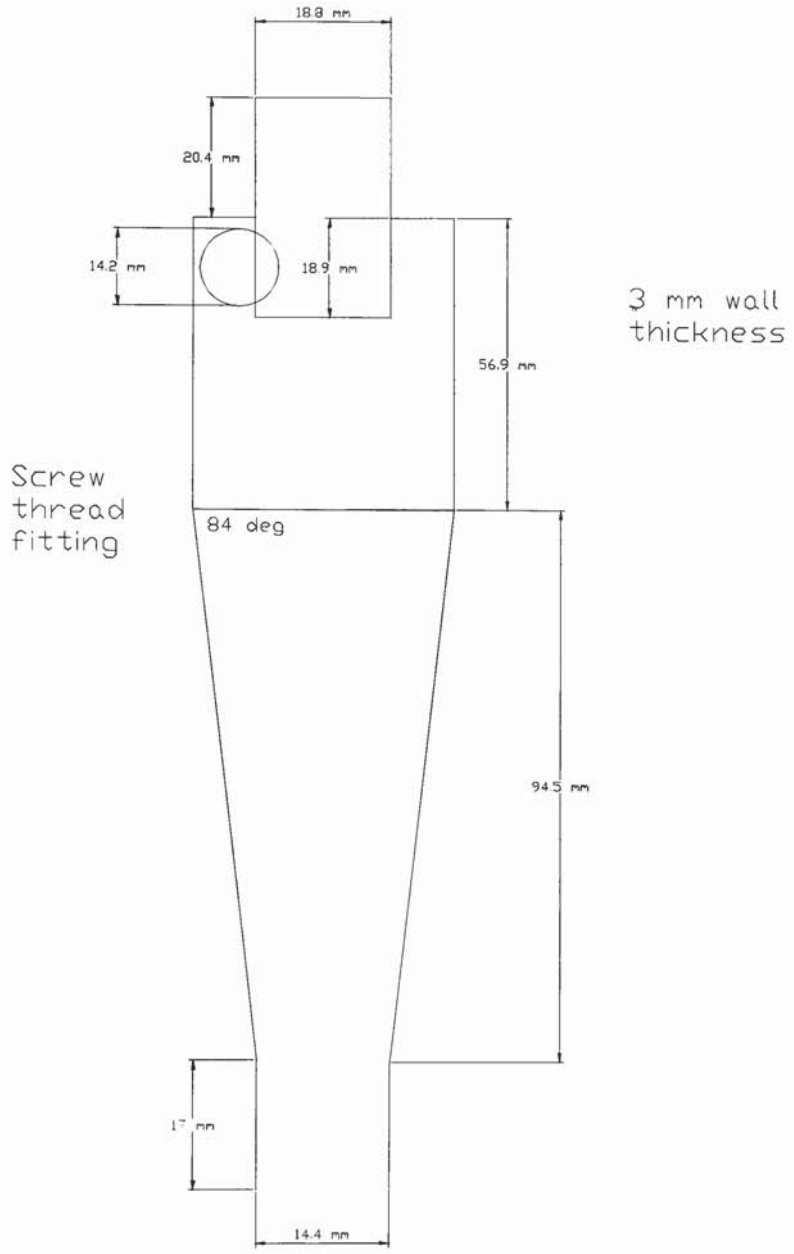

Fig. 37 Cyclone design and dimensions.

9.3 DIRECT-CONTACT HEAT EXCHANGER DESIGN

There are four general classifications for direct-contact gas-liquid heat transfer:

- Simple gas cooling
- Gas cooling with vaporisation of coolant
- Gas cooling with partial condensation
- Gas cooling with total condensation

These processes are exceedingly complex and different sets of relations describe each process. The quenching of pyrolysis vapours may be considered to involve gas cooling with partial condensation. Typical equipment used for direct-contact heat transfer includes:

- Baffle-tray columns
- Spray columns
- Packed columns
- Cross-flow columns
- Pipeline contactors

Design methods for these were summarised in 1961 and 1972 by Fair (113, 114). The most commonly used industrial equipment is the baffle-tray column and the spray columns. Evaluation of available data shows that they typically have a performance in which the number of transfer units (NTU) is only about 1. This value is low due to the occurrence of back-mixing, and in the case of baffle-trays the large gas-side pressure drop. As the pyrolysis process presents a significant fouling problem, only baffle-tray columns will be considered here.

9.3.1 MODELING OF DIRECT CONTACT HEAT EXCHANGERS

One of the reasons direct-contact heat exchangers are not more prevalent in industry is the lack of reliable design and performance prediction methods. This is because direct-contact heat exchangers are difficult to analyse for the following reasons:

- Vapour loading and heat and mass transfer rates decrease continuously as condensation occurs.
- The velocity of the vapour in a direct-contact device varies greatly with distance travelled due to the continuous condensation.
- The latent heat of condensation is high and therefore a large ratio of liquid-to-vapour mass flux occurs. This is not a typical mass transfer experience so experimental data is scarce.

- In-condensable gases are normally present and their effects on the mass transfer rate are difficult to predict under the varying flows experienced.
- In many situation transition from turbulent to laminar flow occurs.

Therefore, the widely use NTU design methodology may not be employed (115). This leaves two principal methods that may be employed; either numerical integration of the rate of mass transfer along the vapour path, or the use of specific design correlations.

9.3.2 Numerical Integration Method

A numerical model for the direct-contact cooling/condensation of pyrolysis vapours with a quenching liquid would require a number of initial assumptions to simplify the problem, these being:

- The exact composition of pyrolysis vapours is not known, therefore an ideal pyrolysis vapour would have to be approximated by the use of key components.
- Specific data on the exact quantities and composition of fugitive vapours that do not condense is not known and this would either have to be assumed from operational data, or calculations would have to be based on complete condensation.

Numerical analysis of the system would require the use of the conservation of mass, momentum and energy equations. In addition expressions for the thickness of the liquid falling film and the gas and liquid mass transfer coefficients would be required. The complexity of this design method and the lack of data makes it currently unsuitable.

9.3.3 General Design Methods

Heat exchangers involving the direct-contact between gas and liquid are designed along the same principles as gas absorbers. The diameter of the exchanger must be large enough to prevent excessive entrainment and flooding. The height of the exchanger must be sufficient to enable the desired approach temperature between the exit gas and entering liquid to be achieved.

9.3.4 BASIC PRINCIPLES

Considering a direct contact heat exchanger, there is clearly a need to be able to calculate the heat exchanger size and volume.

For a differential element of height dz and cross section S, the total required volume may be calculated from:

$$V_T = \int_0^{Z_T} SdZ = \int_0^{Q_T} \frac{dQ}{Ua(t_g - t_l)} \qquad \textbf{Eq. 134}$$

Where

a = interfacial area.
t_g = gas temperature.
t_l = liquid temperature.
Q_t = total energy transferred.
U = overall heat transfer coefficient.
V_T = total volume.
Z_T = total exchanger height.

And

$$Z_T = \frac{V_T}{S} = \frac{Q_T}{Ua\Delta t_m S} \qquad \textbf{Eq. 135}$$

Ua, the average overall volumetric heat transfer coefficient, is a function not only of individual phase transfer coefficients, but also of the degree and direction of mass transfer. The mean temperature difference, Δt_m, is normally based on the assumption of plug flow, but it is obvious that axial mixing will have an effect.

The overall volumetric heat transfer coefficient, Ua, can be related to the film transfer coefficients, $h_l a$ and $h_g a$, for the case of partial condensation with gas cooling (as occurs in pyrolysis gas quenching) by:

$$Ua = \frac{1}{\frac{1}{h_l a} + \left(\frac{1}{\alpha h_g a}\right)\left(\frac{Q_g}{Q_T}\right)} \qquad \textbf{Eq. 136}$$

Where α, a correction factor for simultaneous heat and mass transfer is given by

$$\alpha = \frac{C_0}{1 - e^{-C_0}} \qquad \textbf{Eq. 137}$$

and

$$C_0 = \frac{N_A c_{g,A}}{h_g a V_T} \qquad \textbf{Eq. 138}$$

Where

C_0 = is a correction factor.

N_A = rate of diffusion of species A.

$c_{g,A}$ = gas heat capacity of component A.

9.3.5 BAFFLE-TRAY COLUMN PERFORMANCE

In baffle-tray columns, gas-liquid contact occurs in the occurs in the curtain of liquid that cascades from plate to plate. Several varieties of baffle plate exist and examples may be seen in Fig. 38 below.

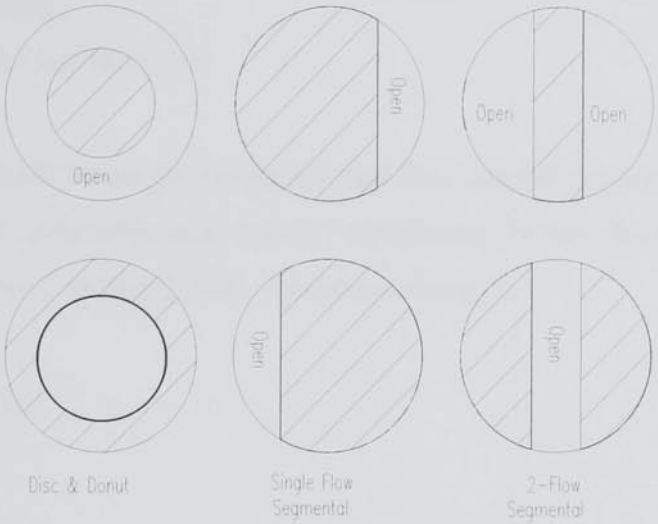

Fig. 38 Sample of available baffle types.

Entrainment flooding determines the vapour capacity of the baffle column. The maximum available vapour velocity is based on either the window or curtain area, whichever is limiting. The window area may be defined as the cross sectional area of the column not occupied by the plate and the curtain area may be defined as the vertical area comprising a single plate spacing. The vapour velocity in either the curtain or window area may be calculated from:

$$v_{c,max} = 1.15\left[\frac{\rho_l - \rho_g}{\rho_g}\right]^{1/2} = \frac{q}{A_c} \qquad \textbf{Eq. 139}$$

$$v_{w,max} = 0.58\left[\frac{\rho_l - \rho_g}{\rho_g}\right]^{1/2} = \frac{q}{A_w} \qquad \textbf{Eq. 140}$$

Where

$v_{c,\,max}$ = maximum allowable velocity in curtain.

$v_{w,\,max}$ = maximum allowable velocity in window.

ρ = density.

A_c = curtain area.

A_w = window area.

q = volumetric gas flowrate.

The values 1.15 and 0.58 are the recommended Souders-Brown coefficients. The value of Ua, the overall volumetric heat transfer coefficient, is best obtained for a complex system like this from correlated data. A standard form is:

$$Ua = C_1 G^m L^n \qquad \textbf{Eq. 141}$$

Where

C_1 = a constant fixed by the baffle spacing and quench liquid type.

G = gas mass velocity.

L = liquid mass velocity.

m & n = system dependent constants.

For the pyrolysis quenching system the constants given above will have to be determined, but data from other similar systems enable the following approximate values to be determined (116). As data become available the accuracy of the estimations will be assessed.

C_1 = 0.026

m = 0.70

n = 0.40

9.3.6 SPECIFICATION OF QUENCH COLUMN

Not enough is known about the temperature differences in the quench column and the expected efficiency to enable a calculation of the required quench column size. Therefore the quench column will be sized according to the gas flows and flooding factors. The intended design for the quench column can be seen in Fig. 39 below.

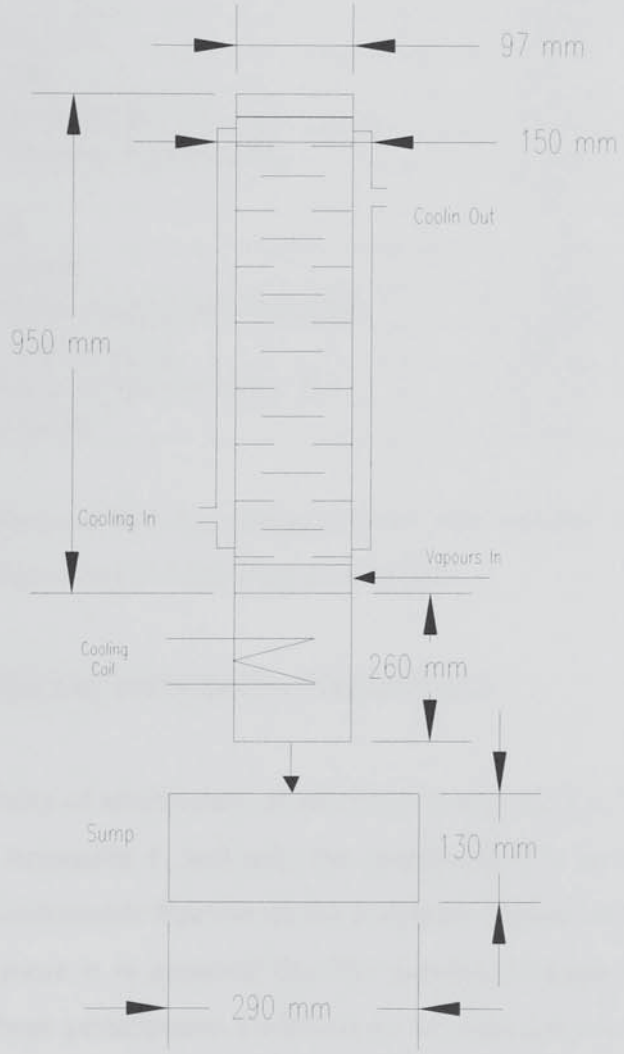

Fig. 39 Specification of quench column.

The disk and doughnuts plates contained within the column have the following specification, calculations of the window and curtain velocity are based on the bottom of the column where the temperature of the vapours will be 400 °C and will therefore have the highest volumetric flowrate:

Table 27 Design parameters of quench column.

Parameter	Value
Volumetric flowrate, m^3/s	0.0044
Temperature, °C	400
Column Diameter, cm	9.7
Plate Diameter, cm	9
Doughnut outside diameter, cm	9.6
Doughnut inner annular diameter, cm	3.4
Plate spacing	2
Number of plates	18
Number of doughnuts	19
Maximum allowable window velocity, m/s	18.3
Actual window velocity, m/s	5.1
Maximum allowable curtain velocity, m/s	36.3
Actual curtain velocity	2.1

From this it can be seen that the design curtain and window velocity limits are well below the limits allowed by the flooding calculations.

9.4 ELECTROSTATIC PRECIPITATOR DESIGN

Due to the complexity of electrostatic precipitator design (E.P.), the model development is documented in Appendix 1, and only the specification is given here. It is assumed that 70 % of the condensable fraction of the pyrolysis vapours is removed in the quench column. Further more it is assumed that the pyrolysis vapour will have been cooled down to 20 °C. These assumptions are based on calculations derived from experimental work carried out on a 1.5 kg/hr fluidised bed reactor by Hague (1).

The electrostatic precipitator specification and performance are given in Table 28 below, for further details see Appendix 1.

Table 28 Design parameters of electrostatic precipitator.

Parameter	Value
E.P. diameter, cm	9.7
E.P. length, cm	20
Electrode wire diameter, mm	0.2
Operating temperature, K	293
Volumetric flowrate, m^3/hr	7.2
Residence time, s	0.7
Corona initiation voltage, kV	8.4
Efficiency at operating voltage of 20 kV, %	99
Efficiency at operating voltage of 10 kV, %	98

The electrostatic precipitator will be directly mounted on top of the quench column and will be wet walled to aid product collection. The arrangement of the quench column and electrostatic precipitator can be seen in Fig. 40 below:

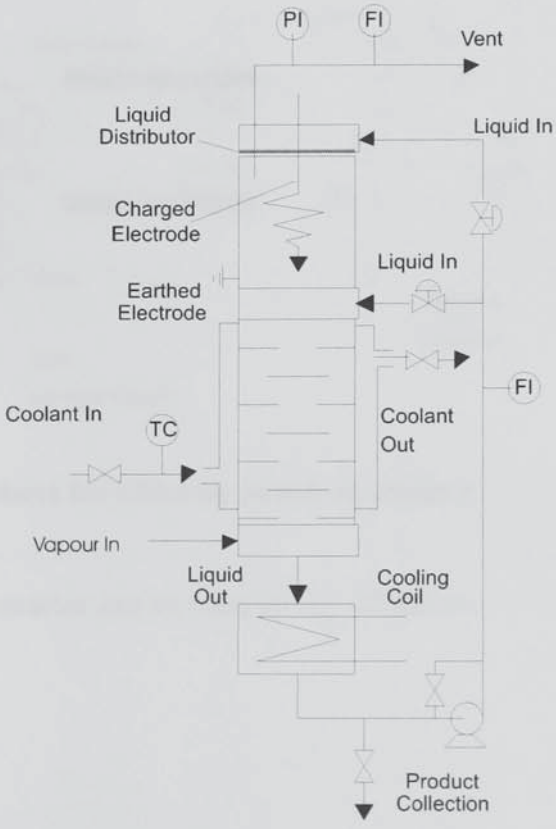

Fig. 40 Quench column and electrostatic precipitator.

10. CONSTRUCTION OF REACTOR

10.1 OVERALL REACTOR DESIGN

The reactor and product collection system were fabricated by the department workshops according to the specifications given in Chapter 5 and 9. A frame was constructed to support the reactor and product collection system. The system was then assembled and all necessary piping, instrumentation and electrical equipment installed. A process flowsheet may be seen in Fig. 41 below.

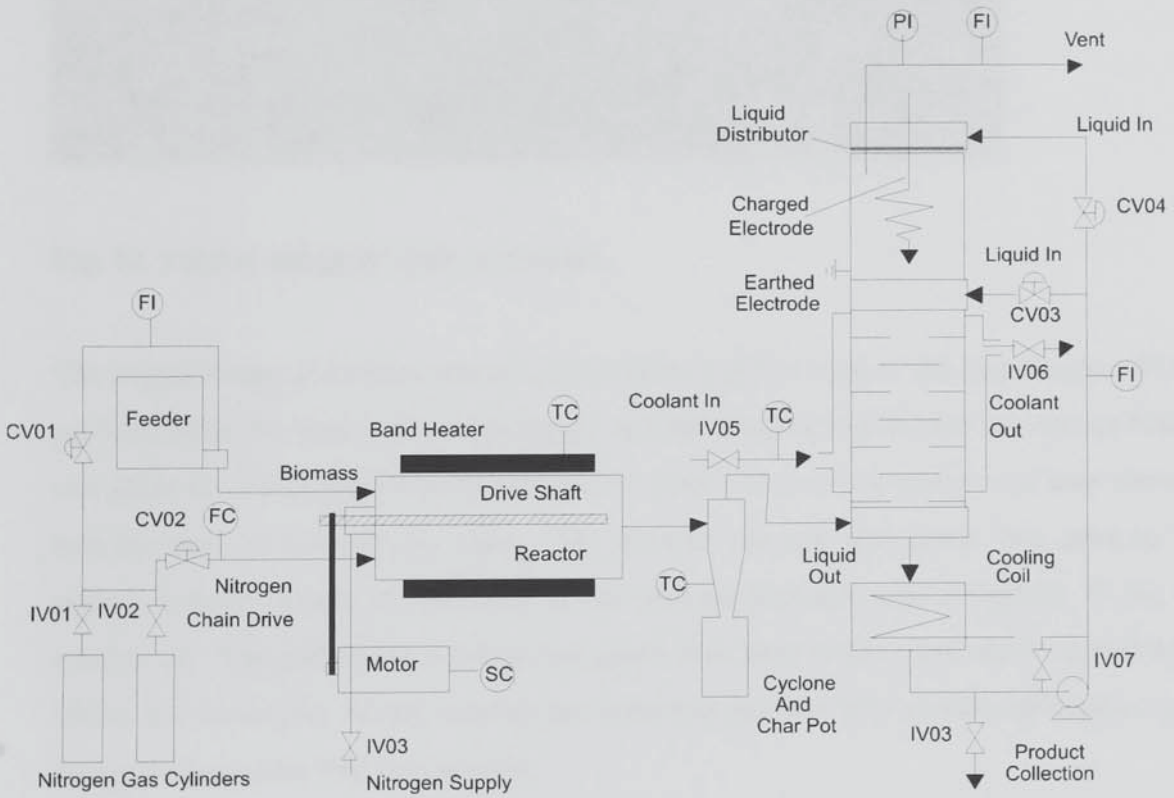

Fig. 41 Process flowsheet for ablative pyrolysis reactor.

A digital image of the reactor can be seen in Fig. 42 below.

Fig. 42 Digital image of scale of reactor.

The digital image shows the reactor construction and the scale of the installation. Wood particles enter the reactor from the feeder and are swept along behind the reactor blades and ablated. The product vapours, gases and solid char exit the reactor and pass through two cyclones to remove the char. The process vapours and gases then pass to the quench column where the majority of the process vapours, approximately 70 %, are condensed. The remaining vapours and gases then pass to the electrostatic precipitator where the remainder of the vapours are removed and the non-condensable gases pass through a gas meter and then to vent.

The major equipment comprising the reaction system and that necessary for successful experimental runs are detailed as follows.

Table 29 Equipment list for reaction system.

Equipment	Quantity	Description Of Function
Wild Bartfield 0.8 kW furnace.	1	Furnace used to preheat nitrogen supply to reactor.
Platon 100 l/min rotameters	3	Used to control supply of nitrogen to reactor.
Accurate 3 kg/hr screw feeder.	1	Used to convey wood feed into reactor.
Hawco 11.5 kW Band heater.	1	Provides necessary temperature and energy for ablation.
RS trace heating tapes.	5	Process pipe heating.
RS digital temperature controllers	3	Temperature control of furnace, band heater and trace heating tapes.
Fenner 1.5 kW drive motor.	1	Linked to drive shaft to provide relative motion required for ablation.
Fenner 12A Sprint controller.	1	Controls drive motor.
Stuart 210w centrifugal pump.	1	Recirculates quench liquid around quench column.
Lab-Plant RC 150 refrigerated recirculator	1	Recirculates refrigerated glycol/water mixture around quench column jacket to remove process waste heat.
Schlumberger gas meter	1	Determines volumetric flowrate of waste gases emitted.
ATI Unicam series 610 gas chromatograph	1	Determines composition of waste gases emitted.
Microlink 3000 data logger	1	Measures and records process temperatures.
P90 Computer	1	Controls Microlink 3000 and records data generated
Assorted pipework, fittings, valves and pressure gauges.	1	Process piping and instrumentation.

10.2 DRIVE SHAFT

The drive shaft, supported by two bearings enters the reactor through the seal housing, which is attached to the front plate of the reactor. This can be seen in Fig. 43 below.

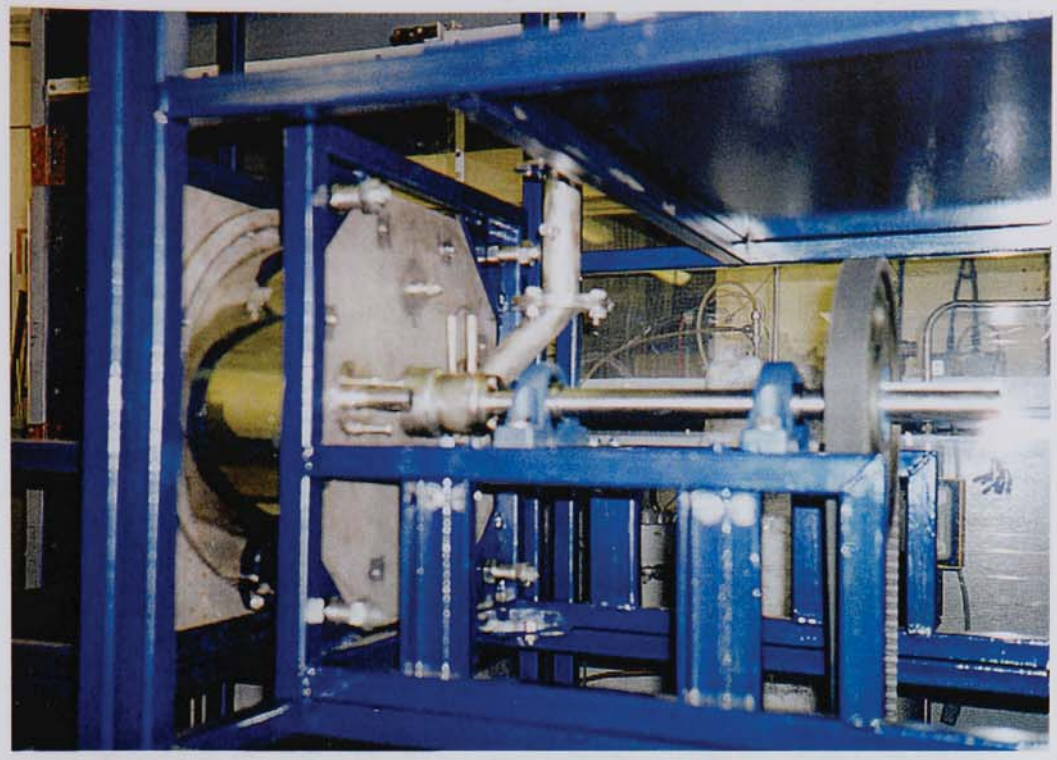

Fig. 43 Drive shaft seal housing.

The drive shaft seal housing contains an aluminium/bronze bush to support the weight of the drive shaft and provide lubrication. A high temperature polymer seal is used in conjunction with a nitrogen purge to prevent product loss. A pulley wheel and belt drive can be seen attached to the drive shaft. This links to the drive motor and controller.

10.3 REACTOR INTERNALS

The ablative pyrolysis reactor uses a bladed approach to provide the requisite high contact pressure and relative motion. In addition the blades are attached to an inner cylinder, the primary function of which is to reduce the available vapour space thereby decreasing the vapour residence time and minimising product cracking. The bladed reactor internals can be seen in Fig. 44 below.

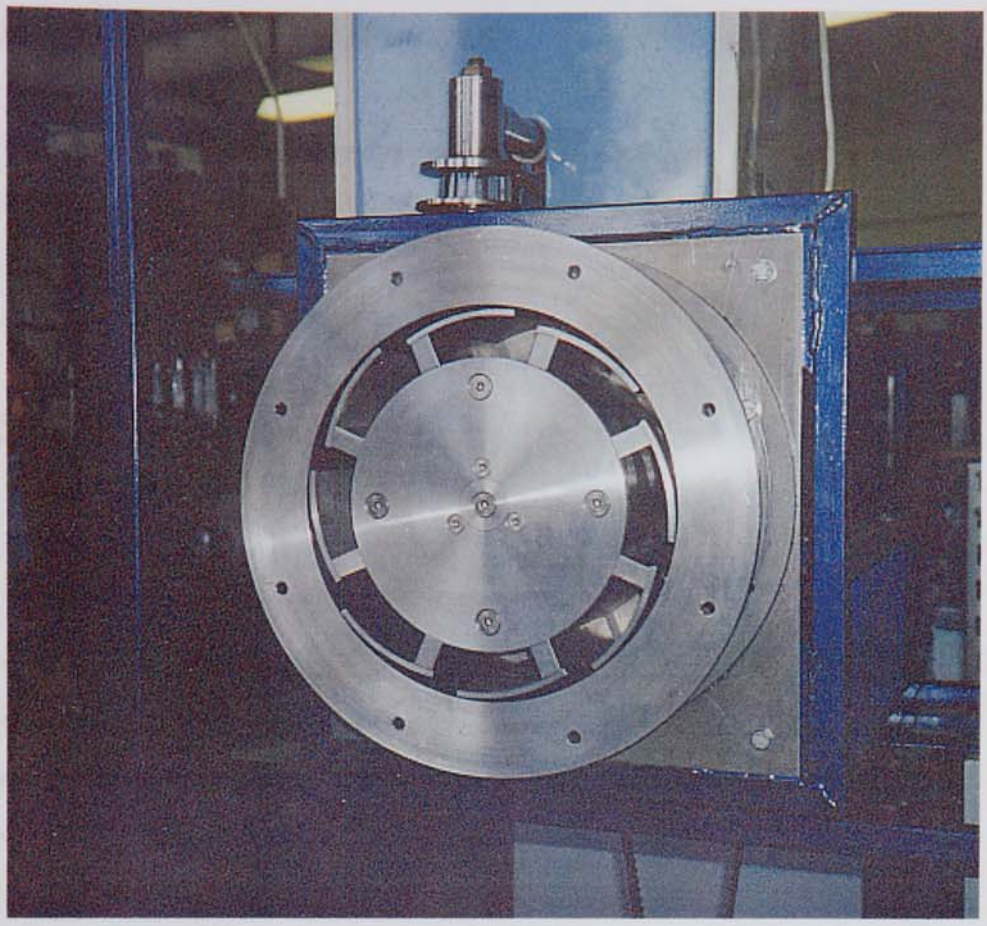

Fig. 44 Digital image of reactor internals.

The curved blades were utilised so as to ensure a constant angle between the blades and the heated outside wall. The blades were fabricated by cutting sections from a cylinder of stainless steel and screwed at the required blade angle to the blocks that can be seen in the diagram above. These in turn are bolted to the internal cylinder, which is attached to the drive shaft and provides the relative motion. The particles enter the reactor from the back and fall to the bottom in a random distribution before being swept along beneath the blades and ablated. Char is entrained out of the back of the reactor also before being removed in two cyclones. Heat input to the reactor is provided by two sources. The primary source is a 5.5 kW ceramic band heater, which heats the outside wall and provides the energy needed for ablation. This also heats the rest of the reactor by conduction and convection. Heated nitrogen is also used to not only provide an inert atmosphere and transport gas but also to help heat the reactor by convection.

10.4 OPERATING PROCEDURE

The procedures detailed below are necessary for the successful operation of the reaction system and should be followed at all times.

Ensure the following initial conditions are met before start up:

1) All heater switches are in the off position. These being the gas pre-heater, the tape heaters and the band heater.
2) All other electrical equipment is off.
3) The following valves are all shut:

- IV01 Nitrogen cylinder isolation valve
- IV02 Nitrogen cylinder isolation valve
- CV01 Nitrogen supply to feeder control valve
- CV02 Nitrogen supply to reactor control valve
- IV03 Nitrogen supply to drive seal isolation valve
- IV04 Product collection isolation valve

4) The following valves are open:

- IV05 Coolant liquid in isolation valve
- IV06 Coolant liquid out isolation valve
- IV07 liquid recycle isolation valve
- CV03 Quench column recycle control valve
- CV04 E.P. recycle control valve

Ensure the following start up procedure is followed.

Pre-start (warm up) procedure:

1) Turn on electrical furnace 3 hours before run commences
2) Open isolation valve IV03 nitrogen supply to drive shaft seal 1 hour before run commences
3) Open either isolation valve IV01 or IV02 Nitrogen supply
4) Open control valve CV01 Nitrogen supply to feeder to a minimum value

5) Turn on band heater and gradually increase to the required operating temperature (500-600 ^{0}C) for 1 hour prior to experimental run.
6) Turn on tape heaters to 450 °C 30 minutes before experimental run
7) Turn on refrigeration unit to –10 °C 30 minutes before experimental run
8) Fill quench column with 2 litres of octane
9) Turn on recycle pump
10) Turn on electrostatic precipitator

Start up procedure:

1) Set CV01 Nitrogen supply to feeder to desired value (60 cm^3/s)
2) Set CV02 Nitrogen Supply to reactor to desired value (60 cm^3/s)
3) Turn on motor to desired rpm (max 315)
4) Turn on G.C.
5) Set Feeder to desired feed rate
6) Start feeder and data logger simultaneously

Shut down procedure:

1) Turn off the feeder
2) Turn off motor
3) Turn off all heaters
4) Set nitrogen to low flowrate
5) Leave system to cool
6) Turn off nitrogen
7) Turn off nitrogen supply to seal housing
8) Turn off chiller
9) Turn off all other equipment

Emergency shut down procedure:

1) Turn off motor
2) Turn off feeder
3) Turn off all heaters

11. PILOT PLANT COMMISSIONING

11.1 INTRODUCTION

This chapter deals with the commissioning of the pilot plant, any problems encountered and where possible any modifications made to surmount these difficulties. Problems will be analysed in chronological order unless there is a significant overlap where problems occurred over extensive time periods, in these cases the problems will be presented in the order that offers the most clarity.

11.2 MOTOR SPECIFICATION

In ablation the pyrolysis particle is moved relative to the heated surface in order to rapidly remove products from the reaction interface. A key feature of ablation is the high contact pressure between the particle and heated surface, which serves to maximise the heat transfer into the particle. Ideally the ablating particle slides on its own film of liquid reaction product, previously termed an "Active" layer. However, in practice biomass particles do not react instantaneously and there is an instant of dry friction before ablation, which leads to significant increases in the frictional load on the drive motor. This is difficult to quantify and makes motor specification problematic.

Initially a 180 W D.C. variable speed motor was specified for the reaction system. The motor had a maximum rpm of 1500 and was connected to the reactor drive shaft using pulley wheels and a belt drive. The pulley wheels were chosen to effect a 4:1 reduction in motor speed in order to enable more torque to be generated. This motor proved to be insufficiently powerful to ablate biomass particles.

A more powerful 370 W D.C. variable speed motor was obtained and fitted. The motor had an integral gearbox that reduced the output speed from 1500 to 315 rpm enabling more torque to be generated. The motor was connected to the drive shaft using a chain drive and toothed cogwheels in a 1:1 ratio. This motor proved partially effective in that it was able to achieve ablation at feed rates of up to 1.5 kg/hr, feed rates in excess of this caused the motor to stall.

A 1.5 kW D.C. variable speed motor was then fitted. The motor had an integral gearbox that reduced the output speed from 1500 to 375 rpm. This was attached to the reactor drive shaft using the same chain drive and toothed cogs. This proved successful in achieving ablation at feed throughputs of up to 2.2 kg/hr, which was the limit of the feeding device employed.

11.3 MICROLINK 3000 DATA LOGGER

The Microlink 3000 is a piece of hardware which converts analogue inputs from thermocouples into digital data which can then be logged using dedicated software such as Windmill™ data logging and management software. The analogue inputs from the thermocouples are passed into an external 3903 thermocouple junction box with up to 15 available channels. This is linked to the Microlink 300 where information first passes to a 3054 interface card which conditions the signals before passing them to a 3040 A.D. converter card which converts the signals from analogue to digital. The digital signals are then passed to a 3701 serial interface card and then to the logging computer.

Problems were encountered due to the use of an electrostatic precipitator (E.P. see Appendix 1) as a part of the product collection system. Whilst the E.P. was stable no problems occurred, however, the E.P. could, on occasion, arc which caused a rapidly collapsing electric field which induced transitory currents in the thermocouple wires. This caused irreversible damage to the 3054 interface card, resulting in it requiring replacement. Initial efforts to resolve the problem involved better electrical insulation of the E.P. but this proved only partially successful. The problem was finally solved by fitting transitory absorption diodes to the 3903 thermocouple junction box to absorb any transitory currents.

11.4 DRIVE SHAFT

The necessary high contact pressure and relative motion between the biomass particles and the reactor heated surface was provided by angled blades attached to a drive shaft which was driven by a motor. The stainless steel drive shaft had a 1 inch diameter and

entered the reactor through a seal house which was attached to the front plate of the reactor. A diagram of the arrangement can be seen in Fig. 45 below

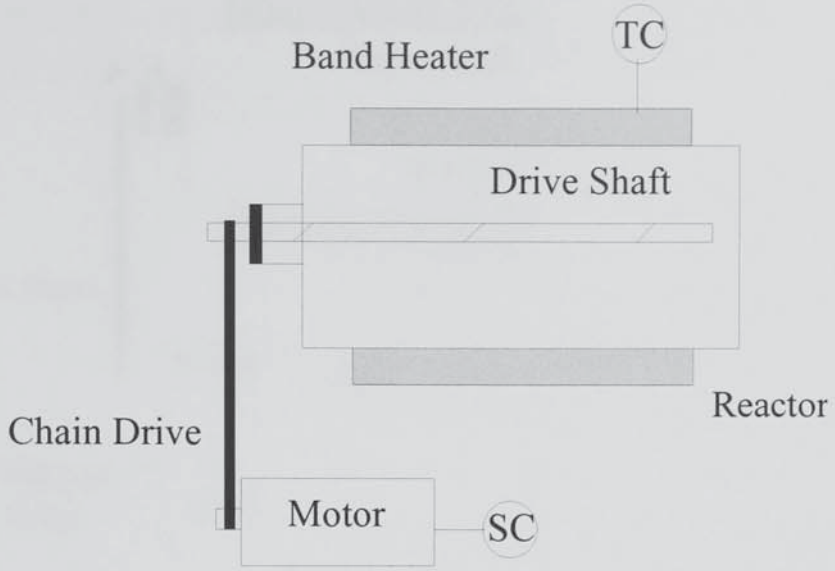

Fig. 45 Initial drive shaft arrangement.

To provide a seal and prevent an escape of pyrolysis vapours the drive shaft enters the reactor through a seal house. This was initially fabricated with a tight clearance from the drive shaft and this combined with a high temperature polymer seal was used to prevent pyrolysis vapours escaping from the reactor. However, during one run the assembly seized causing the motor mounting to warp and bend until sufficient slack was obtained for the drive chain to slip. When the assembly was dismantled it was discovered that pyrolysis vapours had been deposited upon the drive shaft inside the seal house and had coked, ultimately leading to the seizure. To prevent this from occurring again the seal house was drilled out to a larger diameter and an aluminium/bronze bush was incorporated to provide extra support and a softer more lubricating surface. In addition, a nitrogen purge was added to prevent any further vapour deposition. This can be seen in Fig. 46 below.

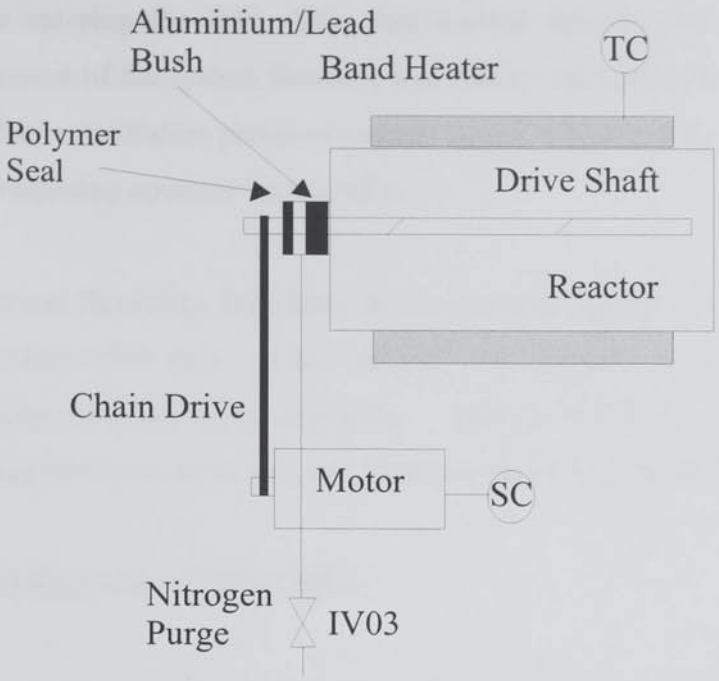

Fig. 46 Drive shaft arrangement.

11.5 QUENCH COLUMN OPERATION

Initially the plates in the quench column were machined to too large a diameter (9.4 cm instead of 9.0 cm), which caused the system to flood at high vapour and liquid flowrates. This was because the vapour velocity in the window area was in excess of the limit determined in Chapter 9. This caused the column to flood, as the quench liquid was unable to cascade down the column. As the vapour flowrate is fixed by reactor throughput and residence time requirements, the only control variable available was the quench liquid flowrate. This had to be operated at a minimum in order to avoid flooding of the quench column, which is not ideal as insufficient cooling is then obtainable. When the quench column flooded, a frothing mixture was produced which was entrained up the column. In severe cases this entered the electrostatic precipitator providing an electrical current pathway. This reduced the efficiency of the electrostatic precipitator to such an extent that continued operation was no longer possible unless action was taken to stop the column flooding. Although this could be prevented by careful control of the vapour and liquid flowrates it was still difficult to predict when flooding would occur due to non-steady state operation. Therefore in order to minimise the impact of the occasional flooding that did occur, a disengagement section, of approximately 4 column diameters, was added to the system to prevent the frothing

mixture entering the E.P. This had limited success due to the fact that a further consequence of the system flooding was that the increased hold-up in the column would starve the recirculation pump of quench liquid, which could cause the pump to loose its prime, requiring operator intervention.

To increase flexibility the plates in the quench column were machined to the correct specification (9.0 cm). This reduced the velocity in the window area, thereby preventing flooding from occurring. This removed the need for a vapour liquid disengagement section so this was removed from the collection system.

11.6 REFRIGERATION UNIT

A refrigeration unit was used to provide the cooling to the quench column jacket. The cooling fluid used was a recirculating glycol/water solution, which was in turn cooled to the desired temperature by the refrigeration unit. It was noted that the refrigeration unit was struggling to maintain its temperature setting. This caused heat accumulation in the quench column as the refrigeration unit could not cope with the duty required. The heat accumulation in the quench column also caused the temperature in the electrostatic precipitator (E.P.) to rise, ultimately resulting in its failure due to an inability to initiate a corona due to arcing. The problem with the refrigeration unit was eventually linked to a faulty weld that had allowed the refrigerant gases to progressively escape. This was repaired and the unit operated satisfactorily.

11.7 ELECTROSTATIC PRECIPITATOR

Problems were encountered with the E.P. in that for the initial sections of an experimental run the E.P. would work at approximately 99% efficiency as designed. Then after an indeterminate amount of time the efficiency would fall which forced the experimental run to be shut down. This was a perplexing phenomenon as the E.P. didn't fail completely, only the efficiency was reduced. A partial failure was difficult to understand and this was compounded by the fact that the system worked perfectly in an air only environment. This can be explained as follows. In a pyrolysis atmosphere using the E.P. specified in Chapter 9 , corona initiation occurs at approximately 9 kV but the system is operated at 20 kV in order to achieve approximately 99 % collection

efficiency. However it was noted that during some experimental runs the operating voltage would drop to about 12 kV and therefore the efficiency would fall (as the efficiency is a function of the applied voltage). It was eventually discovered that a small film of pyrolysis oil could build up on the walls of the E.P. This formed a conductive pathway between the charging electrode and collection electrode, which conducted at a voltage of about 12 kV. This was sufficiently high a voltage for corona initiation to still occur, but at this low voltage the collection efficiency was impaired. This problem was difficult to identify as when the system was dismantled and tested in an air atmosphere, where corona initiation occurs at 6 kV, the problem did not reoccur as a voltage of 12 kV, at which point the oil film started to conduct, could not be achieved. The problem was eventually deduced and rectified by fitting an insulating sheath to the charging electrode. This only proved partially successful as the extremely high voltages employed caused an arc through the insulation and onto the liquid film. This in turn provided a conductive pathway to collection electrode and both voltage and efficiency would fall.

In order to prevent the conducting liquid film from forming in the first place, the electrostatic precipitator length was increased from 20 cm to 45 cm. This increased the operating efficiency from 99% to 99.9%. This prevented the conducting film of pyrolysis oil from forming thereby preventing the drop in voltage from occurring. This enabled the electrostatic precipitator to operate efficiently without any further problems.

11.8 BIOMASS FEEDER

A number of problems were encountered with the biomass feeder which are described as follows:

- Problems were encountered with the biomass feeder due to its inability to feed particles with a size greater than 5x4x10 mm. Particles in excess of this size blocked the screw feeder necessitating in reactor shutdown. This size particle is undesirable as it is difficult and expensive in time and effort to produce due to its small size. The pyrolysis reactor designed is capable of handling particle sizes with a cross section of up to 6 mm^2 (with the length being limited by operational requirements, say <20

mm) which would be a preferable particle size to use, however this would require the purchase of a new feeder which was not feasible.

- Problems were encountered in that the feeder was limited to a maximum feed rate of 3 kg/hr. Modeling of the reactor revealed that it would be capable of operating at an average capacity of 30 kg/hr. Therefore the reactor is operating significantly below capacity. This leads to low vapour product flowrates, requiring significant quantities of nitrogen gas in order to keep the vapour residence time down to acceptable limits. This is clearly undesirable as the reactor was not tested to the limit of its capacities and also because nitrogen is an expensive resource.

- The feeder hopper was limited to an operational capacity of approximately 1.5 kilograms of pine wood particles. This restricted experimental run times at maximum feeder throughput to 60 minutes, which is not ideal.

- The biomass feeder has an internal rubber lining which is used to provide an airtight seal, which is vital for successful pyrolysis experiments. The action of the screw feeder forced particles against this rubber lining, which eventually failed due to the constant attrition. This was fixed with a rubber patch and some adhesive. This can only be a short term solution and either a new rubber lining or preferably a new feeder should be purchased.

12. EXPERIMENTAL MASS BALANCES AND RESULTS

12.1 INTRODUCTION

This chapter details the mass balances and analyses obtained for successful experimental runs. Although more runs were performed than described in this chapter many of these were commissioning runs and therefore were incomplete as problems were identified which required corrective actions. The following assumptions were made in the determination of the experimental mass balances:

- All of the biomass fed to the reactor is ablatively pyrolysed with no unconverted biomass remaining. The justification for this assumption being based upon visual observation and sieving of the product char.
- Any increase in mass of the process piping will be solely attributed to char deposition. This is justified as the process piping is trace heated to 450 ^{o}C to prevent product vapour condensation.
- A hold up of 40g of product liquid is assumed for the disk and doughnut plates housed in the quench column unless the true value was actually measured. This assumption is based upon an average value determined from three experimental runs. These values were determined by dismantling and weighing the disk and doughnut section during early commissioning runs. This practice was discontinued due to the intensive labor requirements and the possibility of product loss due to spillages. It is difficult to know what the true hold up was but the low liquid yields combined with the low mass balance closures tend to support the theory that the hold up in the column was greater than estimated.

12.2 EXPERIMENTAL MASS BALANCES

The experimental mass balances on a dry wood yield basis are given in Table 30 below together with pertinent experimental operating conditions. A description of each run is presented after Table 30 detailing any problems and points of interest that are associated with the run. For Runs NR01 and NR02 a gas chromatograph was unavailable for gas analysis, therefore the gas analysis and consequently mass balance closure is not given and this is indicated by an asterix, *.

Table 30 Experimental mass balances for ablative runs.

Run Number	NR01	NR02	NR05	NR06
Date	19/10/98	20/2/99	22/3 99	8/4/99
Wood type	Pine	Pine	Pine	Pine
Wood feed, g wet basis	1674	105	500	708
Run time, s	5880	2460	2940	2363
Feed rate, kg/hr wet basis	1.02	0.15	0.61	1.07
Wood moisture content, % dry basis	8	11.1	9.7	10
Reactor surface temperature, °C	547	550	530	560
Vapour temperature, °C	421	300	266	292
Relative velocity, m/s	12.1	12.1	12.1	12.1
Vapour residence time, s	1.87	2.5	4.53	1.93
Liquid moisture content, %	22	14	18.97	26
Char yield, %	15.65	9.5	21.7	21.35
Organics yield, %	42.05	45.15	41.26	41.8
Water yield, %	10.51	7.35	9.66	14.25
Gas yield, %	*	*	13.2	19.62
Closure, %	*	*	85.82	97.02
CH_4, %	*	*	2.6	2.2
CO_2, %	*	*	50.65	32.96
C_2H_4, %	*	*	0.46	0.47
C_2H_6, %	*	*	0.88	0.64
H_2, %	*	*	2.95	1.82
C_3H_6, %	*	*	12.66	2.07
CO, %	*	*	29.78	59.76

Run Number	NR07	NR08	NR10	NR11
Date	27/4/99	26/5/99	23/8/99	7/10/99
Wood type	Pine	Beech	Pine	Pine
Wood feed, g wet basis	1219	1041	1282	1044
Run time, s	5100	1640	3610	3600
Feed rate, kg/hr wet basis	.86	2.28	1.28	1.044
Wood moisture content, % dry basis	10.1	10.4	10	12.5
Reactor surface temperature, °C	511	555	570	580
Vapour temperature, °C	325	332	300	291
Relative velocity, m/s	12.1	12.1	12.1	12.1
Vapour residence time, s	1.95	1.47	2.05	1.52
Liquid moisture content, %	14.1	14	38	21.3
Char yield, %	18.09	13.83	20.9	20.58
Organics yield, %	42.21	54.15	35.64	48.05
Water yield, %	14.53	10.71	23.66	14.34
Gas yield, %	17.99	12.37	14.33	11.45
Closure, %	92.90	91.06	94.53	94.43
CH_4, %	2.67	2.7	3.51	3.4
CO_2, %	30.07	46.27	33.3	32.9
C_2H_4, %	0.69	0.37	.4	.2
C_2H_6, %	0.9	0.66	.7	2.0
H_2, %	1.91	1.2	1.34	1.86
C_3H_6, %	2.32	0.2	0.70	0.11
CO, %	61.45	48.66	59.97	59.3

NR01 The first commissioning run used a 180 W D.C. variable speed motor to provide the power and relative velocity for the reactor blades. The wood used was Pine wood and was rectangular in shape with dimensions of 2 x 2 x 11 mm. The reactor was capable of ablating these particles at a feed rate of up to 1.02 kg/h before the frictional load became to great for the drive motor.

NR02 For this commissioning run larger pine wood particles which were rectangular in shape with dimensions of 5 x 4 x 10 mm were used as they were easier and less time intensive to prepare. Due to the increased surface area of the wood particles they were more likely to suffer dry friction, the instant when the particle first enters the reactor and the active layer isn't present to provide lubrication, which could cause the motor to stop. In addition they also had a larger friction factor when the active layer was present due to their increased surface area. At high feed rates the frictional load could prove to great for the motor and force it to stop, this limited the reactor to a maximum capacity of 0.15 kg/hr. This was clearly too low and therefore the drive motor was changed to a more powerful 330 W D.C. variable speed motor, see Chapter 11.

NR05 This run used the same pine wood particles as the previous run with dimensions of 5 x 4 x 10 mm. The 330 W motor proved capable of ablating wood particles at feed rates of upto 0.61 kg/hr before the frictional load became to great for the motor to cope. It was during this experiment that the drive shaft jammed, see Chapter 11, damaging the motor mounting. A decision was made to use this opportunity to change the motor to a 1.5 kW D.C. variable speed motor.

The 1.5 kW motor proved capable of ablating the 5 x 4 x 10 mm pine wood particles at the maximum capacity of the feeder, which proved to be 1.28 kg/hr. An additional feed material, hammered milled beech wood, was tested in run NR08. This had average dimensions of 1 x 4 x 8 mm, essentially flat chips, and was capable of being fed at feed rates of up to 2.28 kg/hr which was the maximum capacity of the feeder.

Experimental runs NR02, NR07 and NR08 produced bio-oil with low water contents, average value of 14 %, which is both expected and desirable. Run NR05 produced a bio-oil with a water content of 18.97 % which is most likely due to the long vapour

residence time of 4.53 seconds. Runs NR01, NR06, NR05 and NR11 produced bio-oils with water contents in excess of 20 % but below 30 %. This is perfectly acceptable and the higher water contents are due to char blockages in the process piping and cyclones. This char catalytically cracks the product vapours producing water and non-condensable gases. This serves to increase the water content of the condensed oils. The larger the quantity of char blocking the pipework the longer the vapour contact time and consequently the more cracked the vapour is with a high liquid product water content.

Run NR10 had pipework and cyclones that were extremely blocked with char which led to the high water content of 38 %.

Mass balances for other fast pyrolysis processes are given in Table 31 below for comparative purposes.

Table 31 Comparative mass balances for various fast pyrolysis processes.

Research Group	Organic Liquids	Char	Gas	Water	Total Liquids	Closure	Temp (°C)	Ref
Aston University This reactor Beech wood	54.15	13.83	12.3	10.71	64.86	91.06	555	
Aston University Ablative Pine Wood	65.9	12.4	9.2	11.5	77.4	98.9	602	9
NREL Ablative Aspen Poplar	55.4	13.1	13.8	11.8	67.2	94.1	625	78
Waterloo University Fluidised bed IEA Poplar Poplar	65.8 51.1	7.7 8.9	10.8 19.0	12.2 17.8	78.0 68.9	96.5 96.8	497 600	60 62
Ensyn Tech. Inc. Transported bed Maple Poplar Poplar IEA Poplar		16.6 17.0 9.0 7.5	10.9 10.0 27.8 32.9		72.6 73.0 63.2 61.7	100.1 100.0 100.0 102.1	500 500 600 650	66 67 68
Twente University Rotating cone Softwood		25	15		60	90		95

It can be seen that the product yields are comparable with those obtained for other fast pyrolysis processes. The mass balance closures are good but not excellent and values are obtained by direct measurement and not by difference methods. Any losses of product, which result in a closure of less than 100 %, are due to liquid product hold-up in the quench column, this being difficult to collect and quantify, and also due to inaccurate gas measurements.

12.3 PYROLYSIS LIQUID ANALYSES

Analysis of the pyrolysis liquids is essential in order to determine their effectiveness as a potential fuel and chemical feed source. The techniques used in the analysis of the liquids produced are:

- Metrohm Titrino titration determination of water content.
- Haque rotary determination of viscosity and stability.
- Filtration determination of solids content.
- High Pressure Liquid Chromatography (HPLC) for a quantitative determination of water soluble compounds.

The Metrohm Titrino is a digital analyser that uses a standard Karl Fischer technique that titrates samples, which are dissolved into a solvent, against a known titrating agent in order to determine the water content.

Viscosity measurements were made using a Haake Rotovisco RV12 to give the viscosity in mPa.s. The rotor cup is fitted with a water jacket supplied by water from a heated bath, controlled to 0.1 ^{o}C, the jacket temperature being independently measured by a standard mercury thermometer. A ramped increasing shear 3 minute cycle (ramp up) was used to determine the liquid viscosity at different shear rates and to identify Newtonian behavior.

Various studies have been conducted into bio-oil physical properties and stability and the reader is referred to Sipila et al. (117) and Diebold et al. (118). The stability of the

oil may estimated using the Viscosity Index (VI), this is a technique for artificially aging an oil and determining its stability over time. The Index compares the viscosity of the original oil to the viscosity resulting after storing the oil at 80 °C for a period of 24 hours. Storing the oil at 80 °C for 24 hours is equivalent to storing the oil for one year at a temperature of 20 °C. Therefore the index is a quick method for determining to what extent the viscosity is likely to change over the course of one year.

The Index can be calculated from:

$$VI = \frac{(\mu_{t2} - \mu_{t1})}{\mu_{t1}} \qquad \textbf{Eq. 142}$$

Where:

VI	=	Viscosity Index
μ_{t2}	=	Viscosity after 24 hours at 80 °C, mPa.s
μ_{t1}	=	Initial viscosity, mPa.s

The char content was determined by measuring solvent insoluble material filtered through a 7 cm Whatman glass microfibre filter paper (particle retention 1.6 μm) at a methanol to pyrolysis liquid ratio of 5:1. At high solvent to liquid ratios it may be assumed that all of the pyrolytic lignin has solubilised and the remaining residue is comprised of char. However, to be certain, increasing solvent ratios should be used until approximately equal readings are obtained.

Table 32 Physical properties of experimental liquids.

Run Number	NR01	NR02	NR05	NR06	NR07	NR08	NR10	NR11
Initial water content, %	22	14	27.9*	26.03	14.10	20.9*	38.00	21.3
Final water content, %	#	#	28.4*	28.12	16.00	22.2*	42.04	23.00
Initial viscosity, mPa.s	#	#	32*	51	122	25*	9	121
Final viscosity, mPa.s	#	#	35*	60	140	27*	9	223
Stability index	#	#	0.09*	0.17	0.14	0.08*	0	0.84
Char content, %	1.61	0.34	0.78	1.45	1.5	1.05	6.02~	0.73

* indicates that a degree of phase separation occurred which effects the result obtained.

\# indicates that the test was not undertaken as the VI wasn't an accepted method at the time of testing.

~ high value due to cyclone blockage and consequently high char carryover.

The viscosity values span a significant range of values and are substantially dependent upon the moisture content of the sample, the degree of phase separation, the operating conditions and the amount of char present in the sample. The general low stability index numbers show that the oils are fairly stable. The exception is the oil from run NR10, this is due to the high char content, which is likely to make the oil more unstable. The char values are generally low with the exception of NR10. Higher char levels were consistent with char blockage of the cyclones and pipe work during operation. The most serious blockage of the cyclones occurred during run NR10 which correlates with the significantly higher char content of the pyrolysis oil.

High Pressure Liquid Chromatography (HPLC)

HPLC analyses the water soluble fraction of the bio-oil obtained by precipitating and filtering off the pyrolytic lignin. In HPLC small concentrations of compounds can be analysed either separately or in mixtures. In the case of pyrolysis products, water soluble components such as sugars, aldehydes, alchohols, etc. analysis is performed on reverse flow columns using a combination of detection methods such as UV absorption and refractive index. This is a non-destructive method of analysis and can be applied to neutral, ionic, low and high molecular mass solutes present in aqueous and organic phases.

The analyses presented in the table below do not allow any trends with temperature to be determined due to the fact that char blockages may have caused vapour cracking and influenced the chemical species and quantities present. As the vapour residence times experienced by the vapours are longer than those used to typically conserve chemical species it is difficult to draw any conclusions from these analyses. However, it appears that the Levoglucosan and Hydroxyacetaldehyde levels appear to be consistent with other similar processes at equivalent operating conditions whereas the Formic Acid levels appear to be quite high.

Table 33 HPLC analysis of raw product liquids.

	NR07	NR08	NR10	NR11
Feedstock	Pine	Beech	Pine	Pine
Moisture Content, %	10.1	10.4	10.0	12.5
Reactor temperature, °C	511	555	570	580
Residence time, s	1.95	1.47	2.05	1.66
Total liquids, %	46.7	64.9	59.3	62.4
Char, %	18.09	13.83	20.9	20.58
Gases, %	12.99	12.37	14.33	10.55
Closure	92.90	91.06	94.53	93.53
Constituents of liquids, % weight				
Glycolic acid	1.46	1.43	1.53	1.54
Xylitol	1.51	1.66	2.56	2.74
Levoglucosan	6.59	5.93	5.90	5.66
Hydroxyacetaldehyde	16.25	13.85	15.17	20.85
Formic acid	12.18	10.50	13.41	15.62
Acetic acid	3.01	3.55	3.56	3.56
Acetol	2.63	3.09	3.43	4.04
g-Butyrolactone	10.72	9.55	0.00	0.00
Methanol	0.00	0.00	0.00	0.00
2-furoic acid	0.00	0.00	0.00	0.00
Methylcyclopentanedione	1.07	0.00	0.00	0.00
Guiacol+other sugars and acids	8.77	3.82	2.87	0.00
Glyceraldehyde	0.00	0.00	0.00	3.09
Ethanol	0.00	0.00	0.00	0.00
Fructose	0.78	0.76	0.29	2.07
Glucose	0.71	0.63	0.31	0.79
Crotyle Alcohol	0.78	0.19	0.96	0.00
Crotonaldehyde	0.005	0.19	0.24	0.00

Pyrolysis gas analysis.

The produced pyrolysis gases were analysed on-line using a Unicam 610 pyrolysis gas analyser (Gas Chromatography). Samples are analysed at 5 minute intervals to allow any deviation in product composition with time to be recorded. The system consists of two parallel chromatographic channels.

System A - for the analysis of hydrogen and carbon monoxide consists of a 10 port valve configuration for inject, backflush/analysis and a thermal conductivity detector (TCD).

System B - for the analysis of the remaining components consists of a 10 port valve configuration for inject, backflush/analysis and a thermal conductivity detector (TCD).

The results obtained from the various experimental runs may be seen in Table 34 below and are compared with other researchers work.

Table 34 Comparison of pyrolysis gas analysis with results from other pyrolysis processes (N_2 free basis, % vol).

	H_2	CO	CO_2	CH_4	C_2H_4	C_2H_6	C_3H_6	Ref.
Aston University This Work								
530°C (NR05)	2.95	29.78	50.65	2.6	0.46	0.88	12.6*	
560°C (NR06)	1.82	59.76	32.96	2.2	.47	.64	2.07	
511°C (NR07)	1.91	61.45	30.07	2.67	0.69	0.9	2.32	
555°C (NR08)	1.2	48.66	46.27	2.7	0.37	0.66	0.2	
570°C (NR10)	1.34	59.97	33.3	3.51	0.4	0.7	0.7	
580°C (NR11)	1.86	59.3	32.9	3.4	0.2	2.0	0.11	
Aston University Cordner Peacocke								
458°C (CR14)		49.1	45.4	4.8	0.7		0.04	9
505°C (CR13)		44.4	48.6	5.9	0.02	0.55		
550°C (CR11)	8.5	43.4	41.6	6.5				
602°C (CR10)	3.6	52.0	36.1	5.7	1.2	1.0		
NREL								31
625°C (Run 34)	3.4	46.2	43.1	4.6	1.3	0.3	0.4	
Waterloo								61
500°C (run 13)	5.9	57.8	26.2	8.4	1.6	0.1	0.1	

It has been proposed that reactor temperature during fast pyrolysis is the most significant influence on composition of the gas products (64). However, the ablative pyrolysis is different in that the reactor may have a high wall temperature, say 555 °C but the vapour temperature may be as low as 300 °C making interpretation difficult. In addition for many of the runs described above char blockage of the process piping occurred leading to product cracking and different gas compositions. Typically product

cracking leads to high CO levels which can be seen in the results for this work as many of the process runs resulted in product cracking due to the catalytically active char.

12.4 RESULTS DISCUSSION

12.4.1 MASS BALANCES

The mass balance closures are acceptable, with losses mostly attributed to product oil hold up within the quench column system. This was unrecoverable due to the complexity of the system. Had larger quantities of biomass been pyrolysed these errors would have been reduced accordingly, eventually becoming negligible. Another source of error is the gas yield and composition results. Problems were encountered in both poor gas chromatograph performance, and occasional due to gas leaks. Problems that did occur with the gas chromatograph include poor calibration, retention time drift and gas pump failure. It is suggested that a more rigorous maintenance and calibration routine is operated.

12.4.2 CHAR YIELDS

The reactor performed extremely well and the product char was a fine free flowing powder and appeared to be visually free of non-ablated wood. Char yields varied from 13.83 % with the beech wood feed to a maximum of 21.7 % with a pine wood feed. The char yield is slightly high, this could either indicate vapour cracking reactions or alternatively that the char was not completely reacted.

12.4.3 ORGANIC LIQUID YIELDS

The product yields are expressed on a dry wood basis and all of the wood fed was assumed to have pyrolysed. The highest organic yield was obtained was 54.15 % at 555°C. As the closure for this run was only 91.06 %, it is expected that there is a significant hold-up of product liquid in the quench column which proved unrecoverable. The organic yields of a number of the experimental runs were not as high as hoped for two reasons. Firstly due to cracking reactions caused by char blockages of the process piping. Secondly due to the fact that the product vapour temperature was typically

below 400 °C, which can cause secondary condensation reactions to occur. Optimisation of the reactor and process piping will remove this problem and increase both liquids yields and quality. Optimisation will include:

- better insulation of the process pipe work and the provision of a more suitable heating piping heating to prevent char accumulation. Currently trace heating tapes heat both the process piping and cyclones. These have a maximum operating temperature of 450 °C and have a high failure rate. These should be replaced where possible, and certainly for the cyclones, with ceramic band heaters which can operate at a higher temperature, supply a higher heat duty and are more reliable.
- Additionally insulation of the reactor, although the reactor wall is maintained at a typical temperature of 550 °C, the reactor front and back plates are typically at a temperature of only 350 °C. Increased insulation should be provided and consideration given to heating of the front and back plates. On a larger scale reactor this would not be as influential a problem due to the increased wall path length.
- The nitrogen supply to the reactor is heated by a furnace which is only capable of heating it to a temperature of 300 °C. This is due to the small path length and surface area of the copper coil which sits within the furnace and the nitrogen flows through. This combined with the low temperature of the front and back plates of the reactor, 350 °C, and the large thermal sink presented by the blade assembly means that the product vapours are typically maintained at a temperature of 330 °C. This leads to secondary condensation reactions which lower the organic yield. A higher nitrogen temperature is essentially and therefore a larger furnace should be utilsed to allow a larger copper coil thereby increasing the nitrogen temperature .

12.4.4 WATER YIELDS

A average water yield from the fast pyrolysis process is 21.13 %, this is high due to the low vapour temperature, 330 °C, and the presence of char blockages is the process pipe work which lead to product cracking. Further work is required to be able to predict the effect of vapour temperatures and residence times on the water yields. Efforts should be made to gain both greater control and a higher operating temperature of the product vapour.

12.4.5 Non-condensable Gas Yields

The gas yield from the fast pyrolysis process is typically 17 % at reactor temperatures of 550 °C and residence times of 2 seconds. These gas yields are high due to product cracking because of contact with hot catalytically active char. Yields of hydrogen and other higher hydrocarbons are high suggesting that vapour degradation to non-condensable gases is occurring. This could be minimised by better heating of the pyrolysis vapours.

12.4.6 Particle size

The reactor proved capable of handling a variety of wood particle sizes, the particle sizes that were used for experimental runs were: 2 x 2 x 11 mm pine wood particles, 5 x 4 x 10 mm pine wood particles and 1 x 4 x 8 mm beech wood particles which were all hand prepared. The 5 x 4 x 10 mm pine wood particles were the maximum size that could be fed by the screw feeder that was used with the reactor.

Manual fed particles were also tested with the reactor to see if they could easily be pyrolysed. The particle sizes were: 6 x 6 x 16 mm rectangular pine wood particles and 6 x 6 x 6 mm square pine wood particles and were both manually prepared. These particle sizes fed easily to the reactor which proved capable of ablative pyrolysing them without any problems. It is desirable to use larger size particles for two main reasons: More effective utilisation of the available space beneath the reactor blades and because larger size particles are both easier and cheaper to produce. It is suggested that the 6 x 6 x 6 mm are the ideal size to be employed with this reactor. This is because they make the most use of the available space beneath the reactor blades, they result in less void space beneath the reactor blades and they have a preferential shape with regard to feed mechanisms.

Another feed source, which was manually fed and tested, which has interesting implications is a hammer milled beech wood with dimensions of 1 x 2 x 2 mm. This material is of a size below the clearance of the reactor blades and therefore unlikely to be pressed against the reactor wall by the blades. This means that a test sample

introduced into the heated reactor, in a nitrogen environment, would successfully pyrolyse. However, it would ablate at a low rate because the blades would not be supplying a high contact pressure as the particles would pass beneath the blade clearance. When tests were conducted it was noted that:

- The pyrolysis rate obtained, determined visually by the rate of vapour production, was low when the blades were stationary or operating at a low relative velocity.
- However when the blades were rotating at a high velocity (tip speed of 12.1 m/s, 315 rpm) the ablation rate increased substantially, determined by a greater production rate of pyrolysis vapour.

This suggests that the blades were generating a vortex, which pressed the wood particles against the heated reactor wall using centrifugal force. It was intended to perform an experimental run with this material, as the biomass feeder used with this reactor was capable of feeding the material at feed rates of up to 4.2 kg/hr. However, before this run could be implemented the reactor band heater failed curtailing any further experimentation. Nevertheless this is an interesting phenomenon which should be investigated.

13. SCALE UP

The concept of scale up can be defined as (119):

"The successful start-up and operation of a commercial size unit whose design and operating procedures are *in part* based upon experimentation and demonstration at a smaller scale of operation."

Successful scale up of chemical processes requires the utilisation of a broad range of technical skills and an appreciation of the total problem. The design methodology may be represented by the diagram given below.

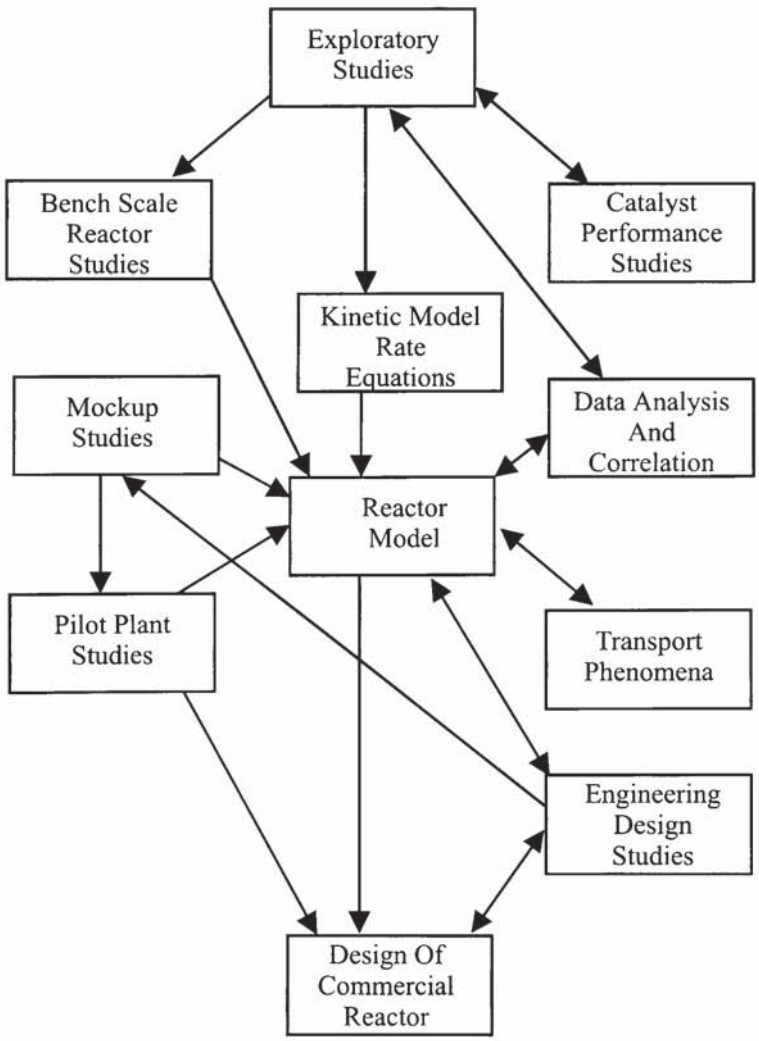

Fig. 47 Scale-up design considerations (119).

Many of the initial exploratory studies and kinetic model determinations for ablation have already been performed by other researchers and discussed in Chapter 2. The challenge in this case is to apply them to a new type of ablative reactor. A qualitative indication of the impact of reactor dimensions on chemical reaction, mass transfer and heat transfer in multiphase reactors is given in the table below

Table 35 General Scale-up Considerations (119).

Phenomenon	Reactor Volume	Length-to-Diameter Ratio	Surface-to-Volume Ratio
Chemical reaction	Significant and determining	Weak and indirectly	Indirectly
Mass transfer	Indirectly	Significant	Indirectly
Heat transfer	Weak and indirectly	Significant	Significant and directly

Solids in particular pose problems due to characteristics such as adhesion to surfaces, adhesion to other solids or self adhesion. They are also difficult to convey or feed requiring special equipment. The problems encountered are variable and dependent on many different factors such as particle size, size distribution and possible impurities.

General differences that may be of particular importance in moving from small scale to commercial size equipment are.

Shape which can lead to differences in agitation, fluid short-circuiting or stagnation zones.

Mode (and scale) of operation resulting in different residence time distributions.

Surface-to-volume ratios, flow patterns and geometry which result in significantly different gradients of concentration and temperatures.

Materials of construction resulting in different contaminant levels.

Flow stability.

Heat addition and removal.

Wall, edge and end effects.

13.1.1 APPLICATION TO ABLATIVE REACTOR

Shape

The shape of the biomass particles does not significantly affect the ablation process as it is predominantly a surface area phenomenon, the vast majority of the pyrolysis process occurs at the interface between the ablating biomass particle and the heated surface. Any pyrolysis of the biomass particle that occurs at sites other than the interface due to the internal reactor temperature will be at a rate several orders of magnitude less and may be considered negligible. Biomass particles with a longer length may ablate at a slightly slower rate due to the inability of a point on reactor wall to supply the heat flux demand as the particle is swept past it. This leads to a slightly lower wall temperature and consequently slightly lower ablation rate. However this is dependent upon the size of the particle and the available heat flux supply and should not be considered a significant factor. The size of the particle is more important if considered from an economic viewpoint. Biomass comminution costs represent a significant proportion of the total operating cost and larger biomass particles are usually cheaper to produce. The size of the biomass particle will be dictated by the size of the reactor used, the setup of the rotating blades and the feeder employed.

The term shape can also be applied to the ablative reactor itself, to scale up an ablative reactor the available surface area for ablation needs to be increased. The reactor designed during this project is cylindrical and the surface area can therefore be increased by increasing the diameter or reactor length. The surface area to volume ratio for a cylinder is equal to 4 divided by the cylinder diameter. Therefore an increase in the reactor diameter decreases the surface area to volume ratio and leads to increased vapour residence times, which is undesirable. The reactor length has no effect upon the surface area to volume ratio so superficially this appears the best way to scale up a reactor. However if the diameter is increased significantly two options become available: either the biomass particle size remains the same which means that potentially more blades may be used in the reactor leading to a better utilisation of the available surface area; or the number of blades remains the same but the size of the biomass particles can be increased leading to reduced biomass comminution costs. In reality for a chosen reactor size a balance must be struck between the limits imposed by vapour residence time requirements; and the fact that biomass comminution cost benefits show

a decreasing return as particle sizes increase, and can lead to added complexity and cost in the feeding arrangements.

The shape of the product collection system is not an issue as it is largely prescribed by design constraints and scale up is largely an issue of increased size rather than complexity and arrangement.

Mode

The mode of the operation, whether the system is run continuously with a limited feed load or continuously with a continuous feed supply, has implications for both the biomass feed system and the product collection system. Currently due to the small size of the reactor the system is run with a limited feed load, with the biomass feeder utilising a sealed hopper with enough wood in it for a single run. In addition, the production collection system is operated in a closed mode with no product removal, excepting of course the necessary venting of waste gases.

A large scale reactor would be run continuously, necessitating an open feeder system rather than a sealed hopper. A seal would be maintained through the use of a non return feeding valve and a purge gas. Provision would have to be made for the removal of char from the cyclones, with the char being used to satisfy the process heating requirements rather than simply being collected as it is currently. The quench column and electrostatic precipitator are currently run in a batch mode with the quench liquid and condensed bio-oil being constantly re-circulated around the system. A continuous reactor would have to have a purge system where the recycle stream was passed through a decanter settler. The bio-oil would be removed and the immiscible quench liquid returned to the column in the recycle.

Surface-to-volume ratios, flow patterns and geometry

Surface-to-volume ratios have already been covered in detail under the heading shape as has the term geometry. Flow patterns are difficult to predict due to the three phase nature of the reactor and the complexities this introduces. Most attention should be focused on the wood particle flow patterns and the distribution beneath the blades. The more effective the distribution and the tighter the packing the larger the reactor

throughputs. It might be necessary to mount the reactor vertically to ensure effective wood particle dispersions.

Materials of construction

The materials of construction are important as the bio-oil is both acidic (pH 2) and unstable with certain contaminants, such as iron, leading to increased instability. Any high temperature parts of the process will require a high grade stainless steel material to prevent rapid corrosion. Parts of the system that are at room temperature could be made from mild steel with a protective polymer coating or perhaps entirely from polymers and plastics.

Flow stability

Flow stability is an important issue in the design of the reactor as the drive motor is more effective if a uniform feed rate is maintained. It is also important if the reactor is operated near its maximum capacity limit, this is because if the feed rate is non uniform certain blades may be subjected to excessive loads and consequently flood leading to operation problems. Another important area requiring flow stability is the quench column liquid flowrate for similar reasons. It is advantageous to run the quench column near its flooding limit as a larger interfacial area is available for heat transfer. However if the flowrate of the quench liquid is not stable this could lead to flooding problems which once initiated require extensive operator input to control.

Wall, edge and end effects

Wall, edge and end effects are not an overriding concern in ablative pyrolysis being more of an issue in fluid flow and mixing problems. Edge effects are important because the distance between the edge of the blade and the heated wall will specify the maximum char particle size which will be produced. The narrower the blade clearance the smaller the char particle size, and correspondingly the less the chance of unreacted biomass passing through the system to the collection cyclones. This is important from an economic viewpoint as the biomass is an integral part of the process economics with an associated cost value.

Heat addition and removal

Due to the concentrated nature and high reaction rates employed during the ablation process, substantial heat input is required which may be difficult to supply on large scale reaction systems. An overview of various applicable technologies is given in Chapter 13.2 below. To summarise only two realistic technologies are available these being either immersion of the whole reactor in a fluidised bed or the use of molten salts or metals to provide the heat input requirements. A careful evaluation of the benefits and disadvantages of the competing systems would need to be made before a decision on the most effective could be made. Electrical heating is not cost effective on large scale applications due to a lower efficiency and is therefore not considered.

13.2 HEATING REQUIREMENTS

13.2.1 GAS-FIRED FURNACES

Gas-fired furnaces primarily use radiant heat transfer from hot flue gases in addition to reradiated heat from the furnace walls to heat reactor walls, predominantly tubular ones, to around 1000 °C. The average heat fluxes that can be obtained are in the region of 31550-63100 W/m^2 (120) with fire box temperatures of 1150-1250 °C. A large optical path length, and hence large furnace, is necessary for a high emissivity and good radiant heat transfer. Typical emissivities for industrial furnaces, 3-6 m a side, are approximately 0.5 meaning that high furnace temperatures would be needed to achieve a given flux than for surfaces with higher emissivities. It should be noted that gas-fired furnaces can be considered to be state of the art technologies.

One particular problem is that pyrolysis for the production of liquid fuel requires that wall temperature reach a maximum of 600 °C to minimise product cracking. This could be difficult to achieve when typical furnace temperature can be double this. Thick reactor walls, and the high heat requirement of the pyrolysing biomass could serve to keep wall temperatures down to the required value, but this is by no means certain.

13.2.2 Fluidised Beds.

The good heat transfer properties of fluidised beds have led to their adoption in circumstances where close control of temperature is required. The presence of particles in a fluidised system results in heat transfer coefficient increases of up to one hundred fold, compared with gas alone at the same velocity.

It is difficult to accurately determine heat transfer correlation's as they appear to be very dependent upon the geometry of the system, on the quality of the fluidisation, and the consequential flow patterns obtained. There is however one almost universal conclusion, that the thermal conductivity of the solids has virtually no influence on the process.

Fluidised beds of small particles generally have high heat transfer rates, the heat transfer coefficient for a bed of hot particles to a wall or jacket is of the order 200 W/m^2K (121), which corresponds to a heat flux of 50000 W/m^2 for a temperature difference of 250 K.

13.2.3 Resistance Heating

Direct electrical resistance heating of the reactor with electrodes at each end of the reactor is a possible method of attaining the required heat fluxes. Due to the low resistance of metal reactors a low voltage would enable a high current to flow giving a large power input, which is desirable. Possible problems would be non-uniform heat fluxes around the reactor, the requirement to electrically isolate the reactor (as against merely grounding), the cost of a very large step-down transformer and also the safety implications of a high current flowing through a reactor.

13.2.4 Induction Heating

Induction heating uses rapidly alternating magnetic fields to induce EMFs within an object. These give rise to induced currents, eddy currents, which circulate within the body of the metal. The eddy currents follow low-resistance paths and therefore may be large, even though the induced EMFs may be small. As a result, eddy currents can produce considerable heating and magnetic effects. Actual working designs include the

induction furnace in which a water cooled coil carrying high frequency current surrounds the sample to be heated. Temperature control could be achieved by varying the inductive power output, via a temperature controller and thermocouple. Problems could be encountered in ensuring uniform fluxes.

13.2.5 Hot Inert Carrier Gas.

Hot inert gases such as steam or nitrogen used to input heat into the reactor requires large amounts of gas at temperatures significantly above the pyrolysis temperature. The biomass vapours formed would be heated to the carrier gas temperature, say 1000 °C, and would rapidly crack. The large quantities of gas would have implications for the product collection system, making it large and more expensive.

13.2.6 Boiling-Condensing Sodium and molten metals and salts.

Sodium is an attractive heat transfer medium at temperatures between 700 °C to 900 °C (122, 123) due to its very high thermal conductivity and heat of vaporisation. This enables very high heat fluxes to be achieved with very small temperature differences, for example 472500 W/m^2 at for temperature differences of 10 °C. However, there are considerable safety implications in using liquid sodium, which may render it unusable. A safer option is the use of a molten metal such a lead or molten salts, temperatures of over 600 °C can easily be achieved and a system is already commercially used by Pyrovac (56).

13.3 LARGE SCALE REACTOR

It was shown in Chapter 6 that an increase in either the reactor temperature or biomass contact pressure will result in an increase in the biomass ablation rate and consequently the reactor throughput. However, the increase in ablation rate is limited and two important points need to be considered. Firstly the reactor temperature must be greater than 450 °C for ablation to occur yet any temperature in excess of 600 °C will lead to substantial product losses (9). Therefore the reactor temperature will be most likely controlled to a value of say approximately 500 °C in order to maximise liquid yields. Secondly, the ablation rate can also be increased by utilising higher contact pressures.

This is limited for two reasons: firstly by the achievable speed of the rotating blades, with an excessive blade speed requiring a complicated drive motor; and secondly by the fact that at high contact pressure rather than the biomass simply ablating it is more likely to be crushed, which is an inefficient use of the power output of the drive motor.

Therefore the single most important factor that needs to be considered for scale up purposes is the reactor surface area. A doubling of available reactor contact area will results in a doubling of the reactor throughput provided that that all other factors remain constant. A large scale reactor is shown in Fig. 48 below.

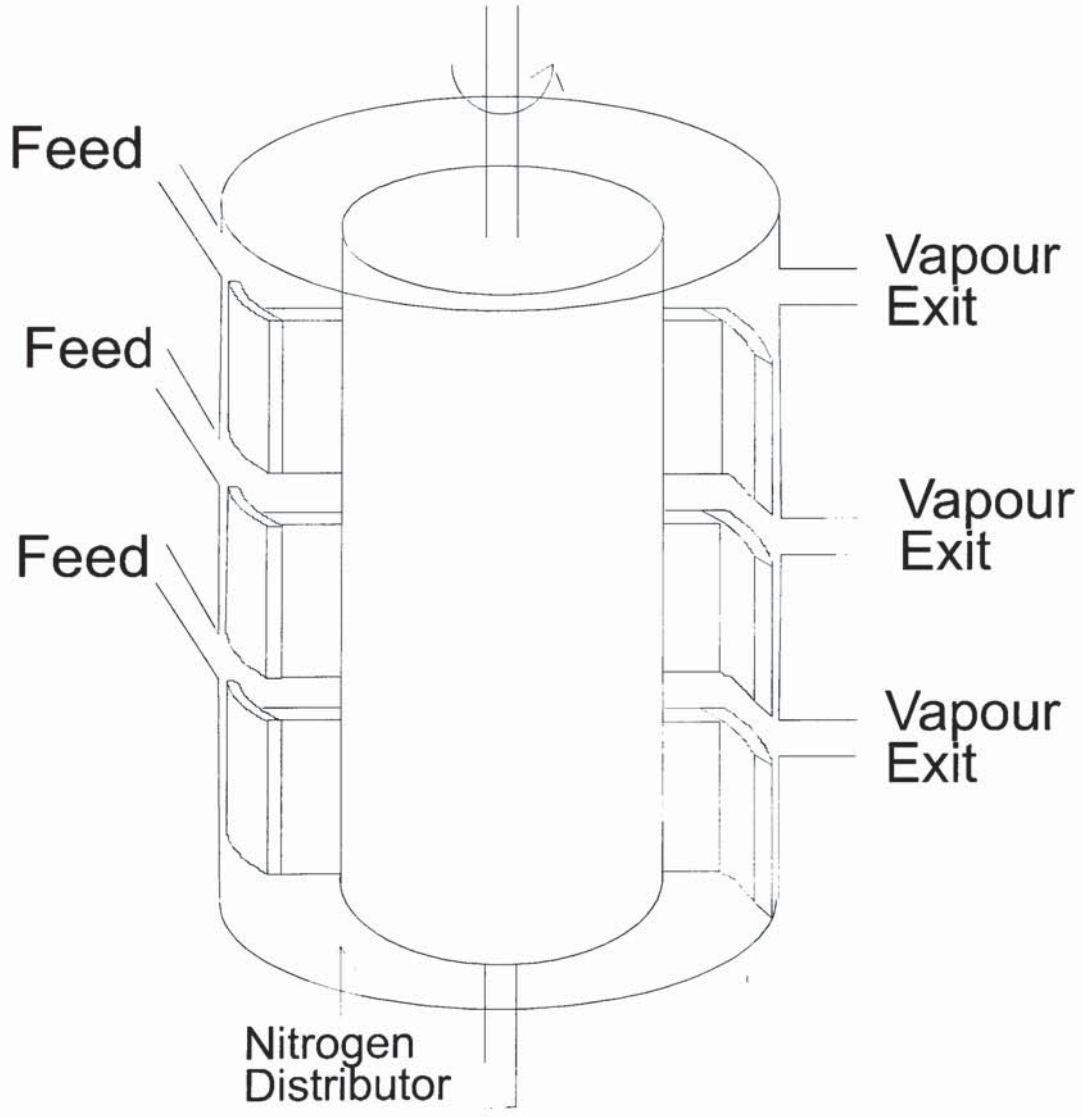

Fig. 48 Scaled up reactor.

Multiple feed points are used because if a large amount of feed was entering at a single location the reactor would be likely to flood or block. The reactor is mounted vertically so that the particles can cascade down the reactor until they become swept along behind the blades. Multiple vapour exit lines are used to provide for both redundancy in design should any become blocked and also to allow the use of smaller multiple cyclones, which are more efficient. The nitrogen distributor is provided as a precautionary measure in case any char settles at the bottom of the reactor instead of being entrained out. If this was to occur nitrogen could be fed through the distributor to force the char out of the reactor.

The product collection system would be similar to that shown in Chapter 9, possible exceptions are that the quench liquid recycle would have to be passed through a decanter/settler to remove the product liquid to prevent any accumulation in the system. In addition it might be advantageous to have multiple, smaller, collection systems rather than one large collection system.

14. DISCUSSION

A novel ablative fast pyrolysis reactor and high efficiency collection system has been modeled, designed, constructed, commissioned and operated. The performance approaches that achieved by processes to date. It is believed that optimisation of the design, specifically the operating parameters, will result in greater operating performance. The reactor design has the added flexibility that it is scaleable in two dimensions, the reactor length and the reactor diameter. This offers easy and effective scale-up of the reactor to commercial applications, this is further discussed in Chapter 13.

The product collection system was designed to be highly efficient and to collect the product vapours in a single unit to reduce complexity and cost. The product collection system was highly efficient and measurements showed the collection efficiency to be approximately 99 % of the condensable vapours on a mass basis.

The reactor proved relatively simple to operate and was reliable under low feed rates. Difficulties were experienced at higher feed rates, these problems will be discussed further in this chapter.

Despite any difficulties experienced and the lower efficiency compared to other reaction systems (at the operating conditions utilised), the reactor is believed to be the best practical option for ablative pyrolysis due to its inherent scaleablity and flexibility. It is also believed to be a highly attractive process for achieving fast pyrolysis as it enjoys cost advantages compared to other fast pyrolysis technologies. The cost advantages will arise primarily from the reactors compact design, the use of conductive rather than convective heat transfer and the substantially lower volumes of transport/inert gas required.

14.1 PROCESS MODELING

The pyrolysis process has been modeled using fundamental equations of state enabling the determination of the ablation rate as a function of biomass type and operating conditions. This in turn has been used to generate a reactor design method, which can

predict reactor throughputs based on reactor geometry and operating conditions. The collection system has also been rigorously modeled enabling the matching of the collection system to the reactor throughput, and the prediction of the collection efficiency.

The modeling process is modular with separate models for: the ablation of the biomass particle, the pressure produced by the relative velocity of the biomass particle, the capacity or maximum feed rate of the chosen reactor design, the reaction products produced by the reactor, the collection efficiency and design of the char cyclone, the design of the quench column and finally the design and efficiency of the electrostatic precipitator. These models are linked with the output of one model forming the input to the subsequent model. This enables the whole process to be modeled and designed with the overall efficiency being calculated.

The model for the ablation of the biomass particle has been validated with operational date from a custom built experimental rig. The model was able to accurately predict the ablation rate at temperatures of up to 550°C. It is more difficult to validate the other modules due to the inability to build different scale reactors, and hence test the accuracy and scaleability of the models, due to the excessive cost this would incur. More experimental runs and scale-up data would be desirable. To aid the design of quench columns operating temperatures, flowrates and collection efficiencies need to be measured so that a volumetric heart transfer coefficient can be determined.

It is however, believed that the overall process design model is valid and could be used as a basis for reactor design and scale-up.

14.2 REACTOR DESIGN

Ablation offers extremely high reaction rates due to the rapid removal of char and other products from the reaction interface. This increases the heat transfer into the particle thereby increasing the reaction rate. Because the primary heat transfer mechanism is conduction and the biomass feed is fed directly into the system there is not a need for large volumes of heating/transport gas. This mimimises cost by reducing the amount of

non-condensable gases required and more importantly by minimising the size and complexity of the product collection system.

The basic reactor design incorporating a cylindrical reactor body with an internal rotating blade assembly is effective and believed to represents the best practical option for achieving ablative pyrolysis. The design is inherently scaleable, with scale-up being feasible in two dimensions, whilst introducing minimal additional reactor complexities. The rotating blade concept allows the residence time of the biomass particles to be de-coupled from that of the gas/vapour residence time. It is also possible to de-couple the reactor wall temperature, at which the biomass reacts, from the gas/vapour temperature enabling a variety of operating regimes. This would in principle allow a high wall temperature to be employed, 600 °C, whilst maintaining the vapour temperature at a lower temperature, 450 °C. This would maximise the ablation rate whilst minimising any secondary vapour phase reactions.

The reactor blades proved effective and versatile. The use of blades cut from a cylindrical tube resulted in curved blades that matched the reactor wall curvature. This enabled a constant blade angle to be maintained. The blades were capable of operating with a wide range of biomass particle sizes without any efficiency impairment. The blades also served to keep the large biomass particles inside the reactor whilst allowing the finer char particles to be entrained out of the reactor. This maximised the usage of the biomass feed and prevented losses of unreacted wood into the collection cyclones. Although the bladed approach increases the reactor complexity this is offset by the reduced complexity of the product collection system (lower gas volumes) and reduced operating costs. In addition a wide variety of feed stocks and sizes can be handled and reactor blockage is extremely unlikely.

The reactor proved to be highly flexible and capable of operating under a wide variety of operating conditions. Particle sizes fed to the reactor included:

- 2 x 2 x 2 mm, 4 x 5 x 10 mm and 6 x 6 x 16 mm rectangular pine wood particles.
- 6 x 6 x 6 mm square pine wood particles

- 1 x 4 x 8 mm hammer milled beech wood particles.
- 1 x 2 x 2 mm fine hammer milled beech wood particles.

All the particles with the exception of the 1 x 2 x 2 mm beech wood particles were ablatively pyrolysed with the contact pressure being generated by the rotating blades. The 1 x 2 x 2 mm beech wood particles were smaller than the blade clearance and therefore could not be swept along beneath the blades. It is speculated that the blades motion generated a centrifugal force, which caused the particles to undergo ablation. The ablation rate in this incidence was believed to be proportional to the angular velocity of the reactor blades and it was visually confirmed that below a minimum velocity the ablation rate was negligible.

14.3 PRODUCT COLLECTION SYSTEM DESIGN

The product collection system was initially tested on Peacocke's (9) ablative reactor and proved extremely efficient. The provision of an ice/acetone condenser and cotton wool filter after the combined quench column/electrostatic precipitator enabled mass measurements of the quantity of condensable products exiting the quench column/electrostatic precipitator. This showed that the collection efficiency was approximately 99% on a mass basis.

Operation on the reactor which is the focus of this thesis (the new reactor) was more problematic due to a number of interrelated factors. The reason that the product collection system worked successfully on Peacocke's reactor (9) was that it has a lower vapour flowrate than that resulting from operation of the new reactor. The higher vapour flowrate on the new reactor caused a number of problems, the main ones being: flooding of the quench column, non steady-state operation of the quench column, poor collection efficiency of the electrostatic precipitator and partial failure of the electrostatic precipitator due to its lower operating efficiency. These problems were either largely or completely rectified by two main modifications: re-machining of the quench column internals to the correct original specification (i.e. they were machined to the wrong specification), and the re-design of the electrostatic precipitator as the one initially in use had been specified for Peacocke's reactor (9). This is discussed further

in Chapter 11. These modifications enabled the product collection unit to operate effectively with a collection efficiency in excess of 99%.

The product collection system collects the liquid product in a single unit. This minimises the collection system complexity, which enables easier operation and also reduces the cost of the collection system. The single collection system also removes the need to produce blends of pyrolysis oil which typically result from multi-stage collection units employed on alternative fast pyrolysis reactors.

It is therefore believed that the relatively simple construction, high efficiency and single liquid product makes this design reliable and the best technique for the collection of pyrolysis vapours currently available.

14.4 CONSTRUCTION AND OPERABILITY

The reactor was simple to operate but in early commissioning runs suffered from a number of problems that had to be corrected. These are discussed in detail in Chapter 11. The system was well designed and any problems encountered were largely connected with equipment failure or unavailability rather than actual design faults. The discussion that follows will be in the order of the reaction sequence; namely the feeder, the reactor, the process piping and cyclones and finally the product collection system.

Feeder

The feeder proved simple to operate and reliable but was generally underspecified in both capacity and in the size of wood chips it could feed. The feeder hopper could contain only approximately 1.8 - 2.2 kg of wood chips (depending on particle size) which is approximately 4 litres of wood chips. At the maximum feed rate the feeder was capable of, 2.2 kg/hr, this gave an operating run time of only one hour. A one hour run time is acceptable but the feed rate of 2.2 kg/hr is over 10 times less than the reactor theoretical capacity and therefore clearly the feeder is insufficiently sized.

The wood chips used, 4 x 5 x 10 mm, were the maximum size that the feeder could handle. The reactor could handle wood chips with a size up to 6 x 6 x 16 mm (although 6 x 6 x 6mm would be preferable for feeder design). Larger wood chips sizes such as 6

x 6 x 16 mm would be more representative of the feed that industrial scale application would use and would also be easier to produce. Therefore a new feeder capable of using large size wood chips with a feed rate of approximately 20 kg/hr and sufficient hopper capacity to operate for one hour at maximum capacity should be sourced.

Reactor

The reactor construction was relatively simple, compact and robust. The blade assembly introduced complexities due to its compact nature, the need for specially fabricated parts (blades) and the desire to have a minimal blade clearance between the blades and the reactor wall. A larger scale installation should be easier to construct as it will not be so small, hence enabling easier machining, access and assembly.

The band heater itself worked well but failed on numerous occasions due to fact that it was linked to a faulty temperature controller. This was eventually identified and rectified, however by this point the numerous failures of the band heater had fundamentally weakened the power supply cable and the occasional failure still resulted. The band heater was more than capable of maintaining the reactor wall at the desired reaction temperature, up to and including 600 °C. Unfortunately the reactor face plates could not be maintained at the required operating temperature as they were not heated. During typical experimental runs the face plates were at a temperature 300-350 °C, even though the reactor wall would be at a temperature of 550-600 °C. A face plate temperature of a minimum of 450 °C would have been desirable to prevent vapour condensation on the face plates. Due to the lower temperature of the face plates, condensed vapour and fine char became deposited on the reactor face, however the amount can be considered negligible. The large mass of the blade assembly also presented a heat sink to the product vapours, helping to maintain the internal reactor temperature at approximately 315 °C, although this is also due in part to the low nitrogen transport gas temperature of 300°C. The result of this is that the internal reactor temperature is less than the required 450 °C needed to prevent secondary condensation reactions and product loss. In order to maximise the rector efficiency the face plates either need to be independently heated or better insulated so as to be at the same temperature as the reactor wall, thus helping to increase the product vapour temperature.

The reactor could be successfully operating without the need for a nitrogen gas supply to entrain particles out of the reactor or for heat transfer purposes. However, at the maximum feed rate of the feeder could supply, 2.2 kg/hr, the vapour residence time, assuming a vapour temperature of 330 °C and no nitrogen, would be approximately 4 seconds and the vapour exit velocity would be 5.5 m/s. This long a residence time at that temperature would lead to substantial secondary vapour phase condensation reaction and lead to a substantial loss of condensable organics. The exit velocity of 5.5 m/s is also below the recommended operability limit's for high efficiency cyclones which is 9 m/s to 27 m/s. If the reactor could be operated at the desired biomass throughput of 10 kg/hr using the same conditions, the vapour residence time would be approximately 1.2 seconds with a vapour exit velocity of 17.4 m/s. Therefore the reactor could be operated at higher capacities without the need for any nitrogen gas, excepting the minimal amounts need for the drive shaft purge.

The reactor drive shaft seal proved effective and the problem of vapour leakage was solved by the use of a nitrogen purge. Initially the drive shaft jammed due to the fact that the clearance between the drive shaft and seal house assembly was too low. Increasing the clearance and the fitting of an aluminium/lead bush to provide a softer more lubricating surface solved this.

Process Piping

The process piping connects the reactor to the twin cyclones, used to remove the char from the hot vapours, and then to the combined quench column/electrostatic precipitator. The process piping must be maintained at a temperature of over 450 °C in order to prevent char sticking and vapour condensation. If this occurs the pipes can either become partially blocked or completely blocked. If the pipes are partially blocked, it forces the product vapours to pass through the char blockage. The char can catalytically crack the product vapours, resulting in a loss of condensable products. The blockages also lead to increased pressure drops which can cause operational problems and a complete blockage forces a shutdown of the reactor.

Tape heaters are used to maintain the process pipes at the required temperature. They are first wrapped around the process pipes and then insulation is applied. The tape heaters used to heat the process pipe work and cyclones are not sufficiently flexible or

robust enough for the task in which they are employed. In particular the daisy chaining of the tape heaters together with the temperature control being provided by a single thermocouple and controller is inadequate to the task. This is because a single point is used to specify the control temperature, however the individual tape heaters are wrapped around different pieces of equipment with different heating requirements. This leads to a non uniform temperature control and localised hot spots and burn outs of the tapeheaters, or to cold spots and hence char deposition in the process pipes. The reason that the tape heaters were run off a single controller is simply the lack of available equipment. Particular attention should be paid to heating the cyclones and char pots as they are essential pieces of equipment and any char blockage here results in char deposition throughout the whole system. Rather than using tape heaters on the cyclones, band heaters should be used as these have a greater heating capacity. This is required on the larger metal items like the cyclones as they present a large thermal sink and are therefore harder to maintain at the required temperature.

Product Collection System

The product collection system is believed to represent the best process for collecting the condensable product vapours. The quench column is ideally suited to collecting pyrolysis vapours as it offers large volumetric heat transfer coefficients due to the fact it employs direct contact heat transfer and it has a high interfacial area. The design is also resistant to fouling problems, which is a key criteria when dealing with pyrolysis vapours. The electrostatic precipitator offers the most effective and cheapest method for removing the residual aerosols from the remaining product stream. By combining the two systems into a single unit, a more compact collection system results and the liquid product is collected in a single unit. This removes the need to blend the various product streams resulting from a number of collection units, which is a feature of other collection systems. This reduces complexity and is also believed to result in better product quality.

The collection system was simple to operate although the centrifugal recirculation pump employed was problematic. Problems experienced involved either varying flowrates or total failure of the pump. It should be replaced with a superior pump, possibly a positive displacement pump as these are better able to deal with fouling liquids.

It proved impossible to operate the quench column at steady state as the refrigeration unit proved incapable of dealing with the heat duty experienced. Additional cooling of the system is required. This will become increasingly important if the reactor is operated closer to its theoretical maximum capacity as the resulting heat duty will be higher.

14.5 RESULTS

High liquid yields of up to 64.9 % on a dry wood basis were achieved, which approaches the performance achieved by other fast pyrolysis processes to date. It is believed that the liquid yield would be higher but for the poor mass balance closure of 91 % which was achieved.

The reactor proved capable of generating an ablation rate of 0.63 mm/s for pine wood at a temperature of 525 °C with a relative velocity of 12.1 m/s. Peacocke (9) performed similar experiments with his reactor and achieved an ablation rate of 0.63 mm/s at a wall temperature of 550 °C. Peacocke (9) did not state the relative velocity employed, only that it was above 1.5 m/s. Therefore a direct comparison of the ablation rates achieved by each reactor cannot be made.

The pyrolysis liquids produced had a variety of water contents. Generally, the water content of the pyrolysis liquids could be expected to be approximately 14-20%, unless char blockage of the process pipelines occurred. If char blockage did occur, this tended to crack the product vapours producing high water contents.

The yields of gas were typical of fast pyrolysis processes with the majority of the gas being comprised of CO and CO_2. During some runs minor amounts of H_2 and CH_4 were present indicating that cracking reaction had occurred, this is backed up by the high water contents of the product oils for these experiments.

15. CONCLUSIONS

15.1 PROCESS MODELING

- A process design model for the reactor has been developed and validated to the extent possible.
- The model enables reaction rates and product compositions to be determined from given operating conditions and feed rates. The model then specifies the reactor and product collection system design and size needed for the specified feed rate.
- The model was able to predict the ablation rate, to within approximately 10%, at temperatures of up to 550°C.
- Further experimental data is needed to further validate the model, particularly where some of the physical property values used have been determined empirically.
- To aid the design of quench columns, operating temperatures, flowrates and collection efficiencies need to be measured so that a volumetric heart transfer coefficient can be determined.
- The model is a valuable tool for scale-up of the reactor to commercial size applications.
- The reactor currently being used is effectively a $1/10^{th}$ slice or segment of the intended reactor length. The model was used to show that this slice has a capacity of 30 kg/hr of wood feed. Therefore the whole reactor would have a capacity of 300 kg/hr, at the reactor diameter used and with the same number of blades employed.

15.2 REACTOR DESIGN

- The reactor was successfully operated at feed rates of up to 2.2 kg/hr, wall temperatures of up to 600 °C and relative velocities of up to 12.1 m/s.
- High liquid yields of up to 64.9 % on a dry wood basis were achieved which is comparable to other fast pyrolysis processes.
- The reactor could be successfully operating without the need for a nitrogen gas supply to entrain particles out of the reactor or for heat transfer purposes.
- The reactor achieved a steady state of operation within two minutes.

- Reactor run times were limited to about one hour due to the lack of capacity of the feeder hopper.
- The rotating blade approached seems to be the most cost effective and practical method for achieving ablative fast pyrolysis. Although the bladed approach increases the reactor complexity this is offset by the reduced complexity of the product collection system (lower gas volumes) and reduced operating costs.
- The reactor construction was relatively simple, compact and robust. The blade assembly introduced complexities due to its compact nature, a larger scale installation should be easier to construct, as it will not be so compact.
- The basic reactor design incorporating a cylindrical reactor body with an internal rotating blade. The reactor is inherently scale-able, with scale-up being feasible in two dimensions, reactor length and reactor diameter.
- The rotating blade concept allows the residence time of the biomass particles to be de-coupled from that of the gas/vapour residence time.
- It is also possible to de-couple the reactor wall temperature, at which the biomass reacts, from the gas/vapour temperature enabling a variety of operating regimes.
- The blades were capable of operating with a wide range of biomass particle sizes without any efficiency impairment.
- The blades also served to keep the large biomass particles inside the reactor whilst allowing the finer char particles to be entrained out of the reactor.
- The use of a drive shaft carbon bush with a high temperature polymer seal and nitrogen purge worked effectively with no vapour losses.
- The product vapour temperature could not reach the required temperature of 450 ^{o}C necessary to minimise secondary condensation reactions and char deposition. Product vapour/gas temperatures were normally in the region of 330 ^{o}C which is clearly insufficient.
- The band heater worked well but the reactor face plates could not be maintained at the required operating temperature. The face plates either need to be independently heated or better insulated so as to be at the same temperature as the reactor wall.
- The reactor blade assembly was not heated and was therefore at a lower temperature than the reactor wall. This lead to char deposition and also presented a heat sink to the product vapours, helping to maintain them at an undesirable low temperature.

- Char removal from the reactor was acceptable but not satisfactory and requires further development.

15.3 PRODUCT COLLECTION SYSTEM DESIGN

- The tape heaters used to heat the process pipe work and cyclones are not sufficiently flexible or robust enough for the task in which they are employed. In particular the daisy chaining of the tape heaters together with the temperature control being provided by a single thermocouple and controller is inadequate to the task.
- Particular attention should be paid to heating the cyclones and char pots as they are essential pieces of equipment and any char blockage here results in char deposition throughout the whole system.
- The product collection system concept was valid and can be considered the best available technique for achieving high collection efficiencies with the minimum of complexity.
- The product collection unit was simple to operate and once optimised was highly efficient (over 99 %).
- The use of an immiscible quench liquid enabled easy separation of the pyrolysis liquids from the quenching liquid.
- The use of a single unit for liquid product collection with a single liquid product stream is both feasible and advantageous. The fact that there is no need to blend liquid product streams should result in a more stable and homogeneous liquid product.
- The liquids recycle pump presented problems in that it was prone to blockages and did not always provide a steady state liquids flowrate.
- The refrigeration unit was not capable of dealing with the heat duty experienced. This lead to an unsteady state operation of the quench column as the temperature of the cooling medium gradually increased.

15.4 RESULTS

- High liquid yields of up to 64.9 % on a dry wood basis were achieved, which is comparable to other fast pyrolysis processes. It is believed that the liquid yield would be higher but for the poor mass balance closure of 91 % which was achieved.
- The reactor proved capable of generating an ablation rate of 0.63 mm/s for pine wood at a temperature of 525 °C with a relative velocity of 12.1 m/s.
- The pyrolysis liquids produced had a variety of water contents, high water contents were experienced for some runs which were due to high vapour residence times and char blockages in the process pipe work and cyclones.
- The yields of gas were typical of fast pyrolysis processes with the majority of the gas being comprised of CO and CO_2. Minor amounts of H_2 and CH_4 were present indicating that cracking reaction had occurred which is backed up by the high water contents.
- Due to the problems encountered with char blockages of the cyclones, the liquid product could have a high char content, which is undesirable.

16. RECOMMENDATIONS

16.1 REACTOR DESIGN

- The reactor works successfully but the model suggests that the reactor is capable of operating at a far higher throughput of 30 kg/hr and the reactor needs to be tested accordingly. This would necessitate a new feeder, drive motor and band heater and is therefore beyond the time scale of this thesis.
    - Higher feed throughputs would require a redesign of the feed tube to prevent feed blockages
- The reactor is also a $1/10^{th}$ slice of a longer reactor. Now that the bladed concept has been proved the design should be tested at its actual full length. This would have a suggested operationally capacity of 300 kg/hr. This would require a complete new experimental rig.
- The effect of the particle size on packing beneath the blades needs to be investigated so that the reactor throughput can be optimised.
- The effect of the blade angle on applied pressure needs to be investigates and the operable limits of blade angle determined.
- The biomass feeder worked well but was limited in the particle sizes it could handle, maximum of 5 x 6 x 10 mm, and the maximum feedrate it could generate, 2.2 kg/hr. It is recommended that in order to test the reactor at its design capacity a new feeder is purchased and retrofitted.
- Larger particle sizes need to be ablated, as this is one of the many features, which make ablation an attractive option. Larger particle sizes are easier and cheaper to produce making the process more economic.
    - Testing with larger particle sizes would require a new feeder and motor. The feeder being required to accommodate the larger particle sizes; and the motor being required due to the fact that larger particles have a larger initial friction and are therefore more likely to cause the drive motor to stall.
- The nitrogen supply to the reactor needs to be pre-heated to a higher temperature; currently it is supplied at an average temperature of 250-300 ^{o}C, with a more suitable temperature being approximately 400 ^{o}C. This would require an additional furnace to be used in sequence with the current single furnace. The higher

temperature is required in order to prevent condensation reactions in the vapour phase which typically occurs at temperatures below 300 °C.

16.2 PRODUCT COLLECTION SYSTEM DESIGN

- The re-circulation pump on the quench column is a centrifugal design, consideration should be given to using a positive displacement pump as this would be more capable of dealing with the more viscous pyrolysis oils which are occasionally pumped round the system and also with any char slurry.
- The re-circulation pump suction pipe should be situated at a level above the base of the tank. This is because the pyrolysis oil settles to the bottom of the tank and therefore is preferentially pumped around the system due to the fact that the current pump suction pipe is situated at the lowest point of the sump tank.
- If the reactor were operated at its maximum capacity of 30 kg/hr, the following considerations would need to be considered.
    - The cyclones are of a sufficient size for up to 30 kg/hr of wood feed, provided that virtually no nitrogen transport gas was used. They would, however, require larger char pots to cope with long runs at high feed throughputs.
    - The quench column would also be likely to overflow at larger wood throughputs due to increased liquid product volumes; this could be offset by periodic draining of the column during operation. Provision was made for this in the original design. A level indicator should be added to the quench column so that it is easy to know when the column needs to be drained.
    - The sump of the quench column should be made larger so that it contains a larger volume of quench liquid and has a greater capacity for storing product liquid.
    - The electrostatic precipitator typically requires a vapour residence time of more than 2 seconds to operate efficiently and at higher vapour rates could not achieve this criteria. This would lead to substantial product loss and therefore a larger electrostatic precipitator would be required. Alternatively, and more simply, as the vapour rate is increased the amount of nitrogen could be decreased accordingly. This would satisfy the E.P. requirements up to a feed rate of 10

kg/hr. Any feed rates in excess of 10 kg/hr would require a new electrostatic precipitator to be designed and constructed.

- The refrigeration unit is unlikely to prove capable of maintaining low temperatures of the sump liquid at higher feed rates. This is due to two reasons: Firstly, there is insufficient contact between the sump liquid and cooled jacket. The sump liquid is cooled by pumping it around the inside of the jacketed column, with the refrigerated glycol being pumped around the jacket. As the flowrate of sump liquid is limited, insufficient cooling of the sump is maintained leading to sump temperatures of up to 90 °C. Provision should be made for some additional cooling of the quench column sump to enable the product collection system to function efficiently.

16.3 CONSTRUCTION AND OPERABILITY

- Due to the low reactor throughput the vapour residence time is currently 1-2 seconds. This can lead to secondary vapour phase reaction and a loss of condensables. Therefore the reactor needs to be operated at a higher throughput of biomass or nitrogen in order to reduce the vapour residence time to less than 2 seconds.
- When a particle initially enters the reactor there is a moment of dry friction before the particle becomes self lubricating. This requires more power from the drive motor, with larger particles having a higher friction. This effect should be investigated and quantified to enable effective drive motor specification.
- The horizontal and vertical reactor concepts need to be investigated to enable the best method of particle dispersion beneath the blades to be identified. Good dispersion is vital to make the most effective use of the available surface area.
- Particle sizes below 1 x 2 x 2 mm appear to be able to be successfully ablated with the contact pressure being generated centrifugally rather than by the blades. This needs to be investigated as it offers a high degree of surface area contact with correspondingly high throughputs. A point to consider is if a high contact pressure could be achieved.
- The cyclones should be heated with ceramic band heaters to a temperature of 450 °C in order to prevent char blockages.

- The process pipe work needs to be better heated in order to prevent char blockages. The current system of daisy chaining multiple tape heaters together and controlling off a single thermocouple and controller is unacceptable and leads to tape heater under performance or burnout. Both of these problems lead to char blockages.
- The gas chromatograph needs a more regular calibration and maintenance schedule in order to maximise its efficiency and robustness.
- The reactor is capable of operating at a far higher feed throughput and needs to be tested accordingly.

16.3.1 Reactor Modeling

- More rigorous experimental evaluation of the ablation model and associated reactor design protocol is necessary. Single particle experiments should be used to validate the theoretical model and the values chosen for the ablative layer thermal conductivity and viscosity. Then the reactor capacity calculation should be verified experimentally.
- A model should be developed for the mechanical abrasion of the product char from the reaction interface so that the model can be used at relative velocities below 1.2 m/s.
- A method for determining the power requirement of the drive motor should be investigated. This should be fairly straightforward to calculate from the friction force generated by the particles.
- Secondary gas vapour phase kinetics should be developed to allow the prediction of product yields with variation in reactor temperature, vapour temperature, char levels and residence time.
- Detailed temperature measurements and collection efficiencies should be taken from the quench column so that a heat transfer coefficient can be determined. This would allow future quench columns to be designed accurately and collection efficiencies predicted.
- The electrostatic precipitator design methodology needs to be tested on large installations so that it can be verified. The small scale installations used in this project are inherently highly efficient which makes it difficult to ascertain the accuracy of the model predictions.

16.3.2 RESULTS

- The results are comparable with those from other similar fast pyrolysis processes under similar conditions. It is recommended that a wider variety of operating conditions and feedstock's are investigated in order to determine the operability limits and flexibility of the reaction system. In particular it would be beneficial to conduct experimental runs where a larger mass of wood was pyrolysed, as this would improve the mass balance closure.

16.3.3 ANALYSIS

- Further work is required on the development of analytical methods for the characterisation of fast pyrolysis liquids. Areas of interest should include a quality specification so that bio-oils from different processes can easily be compared.
- The on-line gas analyser needs a more rigorous calibration and maintenance schedule in order to guarantee accurate results. Problems were encountered with retention time drift and unconditioned columns.

16.3.4 MECHANISMS AND PATHWAYS

- Biomass mechanism and pathways require further study. It is difficult to predict the effect of biomass type, ash content, moisture content and the reactor operating conditions on the product yields. This is complex area with many interactions and therefore difficult to predict using kinetic mechanisms. An area of interest is the use of neural nets, which are highly efficient at determining outputs from complex systems based on a range of inputs.
- Secondary gas phase reactions and kinetics need further investigation so as to enable the effect of reactor operating conditions on product yields, hence allowing the optimisation of reactor design.

17. NOMENCLATURE

Property	Symbol	Units
Ablation velocity	V	m/s
Applied normal force	F_n	N
Biomass decomposition temperature	T_m	K
Biomass dry density	ρ_w	kg/m^3
Calculation term	C_n	
Calculation term	Θ	
Calculation term	C	
Frictional force	F_t	N
Latent heat of fusion	h_{sw}	J/kg
Length of sliding contact	L	M
Liquid density	ρ	kg/m^3
Liquid thermal conductivity	K	W/m K
Liquid thermal diffusivity	α	m^2/s
Liquid viscosity	μ	$N\ s/m^2$
Moisture content	M	wt/wt dry basis
Moisture enthalpy of fusion	h_{mf}	J/kg
Moisture specific heat capacity	C_{pm}	J/kg
Penetration distance into wood	d_0	M
Pressure distribution	P(x, z)	N/m^2
Pressure distribution	P(x)	N/m2
Pressure on cylinder	P_n	Pa
Relative motion gap	h(x)	M
Specific heat capacity of liquid	C_p	J/kg K
Specific heat capacity of wood	C_{pw}	J/kg K
Steel thermal conductivity	k_s	W/m.K
Steel thermal diffusivity	α_σ	m^2/s
Tangential velocity	U	m/s
Temperature of wood	T_0	K
Wall temperature	$T_w(x)$	K
Width of sliding contact	B	M
Wood temperature	T(y)	K
x-direction volumetric flowrate	Q_x	m^3/s
z-direction volumetric flowrate	Q_z	m^3/s

18. REFERENCES

1 Hague, R.A., "The Pre-Treatment And Pyrolysis Of Biomass For The Production Of Liquids For Fuels And Speciality Chemicals", Ph.D. Thesis, Aston University, 1998.

2 Tillman, D.A., "Energy from Wastes: An Overview of Present Technologies and Programs", Fuels from Wastes, Anderson, L.L. and Tillman, D.A. (eds.), Academic Press, Inc. (London) Ltd. 1977, p 17-40.

3 Bio-Alternative SA, "Technique de carbonisation et de pyrolyse", Pyrolysis as a Basic Technology for the Large Agro-Energy Projects, Mattucci, E., Grassi, G and Palz, W (eds.), 1989, p 205.

4 Luengo, C.A. and Cencig, M.O., "Biomass Pyrolysis in Brazil: Status Report", Biomass Pyrolysis Liquids Upgrading and Utilisation, Bridgwater, A.V. and Grassi, G. (eds.), Elsevier Applied Science, London, 1991, p 299-309.

5 Milne, T.A., "Pyrolysis - The Thermal Behavior of Biomass Below 600°C", A Survey of Biomass Gasification, Reed, T.B., (ed.), Solar Energy Research Institute, Colorado, USA, July 1979, p II:95-132.

6 Graham, R.G., Bergougnou, M.A., Mok, L.K.S. and de Lasa, H.I., "Fast Pyrolysis (Ultrapyrolysis) of Biomass Using Solid Heat Carriers", Fundamentals of Thermochemical Biomass Conversion, Milne, T.A. and Mudge, L.K. (eds.), Elsevier Applied Science Publishers, London and New York, 1985, p 397-410.

7 Graham, R.G., "A characterization of the Fast Pyrolysis of Cellulose and Wood Biomass", Ph.D. thesis, February 1993, University of Western Ontario, London, Ontario, Canada.

8 Lédé, J., Verzaro, F., Antoine, B. and Villermaux, J., "Flash Pyrolysis of Wood: direct measurement and study of ablation rate", Fuel, 64, 1985, p 1514-1520.

9 Peacocke G.V.C., Ph.D. Thesis, University of Aston [1994]

10 British Electrical International, "Modern Power Station Practice", Volume E, Chemistry and Metallurgy, Pergamon Press.

11 Rossi, A., "Fuel characteristics of wood and nonwood Biomass Fuels", Progress in Biomass Conversion, Vol. 5., Tillman, D.A. and Jahn, E.C., (eds), Academic Press, New York, 1984, P 69-99.

12 Antal Jr, M.J., "Biomass Pyrolysis: A Review of the Literature Part I - Carbohydrate Pyrolysis", Advances in Solar Energy, Boër, K.W. and Duffie, J.A., Vol. 1, Plenum Press, 1983, p 61-111.

13 Piskorz, J., Radlein, D. and Scott, D.S., "Thermal Conversion of Cellulose and Hemicellulose in Wood to Sugars", Advances in Thermochemcial Biomass Conversion, Ed. Bridgewater, A.V., 1994, P.1432-1440.

14 Glaser, W.G., "Lignin", Fundamentals of Thermochemical Biomass Conversion, Overend R.P., Milne, T.A. and Mudge, L.K. (eds), Elsevier Applied Science Publishers, New York, 1985, p 61-76.

15 Graboski M. and Bain R., "Properties of Biomass Relevant to Gasification", A Survey of Biomass Gasification, Reed, T.B., (ed.), Solar Energy Research Institute, Colorado, USA, July 1979, p II:21-66.

16 Goldstein, I.S., "Composition of Biomass", Organic Chemicals from Biomass, Goldstein I.S., (ed.), CRC Press, Boca Raton, Florida, 1981, p 9-18.

17 Shafizadeh, F., "Pyrolysis and Combustion of Cellulosic Materials", Advan. Carbohydr. Chem. 1968, P419-474.

18 Antal Jr, M.J., "Biomass Pyrolysis: A Review of the Literature Part II - Lignocellulose Pyrolysis", Advances in Solar Energy, Boër K.W. and Duffie J.A., Vol 2, Plenum Press, 1985, P 172-255.

19 Richards, G.N., "Chemistry of Pyrolysis of Polysaccharides and Lignocellulosics", Advances in Thermochemical Biomass Conversion, Bridgwater, A.V. (ed.), Blackie, Glasgow, 1994, P 727-745.

20 Scott, D.S., Piskorz, J. and Radlein, D., "Sugars from cellulosics by the Waterloo Fast Pyrolysis Process", Pyrolysis and Gasification, Ferrero, G.L., Maniatis, K., Buekens, A. and Bridgwater A.V. (eds), Luxembourg, May 1989, Elsevier Applied Science Publishers, 1989, London, p 201-208.

21 Soltes E.j. and Elder, T.J., "Pyrolysis", in Organic Chemicals from Biomass, Goldstein. I.S. (ed.), CRC Press, Boca Raton, Florida, 1981, p 63-100.

22 Ramiah, M.V., "Thermogravimetric and Differential Thermal Analysis of cellulose, hemicellulose and lignin", J. Appl. Poly. Sci., 1970, 14, p 1323-1337.

23 Williams, P.T. and Besler, S., "Thermogravimetric Analysis of the Components of Biomass" Advances in Thermochemical Biomass Conversion, 1994, Bridgwater, A.V., (ed.), Blackie Academic and Professional, Glasgow, p 771-783.

24 Varhegyi, G., Szabo, P., "Kinetics of the Thermal decomposition of cellulose, hemicellulose, and sugar can bagasse", Energy and Fuels, 3, 1989, p 329-335.

25 Avni, E., Davoudzadeh, F. and Coughlin, R.W., "Flash Pyrolysis of Lignin", in Fundamentals of Thermochemical Biomass Conversion, Overend, R.P., Milne, T.A. and Mudge, L.K. (eds.), Elsevier Applied Science Publishers, New York, 1985, P 329.

26 Avni, E., Coughlin, R.W., Solomon, P.R. and King, H.H., "Mathematical Modeling of Lignin Pyrolysis, Fuel, 64, 1985, p 1495.

27 Klein, M.T. and Virk, P.S., "Primary and Secondary Lignin Pyrolysis Reaction Pathways", Ind. Eng. Chem. Fund., 22, 1983, p 35.

28 Petrocelli, F.P. and Klein, M.T., "Simulation of Kraft Lignin Pyrolysis", Fundamentals of Thermochemical Biomass Conversion, Overend R.P., Milne T.A. and Mudge, L.K. (eds.), Elsevier Applied Science Publishers, New York, 1985, p 257.

29 Diebold J.P. (Workshop Chairman) in Proceedings of the Specialist Workshop on the Fast Pyrolysis of Biomass, Copper Mountain, USA, SERI/CP-622-1096, Solar Energy Research Institute, Golden, Usa, October 1980.

30 Evans, R.J. and Milne, T.A. "Molecular Characterisation of the Pyrolysis of Biomass 2: Fundamentals", Energy and Fuels, 1987, Vol 1, 4, p 311-319.

31 Diebold, J.P. and Scahill, J., "Production of Primary Pyrolysis Oils in a Vortex Reactor", in pyrolysis oils from biomass, Producing Analyzing and Upgrading, Soltes, Ed. J., and Milne, T.A., (eds.), ACS Symposium Series 376, 1988, p 31-40.

32 Diebold, J.P., "Ablative Pyrolysis of Macroparticles of Biomass", Proceedings of the Specialists' Workshop on Fast Pyrolysis of Biomass, Copper Mountain, 1980, SERI/CP-622-1096, Solar Energy Institute, Golden, Colorado, p 237-251.

33 Lédé, J., Panagopoulos, J. and Villermaux, J. "Experimental Measurements of Ablation Rate of Wood Pieces, Undergoing Fast Pyrolysis by Contact with a Heated Wall", Pre-prints of ACS Symposium series, 1983, 28, No. 5, p 383-389.

34 Bridge, S.A., "flash pyrolysis of biomass for liquid fuels" M.Phil. thesis, Aston university, England, November 1990.

35 di Blasi, C., "Analysis of Convection and Secondary Reaction Effects within Porous Solid Fuels Undergoing Pyrolysis", Combustion Science and Technology, 90, 1993, p 315-340.

36 di Blasi, C., "Numerical Modeling of Wood Pyrolysis-Effects of Pressure Boundary Conditions", La Rivista dei Combustibili, 46, 9, September 1992, p 265-279.

37 di Blasi C., "Modeling and Simulation of Combustion Processes of Charring and Non-charring Solid Fuels", Prog. Energy Combust. Sci., 19, 1993, p 71-104.

38 Bilbao, R., Arauzo, J. and Millera, A., "Kinetics of Thermal Decomposition of Cellulose. Part I. Influence of Experimental Conditions", Thermochimica Acta., 1989, 143, p 149-159.

39 Bilbao, R., Arauzo, A. and Millera, A., " Kinetics of Thermal Decomposition of Cellulose. Part II. Temperature Difference Between Gas and Solid at High Heating Rates", Thermochimica Acta., 1987, 120, p 133-141.

40 Bradbury, A.G.W., Sakai, Y. and Shafizadeh, F., Journal of Applied Polymer Science 23, 1979, p 3271-3280.

41 Shafizadeh, F., "Pyrolytic Reactions and Products of Biomass", Fundamentals of Thermochemical Biomass Conversion, Overend, R.P., Milne, T.A. and Mudge, L.K. (eds.), Elsevier Applied Science Publishers, New York, 1985, p 183-218.

42 Koufopanos, C., Maschio, G., Paci, M. and Lucchesi, A., "Some Kinetic Aspects on the Pyrolysis of Biomass and biomass Components", Energy from Biomass, 3rd E.C. Conference, Venice, Italy, March 1985, Palz, W., Coombs, J. and Hall, D.O. (eds.), Elsevier Applied Science Publishers, London, 1985, p 837-841.

43 Maschio, G., Koufopanos, C. and Lucchesi, A., "Thermochemical Conversion of Biomass: Mathematical Model's on the Lignocellulosic Materials Pyrolysis", Biomass for Energy and Industry, 4th E.C. Conference, Orléans, France, May 1987, Grassi, G., Delmon, B., Molle, J.F. and Zibbetta, H. (eds.), Elsevier Applied Science Publishers, London, 1987, p 1007-10012.

44 Vovelle, C., Mellottee, H., and Delfau, J.L., "Kinetics of Thermal Degradation of Wood and Cellulose by TGA Comparison of the Calculation Techniques", CNRS, France, internal report, 1987.

45 Bilbao, R., Millera, A. and Arauzo, J., "Thermal decomposition of lignocellulosic materials: influence of the chemical composition"., Thermochimica Acta., 1989, 143, 149-159.

46 Bilbao, R., Millera, A. and Arauzo, J., "Kinetics of weight loss by thermal decomposition of different lignocellulosic materials. Relation between the results obtained for isothermal and dynamic experiments", Thermochimica Acta., 1990, 165, 103-112.

47 Stamm, A.J., Ind. Eng. Chem., 48, 1956, p 413.

48 Thurner, F. and Mann, U., "Kinetic investigation of wood pyrolysis", Ind. Eng. Chem. Process des. Dev. 1981, 20, 3, 482-488.

49 Tran, D.Q. and Rai, C., "A Kinetic Model for the pyrolysis of douglas fir bark", Fuel 57, 1978, p 293-298.

50 Samalada, M.C. and Vasaols, I.C., "A kinetic approach to the flash pyrolysis of biomass in a fluidised bed reactor", Fuels, 1991, 70, p 883-889.

51 Lidén, A.G., Berruti, F. and Scott, D.S., "A Kinetic Model for the Production of Liquids from Flash Pyrolysis of Biomass", Chem. Eng. Comm., 1988, 65, P 207-221.

52 Diebold, J.P., "The Cracking Kinetics of Depolymerised Biomass Vapours in a Continuous Tubular Reactor", MSc Thesis, Colorado School of Mines, Golden, USA, 1985.

53 Gorton, C.W. and Knight, J.A., "Oil From Biomass by Entrained-Flow Pyrolysis", Biotech. and Bioeng. Symp., No. 14, 1984, p 14-20.

54 Vasaolos, I., Stoikos, T., Samolada, M., Achladas, G. and Papamargaritas, C., "Production and Utilisation of Synthetic Liquid Fuels", Energy from Biomass 4, 3rd Contractors meeting, Paestum, 25-27 May, 1988, CEC DG XII, Brussels, p 510-515.

55 Piskorz, J., Scott, D.S., and Radlein, D., "Composition of Oils Obtained by the Fast Pyrolysis of Different Woods", Pyrolysis Oils from Biomass, Producing, Analysing and Upgrading, Soltes, E.J. and Milne, T.A. (eds.), ACS Symposium Series 376, American Chemical Society, Washington DC, 1988, p 167-178.

56 Roy C., Yang, Y., Blanchette, D., Korving, L., de Caumia, B. and Pakdel, H., "Development of a novel vacuum pyrolysis reactor with improved heat transfer potential", pp 351-367 in Developments in thermochemical biomass conversion, Eds Bridgwater, A.V. and Boocock, D.G.B., (Blackie 1997)

57 Bridgwater, A.V. and Peacocke, G.V.C., "Fast Pyrolysis Proceses For Biomass", Sustainable and Renewable Energy Resources, vol.4, pp. 1-73, 1999.

58 Maniatis, K., Baeyens, J., Peeters, H. and Roggeman, G., "The Egemin flash pyrolysis process: commissioning and results", pp 1257-1264 in Advances in thermochemical biomass conversion, Ed. Bridgwater, A.V. (Blackie 1993)

59 Maniatis, K., Baeyens, J., Roggeman, G., Peeters, H., "Flash Pyrolysis of Biomass in an Entrained Bed Reactor", Final report of EEC Contract JOUB 0025, 1993.

60 Scott, D.S., and Piskorz, J., "The Flash Pyrolysis of Aspen-Poplar Wood", Can. J. Chem. Eng. 60, Oct 1982, p 666.

61 Scott, D.S. and Piskorz, J., "The Continuous Flash Pyrolysis of Biomass", Can. J. Chem. Eng. 62, Jun 1984, p 404.

62 Scott, D.S., Piskorz, J. and Radlein, D., "Liquid Products from the Continuous Flash Pyrolysis of Biomass", Ind. Eng. Chem. Process Des. Dev. 24, 1985, p 581.

63 Scott, D.S, Piskorz, J., Grinshpun, A. and Graham, R.G., "The Effect of Temperature on Liquid Product Composition from the Fast Pyrolysis of Cellulose", in ACS Symposium on Production, Analysis and Upgrading of Pyrolysis Oils from Biomass, Denver, Colorado, April 1987, p 1.

64 Scott, D.S., Piskorz, J., Bergougnou, M., Graham, R.G. and Overend, R.P., "The Role of Temperature in the Fast Pyrolysis of Cellulose and Wood", Ind. Eng. Chem. Process Des. Dev. 27, 1988, p 8.

65 Scott, D.S. and Piskorz, J., "The Composition of Oils Obtained by the Fast Pyrolysis of Different Woods", in ACS Symposium on Production, Analysis and Upgrading of Pyrolysis Oils from Biomass, Denver, Colorado, April 1987, p 215.

66 Graham, R.G., Freel, B.A., Bergougnou, M.A., "The Production of Pyrolytic Liquids, Gas and Char from Wood and Cellulose by Fast Pyrolysis", in "Research in Thermochemical Biomass Conversion", Bridgwater, A.V., Kuester, J.L. (eds.), Elsevier, p629, 1988

67 Graham, R.G., Bergougnou, M.A., Mok, L.K.S. and de Lasa, H.I., "Fast Pyrolysis (Ultrapyrolysis) of Biomass Using Solid Heat Carriers" in Fundamentals of Thermochemical Biomass Conversion, (eds) Overend, R.P., Milne, T.A. and Mudge, L.K., Elsevier Applied Science Publishers, New York, 1985, p 397.

68 Graham, R.G. and Huffman, DR, "Commercial aspects of rapid thermal processing (RTP™)", Proc. Power Production form Biomass II Conference, Espoo, Finland, April 1995 (VTT 1995)

69 Underwood, G., "Commercialisation of fast pyrolysis products", in 'Biomass thermal processing', Eds. Hogan, E., Robert, J., Grassi, G. and Bridgwater, A.V. pp 226-228, (CPL Scientific Press, 1992)

70 Trebbi, G., Rossi, C. and Pedrelli, G., "Plans for the production and utilisation of bio-oil from biomass fast pyrolysis", pp 378-387, Advances in Thermochemical Biomass Conversion, Bridgwater AV, Boocock DGB (eds.), Blackie, 1997

71 Graham, R.G., Freel, B.A., Huffman, D.R. and Bergougnou, M.A., "Applications of rapid thermal processing of biomass", in Advances in Thermochemical Biomass Conversion, Vol. II, Ed. Bridgwater, A.V., Blackie, (London 1993) pp 1275-1288

72 Graham, R.G., "Flash-Pyrolysis Liquid Fuels Production", Paper presented at 1st EC Forum on Electricity Production from Biomass and Solid Wastes by Advanced Technologies, Florence, Italy, 27-29 November, 1991

73 Huffman, D.R., Vogiatzis, A.J., Graham, R.G., Freel, B.A., "The Characterisation and Combustion of Fast Pyrolysis Bio-Oils", paper presented at: 1st European Forum on Electricity Production from Biomass and Solid Wastes by Advanced

Technologies, Eds. Grassi, G. and Bertini, L., November 27-29 1991, Florence, Italy

74 Shihadeh,, p 281 in Biomass Pyrolysis Oil Properties and Combustion, Ed. Milne, TA., (NREL 1994)

75 Freel., B.A. and Huffman, D.R., "Applied bio-oil combustion", p 309-315 in Biomass Pyrolysis Oil Properties and Combustion, Ed. Milne, TA., (NREL 1994)

76 Roy, C., De Caumia, B. and Pakdel, H., "Preliminary feasibility study of the biomass vacuum pyrolysis process", in: Bridgwater, A.V., and Kuester, J.L., (Eds) Research in Thermochemical Biomass Conversion, pp 585-596 (Elsevier Applied Science 1988)

77 Roy, C., De Caumia, B. and Plante, P., "Performance Study of a 30 kg/h Vacuum Pyrolysis Process Development Unit", 5th European Conference on Biomass for Energy and Industry, (Elsevier Applied Science, 1990)

78 Diebold, J.P., and Scahill, J.W., "Ablative Entrained Flow Fast Pyrolysis of Biomass", proceedings of the 16th Biomass Thermochemical Conversion Contractors Meeting, Portland, Oregon USA, 1984, p 319-347.

79 Diebold, J.P. and Scahill, J.W., "Progress in the Entrained Flow, Fast Ablative Pyrolysis of Biomass" proceedings of the 12th Biomass Thermochemical Conversion contractors Meeting, Washington, USA, 18-19 March, 1981.

80 Diebold, J.P. and Scahill, J.W., "October 1981 Update on the Progress in the Entrained Flow, Fast Ablative Pyrolysis of Biomass", 13th Biomass Thermochemical Conversion Contractors Meeting, Arlington, USA, 27-29 October, 1981, p 332-365.

81 Diebold, J.P. and Scahill, J.W., "Ablative fast Pyrolysis of Biomass in the Entrained Flow Cyclonic Reactor at SERI", 14th Biomass Thermochemical Conversion Contractors Meeting, Arlington, USA, 23-24 June, 1982, 9 272-311.

82 Diebold, J.P. and Scahill, J.W., "Ablative Fast Pyrolysis of Biomass in the Entrained Flow Cyclonic Reactor at SERI", 15th Biomass Thermochemical Conversion Contractors Meeting, Atlanta, USA, 16-17 March, 1983, p 300-357.

83 Diebold, J.P. and Power, A.J., "Engineering Aspects of the Vortex Pyrolysis Reactor to Produce Primary Pyrolysis Oil Vapours for Use in Resins and Adhesives", Research in Thermochemical Biomass Conversion, Bridgwater, A.V., and Kuester, J.L. (eds), Elsevier Applied Science Publishers, London and New York, 1988, p 609 - 628.

84 McKinley, J., "Biomass Liquefaction Centralised Analysis", July 1989, Project No. 4-03-837, Final Report for EMR Canada, Ottawa, Canada.

85 Lédé, J., Li, H.Z. and Villermaux, J., "Fusion Like Behaviour of Biomass Pyrolysis", ACS, Vol. 32, 2, Production, Analysis and Upgrading of Oils from Biomass, Ratcliffe, C.T., Suuberg, E.M. and Vorres, K.S. (eds.), 1987.

86 Lédé, J., Li, H.Z., Villermaux, J. and Martin, H., "Fusion Like Behaviour of Wood Pyrolysis", J. Anal. Appl. Pyr., 10, 1987, p 291-308.

87 Lédé, J., Li, H.Z. and Villermaux, J., "Pyrolysis of Biomass: Evidence for a Fusion Like Phenomenon", ACS Symposium Series 376 , Pyrolysis Oils from Biomass: Producing, Analysing and Upgrading, Soltes, E.J. and Milne, T.A. (eds.), 1988, p 66-78.

88 Martin, H., Lédé, J., Li, H.Z., Villernmaux, J., Moyne, C. and Dégiovanni, A.M., "Ablative Melting of a Solid Cylinder Perpendicularly Pressed Against a Heated Wall." Int. J. Heat and Mass Transfer, Vol. 29, 9, 1986, p 1407-1415.

89 Ayres, W.A., "Commercial Application of Wood Derived Oil", Energy Progress, Vol. 7, No. 2, June 1987, p 77-79.

90 Ayres, W.A., "Commercial Applications of Oxygenated Oil derived from an Entrained Flow Ablative Fast Pyrolysis System", Energy from Biomass and Wastes XII, 1988, Klass, D.L. (ed.), IGT, Chicago, 1991, p 1141-1151.

91 Kansas City Star, 11 August 1989, p 5C.

92 Johnson, D.A., Ayres, W.A. and Tomberlin, G., "Scale up of the Ablative Fast Pyrolysis Process", in Biomass Thermal Processing, 23-25 October 1990, Ottawa, Canada, CPL Press, Newbury 1992, p 236-240.

93 Johnson, D.A., Tomberlin, G., and Ayres, W.A., "Conversion of Wood Waste to Fuel Oil and Charcoal", Energy from Biomass and Wastes XV, 25-29 March 1991, Washington, D.C., IGT Chicago, 1991, p 915-925.

94 Johnson, D.A., Maclean, Feller, J., Diebold , J.P. and Chum, H., "Ablative Fast Pyrolysis: Prototype Plant", American Chemical Society Annual Meeting, 28 March - 2 April 1993, Denver, Colorado, USA, proceedings to be published in Biomass and Bioenergy, 1994.

95 Wagenaar, B.M., Kuipers, J.A.M., Prins, W. and Van Swaaij, W.P.M., "Hydrodynamics of the rotating cone pyrolysis reactor", Biomass for Energy, Industry and the Environment, Athens, 22-26 April 1991, Grassi, G., Collina, A and Zibetta, H. (eds.), Elsevier Science Publishers, p 732-736.

96 Wagenaar, B.M., Kuipers, J.A.M., Prins, W. and Van Swaaij, W.P.M., "The Rotating Cone Flash Pyrolysis Reactor", Advances in Thermochemical Biomass Conversion, Interlaken, Switzerland, 11-15 May 1992, Blackie, Glasgow, 1994, p 1122-1133.

97 Van Swaaij, W.P.M., Kuipers, J.A.M., Prins, W. and Wagenaar, B.M., "The Rotating Cone Flash Pyrolysis Reactor", Energy from Biomass: Progress in Thermochemical Conversion, Proceedings of the EC Contractors Meeting, 7 October 1992, Grassi, G. and Bridgwater, A.V. (eds.), EUR 15389 EN, CEC DG XIII, Brussels, 1994, p 43-50.

98 Wagenaar, B.M., "The Rotating Cone Reactor for Rapid Thermal Solids Processing", Ph.D. Thesis, University of Twente, Enschede, the Netherlands, 1994.

99 Prins, W. and Wagenaar, B.B., "Review of the Rotating Cone Technology For Flash Pyrolysis of Biomass", Biomass Gasification & Pyrolysis, State of the Art and Future Prospects, M Kaltschmitt and AV Bridgwater (eds.)

100 Bridgwater, A.V. and Peacocke, G.V.C., Ablative Pyrolysis Reactor Design And Specification, not published.

101 Batchelor, G.K., 1967, "An Introduction to Fluid Dynamics", Cambridge University Press, Cambridge, United Kingdom, pp. 219-222.

102 Moallemi, M.K., Webb, B.W. and Viskanta, R., "An experimental and Analytical Study of Close-Contact Melting", Transaction of the ASME, Vol. 108, November 1986, p 894-899.

103 Saito, A., Yoshio, U., Masahiro, A. and Katayama, K., "On Close Contact Heat Transfer with Melting: Experimental Study", Bulletin of JSME, Vol. 28, No. 240, June 1985, p 1142-1149.

104 Saito, A., Yoshio, U., Masahiro, A. and Katayama, K., "On Close Contact Heat Transfer with Melting: Analytical Study", Bulletin of JSME, Vol. 28, No. 242, August 1985, p 1703-1709.

105 Bejan, A., "The Fundamentals of Sliding contact Melting and Friction", Journal of Heat Transfer, Vol. 111, February 1989, p 13-20.

106 Litsek, P.A. and Bejan, A., "Sliding Contact Melting: The Effect of Heat Transfer in the Solid Parts", Transactions of the ASME, Vol. 112, August 1990, p 808-812.

107 Peacocke, G.V.C., Russell, P.A., Jenkins, J.D. and Bridgwater, A.V., "Physical Properties Of Flash Pyrolysis Liquid", Biomass and Bioenergy, Vol. 7, No. 1-6, pp. 169-177, 1994.

108 Toft, A.J., "A comparison of integrated biomass to electricity systems.", Ph.D. Thesis, Aston University, 1996.

109 Andrews, R.G., Zukowski, S. and Patnaik, P.C., "Feasibility Of Firing An Industrial Gas Turbine Using A Biomass Derived Fuel", Developments In Thermochemical Biomass Conversion, p. 495-506, eds. Bridgwater, A.V. and Boocock, D.G.B., 1997.

110 Diebold, J.P., Scahill, J.W., Czernik, S., Phillips, S.D. and C.J. Feik, "Progress In The Production Of Hot-Gas Filtered Biocrude Oil", Bio-Oil Production & Utilisation, p.66-81, cpl Press, eds. Bridgwater, A.V. and Hogan, E.N., 1996.

111 Stairmand, C.J., Trans. Inst. Chem. Eng. 29, 356. Design and performance of cyclone separators.

112 Chemical Engineering Volume 6, pp.403, 6th edition, Sinnott, R.K., Pergamon Press, UK, 1994.

113 Fair, J.R., "Design of Direct-contact Gas Coolers", Petro/Chem Engineer, August 1961, p 57-.

114 Fair, J.R., "Process Heat Transfer By Direct Fluid-Phase Contact", AIChE Symposium series, No. 118, Vol. 68, p 1-11.

115 Kreith, F. and Bharathan, D., "Heat Transfer Research for Ocean Thermal Energy Conversion", Journal of Heat Transfer, Vol. 110, Feb. 1998, p 5-21.

116 Fair, J.A., "Designing Direct-Contact Coolers/Condensers", Chemical Engineering, June 12, 1972, p. 91-100.

117 Sipila, K., Kuoppala, E., Fagernas, L. and Oasmaa, A., "Characterisation of biomass-based flash pyrolysis oil", Biomass and Bioenergy, p. 103-113, vol. 14, no. 2, 1998

118 Diebold, J.P., Milne, T.A., Czernik, S., Oasmaa, A., Bridgwater, A.V., Cuevas, A., Gust, S., Huffman, D., Piskorz, J., "Proposed specification for various grades of pyrolysis oil", Developments in Thermochemical Biomass Conversion, Bridgwater, A.V. and Boocock, D.G.B. (eds.), Blackie academic and professional, p. 443-4481997.

119 Bisio, A. and Kabe, R.L., Scale-up Of Chemical Processes, Wiley-Interscience, United States, 1985

120 Diebold, J. and Scahill, S., "Ablative Entrained Flow Fast Pyrolysis Status", Solar Energy Research Institute, Golden, Colorado.

121 Sinnot, R.K., "Chemical Engineering", Volume 6, 1993, Pergamon Press, England.

122 Keen, R. and Koontz, R., 1970, "Operational Considerations." in Sodium Technology. North America Rockwell (Atomics International). Canoga Park, CA, Sect. 7, p.3-24.

123 Dunn, P.O. and Reay, D., 1978, Heat Pipes, 2nd edition. Pergamon Press, New York.

APPENDIX 1: ELECTROSTATIC PRECIPITATOR MODELLING

1. INTRODUCTION

Pyrolysis of biomass produces vapours consisting of condensable organics, water and non-condensable gases at temperatures of up to 450 °C. To completely condense the desired product in the presence of large quantities of non-condensable would require considerable heat transfer area using conventional heat exchangers; in addition the vapour comprises a mixture of micron sized particles and water vapour, with the vapours presenting considerable fouling problems. This would increase the complexity and cost of any conventional heat exchanger employed.

It is intended to design and construct an electrostatic precipitator to be used to coalesce the vapours formed during fast pyrolysis of biomass. The vapours will initially be cooled using a conventional heat exchanger or direct contact heat exchanger with a liquid quench to approximately 20 °C. At this temperature the majority of the pyrolysis product is in the form of entrained vapour/liquid and electrostatic precipitation is an effective way of collecting the resulting aerosol.

Electrostatic precipitation is used to separate particles or aerosols from process gases. In electrostatic precipitation the forces used to separate the particulate from the gas stream are applied directly to the particles themselves. Therefore, the energy needed to effect separation is considerably less than for other types of gas cleaning equipment. The electrostatic precipitation process consists of three basic steps: particle charging, particle collection on a collection electrode and removal of the collected particle from the collection electrode. Particle charging in precipitators is due to ions produced by a generated corona. The charged particles are then subjected to an applied electromagnetic field which forces them towards the electrostatic precipitator wall where they are collected.

Theoretical and empirical equations are used to model an electrostatic precipitator to determine parameters such as the corona initiation voltage, current flow, field strengths, particle migration velocities, required precipitator size and collection efficiency. No

published model or design protocol appears to be available in the current literature and design appears to be vary much based on scale up from pilot plant test and upon the designers experience; although companies working in the area of electrostatic precipitator design usually have an in-house model available. Equations have been used from a variety of sources (1, 2, 3, 4) and as a consequence 3 different types of units are used. These being the Cgs system (centimetres, grams, seconds), the MKS system (Metres, Kilograms, Seconds), and the Electrostatic Units system (ESU). These different units can best be represented by Table 1.1

Table 1.1 Units in use and conversion factors.

Quantity	Cgs	MKS	ESU	Conversion factor of ESU to MKS
Length	cm	M	cm	10^{-3}
Time	s	S	s	1
Mass	g	Kg	g	10^{-3}
Charge	C	C	stC	$3.33*10^{-10}$
Charge per electron	$1.6*10^{-19}$ C	$1.6*10^{-19}$ C	$4.8*10^{-10}$ stC	$3.33*10^{-10}$
Voltage	kV	V	stV	300
Current	A	A	stA	30000
Field strength	kV/cm	V/m	stV/cm	$3.33*10^{-10}$

The following sections give an overview of how the fundamental equations are derived and some of the requirements and problems associated with electrostatic precipitator design. Section **Error! Reference source not found.** details how the process was modelled and the steps taken in arriving at a final design.

2. CORONA GENERATION

Electrostatic precipitators require a large amount of gas ions for the charging of aerosol particles. This is accomplished by a gaseous discharge called a corona. The generation of a corona occurs in a region of high electrical stress. In this case the electrical stress is provided by the application of a high DC voltage to an electrode system consisting of a negatively charged wire as one electrode with a cylinder as the outer positively charged

electrode. This will produce a non-uniform electric field. Near the wire the electric field strength is be high and decreases rapidly with distance from the wire surface.

Process gases consist mainly of uncharged molecules and molecular gases. These molecules are virtually unaffected by the application of an electric field and hence practically no current would flow between the electrodes. However, if the gas molecules are exposed to radiation, some of the molecules will become ionised, thus creating a positive ion and a free electron. Both the positive ion and free electron are effected by the electric field and move towards their respective electrodes. This causes a current to flow between the electrodes, although it is only a small amount. However, in the region of the wire electrode the electric field strength is high and the free electrons in this region are accelerated to high velocities [high electrical mobilities]. These electrons have sufficient energy to release subsequent electrons on impact with neutral gas molecules, creating more electrons and positive ions. This process occurs repeatedly, generating large quantities of electrons and positive ions, and is known as the avalanche process.

2.1 ELECTRON ATTACHMENT

The electric field strength diminishes rapidly with distance from the wire electrode, therefore the velocities of the electrons diminish until they no longer possess sufficient energy to initiate ionisation of the molecular gases. This limit defines the corona glow region.

Outside of this region collisions between electrons and molecules of electronegative gases results in the capture of electrons to produce negative ions. These in turn would be effected by the electrical field and move towards the positive electrode. This also constitutes current flow, the magnitude of the current flow depending upon the ion mobility and the strength of the electric field.

The negative ions formed from the electronegative gases are more stable (lower binding energy) than the molecules from which they originated. The negative ions drift slowly towards the collection electrode, resulting in the build-up of a significant space charge.

The space charge is necessary to stabilise the avalanche region and prevent sparking from occurring.

The electrical limits for operation of an electrostatic precipitator are governed by the corona onset voltage and the sparkover voltage. For negative corona, Shale (5) found that both corona onset voltage and sparkover voltage are influenced by gas temperature and pressure. Ion mobility increases with increasing temperature resulting in a reduced sparkover onset voltage. This in turn limits the electric field strength that can be used and hence the precipitator performance.

3. THE ELECTRIC FIELD

Corona generation occurs when the field strength is sufficient to produce ionising collisions between the generated electrons and the process gases. This is obviously dependent upon the ionisation potentials of the gases present and the mean free path between collisions. It is not practical to derive this from a theoretical basis for a mixture of gases and it is therefore determined empirically. As an empirical relationship is not available for pyrolysis gases it will be assumed that they are equivalent to air, based on their similarly high nitrogen content. The field strength at which corona generation begins in air has been shown semi-empirically by Peek (6) to begin at an electric field strength E defined by

$$E_C = 3 \times 10^6 m\left(\delta + 3.0\sqrt{\frac{\delta}{a}}\right) \qquad \textbf{Eq. 3.1}$$

Where:

E_C = Electric field strength required for onset of corona generation [V/m]

a = The radius of the corona wire [m]

m = Wire roughness factor [1-0]

δ = The relative gas density = $[T_0/T][P/P_0]$

P = The pressure of the gas [atm]

T = The temperature of the gas [K]

T_0 = 298 k

P_0 = 1 atm

This can be integrated from the corona wire to the collection electrode to give the applied voltage at which corona generation occurs.

$$V_C = 3 \times 10^6 am\delta\left(1 + 0.03\sqrt{\frac{\delta}{a}}\right)\ln\left(\frac{b}{a}\right) \qquad \textbf{Eq. 3.2}$$

Where:

b = the radius of the collection electrode [m]

Applied voltages greater than V_C will lead to a corona discharge with a current flow through the interelectrode region.

Alternatively, in electrostatic units the corona onset field strength is given by

$$E_C = 30m\delta\left(1 + 0.3\sqrt{\frac{\delta}{a}}\right) \qquad \textbf{Eq. 3.3}$$

and the corona initiation voltage is given by

$$V_C = \left(30am\delta + 9m\sqrt{a\delta}\right)\ln\frac{b}{a} \qquad \textbf{Eq. 3.4}$$

The electric field in an electrostatic precipitator is due to two components: the surface charges on the electrodes due to the applied voltage and the space charge due to the ions and charged particles in the interelectrode region. Either of these factors can play the dominant role in the determination of the resultant electric field strength. Also, the make-up of the space charge can vary greatly over the precipitator length due to the removal of the charged particles from the interelectrode region.

The electric field equations for a wire-cylinder electrode system can be reduced to a one-dimensional problem if end effects are ignored. For no current flow the field strength (E) at any radius (r) within the cylinder can be determined from.

$$E = \frac{V}{r \ln\left(\frac{b}{a}\right)} \qquad \textbf{Eq. 3.5}$$

If the voltage is increased, the electric field strength will increase until corona generation occurs. The resultant space charge modifies the expression given in equation 3.3. The electric field in the interelectrode region is also dependent upon the space charge density and may be found by solving Poisson's equation for cylindrical co-ordinates.

$$\frac{d^2V}{dr^2} + \frac{1}{r}\frac{dV}{dr} + 4\pi\rho = 0 \qquad \textbf{Eq. 3.6}$$

Where

ρ = space charge density (stC/cm^2)

The space charge density can be determined, for the case of a single current transport species (ions, free electrons, or charged particle), by the following relationship.

$$j = \rho B E \qquad \textbf{Eq. 3.7}$$

Where

B = Mobility ($cm^2/sec.stV$)

j = Current density (stA/cm^2)

If multiple space charge carriers are present than an equivalent or effective mobility is required.

By using the relationship

$$E = -\frac{dV}{dr} \qquad \textbf{Eq. 3.8}$$

and noting that the current density is related to the current per unit length of wire (i) by

$$j = \frac{i}{2\pi r} \qquad \textbf{Eq. 3.9}$$

equation 3.4 can be rearranged and integrated to give.

$$E = -\frac{dV}{dr} = -\left[\left(\frac{C}{r}\right)^2 + \left(\frac{2i}{B}\right)\right]^{1/2} \qquad \textbf{Eq. 3.10}$$

Where

C = a constant of integration

Note that C is constant only with respect to r, and in general will depend upon corona voltage and current and also the diameter of the corona wire and collection electrode.

C may be evaluated by using the boundary condition at the outer radius of the corona glow region near the wire. Denoting the field strength at his point as E_C and the corresponding radius as r_0:

r_0 = Radius of corona glow region ≈ Radius of corona wire a (m)

The voltage current-relationship can be determined by the integration of equation 3.8 between the limits r = a and r = b to give

$$V = V_C + aE_C\left\{\left[1+\left(\frac{b}{E_C a}\right)^2 \frac{2i}{B}\right]^{1/2} - 1 - \ln\frac{1+\left[1+\left(\frac{b}{E_C a}\right)^2 \frac{2i}{B}\right]^{1/2}}{2}\right\} \qquad \textbf{Eq. 3.11}$$

This derivation applies specifically to a single current carrying species where B is the mobility of the current carrier and i the current flowing at that applied voltage. If multiple charge carriers are present then an effective mobility must be calculated. In precipitators most of the current is carried as negative ions, this is because the electrons can not penetrate far into the interelectrode region due to capture and the particulate mobility is relatively slow, approximate mobilities of electrons, ions and particulates are $6.6x10^{-2}$, $2.2x10^{-4}$ and $5x10^{-7}$ $m^2/V.s$ respectively (1). However, it is the relatively low mobility of the particulate that provides a large, sluggish space charge and therefore it cannot be ignored in the calculation of the electric field strength.

3.1 PARTICLE AND SPACE CHARGE EFFECT

Particles in suspension in a gas stream usually become fully charged in about 10^{-2} seconds or less on entering a precipitator (this can easily be proves by substituting values into the equation for particle charge as a function of time Eqn 4.2). Collection of the particles is a slower process, therefore, the interelectrode region is populated by gas ions and charged particulates of the same polarity. The particulate space charge adds to the ion space charge and serves to weaken the field strength near the corona wire and to reduce the current flowing. The effect of the particulate space charge on the corona may be determined by assuming that the particle space charge is proportional to the precipitation field at any given cross section and decreases with precipitator length.

The space charge, ρ_1, (ESU units) carried by the dust per unit volume of gas, in a uniform field E is given by

$$\rho_1 = \frac{\frac{3k}{k+2} ES}{4\pi} \qquad \textbf{Eq. 3.12}$$

Where

k = Relative permittivity of particle

S = Surface area of dust particle per unit volume of gas (cm^2/cm^3)

The space charge per nit volume attributable to the ion current is given by

$$\rho = \frac{2i}{4\pi BrE} \qquad \textbf{Eq. 3.13}$$

Substituting into Poisson's equation, and letting

$$\frac{3k}{k+2} = \phi \qquad \textbf{Eq. 3.14}$$

gives

$$\frac{dE}{dr} + \frac{E}{r} - \frac{2i}{BrE} - \phi ES \qquad \textbf{Eq. 3.15}$$

This can be integrated to give

$$E = \left[\left(\frac{a^2 E_C^2}{r^2} + \frac{i}{B(\phi Sr)^2} \right) \exp(2\phi Sr) - \frac{i}{B} \left(\frac{2}{\phi Sr} + \frac{1}{(\phi Sr)^2} \right) \right]^{1/2} \qquad \textbf{Eq. 3.16}$$

if ϕS is small, the exponential term may be expanded, reducing the equation to an approximate form. For large radii [and specifically at the collection electrode], where $a^2/r^2 >> 1$, the field strength can be approximated by

$$E = \sqrt{\frac{2i}{B}} \left(\frac{\phi Sr}{3} + 1 \right) \qquad \textbf{Eq. 3.17}$$

and the field strength at the wire surface can be approximated by

$$E = E_o \exp(\phi Sr) \qquad \textbf{Eq. 3.18}$$

3.2 PARAMETERS INFLUENCING THE ELECTRIC FIELD

The electric field in an electrostatic precipitator can be altered by both design and operating parameters. The maximum allowable current is determined by the electrical breakdown of gases within the interelectrode region or in the deposited particulate layer. The current-voltage relationship can be altered by varying the wire electrode diameter, with wire sizes of 0.3 cm being a reasonable average. The larger the wire size the higher the rate of current increase with voltage and the higher the corona initiation voltage. The value of this is somewhat dependent upon the system, a large wire size means you need a larger corona initiation voltage and the sparkover limit is reached at lower voltages, both of which are a disadvantage and limit operation of the precipitator. However, the rate of degradation of field strength as a function of distance from the corona wire is reduced giving a higher field strength at the collection electrode resulting in an improved collection efficiency. The decision to use a large or small wire diameter will be process specific and will depend upon the available power supply, process gases, sparkover potential and desired collection efficiency and therefore cannot be quantified here.

4. PARTICLE CHARGING

In electrostatic precipitation the particle must be charged for the electric field to impose a driving force. This force is the predominant factor in the removal of the particulate from the gas stream, and is proportional to the particle charge and the electric field strength.

There are two mechanisms for the charging of particles, field charging and diffusion charging. Both mechanisms apply to the charging process, however, each is increasingly significant for particles within a particular size range. Field charging is the dominant mechanism for particles which have a diameter greater than 1 μm and diffusion charging is predominant for particles with a diameter less than 0.4 μm. In the intermediate range both mechanisms apply and must therefore be considered simultaneously. In the case of the design of an electrostatic precipitator to be used to coalesce vapours formed during fast pyrolysis, it is necessary to know the range of

particle sizes present in the pyrolysis vapours. Vapours from a pyrolysing wood rod have previously been blown across the detector from a Malvern particle size analyser and the following particle size analysis obtained.

Table 4.1 Particle size analysis of pyrolysis vapour.

Size Microns	% Under	Size Band Range Microns	% in Range
118.4	100.0		
54.9	100.0	118.4-54.9	0.0
33.7	99.7	54.9-33.7	0.3
23.7	94.3	33.7-23.7	5.4
17.7	52.6	23.7-17.7	41.7
13.6	50.6	17.7-13.6	2.0
10.5	50.5	13.6-10.5	0.1
8.2	31.7	10.5-8.2	18.8
6.4	25.1	8.2-6.4	6.6
5.0	21.2	6.4-5.0	3.8
3.9	15.7	5.0-3.9	5.6
3.0	10.2	3.9-3.0	5.5
2.4	6.8	3.0-2.4	3.4
1.9	4.7	2.4-1.9	2.2
1.5	3.2	1.9-1.5	1.4
1.2	2.4	1.5-1.2	0.8

The majority of the particle fall within the particle size range 23.7-17.7 μm and 10.5-8.2 μm, therefore, only field charging will be considered in the determination of particle charge. To accurately design an electrostatic precipitator, the design should be performed on an incremental basis, however, as this is time consuming and the accuracy of the particle size analysis has not been validated a worst case scenario will be assumed and an average particle size of 1 μm chosen.

Field charging is related to the ordered motion of ions due to an electric field resulting in collisions between ions and suspended particles in a gas stream. If the ions are retained by the particles then the particles become electrically charged. In the theoretical analysis of field charging, three simplifying assumptions need to be made:

1 The particles are considered to be spherical.

2 The field from one particle does not influence the field in the vicinity of adjacent particles.

3 The particles and ions are suspended in a constant electric field.

As the ions pass into a region near a particle, internal charges of the dust particle are redistributed so that an attractive force exists between the ion and particle. As ions continue to impinge on the particle the charge will increase until a sufficient electric field is established in the vicinity of the particle to prevent additional ions reaching the particle.

The saturation charge is the maximum charge attainable by a particle and can be determined from

$$q_S = 12\frac{k}{k+2}\pi\varepsilon_0 p^2 E_0 \qquad \textbf{Eq. 4.1}$$

Where

q_S = Saturation charge (coulombs)

k = Relative permittivity

ε_0 = Permittivity of free space = $8.854*10^{-12}$ $C^2J^{-1}m^{-1}$

p = Particle radius (m)

E_0 = Undisturbed electric field strength (V/m)

The relative permittivity of most substances ranges between 1 and 10, an average permittivity value for pyrolysis vapours is not known so a value of 1 will be specified

The expression of charge as a function of time can be given by

$$q_t = 12\frac{k}{k+2}\pi\varepsilon_0 p^2 E_0 \frac{t}{t+\tau} = q_s \frac{1}{1+\frac{\tau}{t}} \qquad \textbf{Eq. 4.2}$$

$$\tau = \frac{4\varepsilon_0}{N_0 eB} \qquad \textbf{Eq. 4.3}$$

Where:

B = Mobility of ion ($m^2/s.V$)

e = Charge of an electron = $1.6*10^{-19}$ C

N_0 = Molecular density (molecules/m^3)

5. PARTICLE COLLECTION

An electrically charged particle in an electric field will be acted on by a force in a direction dependent on the polarity of the charge and the direction of the field. If the electrostatic forces dominate, the particle will move towards the collection electrode with a velocity determined by the magnitude of the electrostatic and viscous drag forces. However, other factors play an important part in determining the collection efficiency.

The four principal forces acting on a particle in an electric field are:

Gravitational force

$$F_g = mg$$

Electrical force

$$F_e = qE$$

Viscous force

$$F_\mu = 6\pi p\mu w$$

Inertial force

$$F_i = mdw/dt$$

Where

q = Charge on particle (Coulombs)

μ = Viscosity of medium (kg/m.s)

p = Particle radius (m)

w = Velocity of particle (m/s)

m = Mass of particle (kg)

g = Acceleration due to gravity = 9.8 m/s^2

A diagram of the forces acting upon a particle can be seen in Fig. 5-1. The main forces, electrical and viscous, are shown in solid lines. The gravitational and inertial and inertial forces can be considered to be negligible in comparison to the electrical and viscous forces and are shown as dotted lines.

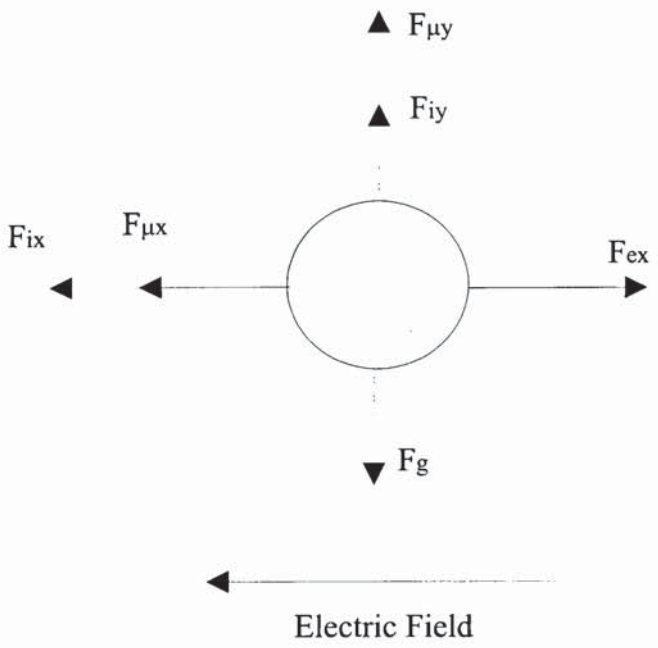

Fig. 5-1 Forces acting upon a negatively charged particle in an electrostatic precipitator.

If we consider a particle suspended in a stationary gas with a co-ordinate system as shown in Fig. 5-1, a force balance yields:

$$\sum F_x = F_e - F_\mu - F_{i(x)} = 0$$

$$\sum F_y = F_g - F_{i(y)} = 0$$

$$\sum F_z = 0$$

The gravitational force is typically at least two decimal orders of magnitude less than the electrical force and can be ignored. Therefore, only the x-direction force is considered.

$$F_e - F_\mu - F_i = 0 \qquad \textbf{Eq. 5.1}$$

Which on substitution of the relevant expressions yields

$$qE - 6\pi p\mu w - m\frac{dw}{dt} = 0 \qquad \textbf{Eq. 5.2}$$

This can be rearranged to give a linear differential equation with constant coefficients and solved for the term w to give.

$$w = \frac{qE}{6\pi p\mu}\left[1 - \exp\left(\frac{-6\pi p\mu t}{m}\right)\right] \qquad \textbf{Eq. 5.3}$$

The term, $\frac{m}{6\pi p\mu}$, denotes the time constant (τ) of the motion; the velocity w essentially reaches its terminal value within five time constants.

The time constant for a 1 μm radius particle, in air at atmospheric pressure, with an assumed density of 10^3 kg/m^3 can be shown to be approximately 0.1 ms. The typical

residence time of a particle in an electrostatic precipitator ranges from 2-5 seconds. Therefore, the exponential part of equation 5.3 can be ignored, giving the expression.

$$w \approx \frac{qE_p}{6\pi p\mu} \qquad \textbf{Eq. 5.4}$$

Where

E_p = The electric field strength at the collection electrode (V/m)

Substituting gives

$$w \approx 12\frac{k}{k+2}\pi\varepsilon_0 p^2 E_0 \frac{1}{1+\frac{\tau}{t}}\frac{E_p}{6\pi p\mu} \qquad \textbf{Eq. 5.5}$$

Where in this case τ is as given earlier

$$\tau = \frac{4\varepsilon_0}{N_0 eB} \qquad \textbf{Eq. 5.6}$$

Which after simplification gives

$$w \approx \frac{2k\varepsilon_0 E_o E_p p}{(k+2)\mu}\frac{1}{\left(1+\frac{\tau}{t}\right)} \qquad \textbf{Eq. 5.7}$$

For particles with high relative permittivities, which have attained a saturation charge, the factor k/k+2 approaches unity and τ/t approaches zero. Therefore, the steady state migration velocity of a particle dependent on field charging is given by

$$w \approx \frac{2\varepsilon_0 E_o E_p p}{\mu} \qquad \textbf{Eq. 5.8}$$

5.1 PARTICLE COLLECTION IN TURBULENT FLOW

In laminar flow the gas velocity through the precipitator and the radial migration velocity of the particles are known and it is simple to determine the length required for 100 % collection provided plug flow is assumed. In most practical precipitators gas flow is turbulent and the motion of a dust or aerosol particle will be the result of the turbulent gas flow and the particle migration velocity (w). Therefore, the trajectory of a single particle can not be easily determined.

Anderson first discovered the equation for collection efficiency in an electrostatic precipitator during field tests in 1919. Deutsch (7) theoretically derived a similar equation in 1922. The collection efficiency equation has been verified by laboratory experiments, and is generally known as the Deutsch equation or the Deutsch-Anderson equation. A number of assumptions were made in the derivation of the equation, these being:

1. The particles are considered to be fully charged immediately on introduction into the collection system.
2. Turbulent and diffusive forces cause the particles to be distributed uniformly in any cross section.
3. The velocity of the gas stream does not affect the migration velocity of the particle.
4. Particle motion is governed by viscous drag where Stokes' Law applies.
5. The particles always move at their electrical terminal velocity.
6. Dust particles are sufficiently separated so that their mutual repulsion can be ignored.
7. The effect of collisions between ions and neutral gas molecules can be neglected.
8. There are no disturbing effects such as erosion, re-entrainment, uneven gas flow distribution, or back corona.

In the central region of the precipitator flow is turbulent, and the magnitude of the migration velocity is small in comparison to the gas velocity. The theoretical derivation of the collection efficiency equation is based on the assumption that there is a region of

thickness (δ) in the boundary layer at the collection electrode where flow will be laminar due to friction between the wall and the gas stream. All the particle in the boundary layer can be assumed to be driven to the wall and collected in a time Δt over a length ΔL. The full derivation will not be given here, being readily available (1), the final equation being of the form.

$$\eta = 1 - \exp\left(-\frac{A}{Q}w\right) \qquad \textbf{Eq. 5.9}$$

Where

η = Collection efficiency
A/v_g = Specific collection electrode area
w = Particle migration velocity (m/s)
A = Area of collection electrode (m^2)
Q = Volumetric flow rate of gas (m^3/s)

5.2 FACTORS INFLUENCING COLLECTION

The collection efficiency equation was developed for ideal condition, however, there are a number of factors that need to be considered which can reduce the collection efficiency.

The gas flow quality or velocity is considered to be identical across the precipitator cross-section, with the collection efficiency equation being applied across the whole. In reality the velocity can vary and the precipitator should be divided into sections radially, with the velocity being determined for each section and the collection efficiency equation being applied separately.

It is assumed in the derivation of the efficiency equation that the particles are retained on the collection surface, this can be achieved in wet wall precipitators or in the collection of liquid aerosols, but this does not necessarily apply for dry materials.

Particles reaching the collection electrode can be re-entrained into the gas stream increasing the upstream particle concentration with a consequential effect upon collector efficiency. It is not currently known if the collected pyrolysis vapours suffer reentrainment, but it is safe to assume that if it does occur it is minimal

The efficiency equation assumes that the particles reach their saturation charge instantaneously on entry into the precipitator. If the charging time is of the order of milliseconds then it can effectively be ignored. However, in precipitators where the current densities must be kept low to prevent sparking, the charging times can be considerable and this factor needs to be considered.

The derivation of the collection efficiency equation applies to a single particle size. Although it can be applied on an incremental particle size basis it has not been done here, this is because a worst case scenario of 1 μm particles has been assumed. Particle size has an effect upon the migration velocity because the ration of charge to mass changes, with the result that larger particles have a higher migration velocity and are collected easier, again this can be calculated on an incremental particle size basis but has not been done so in this case. There is also the fact that charging mechanisms vary depending upon the particle size and field charging has been specified in this case. For the collection efficiency equation to be used accurately, it needs to be applied to each particle size present.

6. BACK CORONA AND SPARKOVER

Electrostatic precipitators are influenced by the collected dust or aerosol layer because the corona current must flow through the collected layer. If the layer has a high electrical resistivity the corona current will be limited and this will limit the magnitude of the particle charge, charging rate and electrical field strength.

A dust or aerosol layer with a high electrical resistivity can limit the power input into a precipitator in two ways. Firstly, high resistivity dust can electrically breakdown at low current densities resulting in a condition called back corona. Secondly, sparkover can occur with clean electrodes due to the electrical breakdown of the gases in the

interelectrode region. However , breakdown of the gases held within the interstitial spaces of a dust layer can occur at conditions much lower than those required in the interelectrode region. This is because the electric field within the dust/aerosol layer is capable of accelerating electrons to ionisation velocities. This results in an avalanche effect, due to impacts with gas molecules, generating large quantities of positive ions and electrons.

The dust/aerosol layer on the collection electrode can cause a voltage drop from that which can be achieved with clean electrodes. The voltage drop can be determined from:

$$V_d = j\lambda x \qquad \textbf{Eq. 6.1}$$

Where

V_d = Voltage drop [v]
j = Current density [amperes/m^2]
λ = Resistivity [ohms/cm]
x = Dust/liquid layer thickness [m]

The field strength in the deposited layer can be determined from:

$$E = j\lambda \qquad \textbf{Eq. 6.2}$$

The breakdown field strength of most industrial gases is typically in the range of 10 to 20 kV/cm.

A localised breakdown of the dust layer will lead to a sudden increase of the interelectrode voltage at the breakdown point, since the voltage drop due to the dust layer is no longer limiting. If the interelectrode voltage is sufficiently high, a spark can be propagated between the two electrodes, i.e. sparkover. This would serve to reduce the current density within the electrostatic precipitator.

Back corona can occur when the generated positive ions at the collection electrode are propelled towards the corona electrode due to the electric field. If they impinge on a negatively charged particle they serve to reduce its charge, or charge it with the opposite polarity.

7. MODELING

An electrostatic precipitator can be modeled by assuming that the Deutsch equation is valid and defines the collection efficiency of the precipitator. To accurately determine the precipitator efficiency the particle sizes need to be divided into a number of increments, and the precipitator also needs to be divided into a number of incremental lengths. Although in this case an assumed value of 1 μm has been specified, it is helpful to show the equations as they would apply if an incremental particle size was used

The model would ideally predict the fractional collection efficiency, η_{ij} for the i^{th} particle size in the j^{th} length of the precipitator. The Deutsch equation would be applied in the form:

$$\eta_{i,j} = 1 - \mathrm{Exp}\left(\frac{-w_{i,j}A_j}{Q}\right) \qquad \textbf{Eq. 7.1}$$

Where

$w_{i,j}$ = Migration velocity of the i^{th} particle size in the j^{th} incremental length.

A_j = Collection plate area in the j^{th} increment.

Q = Volumetric flow rate [m^3/s].

The Deutsch equation assumes that the migration velocity is constant over the collection area, therefore, it is necessary to make the increments sufficiently small so that electric field strength and the charge accumulated by a particle effectively constant over the increment. The fractional collection efficiency for a particle size over the entire length of precipitator is given by

$$\eta_i = \frac{\sum_j \eta_{i,j} N_{i,j}}{Ni,1} = \frac{\sum_j \left(1 - Exp\left(\frac{-w_{i,j}A_j}{Q}\right)\right) N_{i,j}}{N_{i,1}} \qquad \textbf{Eq. 7.2}$$

Where

$N_{i,j}$ = Number of particles in the i^{th} particle range per cubic meter of gas entering the j^{th} increment.

$N_{i,1}$ = $N_{i,0}$, the number of particles of the i^{th} size per cubic meter of gas in the inlet size distribution.

$N_{i,j}$ can be written in the form

$$N_{i,j} = N_{i,j-1} - \left(1 - Exp\frac{-w_{i,j-1}A_{j-1}}{Q}\right) N_{i,j-1} = N_{i,j-1} EXP\left(\frac{-w_{i,j-1}A_{j-1}}{Q}\right) \qquad \textbf{Eq. 7.3}$$

The overall efficiency for the entire aerosol is determined by

$$\eta = \sum_i \eta_i P_i \qquad \textbf{Eq. 7.4}$$

Where

P_i = The mass percentage of the i^{th} particle size in the inlet size distribution.

7.1 SPACE CHARGE EFFECTS

The presence of particles in the interelectrode region significantly influences the voltage-current characteristics of an electrostatic precipitator. The particles cause an increased voltage for a given current compared to a dust free condition, with an increased possibility of sparkover. This is due to the reduced mobility of the charge carriers as the faster ions become attached to the slower moving particulates, thus creating a space charge. This space charge influences the electric field strength

(increasing it), leading to an increase in both the collecting field strength and particle charging field strength, and therefore enhancing collection efficiency. The space charge is due to the presence of particulates and is therefore a function of length along the precipitator, requiring its determination on an incremental basis.

The current density at the collection electrode is due to charge transported by ions and particulates, with virtually all of the generated free electrons being captured in the interelectrode region. The current density can be determined from

$$j_T = E_o\rho_i B_i + E_o\rho_p B_p = E_o\rho_T B_e \qquad \textbf{Eq. 7.5}$$

Where

j_T = Total current density, A/m^2
E_o = Average electric field, V/m
B_i = Ion mobility, $m^2/S.V$
ρ_i = Charge on ions, C/m^3
B_p = Particle mobility, $m^2/S.V$
ρ_p = Charge on particulate, C/m^3
ρ_t = $\rho_p + \rho_i$
B_e = Effective mobility of ions and particulate, $m^2/S.V$

The effective mobility can be defined as:

$$B_e = \frac{\rho_i B_i + \rho_p B_p}{\rho_T} \qquad \textbf{Eq. 7.6}$$

B_e can be determined as follows

$$\frac{j_p}{j_T} = \frac{E_o\rho_p B_p}{E_o\rho_p B_p + E_o\rho_i B_i} \qquad \textbf{Eq. 7.7}$$

j_p is determined by determining the charge on the particles in the interelectrode region in a specific incremental length and multiplying this by an estimated particle removal rate. The current density due to the particulate an be assumed to be small compared to the total current density ($j_i >> j_p$), and the mobility of the ion charge carriers is, on average, 200 times that of the particulate. Equation 7.7 can then be reduced to

$$\frac{j_p}{j_T} \cong \frac{\rho_p B_p}{\rho_i B_i} \cong \frac{\rho_p B_p}{\rho_i (200 B_p)} = \frac{\rho_p}{200\rho_i} \qquad \textbf{Eq. 7.8}$$

After manipulating the preceding equations, the effective mobility may be determined from

$$B_e = B_i \left(\frac{j_T}{200 j_p + j_T} \right) \qquad \textbf{Eq. 7.9}$$

This gives a basis for estimating the effect of particulate space charge on the voltage-current characteristics. Sources of possible error include the assumption that the particle current is insignificant and that the ion mobility is approximately 200 times that of the particle [average value of useful data, particle mobility varying with size] (1).

7.2 DATA REQUIREMENTS

To enable the spreadsheet to operate a number of data inputs are required, these are best summarised in Table 7.2 and Table 7.3 below. The table below gives the gas composition, flow rates and the mobilities of the gaseous ions formed in the corona glow region.

Table 7.2 Gas flow composition and mobilities.

Component	R.M.M	lt/h	kg/s	Mobilities $m^2/s.V$
CO	28	21.6359	9.71239E-06	0.000114
CO_2	44	13.6136	9.60326E-06	0.000098
CH_4	16	3.4034	8.73024E-07	0.00008

C_2H_4	28	0.7293	3.27384E-07	0.00008
C_2H_6	30	0.2431	1.16923E-07	0.00008
N_2	28	2391.375	0.001073492	N.A.
C_3H_8	44	0	0	0.00008
Liquid	600	0.055833	1.86111E-05	N.A.
Water	18	0	0	N.A.
Total		**2431.056**	**0.001112736**	

The table below gives an example of a typical physical arrangement of the precipitator, its operating parameters and the physical constants (some of which are assumed) of the particles and gases within the precipitator for products exiting a char cyclone fitted to a pyrolysis reactor.

Table 7.3 Example electrostatic precipitator configuration and physical properties.

Parameter	Units	Value
Operating Voltage	V	25000
Wire Electrode Radius	M	0.001
Tube Electrode Radius	M	0.0375
Tube Length	M	0.4381
Assumed efficiency	%	100
No of incremental lengths		10
Operating Temp	K	289
Operating Pressure	N/m^2	138685
Relative Permittivity		1
Average particle size	μm	2
Wire Roughness factor		0.8
Relative Air Density		1.031142
Viscosity of medium	kg/m.s	0.000018
Density of gas	g/cm^3	0.001205
Permittivity of free space	F/m	8.85E-12
Particle Density	kg/m^3	1200

7.3 SPREADSHEET CALCULATIONS

The spreadsheet developed calculates the overall precipitator efficiency by following a set program. This can be represented as follows.

1 Input Data.

2 Calculate incremental efficiency from assumed overall efficiency.

3 Calculate number of particles in each increment and the number of particles removed in each increment.

4 Determine corona initiation voltage and field strength.

5 Calculate average field strength for particle charging.

6 Calculate particle saturation charge, determine space charge due to particulates.

7 Calculate voltage-current relationship for each increment.

8 Calculate collecting field strength at the collecting electrode.

9 Determine migration velocity of particles.

10 Determine incremental efficiency from migration velocity.

11 Determine overall efficiency.

12 Use new incremental efficiency for step 2, repeat process until convergence is achieved.

The output from the spreadsheet gives the calculated operating efficiency and required operating current as a function of the interelectrode gases physical properties, the operating voltage and the electrostatic precipitator geometry.

8. RESULTS

The model developed is still in the validation stage, however, preliminary indications are encouraging. Two prototype electrostatic precipitators have been designed according to this design methodology, one is a conventional E.P and is in service on a 1.5 kg/h fluidised bed pyrolysis reactor. The other is a wet walled E.P, with octane being the liquid media, and is in service on a 3.5 kg/h ablative fast pyrolysis reactor. The wet walled E.P. was designed to be fitted on top of a quench column enabling capture of the pyrolysis vapours in a single piece of equipment with significantly reduced fouling. The novel combined design has been tested and is highly efficient. The two E.P.s will be used to generate design information to improve the electrostatic precipitator design methodology. Initial findings are:

- The wire roughness factor can be taken to be 0.8 with the materials we are using.
- The corona initiation voltage in pyrolysis gas appears to be 20% larger than that which would be required in air, although this result is subject to the quantities of transport gas used and conformation with different size E.P.'s.
- The small size of the E.P.'s being employed leads to a very high electric field strength at the collection electrode. This in turn enables efficiencies of 100 % to be achieved, both by modeling and by experimental conformation.

9. RECOMMENDATION

Although a model for the determination of the efficiency of an electrostatic precipitator has been developed a number of areas and assumptions need investigating and justifying. These can fall into the following categories.

- The use of an empirical equation developed for an air system to determine the corona initiation voltage will need investigating as it has an effect on the overall efficiency. Ideally an empirical equation specifically for pyrolysis gases will be determined.
- The effective mobility is determined based on an assumption about the relative amounts of charge carried by ions and particles, this is because the particle mobility can not be calculated directly. However, tabulated data is available and may be of some use in validating the above assumption.
- The model developed is based on a single particle size and should be modified to allow the efficiency to be determined on an incremental particle size basis.

1 S. Oglesby, Electrostatic Precipitation, Marcel Dekker, INC., 1978.

2 W.C. Hinds, Aerosol Technology, John Wiley & Sons, INC., 1982.

3 H.J. White, Industrial Electrostatic Precipitation, Addison-Wesley, Reading, Mass., 1963.

4 H.E. Rose, A.J. Wood, An Introduction To Electrostatic Precipitation In Theory And Practice, Constable & Company LTD, London., 1966.

5 C.C Shale, W.S. Bowie, J.H. Holden, and G.R. Strimbeck, U.S. Bur. Mines Rep. Invest. 6325 (1963).

6 F.W Peek, Dielectric Phenomena in High-Voltage Engineering, 3rd ed., McGraw-Hill, New York, 1939.

7 W. Deutsch, Ann. Phys. (Leipzig) 68, 335-344 (1922).